ANALYSIS AND SYNTHESIS OF MECHANICAL ERROR IN RAPID PROTOTYPING PROCESSES USING STOCHASTIC APPROACH

SANAT AGRAWAL

to the
DEPARTMENT OF MECHANICAL ENGINEERING
INDIAN INSTITUTE OF TECHNOLOGY, KANPUR

March, 2001

ANALYSIS AND SYNTHESIS OF MECHANICAL ERROR IN RAPID PROTOTYPING PROCESSES USING STOCHASTIC APPROACH

A Thesis Submitted
in Partial Fulfilment of the Requirements
for the Degree of

Doctor of Philosophy

by
SANAT AGRAWAL

to the

DEPARTMENT OF MECHANICAL ENGINEERING
INDIAN INSTITUTE OF TECHNOLOGY, KANPUR

March, 2001

Dedicated

to

All My Teachers

CERTIFICATE

It is certified that the work contained in the thesis entitled **Analysis and Synthesis of Mechanical Error in Rapid Prototyping Processes Using Stochastic Approach**, by **Sanat Agrawal**, has been carried out under my supervision and that this work has not been submitted elsewhere for a degree.

Dhande
28/3/01

Dr. Sanjay Govind Dhande
Professor, ME & CSE
Department of Mechanical Engineering,
Indian Institute of Technology, Kanpur.

March, 2001

SYNOPSIS

Analysis and Synthesis of Mechanical Error in Rapid Prototyping Processes Using Stochastic Approach

A Thesis Submitted
in Partial Fulfilment of the Requirements for the Degree of
Doctor of Philosophy

by

Sanat Agrawal
Roll no. 9410563

Thesis Supervisor Dr. Sanjay Govind Dhande

to the

Department of Mechanical Engineering
Indian Institute of Technology, Kanpur

March, 2001

Rapid Prototyping, RP in short, is a layered manufacturing process to make prototypes fast from CAD data. RP is emerging as a key prototyping technology with its ability to produce even complicated parts within hours. RP is a term which embraces a range of new technologies for producing accurate parts directly from CAD models, in a few hours, with little need for human intervention. This means that designers have the choice of making physical models of the conceptual design more frequently, allowing them to assess the form, fit and functionality of the design. This also allows them to discuss manufacturing issues with an easy-to-interpret prototype which can be held, viewed, studied, tested and compared. As a result, a product is improved and the product development cycles and costs substantially reduced.

RP systems take the solid model of a part as an input and make a physical model or prototype without using tools or fixtures. Unlike conventional machining processes, which remove material to obtain a desired shape, RP systems are additive in nature. A part is built progressively, layer by layer. This technology has also been referred to as layered manufacturing technology, free-form fabrication, model making, desktop manufacturing, etc.

The layer by layer manufacturing technologies poses several accuracy issues. Some of these issues are technical and may be as a result of software and hardware limitations, while others may be due to finishing operations. There are limitations in CAD to RP translation which generally take place in the CAD system itself, for e.g., tolerance for tessellation, convex boundary error, flipped normal, mid-line node, etc. The dimensions of the delivery systems of RP determine the minimum feature size that can be built in the RP system. RP parts usually exhibit a staircase effect on slanted and curved surfaces because of the layering process. Areas that overhang the prior layer must be supported to prevent their curl deformation. Orientation of the build is to be determined considering several factors, such as, surface finish, build time, distortion, etc.

The RP systems consist of mechanisms to move optics, build head, elevator platform, Z-stage platen, etc. The links of a mechanism are manufactured with some tolerances on the link lengths and clearances at the joints. The tolerances and clearances cause mechanical error in the desired position of the tool or the platform. Mechanical Error is a significant accuracy issue in RP processes. A search of the literature has yet to disclose any work on analysis and synthesis of mechanical error in RP processes. The objective of the present work is the analysis and synthesis of mechanical error in RP processes. Three RP processes, Laminated Object Manufacturing (LOM), Fused Deposition Modeling (FDM) and StereoLithography (SL) are considered. Using the stochastic approach, a methodology for analysis as well synthesis for mechanical errors such as tolerances and clearances of salient feature dimensions of these three RP processes have been studied. In order to achieve a desirable performance accuracy of an RP process, it is necessary to allocate optimally the levels of tolerances and clearances. This aspect is also studied in the present work.

While designing a mechanism either for function generation or for path generation or for rigid-body guidance, it is necessary to take into account not only the structural error but also the mechanical error. Mechanical error in mechanisms has been dealt considerably in the past literature. Indiscriminate allocation of tolerances and clearances may lead to unacceptable deviation of the output. On the other hand, the cost of manufacturing and assembling such a mechanism with stringent values of tolerances and clearances may be prohibitive. A designer would, therefore, like to assign tolerances and clearances such that the mechanical error is within the specified limits and the levels of tolerances and clearances are as high as possible.Tolerances and clearances are random in nature. The stochastic approaches have been found to be more suitable for both analysis and synthesis of mechanical error. In the present work mechanical error in RP processes is studied using the stochastic approach.

Chapter 1 of the thesis gives an overview of RP processes. It describes three

RP processes LOM, FDM and SL in brief. The accuracy issues in RP processes are discussed. A review of the literature pertaining to analysis and synthesis of mechanical error in mechanisms is presented.

Chapter 2 of the thesis presents a unified approach for studying the effects of manufacturing errors in RP processes. It gives random errors associated with link lengths, joints in linkages, coordinates of a point and orientation of a link. Stochastic model of an RP process is discussed. The coordinates of a point on the work surface traced by the laser beam or the tip of the extruder head is expressed as a function of random variables involved in the process. If there are n random variables V_1, V_2, ..., V_n involved in the process then the coordinates of the point are given by $x(V_1, V_2, \ldots, V_n)$, $y(V_1, V_2, \ldots, V_n)$ and $z(V_1, V_2, \ldots, V_n)$. The methodology to associate any given range of a dependent variable x, y or z with its corresponding probability is given. For normally distributed random variables, the dependent variable may as well be taken as normal for more than five random variables. For a given probability, the range of a dependent variable is evaluated from the variance of the dependent variable. The variances of the dependent variables x, y and z are expressed in terms of the influence coefficients $\left(\frac{\partial x}{\partial V_i}\right)^2$, $\left(\frac{\partial y}{\partial V_i}\right)^2$and $\left(\frac{\partial z}{\partial V_i}\right)^2$.

Chapter 3 performs analysis of mechanical error in LOM. The LOM process cuts and binds foil . Geometric model of the LOM process consists of rollers, work surface, location of the laser source, etc. The geometric model allows to express a point on the contour of a slice on the LOM sheet. The work surface and the laser beam is expressed parametrically and the intersection of the laser beam and the work surface is found. Newton-Raphson method is used to solve the transcendental equations. Expressions for the influence coefficients and the partial derivatives needed for them are derived. A numerical example is given for a set of input values. The variances D[x], D[y] and D[z], and their sum are listed for a grid of points on the work surface. The three-sigma bands of error in tracing several lines on the work surface is plotted. This is the band with probability 0.9973.

Chapter 4 performs analysis of mechanical error in FDM. The FDM process comprises of an extruder head moving in XY-plane. The tip of the extruder head deposits material on the Z-stage platen. It draws the contour of a slice on the platen and fills the contour with roads. Geometric model of the FDM process consists of links, hinge joints, location and orientation of Z-stage platen, etc. The expression for a point on the contour of a slice traced by the nozzle tip is found. The influence coefficients and the partial derivatives needed for them are derived. A numerical example is presented for given tolerances and clearances, and other input values. The variances and their sum are listed for a grid of a points traced by the nozzle tip. The three-sigma bands of error in tracing few example curves is plotted.

Analysis of mechanical error in SL is presented in Chapter 5. In the SL process, the laser beam moves across the surface of a photocurable liquid acrylate resin in a vat and traces the contour of a slice. Geometric model of the SL process consists of the location of the laser source, orientation of the mirrors, location and orientation of the elevator platform, etc. Parametric representation of the ray incident on the mirror is found. For a desired reflection from the galvanometer-driven mirror, the orientation of the mirror and the intersection of the incident ray and the mirror is found. Newton-Raphson method is used to solve the non-linear equations. Expression for a point on the contour of a slice is drawn by the laser on the resin surface is derived. A numerical example for a set of input values gives the list of variances. The three-sigma bands of error for few example curves are also plotted.

Chapters 2, 3, 4 and 5 deal with the analysis of mechanical error in RP processes. The synthesis part is the inverse of the above problem. In synthesis, the designer has to decide the levels of tolerances on the random variables V_i for certain allowable tolerance limits on the dependents variables x, y and z. Chapter 6 deals with the optimal allocation of tolerances and clearances in RP processes. Since the constraints are linear functions of design variables, therefore, the optimization is done using Lagrange Multiplier Technique. Optimal allocation of tolerances and clearances is done in the LOM, FDM and SL processes. Optimization is also done using Genetic Algorithm, GA in short, for FDM and SL. The optimum values of variances of random variables obtained using Lagrange method and GA are compared.

The conclusions of this work are presented in Chapter 7. The scope of further work has also been discussed in this chapter.

ACKNOWLEDGMENTS

I would like to express my deep sense of gratitude to my thesis supervisor Prof Sanjay Govind Dhande for his guidance over the past few years and for his patience during the progress of the work. I would also like to thank him for his interest and invaluable suggestion during the preparation of this document.

I express my sincere gratitude to Prof Kalyanmoy Deb for his suggestions during the synthesis part of the problem and for his encouragement during the progress of the work. His suggestions and explanations in using Lagrange multiplier technique and real coded genetic algorithm were of great help. I gratefully acknowledge him for providing me the code for GA in C language.

I am grateful to Prof A K Mallik, Prof B Sahay, Prof Prashant Kumar, Prof K K Saxena, Prof N N Kishore, Prof Vijay Gupta, Prof Sudipto Mukherjee, Prof S K Choudhry, Prof P S Ghoshdastidar, Prof Gautama Biswas, Dr Amitabha Mukerjee and all the faculty members of the institute for the courses they taught me and for their moral support during this work. I thank Dr K C Goel and Dr C M Singhal for the medical care provided to me.

I express my sincere thanks to Mr A D Bhatt for the support and encouragement during our dissertations. I thank Shiva Prasad who was an instant help during my computation. I thank Saurabh Vishal for the moments shared together during the final phases of our respective theses.

I would be filled with nostalgia when I remember the light moments shared with Atulji, Charu bhabhi and children. Their company and their constant encouragement kept us cheerful. I enjoyed the company of Mahesh Gupta and Kushal Qanungo during sports and leisure time in hall V. I gratefully acknowledge their support during my dissertation.

I wish to thank all CAD lab members KVND Ramesh, Subhash Mishra, PVM Rao, Jakka Venkatesh, Palanisami, Kumaraswami, Rahul, Bansal, M Anil, Manoj, Siddharth, Anil, Puneet, Mukul, Sarvanakumar and M L Jain for their help in various ways during the course of my thesis work. My sincere thanks to the staff of CAD Project Laboratory for their help and cooperation during the thesis work.

I thank my friends in the campus and outside for their moral support. I thank Sudhir, Satya Prakash, Dwarika, Ashutosh Mishra, Jugal, Mini Ghosh, Sanjay Kumar, B N Singh, Jilaniji, Anupam Gupta and Rajiv Awasthi.

I express my deep sense of gratitude to my wife Ranjana for her cooperation and endurance during the thesis work. Her constant support and encouragement while she herself was completing her dissertation will always be cherished.

Finally, I wish to express my heartfelt thanks and gratitude to my parents, brother, sister and all family members for their constant support and encouragement during the work.

28/3/01

(Sanat Agrawal)

Contents

List of Figures

List of Tables

List of Symbols

a_i	influence coefficient $\left(\frac{\partial x}{\partial V_i}\right)_m^2$
b_i	influence coefficient $\left(\frac{\partial y}{\partial V_i}\right)_m^2$
c_i	influence coefficient $\left(\frac{\partial z}{\partial V_i}\right)_m^2$
c_{ij}	radial clearance in the pair ij
C_{jk}	covariance of the dependent variable V_j and V_k
DSUM	sum of the variances of the dependent variable x, y and z
D[V_i]	variance of the random variable V_i
D[x]	variance of the dependent variable x
E[w]	expected value of the dependent variable w
$\mathbf{FN_1}$	unit vector normal to the mirror plane GHIJ in SL
l_i	nominal length of the i^{th} link
$\mathbf{l}$(t)	parametric representation of the line AC in LOM in $X_1Y_1Z_1$ frame
l_{1fixed}	length of the portion of link 1 in FDM where there is no motion
l_{1max}	maximum variation of the length of link 1
l_{3fixed}	length of the portion of link 3 in FDM where there is no motion
l_{3max}	maximum variation of the length of link 3
m[V_i]	mean of the random variable V_i
m[x]	mean of the dependent variable x
M	modified cost function
$\mathbf{p}_1(u, v)$	parametric representation of a cylindrical surface in $X_1Y_1Z_1$ frame
$\mathbf{q}$(u,w)	parametric representation of the bilinear surface ABDC in LOM in XYZ frame

$\mathbf{q}_1(r,s)$	parametric representation of a cylindrical surface in $X_1Y_1Z_1$ frame
$\mathbf{q}_2(r,s)$	parametric representation of a cylindrical surface in $X_2Y_2Z_2$ frame
$\mathbf{Q}(t)$	parametric representation of the ray **EG** in LOM in XYZ frame
$\mathbf{r}(\mathrm{t})$	ray **EF** in the base frame $X_0Y_0Z_0$ in SL
$[r2\_tf]$	position vector $[\mathbf{r}_2(\mathrm{t})]$ at $t = tf$ in SL
R_i	actual length of the i^{th} link
R_{i1}	equivalent length of the i^{th} link
sq	value of the parameter s at the point Q in SL
tf	value of the parameter t at the point F in SL
$[t02\_3]$	third column of $[T_2^0]$ in SL
$[t21\_3]$	third column of $[T_1^2]$ in SL
$[T_j^i]$	homogeneous transformtion matrix of the frame $X_iY_iZ_i$ with respect to the frame $X_jY_jZ_j$
V_i	random Variable
$[w1\_sq]$	postion vector $[w_1]$ at $s = sq$ in SL
$(x'_{ij},\, y'_{ij})$	coordinates of the pin axis in $x'_{ij}y'_{ij}$ frame

Greek Symbols

γ	angle made by a link with a plane perpendicular to its socket
ϵ_i	error on a random variable
θ	azimuth angle of the laser beam
$\lambda_1,\, \lambda_2,\, \lambda_3$	lagrange multipliers
ρ_i	variance of the random variable V_i
σ	standard deviation of error at a point on the work surface
ϕ	zenith angle of the laser beam

Chapter 1

INTRODUCTION

1.1 Introduction to Rapid Prototyping

Rapid prototyping is emerging as a key prototyping technology with its ability to produce even complicated parts within hours. Prototyping is an essential part of the product development cycle required for assessing the form, fit and functionality of a design before a significant investment in tooling is made. Until recently, prototypes were largely hand-made by skilled craftsmen, adding weeks or months to product development time.

Rapid Prototyping (RP, in short) is a term which embraces a range of new technologies for producing accurate parts directly from CAD models, in hours, with little need for human intervention. This means that designers have the choice of making physical models of the conceptual design more frequently, allowing them to check the form and assembly of the design. This also allows them to discuss manufacturing issues with an easy-to-interpret prototype which can be held, viewed, studied, tested and compared. Consequently, a product is improved and product development cycles and costs substantially reduced. It has been claimed that RP can cut new product costs by upto 70% and product development time by upto 90% [95].

RP systems take the solid model of a part as an input and fabricate a physical model or prototype without using tools or fixtures. Unlike CNC machines, which remove material to obtain a desired shape, RP systems are additive in nature. A part is built progressively, layer by layer. This technology has also been referred to as layered manufacturing technology, free-form fabrication, desktop manufacturing, model making, low-volume manufacturing, material incress manufacturing, etc [2].

1.1.1 Process sequence of Rapid Prototyping

The RP process starts with the creation of a solid model and ends with a finished prototype. The process sequence of rapid prototyping consists of the following four tasks:

- Geometric Modeling
- Data conversion and checking
- Part building
- Postprocessing

The process sequence is shown in Fig. 1.1.

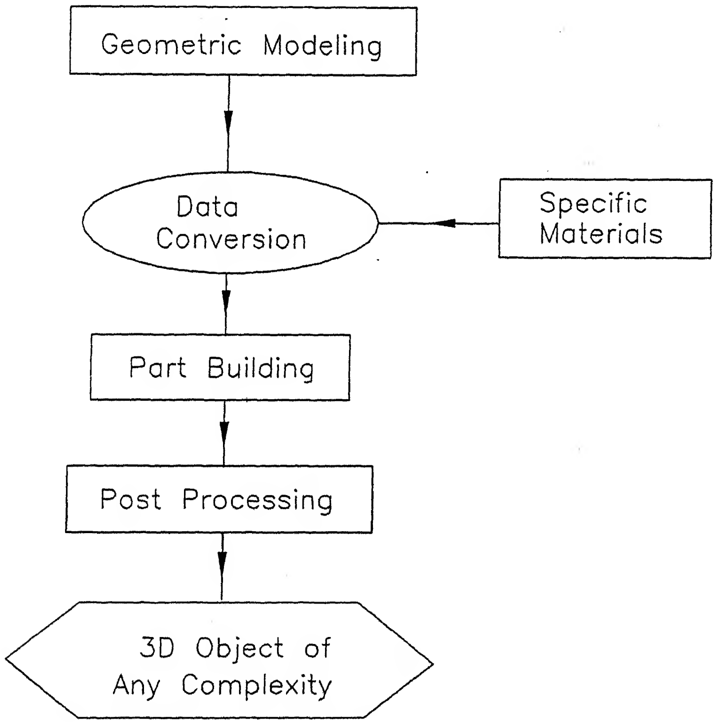

Figure 1.1: Process Sequence of RP Processes

Geometric Modeling

Creating an accurate and complete solid model is a general prerequisite of RP processes. The solid model must be a closed volume. There are several solid modelers available, for e.g., Pro/ENGINEER, I-DEAS, Unigraphics, CADDS 5i and CATIA. Geometric models can also be constructed using data from Computerized Axial Tomography (CAT), Magnetic Resonance Imaging (MRI), reverse engineering, etc., depending upon the need.

Data Conversion and Checking

Geometric data of a model is transferred from a CAD system to an RP system primarily through the STL (STereoLithography) file format. This format has become a *de facto* standard for interfacing with RP systems. The solid model is converted to STL format. The STL is a faceted format and consists of connected three dimensional triangles representing the part shape. The vertices of the triangle are ordered to indicate which side of the triangle contains the part mass [62]. From a mesh generation point of view, triangular meshes are easy to generate than quadrilateral meshes. This is because a triangle is a simplex while a quadrilateral is not [133, pp. 930]. Some RP processes cannot effectively handle sliced models, (or "$2\frac{1}{3}$D" models, as referred to in literature by Dolenc and Mäkelä [32]), and so a faceted model is taken and sliced again. This is because the sliced model cannot be positioned arbitrarily in the workspace of an RP system [32].

The translation from CAD to RP results in some errors. The typical errors are flipped normals, mid-line node, closure errors (holes) and truncation errors [36]. The validity of the STL file is verified using a correction software and the file is repaired.

Part Building

This process starts with placing the STL file for the optimum part orientation, and extracting the slice information from it, checking the slices for any open curves and other defects and repairing them, adding the part-building parameters, if any, and sending the file thus created to the RP machine. The machine then builds the part described by the file, and this process requires no or minimal human intervention. The part is thus built by the machine.

Postprocessing

In the postprocessing stage, some manual operations are done and these operations require expertise of the operator. The manual operations includes removal of supports and excess material, if any, and postcuring, if required.

1.1.2 Overview of RP processes

1.1.2.1 Laminated Object Manufacturing Process

The Laminated Object Manufacturing (LOM) process from Helisys Inc. cuts and binds foils as illustrated in Fig. 1.2. The undersurface of the foil has a thermoplastic binder that, when pressed by a heated roller, causes it to glue to the previous foil. The foil is cut by a CO_2 laser following the contour of the slice. A computer controlled

XY positioning device and a set of mirrors are used to direct the laser beam. To help the removal of excess material once the parts have been built, the exterior of the slice is hatched, as opposed to the stereolithography process where the interior is hatched. This excess material remains in place during the build process to act as support. The thickness of the foil is not constant. Therefore, a sensor measures the current foil thickness, and the foil is sliced accordingly.

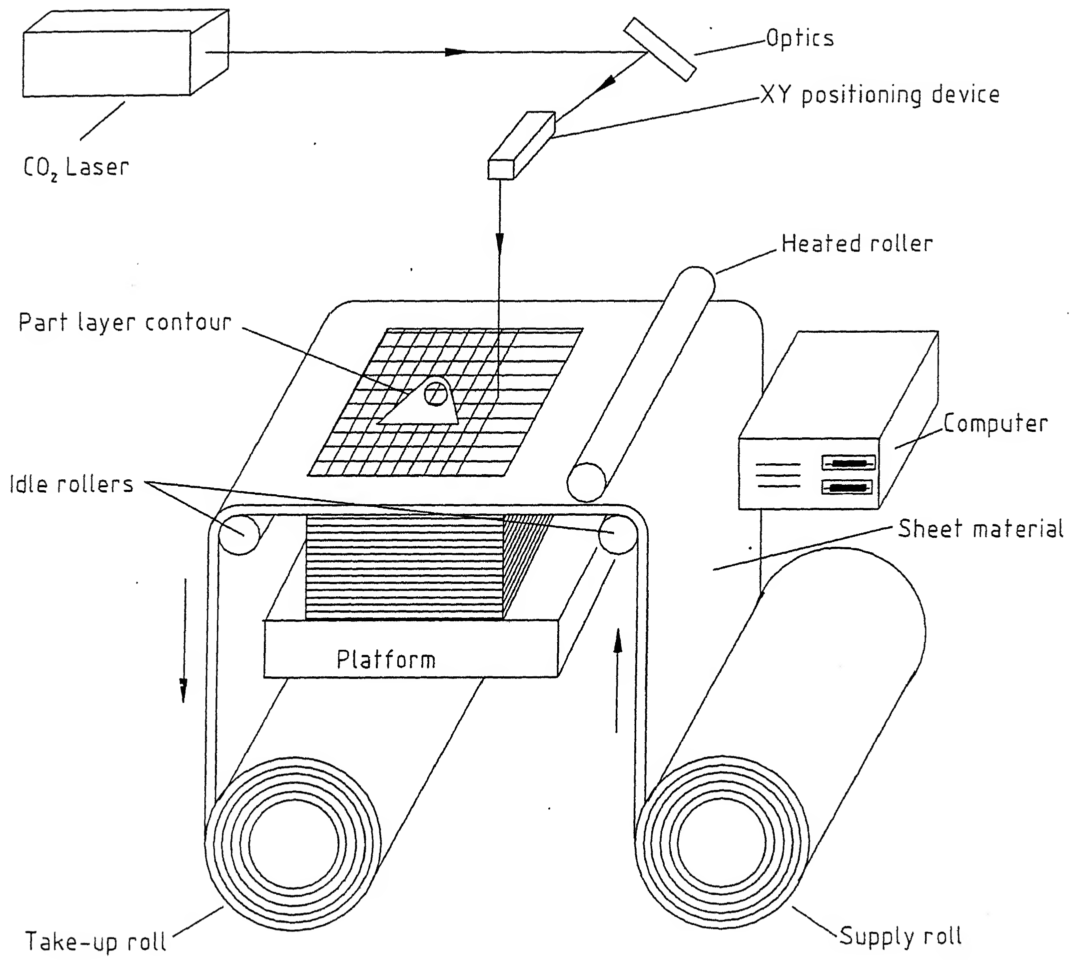

Figure 1.2: A Schematic Diagram of the LOM Process

The Helisys product line consists of LOM-1015Plus and LOM-2030H machines. Material thickness in LOM-1015Plus is from 0.08 to 0.25 mm (0.003 to 0.008 in) and the maximum part envelope size is 381×254×356 mm (15×10×14 in) [55]. Part accuracy is ± 0.125 mm (± 0.005 in) anywhere in the work envelope [2, 95, 31]. The LOM process can produce parts from paper, plastics, metal foil, composites and ceramics in sheet form [112, 63, 2].

Advantages of LOM include a wide variety of organic and inorganic materials which can be used. Speed is another strong point of LOM. As only the outlines of the parts need to be traced by the laser, this method is very fast. This method is

best suited for building large parts. The process produces virtually no internal stress and associated undesirable shrinkage and warping [55, 95]. The procedure is not well suited for manufacturing parts with thin walls in z direction and hollow parts. The parts are strong in x and y directions and have a tendency to delaminate in z direction in intricate parts [62, 112]. Other disadvantages of this technology are that there is a large amount of scrap, the machine must be constantly manned, parts need to be hand-finished and the shear strength of the part is limited by the bonding strength of glued layers [95].

1.1.2.2 Fused Deposition Modeling Process

In the Fused Deposition Modeling (FDM) process from Stratasys Inc., a spool of 1.27 mm (0.05 in) diameter filament feeds into the unit's extruding head. The extruder head moves in the XY-plane (See Fig. 1.3). The filament is melted to liquid inside the extruder head at 82°C (180°F) by a resistance heater. FDM produces parts from solid CAD models. The model is then converted into STL format in the CAD system and sent to the FDM slicing software, called QuickSlice. There the .STL file is sliced into thin cross sections of desired thickness, creating a .SLC file.

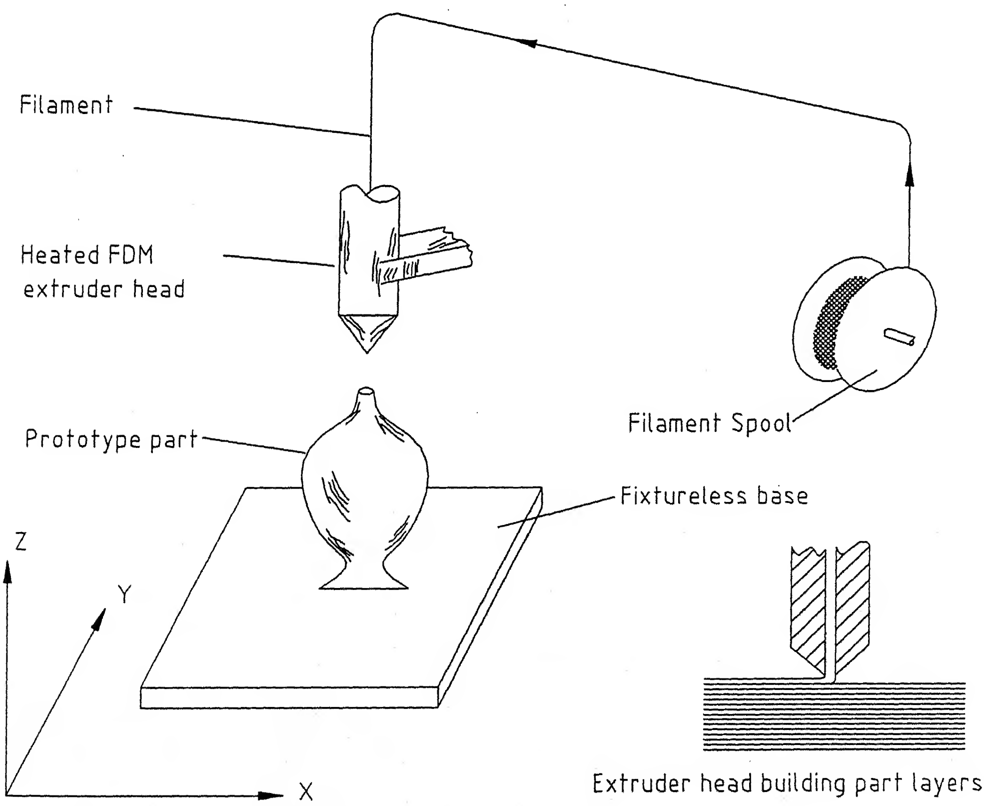

Figure 1.3: A Schematic Diagram of the FDM Process

Supports are created for overhanging parts and sliced as well. The sliced model

and support are converted into a .SML file (Stratasys Machine Language file) that contains actual instructions for the FDM machine. A tool path is generated which is followed by the numerically controlled extruder head. As the head moves in X and Y directions following the tool path, the thermoplastic material is extruded out of a nozzle and then deposited in ultra thin layers, one layer at a time. Since the envelope surrounding the head is maintained at a temperature below the melting point of material, the extruded material quickly solidifies [63, 95]. The extruder head has two nozzles, one for the part material and the other for the support material. The support can be easily removed by breaking away. The part is built on a foam foundation attached on a Z-stage platen. The Z-stage platen moves downwards as the part is built progressively.

The system uses ABS — a tough nylon-like thermoplastic, ABSi — a high impact ABS, machinable wax, investment casting wax, elastomers, etc., as modeling materials.

The specification of FDM2000 are as follows. The work envelope is 254×254×254 mm (10×10×10 in). The operator may select a road width between 0.254 and 2.54 mm (.010 and .100 in) and a layer thickness between .05 and .762 mm (.002 to .030 in). Models can be produced within an accuracy of ± 0.127 mm (± 0.005 in) [114].

The FDM system has two position sensors. Theses sensors are to place the extruder head in the home position before starting the part build. They do not sense the position of the head during part build.

This system may be viewed as a desktop prototyping facility in a design office since the modeling materials are cheap, non-toxic, odorless and environmentally safe. A wide range of material is available in various colors. Parts made by this method have a high stability since they are not hygroscopic. The system doesn't waste material during or after producing the model. No postcuring of model is required [13]. A drawback of the FDM process is that the surface finish of a part is poor relative to other processes.

1.1.2.3 Stereolithography Process

The StereoLithography Apparatus (SLA) system from 3D Systems Inc. is the most representative system running on StereoLithography (SL) process. The SL process starts with a solid CAD model of an object that is downloaded to a slicing algorithm, which cuts the CAD model into many thin layers. The part itself is built in a vat of liquid acrylate or epoxy resin that solidifies when the laser light hits it (See Fig. 1.4). An elevator platform rests below the liquid surface at a distance equal to the thickness of the first bottom-most layer of the part to be built. An ultraviolet laser beam from

the HeCd-laser is deflected by the galvanometer-driven mirrors and scribes the contour of a slice of the part on the resin surface. A second, HeNe-laser is used to ensure that the surface of the liquid is in correct location [60, 31].

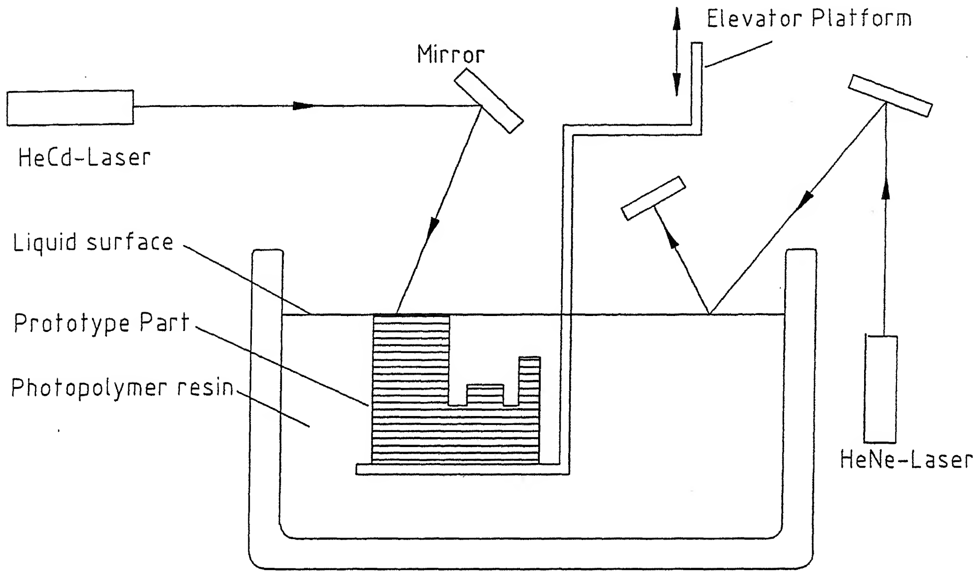

Figure 1.4: The Schematic Diagram of Stereolithography Process

The interior of the contour is then hatched using a hatch pattern. After a layer is built, the elevator platform is lowered a programmed distance so that a new coating of liquid resin covers the solidified layer. A recoater blade then sizes the coating depth. The laser draws a new layer on top of the first layer and the part is built layer by layer from the bottom up. Finally the part is removed from the vat and placed in a curing oven, which floods the object with ultraviolet light to complete the polymer solidification process [2, 95]. For parts with overhanging geometry, support structures are created that attach to the elevator platform to support the part while it is being built [63, 62]. Postprocessing for the SL process include removal of excess resin, postcuring, and surface finishing as required.

The SL product line consists of SLA 190, SLA 250, SLA 500, SLA 3500, SLA 5000 and SLA 7000. The SLA 250/50 specifications are as follows. The layer thickness can be selected between .063 and .76 mm (.0025 and .03 in) [60, 74]. The minimum recommended layer thickness is .1 mm (.004 in) [1]. The laser beam spot size is .20 – .28 mm (.008 – .011 in). The build envelope size is 250×250×250 mm (10×10×10 in). The vertical resolution of the above platform is .0025 mm (.0001 in). Platform repeatability is .013 mm (.0005 in). Scan resolution and scan repeatability are .008 mm (.0003 in) and .130 mm (.005 in) respectively. Part accuracies are ± .127 mm (± 0.005 in) [2, 95].

The SL process produces a surface finish that is comparable to that of NC milling.

The process is reasonably fast and accurate [95]. A part with intricate features can be made with virtually no limitations. The area of application of the process is restricted due to expensive, smelly and toxic material.

1.1.3 Performance Parameters of RP Processes

The layer by layer manufacturing technologies poses a unique set of issues, irrespective of the techniques involved in the fabrication of layers. Some of these issues are technical and may be as a result of software and hardware limitations, while others may be due to the finishing operations. There are limitations in CAD to RP translations which generally take place in the CAD system itself. The best output that can be obtained from a machine driven by the CAD software cannot be better than the accuracy used in the CAD system. Several process parameters of RP which affect the accuracy of RP processes are as follows:

(i) Accuracy Issues in CAD to RP Translations

(a) Tolerance for Tessellation

As discussed earlier, the tessellation process is the translation of the surfaces of CAD model into triangular facets. In order to generate the faceted format the CAD system asks the user the acceptable tolerances. These tolerances can be the largest distance from the true surface to the triangle, or the largest distance from the true surface to a side of the triangle. The latter is termed as chordal tolerance (See Fig. 1.5). The smaller the tolerance, and more irregular the surface is, the larger the number of triangles required to represent the surface. The RP technologies has spot sizes between .127 – 2.5 mm (.005 – .100 in) [36]. Therefore, very small tolerances become meaningless. Large number of facets increase the .STL and slice file size and the user has to strike a balance between accuracy and file size.

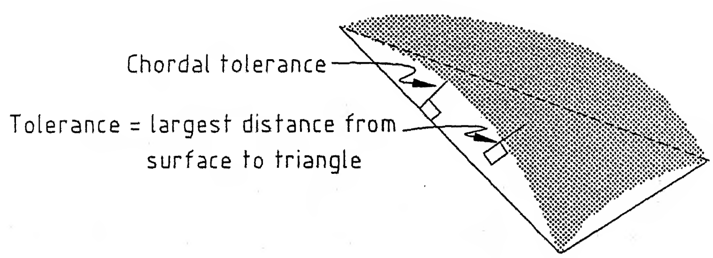

Figure 1.5: Tolerances in Faceted Formatting

(b) Convex Boundary Error

The tessellation results in a smaller object where the object is convex, whereas it results in added material where the object is concave (See Fig. 1.6). Since most RP systems are typically sanded to obtain good surface finish, the locations short on material will be even more distant from the original desired surface, whereas the locations with added material can be sanded to accurate dimensions.

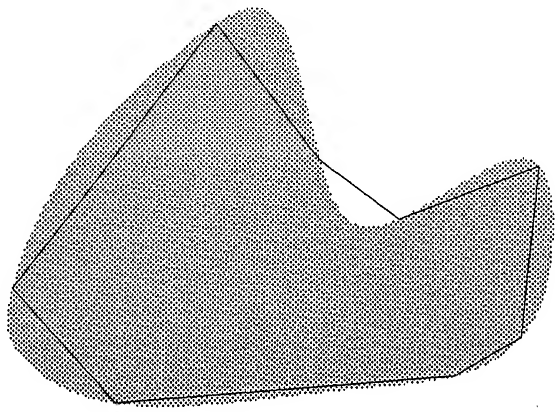

Figure 1.6: Convex Boundary Error Issue

(c) Flipped Normals

Occasionally, the computed normal of a triangle obtained from translation is in the opposite direction, or is just plain wrong, and must be corrected. They are corrected by using some heuristic rules on adjoining triangles, or simply based on a new cross product [36].

(d) Mid-Line Node

The basic rule to check the .STL file is that each edge of a triangle is shared by two triangles. Figure 1.7a illustrates an erroneous triangularization and Fig. 1.7b, a correct one. The case in Fig. 1.7a results in an incorrect model of the object and in a failure of the slicing algorithm.

(e) Closure Errors

Round-off errors during tessellation cause one point to be at multiple locations at the same time. Thus triangles are formed, and a thin hole is present in the finished model (See Fig. 1.8). In order to correct such an error, points that are within an infinitesimal distance, say delta, are considered, and the triangles they individually form are checked to see whether they share a common edge. It is to be noted that for a very small chordal tolerance, two legitimate points are very close to each other and it becomes difficult to differentiate between legitimate

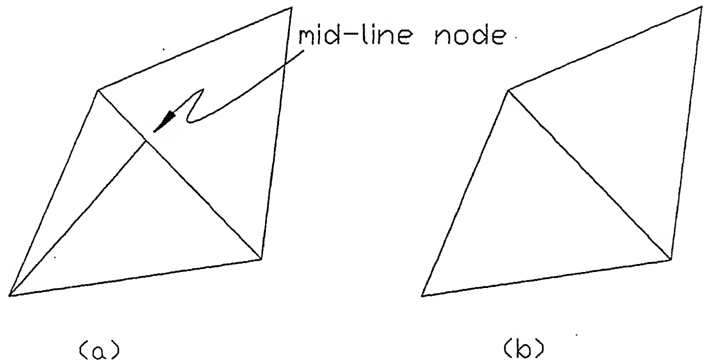

Figure 1.7: Mid-Line Node

points and round-off error. Round-off errors also result in overlapping facets, and non-manifold edges, points and faces [63].

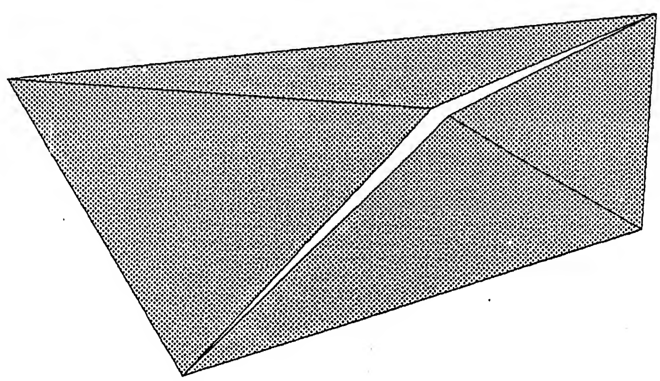

Figure 1.8: Closure Error Causing Hole in Model

(ii) Laser Beam or Nozzle Diameter

The dimensions of the delivery systems of RP determine the minimum feature size that can be built in an RP system. For laser based systems, the minimum wall thickness in a part would be the width of a single cured line. This is related to laser beam diameter and cure depth. The laser beam diameter used in SL is typically .254 mm (.01 in). For a photomask system such as Solid Ground Curing by Cubital Inc., the minimum feature size would be related to the resolution of the mask. A resolution of 200 dot per inch would result in a minimum feature size of .127 mm (.005 in). The minimum road width in FDM1650 for T12 tip is .305 mm (.012 in).

The laser beam in SL systems is typically at some height above the part, and the part can be located at any point in the vat. In SLA 250, the laser is directed at the resin from a point 500 mm (20 in) above the surface of the vat and draws on an area of 254×254 mm (10×10 in). This causes the deviation of the beam by around 15° at the edges of the part. This leads to a part that is shingled and the surface finish

quality suffers significantly. For a typical layer thickness of .254 mm (.01 in) and an overcure of .1524 mm (.006 in), the variation in dimension of a part at the extreme corner of platform is .127 mm (.005 in) [36].

(iii) Staircase Effect and Adaptive Slicing

Parts usually exhibit a visible staircase effect on slanted and curved surfaces because of layering process. It causes the surface finish quality to suffer significantly. Adaptive slicing remedies this error by allowing the part to be build at variable layer sizes. Orientation of the part can also be occasionally used to mitigate this error. Note that uniform slicing may lead to omission of flat areas (areas parallel to slicing direction) and peaks from the part. Dolenc and Mäkelä [32] have presented an adaptive method handling flat areas and restricting the staircase effect to a user-specified tolerance. Kulkarni and Dutta [73] have given a procedure for adaptive slicing to redress the staircase effect and containment problem. Jamieson et al [61] have presented a methodology to develop direct and adaptive slicing of CAD models for RP processes. Sabourin et al [105] have performed adaptive slicing using stepwise uniform refinement. This method is well suited for execution in parallel computer. Tata et al [118] have presented an adaptive slicing algorithm that can vary the layer thickness considering the geometry of the part. Tyberg and Bøhn [122] present a new approach to adaptive slicing that significantly reduces fabrication time.

Hope et al [57, 58] have presented an adaptive slicing method for improving the surface finish and decreasing build time. They used sloping boundary surfaces rather than stepped edges.

(iv) Supports

A majority of the RP processes require the part geometries to be supported as the part is being built. In contrast to conventional machining methods, RP processes do not require part specific fixtures and tooling, and the process is fully automated.

In the SL process, base supports are built on the elevator platform and the part building starts on them. It ensures that the recoater blade does not strike the platform upon which the part is being built. Additionally, it allows for the safe removal of the part from its platform and thus preserves its surface finish.

Areas that overhang the prior layer must be supported to prevent their deformation, known as curl. An overhang that extends beyond 1.27 mm (.05 in) will exhibit curl when unsupported [60]. In SL, arches or convex surfaces support themselves as long as the overhang between successive layers is small. "Islands" are layers of the part geometry that would otherwise be unconnected to any other section of the part. Islands must be anchored to the platform or to the part itself.

(v) Part Orientation

Several factors contribute to the determination of the orientation of a build. Some of these factors are: surface finish, build time, shrinkage, curling, distortion, support structures, roundness/flatness, resin flow, material cost and trapped volume [93]. The surface finish is usually the most important issue. Higher resolution of curved surfaces are obtained by orienting them in such a way that their normals lie in the horizontal plane. The build time, which depends upon the number of layers involved, can be minimized by careful selection of the part orientation.

Cheng et al [18] determine the optimal part orientation for multi-objectives such as part accuracy and build time. Xu et al [129] have obtained optimal the orientation with adaptive slicing in SL process taking into consideration build time, accuracy and stability of the part. Xu et al [130] have given an algorithm to determine the optimal part orientation for different RP processes considering accuracy, surface finish, build time and cost.

There are several works on other accuracy issues, for e.g., part distortion, benchmark component, part accuracy, etc. Weidermann et al [125] investigate the influence of material and process parameters on part distortion to facilitate the selection of resins in the SL process. Lee et al [82] consider the accuracy in vertical direction in powder-based RP processes. Here the unsintered powder in layers, which act as support, undergo downward displacement due to their weight.

Ippolito et al [59] deal with the development, manufacture and testing of a benchmark component to investigate the dimensional accuracy and surface finish. Childs and Juster [19] have designed a benchmark component to assess not only linear accuracies but geometric tolerances, repeatability and resolution limits of several RP processes. Lynn-Charney and Rosen [84] have presented an empirical model for the accuracy of a part in the SL process as specified by a set of tolerances on the part. They have used a process planning method based on response surfaces that capture the relationship among part surfaces, tolerances, and process variables.

(vi) Machine Accuracy

The accuracy of a fabricator is its ability to faithfully generate a particular geometrical shape and size. Let us use the term "tool" for a curing or sintering laser beam, material-stream from extrusion or particle-jet nozzle in an RP system. Machine accuracy relates to how close to a predetermined position the RP machine can place its tool [14]. Accuracy is partially a statistical phenomena. A set of measurements, no matter how closely done, always involve some variation. This occurs because the factors that affect accuracy and measurement include random effects that cannot be eliminated and cannot be controlled.

Machine accuracy is different from part and process accuracy. Machine accuracy of an RP process involves the following matters:

- Repeatability of the laser beam / build head position
- Functioning of machine calibration algorithm
- Functioning of machine levelling system
- Functioning of the scanning system
- Correctness of machine instructions issued by the software
- Repeatability of the elevator platform / Z-stage platen

There are mechanisms in RP systems to move optics / build head and elevator platform / Z-stage platen. Tolerances on the link lengths and clearances in the joints of the mechanisms cause mechanical error in their desired position. Mechanical error affect the accuracy and repeatability of the laser beam / build head position and elevator platform / Z-stage platen position. The objective of the present work is to find the mechanical error in RP processes. Three RP processes, LOM, FDM and SL are considered. Mechanical error in mechanisms has been dealt with considerably in the past literature [43, 28, 117, 30, 86, 102, 80]. A search of the literature has yet to disclose any work on analysis and synthesis of mechanical error in RP processes.

1.2 Analysis of Mechanical Error in Mechanisms: A Brief Review

Clearances in the joints and tolerances on the link lengths of linkages may cause mechanical error of appreciable magnitude. While designing a mechanism either for function generation or for path generation or for rigid-body guidance, it is necessary to take into account not only the structural error but also the mechanical error. By assigning stringent values of tolerances and clearances, one may get actual tolerances quite close to the desired one. However, the cost of manufacturing and assembling such a mechanism may be prohibitive. On the other hand, indiscriminate allocation of tolerances and clearances may lead to unacceptable deviation of the output. A designer would, therefore, like to assign tolerances and clearances such that the mechanical error is within the specified limits and the levels of tolerances and clearances are as high as possible.

Several attempts have been made to analyze path and function generating mechanisms. There are two distinct approaches — deterministic and stochastic. The

deterministic approaches are based upon worst-case analysis of individual tolerances [121, 53, 68, 75, 34, 5, 98, 107, 16, 39, 37, 83, 22, 120]. Deterministic approaches give highly conservative estimates and do not reflect the overall behaviour of the mechanisms. Besides in most of these studies, either tolerances [53, 75, 65, 16, 39, 37, 22] or clearances [121, 68, 120] are considered. In contrast stochastic approaches have been found to be more suitable for both analysis and synthesis of mechanical error [43, 28, 117, 30, 86, 102, 80, 87]. There are several other statistical approaches by [43, 21, 10, 6].

The effects of both tolerances and clearances have been considered in [28, 86, 87, 80, 83]. Rao [98] considered elastic deformation along with tolerances and clearances, whereas Choubey and Rao [21] and Sutherland and Roth [117] considered structural error along with tolerances only.

The error analysis by Tuttle [121] is perhaps the earliest treatment of the subject. He gave a treatment for the estimation of average error due to clearance effects alone, but geometry of linkages did not enter into the analysis. Knappe [65] has given an approach which permits calculation of the maximum output tolerance as well as the relative effect of each individual tolerance on the output. Hartenberg and Denavit [53] estimated the mechanical error on function-generating four-bar linkage on the basis of maximum allowable tolerance on each link separately; and the maximum error was shown to be the sum of errors due to individual links. Garrett and Hall [43] have applied a statistical method for mechanical error analysis of function-generating mechanisms. The effects of manufacturing tolerances and clearances are presented in the form of mobility bands for the linkages. The effects of clearances on mechanical error was taken into account by Kolhatkar and Yajnik [68]. They treated joint clearances as "equivalent clearance links" and determined the maximum output error in four and six bar function-generating mechanisms. They drew a number of simple conclusions for four-bar linkage. Lakshminarayana and Narayanamurthi [75] have shown that for complex mechanisms it is convenient to base the analysis on individual loop closure equations rather than on complex input-output relationship for the complete linkage. The total output deviation is obtained by adding the absolute values of the deviations due to individual link lengths.

Dhande and Chakraborty [28, 15] used a stochastic model for mechanical error analysis of function-generators. Dubowsky et al [34] utilizes optimization technique to identify the dimension which contributes to the mechanical error. The probabilistic analysis by Baumgarten and van der Werff [10] utilizes a finite-element description of the kinematic chain. A band of error which would contain 99% of the coupler path of a population of randomly assembled mechanisms is plotted. Chatterjee and Mallik [16] derived the equations for the position error of a coupler curve as functions of crank

angle, the link lengths and the error in link lengths. Mallik and Dhande [86] used a stochastic approach for mechanical error analysis of path-generating mechanisms. Fenton et al [39, 22] have presented a method for error analysis of multi-loop planar mechanisms. Lin and Chen [83] presented a generalized error analysis methodology. They presented an error matrix to account for the effects of error motions due to joint clearances. Ting and Zhu [120] presented a kinematic model and applied N-bar rotatability laws to identify the worst position and orientation errors due to the joint clearances of linkages and manipulators.

Several authors have considered sensitivity of mechanisms to the tolerances and clearances. Coit and Riley [23] have analyzed the sensitivity of the output of an inverted slider-crank straight line generator to the link length tolerances. A link length ratio at which tolerances have the most desirable effects on the linkage can be selected. Faik and Erdman [37] have proposed a method to synthesize a four-bar linkage with a prescribed sensitivity value using synthesis solution space. They compute the maximum allowable tolerances on link lengths to achieve the desired accuracy on link angles. Lee and Gilmore [80] presented the " effective link length" model which considered tolerances on link length, radial clearance and pin center location as random variables. They presented a method to determine the sensitivities of the output variables with respect to the random variables.

There are several other approaches to consider the effect of tolerances and clearances on mechanical error in mechanisms. Sukhija and Rao [115] have applied information theory for optimum synthesis of path-generating mechanisms. The theory utilizes the concept of entropy, a measure of uncertainty. Optimum allocation of tolerances on link length is also carried out. Ting and Long [119] used Taguchi's concept to determine the performance quality and tolerance sensitivity of mechanism in the early stages of design synthesis. They introduced a Jacobian matrix to relate the performance variation and dimensional tolerances. Rao and Hati [99] have considered the design of a spherical four-revolute function-generating mechanism, with the objective of minimizing structural error and manufacturing cost using game theory. Lee, Gilmore and Ogot [81] have considered dynamically driven planar kinematic chains, either open-loop or closed-loop, with uncertainties in tolerances and clearances. They presented probabilistic models and method to allocate tolerances on link lengths and radial clearances. Shi [108] has used the reliability concept for synthesis of mechanical error in spatial linkages.

There are several works on the error analysis of cam, journal bearings, spatial mechanisms and other mechanisms [27, 29, 124, 116, 49, 51, 30, 106, 4]. Weiliang and Qixian [126] have established the stochastic models of spatial joints by introducing the concept of "clearance characteristic element" and "clearance space". Probability

distribution and stochastic characteristic of accumulated kinematic error are analyzed using Monte Carlo simulation. Yufeng and Jiangqin [132] used matrices to obtain tolerances on structural and kinematic parameters of robot manipulators. Zhu and Ting [134] presents probabilistic analysis to examine the performance uncertainty due to joint clearances in robots. Hati and Rao [54] and Wu and Dalal [128] have given their approach to find optimum machining conditions.

Many researchers have considered optimal tolerance allocation in assembly [111, 94, 88, 89, 7, 78, 79, 47]. Balling et al [6] have done worst-case analysis of tolerances in design optimization. Graves [46] has reviewed four basic tolerancing formulae that have appeared in the literature and shown that each solves a slightly different problem. He has focused on the more general problem of determining the assembly tolerance and component tolerance simultaneously to minimize the total cost of assembly and use of a product.

Several attempts have been made for optimum design of mechanisms [20, 42, 91, 92, 41, 50, 96, 17, 9, 70, 76, 77]. Root and Ragsdell [104] have given a survey of optimization techniques applied to the design of mechanisms. Barker and Baumann [8] developed the concept of four-bar solution space. Optimization methods for engineering design is discussed in [12, 35].

1.3 Synthesis of Mechanical Error in Mechanisms: A Brief Review

A significant development in the treatment of tolerances and clearances is their optimal allocation so as to restrict the mechanical error within specified limits. Dhande and Chakraborty [28, 15] used a stochastic model and an equivalent linkage model to allocate tolerances and clearances in four-bar function-generators. Sutherland [117] has given a method for synthesis of mechanism taking into account structural and mechanical error due to tolerances. The dimensions and tolerances of a mechanism can be obtained for a given maximum allowable function generating error while minimizing the manufacturing cost. Bakthavachalam and Kimbrell [5] have considered synthesis of four-bar path-generating mechanisms as an optimization problem under inequality constraints. Equality constraints are modified by introducing tolerances and clearances and thereby, the difficulty in satisfying the equality constraints exactly are eliminated. By this modification, the objective function is also changed. The penalty function approach is used.

Rao [98] has suggested an iterative method for the synthesis of mechanism taking into account the effect of link deformations, tolerances and joint clearances. However,

tolerances and joint clearances were specified prior to the synthesis of mechanism. Choubey and Rao [21] have suggested a method for minimizing the structural error together with the mechanical error due to manufacturing tolerances on the link dimensions. Nominal link length are obtained prior to tolerance allocation. The mechanical error is treated as a deviation of structural error. Tolerances are then allocated with reference to the position of maximum error to limit the mechanical error below a specified value. Sharfi and Smith [107] proposed a method for tolerance and clearance allocation in multi-loop planar mechanisms based on the output sensitivity with respect to the link lengths. Tolerances and clearances are allocated as a result of the synthesis of mechanical error.

Mallik and Dhande [86] developed a stochastic model for the synthesis of mechanical error in four-bar path-generating linkages. They analyzed the mechanical error in the path of a coupler point for the three-sigma band of confidence level. A synthesis procedure to allocate tolerances and clearances so as to restrict the output error in the path of coupler point within specified limits is developed. They found that the mechanical error of the coupler-point path is dependent on whether one considers the original mechanism or its cognate [52, 109] mechanisms. Rhyu and Kwak [102] have presented a procedure for optimal stochastic design of mechanisms considering tolerances and clearances. A weighted sum of the mechanical error and the manufacturing cost is minimized for the optimal allocation of tolerances and clearances. Fenton et al [39, 22] have presented a method for error analysis and tolerance synthesis of multi-loop planar mechanisms.

1.4 Objective and Scope of the Present Work

In the present work mechanical error in RP processes is studied using the stochastic approach. The coordinates of a point on the work surface traced by the laser beam or the tip of the extruder head is expressed as a function of random variables involved in the process. If there are n random variables $V_1, V_2, \ldots, V_n$ involved in the process then the coordinates of the point are given by $x(V_1, V_2, \ldots, V_n)$, $y(V_1, V_2, \ldots, V_n)$ and $z(V_1, V_2, \ldots, V_n)$. The methodology to associate any given range of a dependent variable x, y or z with its corresponding probability is given. For a given probability, the range of a dependent variable is evaluated from the variance of the dependent variable. The variances of the dependent variables x, y and z are expressed in terms of the influence coefficients $\left(\frac{\partial x}{\partial V_i}\right)^2$, $\left(\frac{\partial y}{\partial V_i}\right)^2$ and $\left(\frac{\partial z}{\partial V_i}\right)^2$.

Chapter 1 of the thesis gives an overview of RP processes. It describes three RP processes LOM, FDM and SL in brief. The accuracy issues in RP processes are discussed. A review of the literature pertaining to analysis and synthesis of mechanical

error in mechanisms is presented.

Chapter 2 of the thesis presents a unified approach for studying the effects of manufacturing errors in RP processes. It gives random errors associated with the link lengths, joints in linkages, coordinates of a point and orientation of a link. Stochastic model of an RP process is discussed.

Chapter 3 performs analysis of mechanical error in LOM. The geometric model for description of the LOM process is presented. This gives expression of a point on the contour of a slice on the LOM sheet. The work surface and the laser beam is expressed parametrically and the intersection of the laser beam and the work surface is found. Newton-Raphson method is used to solve the transcendental equations. Expressions for the influence coefficients and the partial derivatives needed for them are derived. A numerical example is given for a set of input values. The variances D[x], D[y] and D[z], and their sum are listed for a grid of points on the work surface. The three-sigma bands of error in tracing several lines on the work surface is plotted. This is the band with the probability 0.9973.

Chapter 4 performs analysis of mechanical error in FDM. It begins with the geometric modeling for description of the FDM process. The expression for a point on the contour of a slice traced by the nozzle tip is found. The influence coefficients and the partial derivatives needed for them are derived. A numerical example is presented for given tolerances and clearances, and other input values. The variances and their sum are listed for a grid of a points traced by the nozzle tip. The three-sigma bands of error in tracing few example curves is plotted.

Analysis of mechanical error in SL is presented in Chapter 5. Parametric representation of the incident ray is found. For a desired reflection from the galvanometer-driven mirror, the orientation of the mirror and the intersection of the incident ray and the mirror is found. Expression for a point on the contour of a slice drawn by the laser on the resin surface is derived. A numerical example for a set of input values gives the list of variances. The three-sigma bands of error for few example curves are also plotted.

Chapters 2, 3, 4 and 5 deal with the analysis of mechanical error in RP processes. The synthesis part is the inverse of the above problem. In synthesis, the designer has to decide the levels of tolerances on the random variables V_i for certain allowable tolerance limits on the dependents variables x, y and z. Chapter 6 deals with the optimal allocation of tolerances and clearances in RP processes. Since the constraints are linear functions of design variables, therefore, the optimization is done using Lagrange multiplier technique. Optimal allocation of tolerances and clearances is done in the LOM, FDM and SL processes. Optimization is also done using Genetic Algorithm, GA in short, for FDM and SL. The optimum values of variances of random

variables obtained using Lagrange method and GA are compared.

The conclusions of this work are presented in Chapter 7. The scope of further work has also been discussed in this chapter.

Chapter 2

STOCHASTIC MODELING OF MECHANICAL ERROR

In any electro-mechanical system the issue of accuracy is important from the point of view of successful operation of the system. If the electro-mechanical system involves mechanical elements such as cams, linkages, gears, screw and nut assemblies, sliding elements, ball bearings, etc., the final performance gets affected due to the manufacturing errors in terms of tolerances and clearances of these machine elements. In order to evaluate the performance of an electro-mechanical system, it is necessary to study the effect of such manufacturing errors on the final performance of the system. The parameters like tolerances and clearances are stochastic in nature. The modeling of the process using a set of variables which are stochastic in nature is now a well established aspect of design methodology in general and for the design of electro-mechanical systems in particular. In the present chapter, a unified approach for studying the effects of manufacturing errors in RP processes has been presented. Using that unified approach, specific studies have been carried out for three major RP processes, namely, Laminated Object Manufacturing (LOM, in short), Fused Deposition Modeling (FDM, in short), and Stererolithography (SL, in short) process. The details of these studies are given in Chapters 3, 4 and 5.

2.1 Introduction

In the LOM process, the sheet material is supplied from a continuous roll on one side of the machine and is taken up on the opposite side (Fig. 1.2). The sheet material moves between two idle rollers. An XY positioning device contains the optical attachment. The laser beam emanates from the optical attachment. The laser beam follows the

contour of a slice and cuts the sheet. In the FDM process, the extruder head is controlled in the XY-plane (Fig. 1.3). In the SL process, the galvanometer-driven mirrors deflect a laser beam emanating from a laser source (Fig. 1.4). The laser beam moves across the surface of a photocurable liquid acrylate resin in a vat and traces the contour of a slice.

Geometric model of an RP process consists of several elements involved in the process. Geometric model of the LOM process consists of rollers, work surface, location of the laser source, etc. Model of the FDM process consists of links, hinge joints, location and orientation of Z-stage platen, etc. Model of the SL process consists of location of the laser source, orientation of mirrors, location and orientation of the elevator platform, etc.

Tolerances and clearances in these elements are random in nature. These random errors are discussed in Section 2.2.

2.2 Random Errors in the Elements of the Geometric Model of an RP Process

The tool of an RP system traces the contour of the slice of a part on a platform. There are several mechanisms, comprising of links and hinges, responsible for the motion of tool and platform. A schematic diagram is shown in Fig. 2.1. The error at a point on the contour depends upon the error in the elements of these mechanisms. The random errors associated with the link lengths, joints in linkages, coordinates of a point and orientation of a link are as follows.

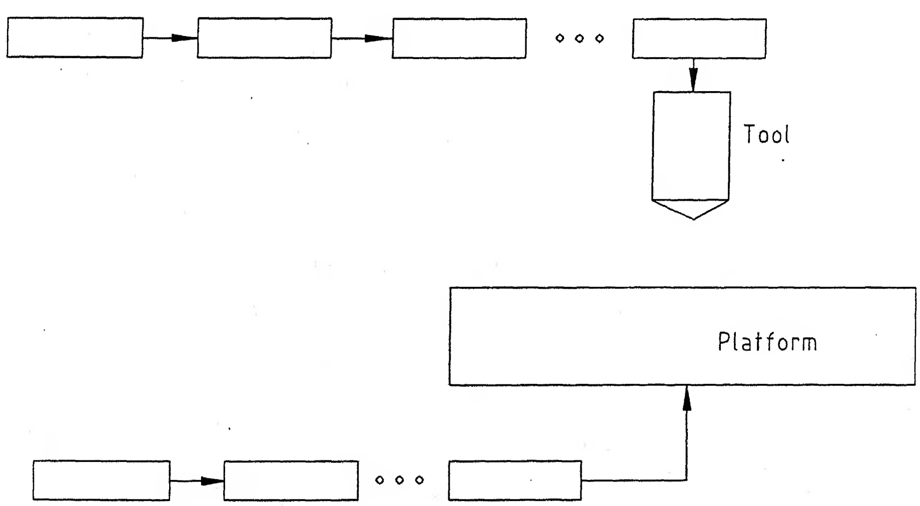

Figure 2.1: An RP Process

2.2.1 Random Error in a Revolute Joint and a Revolute Dyad

Figure 2.2 shows a revolute dyad having links of nominal lengths l_1 and l_2 and pin joints 12, 23 and k1. Let ϵ_i be the tolerance coefficients defined as the tolerance per unit nominal length of the i^{th} link. The actual lengths R_i are given by

$$R_i = l_i + \epsilon_i l_i \qquad\qquad i = 1,2 \tag{2.1}$$

where R_i are now random variables.

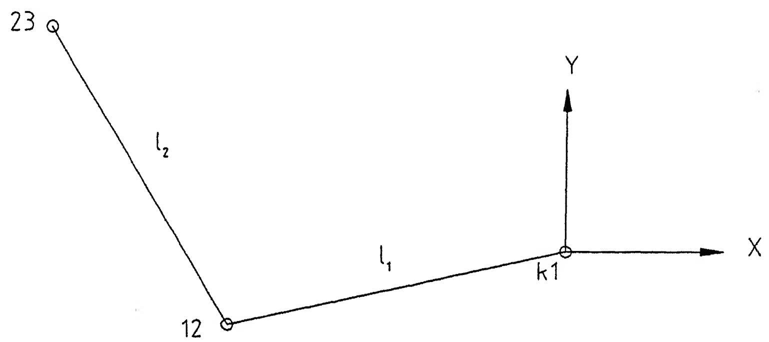

Figure 2.2: A Revolute Dyad

There is some clearance always present between the pin of a link i and the race of its adjacent link j as shown in Fig. 2.3. Let us choose a two dimensional, Cartesian, local coordinate system $x'_{ij}y'_{ij}$ so that the x'_{ij}-axis is coincident with the center line of the link ending in the race and the origin is at the center of the race. The axis of the pin always lies within a circle of radius r_{ij} and center at the origin of the coordinate system $x'_{ij}y'_{ij}$ where r_{ij} is the radial clearance of the hinge between i^{th} and j^{th} links. When the mechanism is in motion the pin axis does not touch the circumference of the circle due to hydrodynamic lubrication. Further, if certain foreign particles are present in the race or if the whole mechanism vibrates, the pin axis may randomly lie anywhere inside the circle. Due to these operating conditions it may be safely assumed that the probability that the pin axis lies at a point inside the circle is the same for all points [28]. If $(x'_{ij},\ y'_{ij})$ are the coordinates of the pin axis then the probability density function is given by

$$f(x'_{ij}, y'_{ij}) = \begin{cases} \dfrac{1}{\pi r_{ij}^2} & \text{if} \quad {x'_{ij}}^2 + {y'_{ij}}^2 \le r_{ij}^2 \\ 0 & \text{if} \quad {x'_{ij}}^2 + {y'_{ij}}^2 > r_{ij}^2 \end{cases} \tag{2.2}$$

The effects of tolerances on the link lengths and clearances in the hinges of a revolute dyad are shown in Fig. 2.4. The equivalent dyad which takes into account

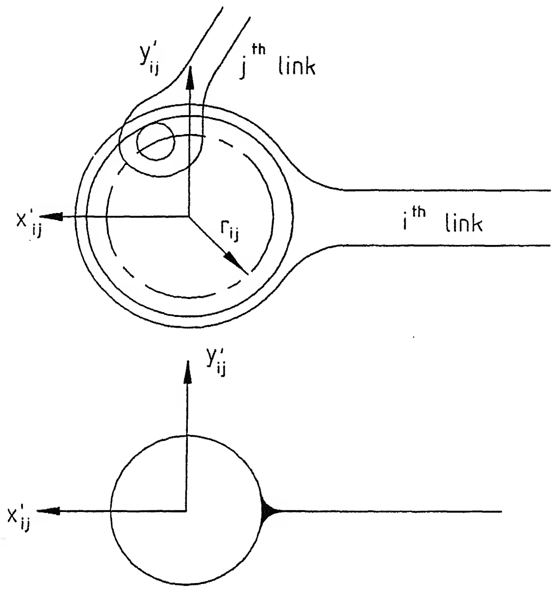

Figure 2.3: Stochastic Model of a Revolute Joint

the stochastic effect is shown by the dashed lines. The link lengths of the equivalent dyad are given by

$$R_{i1}^2 = (R_i + x'_{ij})^2 + {y'_{ij}}^2$$

Or,

$$R_{i1} = R_i + x'_{ij} \qquad \text{i} = 1,2 \qquad (2.3)$$
$$\text{j} = 1,2$$

So there are five random variables involved in the model of a revolute dyad. If these are denoted by V_1, V_2, ..., V_5 then

$$\begin{aligned} V_i &= R_i \qquad \text{i} = 1,2 \\ V_3 &= x'_{12} \\ V_4 &= x'_{23} \\ V_5 &= x'_{k1} \end{aligned} \qquad (2.4)$$

As has been observed in practice the link lengths are assumed to be normally distributed. Therefore the mean values m[V_i] and the variances D[V_i] of the random

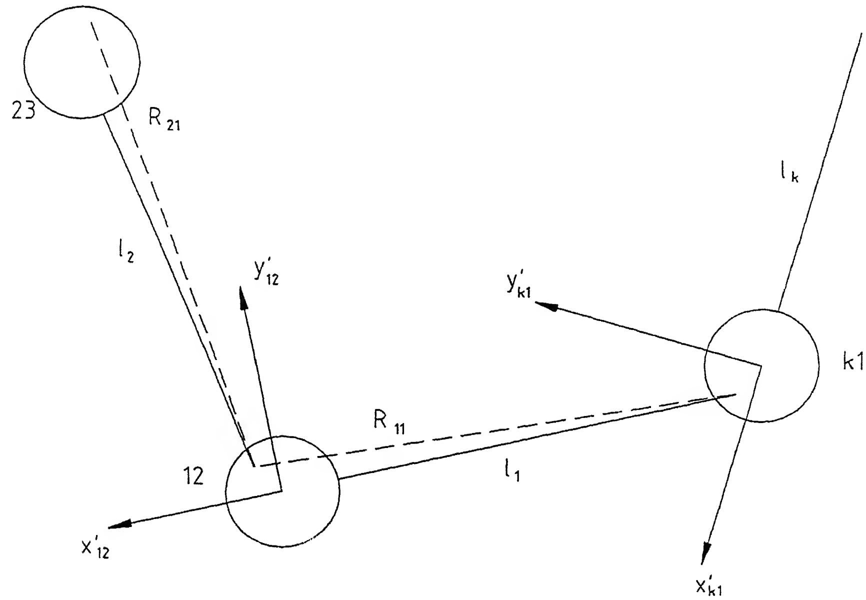

Figure 2.4: Stochastic Model of a Revolute Dyad

variables are given as follows [28]:

$$\begin{aligned}
m[V_i] &= l_i \qquad \text{i} = 1,2 \\
D[V_i] &= \left(\frac{\epsilon_i l_i}{3}\right)^2 \qquad \text{i} = 1,2 \\
m[V_3] &= m[V_4] = m[V_5] = 0 \\
D[V_3] &= \frac{r_{12}^2}{4} \\
D[V_4] &= \frac{r_{23}^2}{4} \\
D[V_5] &= \frac{r_{k1}^2}{4}
\end{aligned} \tag{2.5}$$

2.2.2 Random Error in a Spatial Revolute Joint

Figure 2.5a shows a revolute joint in a spatial mechanism. It is assumed that there is no wobbling of the pin in the socket. The socket and the pin are connected to links 1 and 2 respectively. O_c is the point of intersection of the axis of link 1 and that of the socket. Consider now a plane τ perpendicular to the socket and passing through O_c. This plane intersects the pin axis at O_p. The distance O_cO_p is the clearance error in the revolute joint. γ denotes the angle made by link 1 with the plane τ.

A coordinate system $S(\hat{\mathbf{i}}, \hat{\mathbf{j}}, \hat{\mathbf{k}})$ is set up with its origin at O_c (Fig. 2.5b). The unit vector $\hat{\mathbf{k}}$ is directed along the axis of the socket. The vector $\mathbf{O_cO_p}$ is uniquely determined by two parameters r and α. These parameters are random in nature. Their ranges are given by $0 \leq r \leq c$ and $0 \leq \alpha \leq 2\pi$; where c is the radial clearance. The limiting area for the random vector $\mathbf{O_cO_p}$ is a circle with its center at O_c and

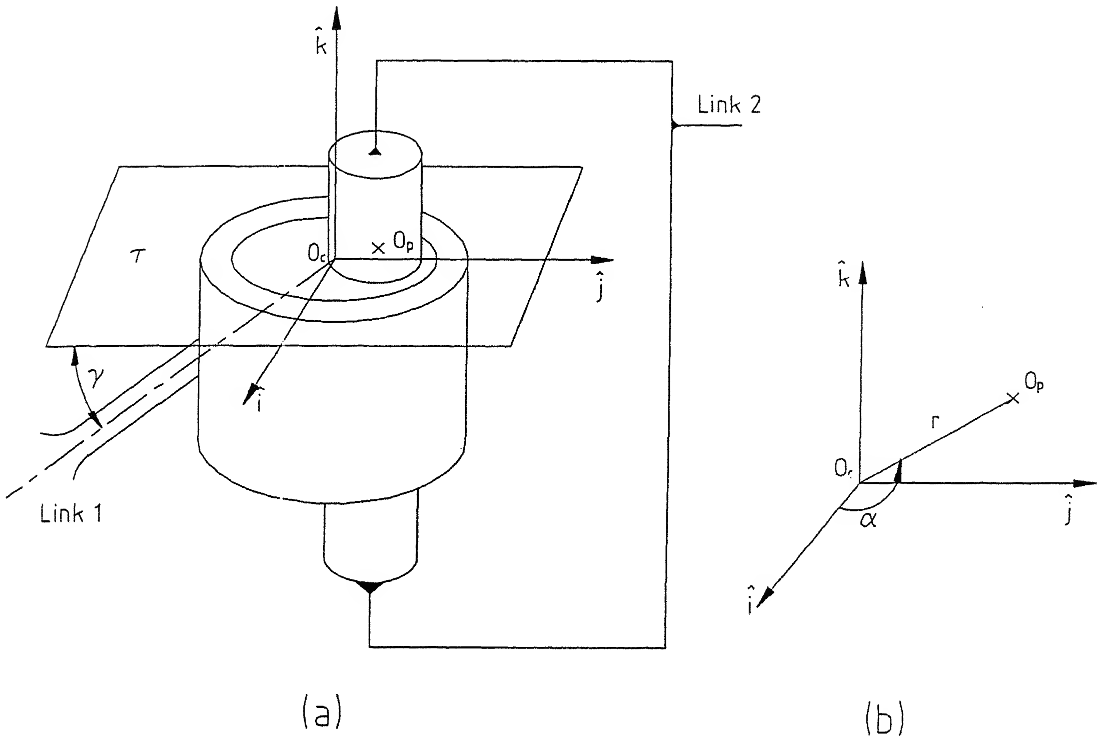

Figure 2.5: Clearance Model for a Revolute Joint in a Spatial Mechanism

radius c. Dhande and Chakraborty [30] have found the mean and the variance of the random error in the spatial joint as discussed in the following.

As has been observed in practice, it is assumed that the probability that at any instant the axis of the pin lies inside or on the circumference of the circle is uniform. If $f(r, \alpha)$ is the joint probability density function and if dA is an elemental area at the tip of the error vector then the probability $f(r, \alpha)drd\alpha$ is proportional to dA. Hence,

$$f(r, \alpha)drd\alpha = k_2 dA \tag{2.6}$$

where k_2 is a proportionality constant.

The constant k_2 and the joint probability density function f(r, α) is given by

$$\begin{aligned} k_2 &= \frac{1}{\pi c^2} \\ f(r, \alpha) &= \frac{r}{\pi c^2} \end{aligned} \tag{2.7}$$

The effective clearance error ϵ along the link axis is given by

$$\epsilon = \frac{r \cos \alpha}{\cos \gamma} \tag{2.8}$$

The mean and the variance of the variable ϵ are given as

$$m[\epsilon] = 0 \tag{2.9}$$

$$D[\epsilon] = \frac{c^2}{4 \cos^2 \gamma} \tag{2.10}$$

For a planar mechanism the angle $\gamma = 0°$. Therefore

$$\begin{aligned} \epsilon &= r \cos \alpha \\ m[\epsilon] &= 0 \\ D[\epsilon] &= \frac{c^2}{4} \end{aligned} \tag{2.11}$$

So expressions (2.8), (2.9) and (2.10) reduce to those for the random variable and its mean and variance, respectively, for a revolute pair in a planar mechanism as in (2.5).

2.2.3 Random Errors in the Coordinates of a Point

Consider a point $P(x_i, y_i, z_i)$ in the model of an RP process, the coordinates of which are in error and tolerances are specified on its coordinates. Tolerances are specified in absolute manner in contrast with the tolerance coefficients for link lengths. Then, these coordinates are random variables in the stochastic model of the RP process. Let ϵ_i, ϵ_{i+1} and ϵ_{i+2} be the absolute tolerances on coordinates x_i, y_i and z_i respectively. The corresponding random variables V_i, V_{i+1} and V_{i+2} are then given by

$$\begin{aligned} V_i &= x_i + \epsilon_i \\ V_{i+1} &= y_i + \epsilon_{i+1} \\ V_{i+2} &= z_i + \epsilon_{i+2} \end{aligned} \tag{2.12}$$

The coordinates of the point are in error due to locating the point in space while fabricating and assembling the RP machine. These are observed to be normally distributed in practice. Assuming normal distribution the means and the variances of the coordinates are given by

$$\begin{aligned} m[V_i] &= x_i \\ m[V_{i+1}] &= y_i \\ m[V_{i+2}] &= z_i \\ D[V_i] &= \left(\frac{\epsilon_i}{3}\right)^2 \\ D[V_{i+1}] &= \left(\frac{\epsilon_{i+1}}{3}\right)^2 \\ D[V_{i+2}] &= \left(\frac{\epsilon_{i+2}}{3}\right)^2 \end{aligned} \tag{2.13}$$

2.2.4 Random Errors in the Orientation of a Link or an Axis

Consider a link AB lying in 3D space (Fig. 2.6). Let XYZ be the base coordinate frame.

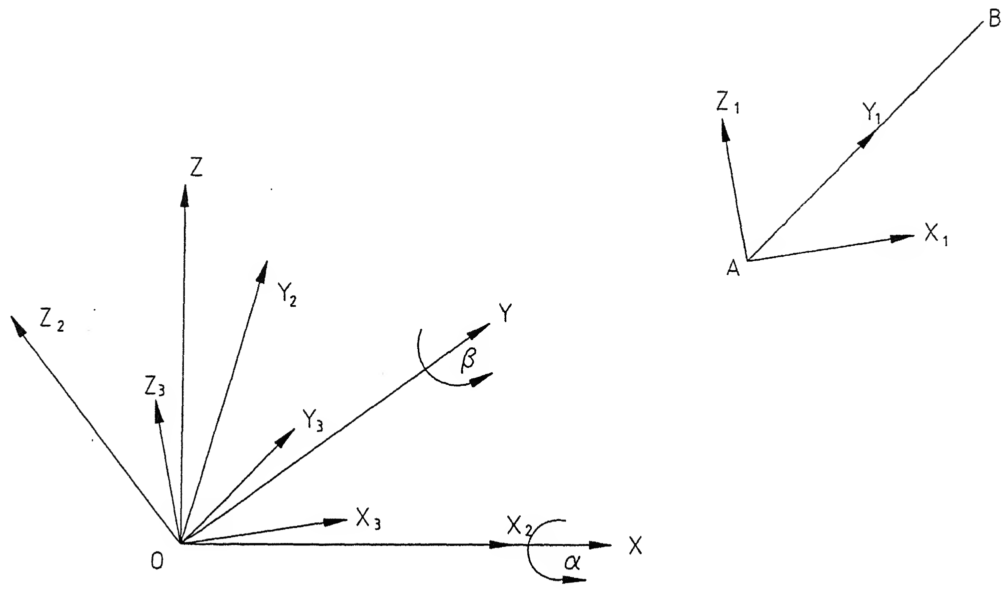

Figure 2.6: The Link AB in XYZ Frame

Let Y_1 be an axis along link AB with origin at A. Let Y_3 be an axis parallel to Y_1 but passing through the origin O of the base coordinate frame. The orientation of a vector $\mathbf{OY}_3$ can be expressed by two successive rotations about two axes in space. So we can express the orientation of Y_3 by two successive rotations α and β about base coordinate axes X and Y respectively. Since Y_1 is parallel to Y_3, therefore, the two angles α and β describe the orientation of Y_1 also.

If the orientation of link AB is in error and ϵ_i and ϵ_{i+1} be the absolute tolerances on angles α and β respectively then the actual angles are given by

$$\begin{aligned} V_i &= \alpha + \epsilon_i \\ V_{i+1} &= \beta + \epsilon_{i+1} \end{aligned} \tag{2.14}$$

Obviously V_i and V_{i+1} are random variables. The angles giving orientation of a link are observed to be normally distributed in practice. Assuming normal distribution of the random variables V_i and V_{i+1}, their means and variances are given by

$$\begin{aligned} m[V_i] &= \alpha \\ m[V_{i+1}] &= \beta \\ D[V_i] &= \left(\frac{\epsilon_i}{3}\right)^2 \\ D[V_{i+1}] &= \left(\frac{\epsilon_{i+1}}{3}\right)^2 \end{aligned} \tag{2.15}$$

2.2.5 Stochastic Model of an RP Process

The coordinates of a point on the work surface traced by the tip of the extruder head or the laser beam can be expressed as a function of random variables involved in the

corresponding process. If there are n random variables V_1, V_2, ..., V_n involved in the RP process under consideration then the coordinates of the point are given by

$$\begin{aligned} x &= x(V_1, V_2, \ldots, V_n) \\ y &= y(V_1, V_2, \ldots, V_n) \\ z &= z(V_1, V_2, \ldots, V_n) \end{aligned} \tag{2.16}$$

Since the dependent variables x, y and z are functions of random variables, therefore, any given range of a dependent variable may be associated with the corresponding probability if the probability densities or at least certain numerical characteristics, such as means m[V_i] and variances D[V_i] of random variables V_i are known. Means and variances of several random variables which may be involved in an RP process have been discussed earlier.

To evaluate the numerical characteristics of x we proceed as follows. As the theorems of random variables are well established for linear functions, the right hand side of Eq. (2.16) is expanded in Taylor series about the means of the random variables and the terms having order two and above are neglected. As a result we get

$$x \simeq x(m[V_i], \quad \text{i} = 1,2,\ldots,\text{n}) + \sum_{i=1}^{n} \left(\frac{\partial x}{\partial V_i}\right)_m (V_i - m[V_i]) \tag{2.17}$$

The term $\left(\frac{\partial x}{\partial V_i}\right)_m$ is a constant for a particular V_i. Let us say

$$A_i = \left(\frac{\partial x}{\partial V_i}\right)_m \tag{2.18}$$

Therefore, x can be expressed as

$$x \simeq x(m[V_i], \quad \text{i} = 1,2,\ldots,\text{n}) + \sum_{i=1}^{n} A_i(V_i - m[V_i]) \tag{2.19}$$

In the present case V_i, i = 1,2,...,n; are independent variables. Independent variables have zero covariance and, therefore, they are uncorrelated [69]. Hence the mean value of x is given by

$$m[x] = x\left(m\left[V_i\right], \qquad \text{i} = 1,2,\ldots,\text{n}\right) \tag{2.20}$$

The expression (2.19) on substituting (2.20) into it reduces to

$$x = m[x] + \sum_{i=1}^{n} A_i(V_i - m[V_i])$$

$$x - m[x] = \sum_{i=1}^{n} A_i(V_i - m[V_i]) \tag{2.21}$$

The expression for the variance D[x] of the dependent variable x can be derived as follows [56]. Variance D[x] is defined as [71]

$$D[x] = E\left(x - m[x]\right)^2$$

where E(w) is the expected value of the dependent variable w. From Eq. (2.21) we get,

$$\begin{aligned} D[x] &= E\left[\sum_{i=1}^{n} A_i(V_i - m[V_i])\right]^2 \\ &= \sum_{j=1}^{n}\sum_{k=1}^{n} A_j A_k \;\; E[\;(V_j - m[V_j])\,(V_k - m[V_k])\;] \\ &= \sum_{j=1}^{n}\sum_{k=1}^{n} A_j C_{jk} A_k \\ &= \{A\}[C]\{A\} \end{aligned}$$

where

$$\{A\}^T = (A_1, A_2, \ldots, A_n)$$

and

$$C_{jk} = \mathrm{Cov}(V_j, V_k) \qquad 1 \leq (\mathrm{j},\mathrm{k}) \leq n$$

If the n random variables V_j are uncorrelated,

$$\mathrm{Cov}(V_j, V_k) = \begin{cases} \mathrm{Var}(V_j), & \mathrm{j} = \mathrm{k} \\ 0, & \mathrm{j} \neq \mathrm{k} \end{cases}$$

i.e., the covariance matrix [C] is diagonal.

In the present case, all the n random variables are independent and hence uncorrelated. Therefore,

$$\begin{aligned} D[x] &= E\left(x - m[x]\right)^2 \\ &= \sum_{i=1}^{n} A_i^2 \;\; \mathrm{Var}(V_i) \\ &= \sum_{i=1}^{n} A_i^2 \;\; D[V_i] \end{aligned}$$

Or,

$$D[x] = \sum_{i=1}^{n} \left(\frac{\partial x}{\partial V_i}\right)_m^2 D[V_i] \qquad (2.22)$$

So expressions for numerical characteristics m[x] and D[x] of the dependent variable x are given by (2.20) and (2.22) respectively.

Similarly, numerical characteristics of the dependent variables y and z can be obtained. Taylor series expansions of y and z neglecting terms of order two and above are given by

$$\begin{aligned} y &\simeq y(m[V_i], \quad \mathrm{i} = 1,2,\ldots,\mathrm{n}) + \sum_{i=1}^{n}\left(\frac{\partial y}{\partial V_i}\right)_m (V_i - m[V_i]) \\ z &\simeq z(m[V_i], \quad \mathrm{i} = 1,2,\ldots,\mathrm{n}) + \sum_{i=1}^{n}\left(\frac{\partial z}{\partial V_i}\right)_m (V_i - m[V_i]) \end{aligned} \tag{2.23}$$

The numerical characteristics of y and z are given by

$$\begin{aligned} m[y] &= y\,(m\,[V_i]\,, \quad \mathrm{i} = 1,2,\ \ldots,\ \mathrm{n}) \\ m[z] &= z\,(m\,[V_i]\,, \quad \mathrm{i} = 1,2,\ \ldots,\ \mathrm{n}) \\ D[y] &= \sum_{i=1}^{n}\left(\frac{\partial y}{\partial V_i}\right)_m^2 D[V_i] \\ D[z] &= \sum_{i=1}^{n}\left(\frac{\partial z}{\partial V_i}\right)_m^2 D[V_i] \end{aligned} \tag{2.24}$$

Let

$$a_i = \left(\frac{\partial x}{\partial V_i}\right)_m^2, \quad b_i = \left(\frac{\partial y}{\partial V_i}\right)_m^2 \quad \text{and} \quad c_i = \left(\frac{\partial z}{\partial V_i}\right)_m^2$$

The terms a_i, b_i and c_i are called influence coefficients of x, y and z respectively.

To associate an exact probability for any dependent variable x, y or z to lie within a certain range, it is necessary to determine distribution functions F(x), F(y) or F(z). Even if the probability density functions of all the random variables were known exactly, it is a difficult task to evaluate the distribution functions F(x), F(y) or F(z) [28].

The evaluation of F(x), F(y) and F(z) can be avoided if we use the central limit theorem regarding functions of random variables. This theorem states that if V_1, V_2, ..., V_i are mutually independent random variables with finite mean and variance then the sum

$$S_i = \sum_i V_i$$

tends to a normal variable if no single variable contributes to the sum as i tends to infinity. It is known that if the function is of the form given in (2.20) or (2.23) and if $i > 5$, then the dependent variable x, y and z may as well be taken as normal [123].

To evaluate the variances D[x], D[y] and D[z], the partial derivatives of x, y and z, respectively, with respect to the variables V_i are to be evaluated. Once the variance of a dependent variable has been found for the RP process to trace a particular point on the work surface, the range of dependent variable is evaluated for three-sigma band of confidence level (with probability 0.9973).

Chapter 3

ANALYSIS OF MECHANICAL ERROR IN LOM

3.1 Geometric Modeling for Description of the LOM Process

The Laminated Object Manufacturing (LOM) process comprises of a sheet material moving between two idle rollers and a laser beam striking the sheet material as shown in Fig. 1.2. The sheet material is supplied from a continuous roll on one side of the machine and is taken up on the opposite side. An optical device moves in the horizontal plane with the help of an XY positioning device. The optical attachment emits the laser beam in vertically downward direction and the laser beam traces the contour of a slice and cuts the sheet [2, 63, 31, 45]. The LOM process has been discussed in detail in Section 1.1.2.1.

The geometric model of the LOM process would allow to express a point on the contour of a slice. The geometric model is discussed below (Fig. 3.1). The rollers are modeled as two cylinders C_1 and C_2 with centers of the front ends at $O_1(a_1, b_1, c_1)$ and $O_2(a_2, b_2, c_2)$, respectively, with respect to a base frame XYZ. The cylinders C_1 and C_2 have radii r_1 and r_2, respectively, and lengths l_1 and l_2 respectively. The axes of the two cylinders are not parallel due to the errors in the location of centers O_1 and O_2 and the errors in the orientation of the two axes. Ideally, the laser beam should be oriented in the vertically downward direction. However, due to mechanical errors in the location and orientation of the optical attachment, the actual orientation of the laser beam is oblique in space. The actual inclination of the laser beam can be described by means of two angles θ and ϕ as shown in Figs. 3.1 and 3.8a. This

general orientation of the laser beam would allow to find the partial derivatives of the coordinates of a point on the work surface with respect to θ and ϕ. In computation, the nominal values of θ and ϕ will be kept such that the mean position of laser beam is vertical.

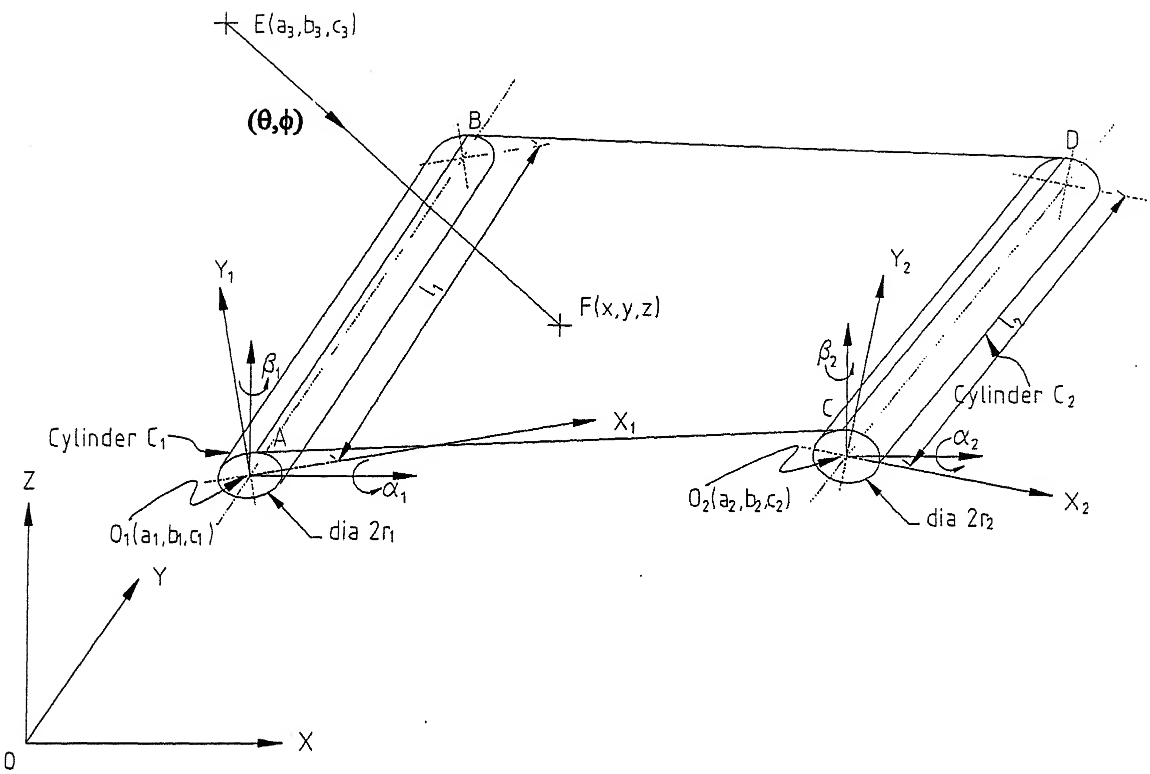

Figure 3.1: Geometric Model of the LOM Process

The source of the laser beam **EF** is at E(a_3, b_3, c_3) and it strikes the work surface ABDC at $F(x, y, z)$. Ideally, the axes of the two cylinders should be along Y direction, but due to mechanical errors they are inclined from the Y direction. A coordinate frame $X_1Y_1Z_1$ is attached at the center of the front end of cylinder C_1 with X_1 and Y_1 axes on the plane of the front end. The frame $X_1Y_1Z_1$ is obtained by two successive rotations α_1 and β_1 about lines passing through O_1 and parallel to $X$and Z directions respectively. Another coordinate frame $X_2Y_2Z_2$ is attached at the center of the front end of the cylinder C_2 with X_2 and Y_2 axes on the plane of its front end. The frame $X_2Y_2Z_2$ is obtained by two successive rotations α_2 and β_2 about lines passing through O_2 and parallel to X and Z directions respectively.

Let $\mathbf{p}_1(u, v)$ and $\mathbf{q}_2(r, s)$ be the parametric representation of the cylindrical surfaces C_1 and C_2 with respect to the coordinates frames $X_1Y_1Z_1$ and $X_2Y_2Z_2$ respectively (Fig. 3.2). The parameters v and s are along the axes of C_1 and C_2 respectively.

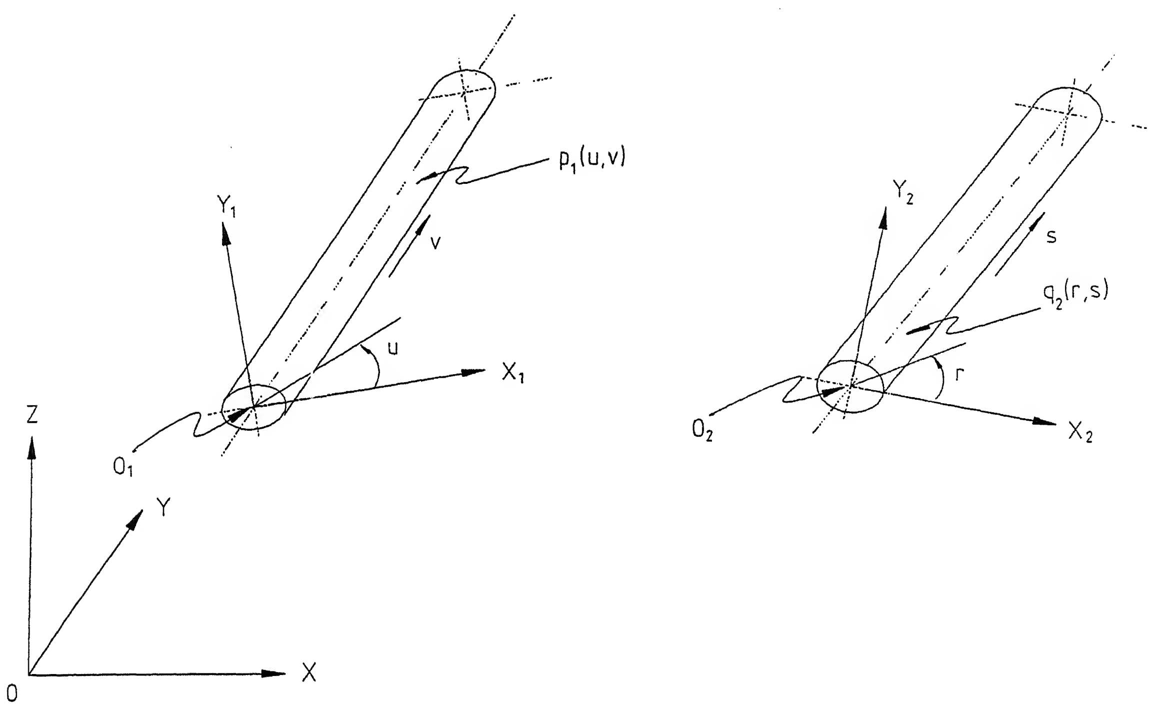

Figure 3.2: The Cylindrical Surfaces $\mathbf{p}_1(u, v)$ and $\mathbf{q}_2(r, s)$

The surface $\mathbf{p}_1(u, v)$ in the frame $X_1Y_1Z_1$ is given by

$$\mathbf{p}_1(u, v) = \left[\begin{array}{cccc} r_1 \cos u & r_1 \sin u & -l_1 v & 1 \end{array}\right] \qquad 0 \le u \le 2\pi, \quad 0 \le v \le 1 \tag{3.1}$$

The surface $\mathbf{q}_2(r, s)$ in the frame $X_2Y_2Z_2$ is given by

$$\mathbf{q}_2(r, s) = \left[\begin{array}{cccc} r_2 \cos r & r_2 \sin r & -l_2 s & 1 \end{array}\right] \qquad 0 \le r \le 2\pi, \quad 0 \le s \le 1 \tag{3.2}$$

The parametric representation $\mathbf{q}_1(r, s)$ of the cylinder C_2 can be expressed in the frame $X_1Y_1Z_1$ as follows. Let $[T_0^1]$ be the homogenous transformation matrix of the frame $X_1Y_1Z_1$ with respect to the frame XYZ. Let $[T_0^2]$ be the transformation of the frame $X_2Y_2Z_2$ with respect to the frame XYZ. Therefore, the frame $X_2Y_2Z_2$ with respect to $X_1Y_1Z_1$, as shown in Fig. 3.3, is given by

$$\left[T_1^2\right] = \left[T_0^2\right]\left[T_1^0\right]$$

$$\left[T_1^2\right] = \left[T_0^2\right]\left[T_0^1\right]^{-1} \tag{3.3}$$

Hence the surface $\mathbf{q}_1(r, s)$ in the frame $X_1Y_1Z_1$ is given by

$$\mathbf{q}_1(r, s) = \mathbf{q}_2(r, s)\left[T_1^2\right] \tag{3.4}$$

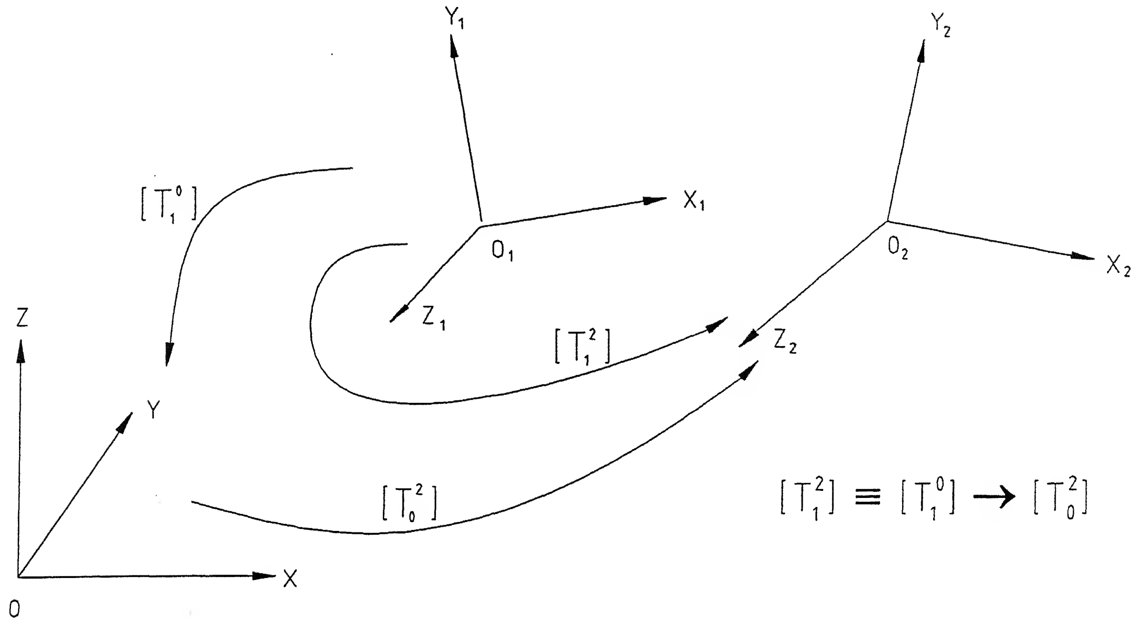

Figure 3.3: Transformations $[T_0^1]$, $[T_0^2]$ and $[T_1^2]$

3.1.1 The Transformation Matrices $[T_0^1]$, $[T_0^2]$ and $[T_1^2]$

The frame $X_1Y_1Z_1$ is obtained from the frame XYZ by a rotation about X by 90^o, a rotation about X by α_1, a rotation about Z by β_1 and a translation (a_1, b_1, c_1), successively, as shown in Fig. 3.4. The frame $X_IY_IZ_I$ from XYZ is obtained by a 90^o rotation about X. The frame $X_{II}Y_{II}Z_{II}$ is obtained from $X_IY_IZ_I$ after two successive rotations, α_1 and β_1 about X and Z directions respectively. The transformation $[T_0^1]$ is given by

$$\left[T_0^1\right] \equiv Rot(X, 90^o) \rightarrow Rot(X, \alpha_1) \rightarrow Rot(Z, \beta_1) \rightarrow Trans(Base, a_1, b_1, c_1)$$

This yields [103]

$$\left[T_0^1\right] \equiv Rot(X, 90^o)\ Rot(X, \alpha_1)\ Rot(Z, \beta_1)\ Trans(Base, a_1, b_1, c_1)$$

Or,

$$\left[T_0^1\right] = \begin{bmatrix} \cos\beta_1 & \sin\beta_1 & 0 & 0 \\ \sin\alpha_1 \sin\beta_1 & -\sin\alpha_1 \cos\beta_1 & \cos\alpha_1 & 0 \\ \cos\alpha_1 \sin\beta_1 & -\cos\alpha_1 \cos\beta_1 & -\sin\alpha_1 & 0 \\ a_1 & b_1 & c_1 & 1 \end{bmatrix} \qquad (3.5)$$

Similarly the matrix $[T_0^2]$ can be obtained as

$$\left[T_0^2\right] \equiv Rot(X, 90^o)\ Rot(X, \alpha_2)\ Rot(Z, \beta_2)\ Trans(Base, a_2, b_2, c_2)$$

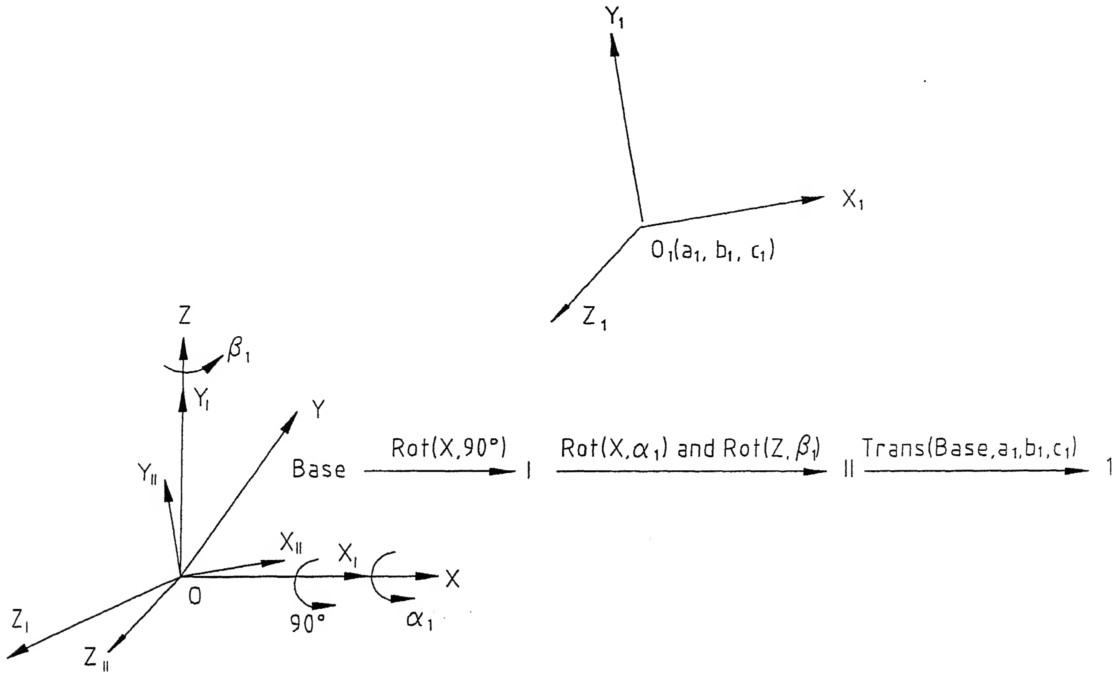

Figure 3.4: The Coordinate Frames XYZ and $X_1Y_1Z_1$

Or,

$$[T_0^2] = \begin{bmatrix} \cos\beta_2 & \sin\beta_2 & 0 & 0 \\ \sin\alpha_2\sin\beta_2 & -\sin\alpha_2\cos\beta_2 & \cos\alpha_2 & 0 \\ \cos\alpha_2\sin\beta_2 & -\cos\alpha_2\cos\beta_2 & -\sin\alpha_2 & 0 \\ a_2 & b_2 & c_2 & 1 \end{bmatrix} \tag{3.6}$$

Substituting $[T_0^1]$ and $[T_0^2]$ in Eq. (3.3) it follows that

$$\begin{aligned}[T_1^2] \quad = & \begin{bmatrix} \cos\beta_2 & \sin\beta_2 & 0 & 0 \\ \sin\alpha_2\sin\beta_2 & -\sin\alpha_2\cos\beta_2 & \cos\alpha_2 & 0 \\ \cos\alpha_2\sin\beta_2 & -\cos\alpha_2\cos\beta_2 & -\sin\alpha_2 & 0 \\ a_2 & b_2 & c_2 & 1 \end{bmatrix} \\ & \times \begin{bmatrix} \cos\beta_1 & \sin\alpha_1\sin\beta_1 & \cos\alpha_1\sin\beta_1 & 0 \\ \sin\beta_1 & -\sin\alpha_1\cos\beta_1 & -\cos\alpha_1\cos\beta_1 & 0 \\ 0 & \cos\alpha_1 & -\sin\alpha_1 & 0 \\ -a_1\cos\beta_1 - b_1\sin\beta_1 & \begin{array}{r}(-a_1\sin\alpha_1\sin\beta_1 \\ +b_1\sin\alpha_1\cos\beta_1 \\ -c_1\cos\alpha_1)\end{array} & \begin{array}{r}(-a_1\cos\alpha_1\sin\beta_1 \\ +b_1\cos\alpha_1\cos\beta_1 \\ c_1\sin\alpha_1)\end{array} & 1 \end{bmatrix}.\end{aligned} \tag{3.7}$$

3.1.2 Mathematical Representation of the Work Surface

The LOM sheet from which the contour of the slice is cut is the work surface. This surface is to be modeled mathematically so as to be able to find a point on the contour of a slice. A point on the contour is obtained by the intersection of the laser beam with the work surface. Consider the following three alternatives to approximate the work surface. In the first alternative the line AC, tangent to the two cylinders, is found such that the end points A and C lie on the front ends of C_1 and C_2 respectively. This gives two points A and C on the work surface. Then two straight lines AB and CD are drawn passing through A and C, respectively, and parallel to the axes of the corresponding cylinders. The work surface can be modeled by a bilinear surface ABDC with the four corner points A, B, C and D as shown in Fig. 3.5.

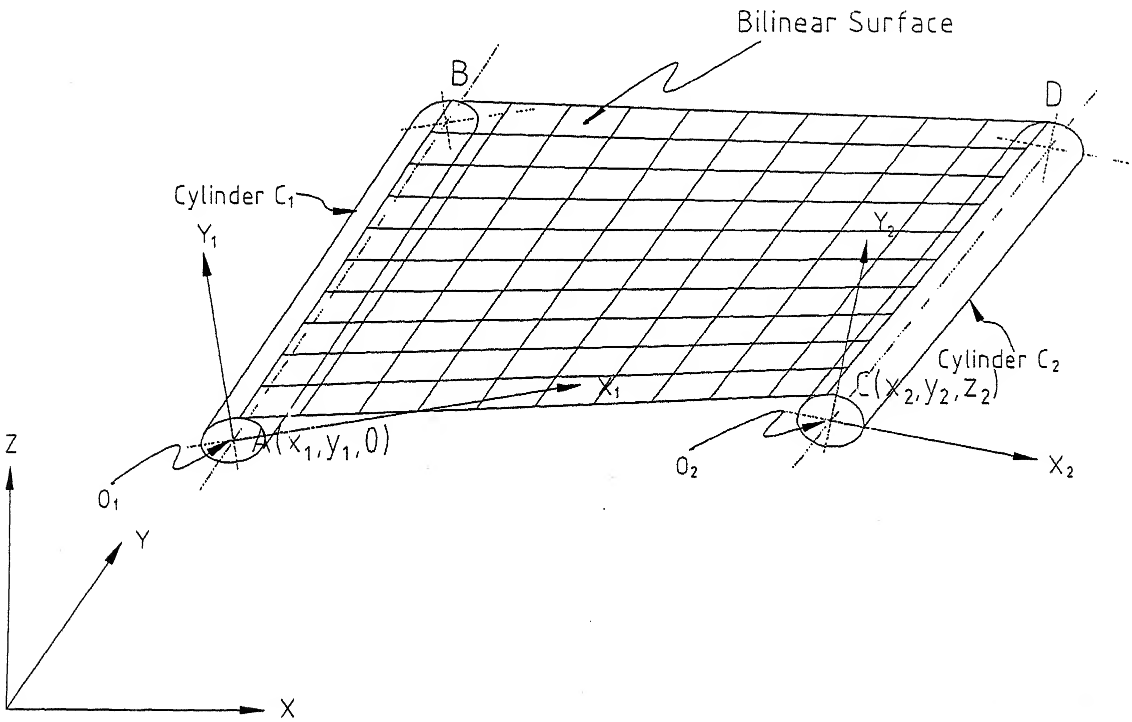

Figure 3.5: Mathematical Model of the Work Surface

The second alternative is to take the two tangents at both front and rear ends of the cylinders. But then AB and CD will be curved lines and wrapping has to be considered to find them. For an approximation, the bilinear surface in the first alternative is good enough as the work surface is not highly curved, and it is a plane when there is no error. The third alternative is to take the highest points on both ends of the two cylinders giving four corner points. A bilinear surface can be obtained with these four points. Obviously, the first alternative is a better representation of a surface tangent to the cylinders as the approximate surface in that case consists of at

least one tangent line.

So the work surface is modeled as in the first alternative. The line AC, tangent to the two cylinders is found such that its end points lie on the front ends of the cylinders. To approximate the surface, two lines AB and CD are drawn parallel to the axes of the corresponding cylinders and passing through the points A and C respectively. Let the points A, B, C and D correspond to four corner points of a unit square in parametric space, $\mathbf{p}(0,0)$, $\mathbf{p}(0,1)$, $\mathbf{p}(1,0)$ and $\mathbf{p}(1,1)$ respectively. A bilinear surface is constructed from these four points as corner points (Fig. 3.6).

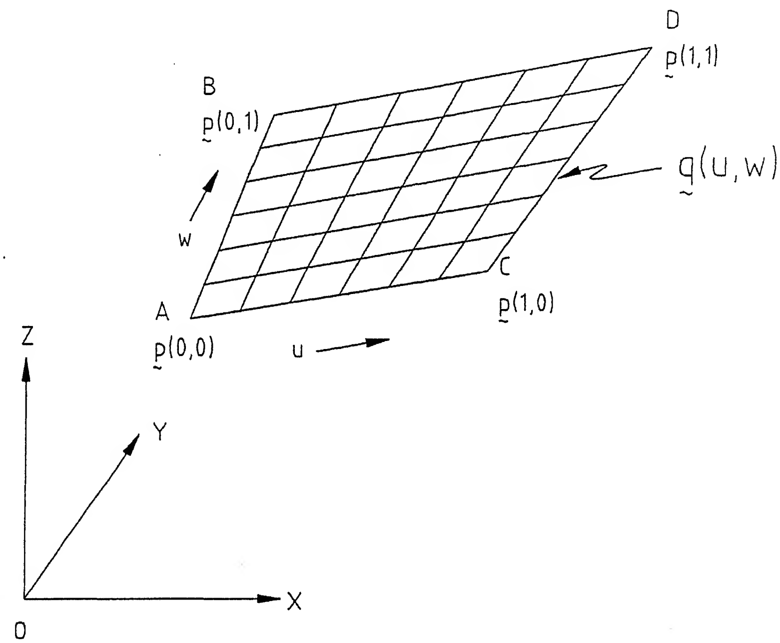

Figure 3.6: The Bilinear Surface ABDC in XYZ Object Space

The coordinates of these four corner points are found in XYZ object space by the desired transformation. The bilinear surface ABDC in the frame XYZ is given by

$$\mathbf{q}(u,w) = \begin{bmatrix} 1-u & u \end{bmatrix} \begin{bmatrix} \mathbf{p}(0,0) & \mathbf{p}(0,1) \\ \mathbf{p}(1,0) & \mathbf{p}(1,1) \end{bmatrix} \begin{bmatrix} 1-w \\ w \end{bmatrix} \tag{3.8}$$

where the four corner points $\mathbf{p}(0,0)$, $\mathbf{p}(0,1)$, $\mathbf{p}(1,0)$ and $\mathbf{p}(1,1)$ are expressed in the object space.

The surface is, in fact, a hyperbolic paraboloid, and therefore, it is a doubly ruled surface.

3.1.3 The End Points of the Edge AC of the Work Surface

The line AC in Fig. 3.5 is tangent to the two cylinders such that its end points A and C lie on the front ends of C_1 and C_2 respectively. Therefore, the normals to the

surfaces $\mathbf{p}_1(u,v)$ and $\mathbf{q}_2(r,s)$ are orthogonal to the line AC at A and C respectively. The other two conditions are that the end points A and C of the line should lie on the front ends of the cylinders C_1 and C_2 respectively. Let $A(x_1,y_1,0)$ and $C(x_2,y_2,z_2)$ be the two points in the frame $X_1Y_1Z_1$, as shown in Fig. 3.7.

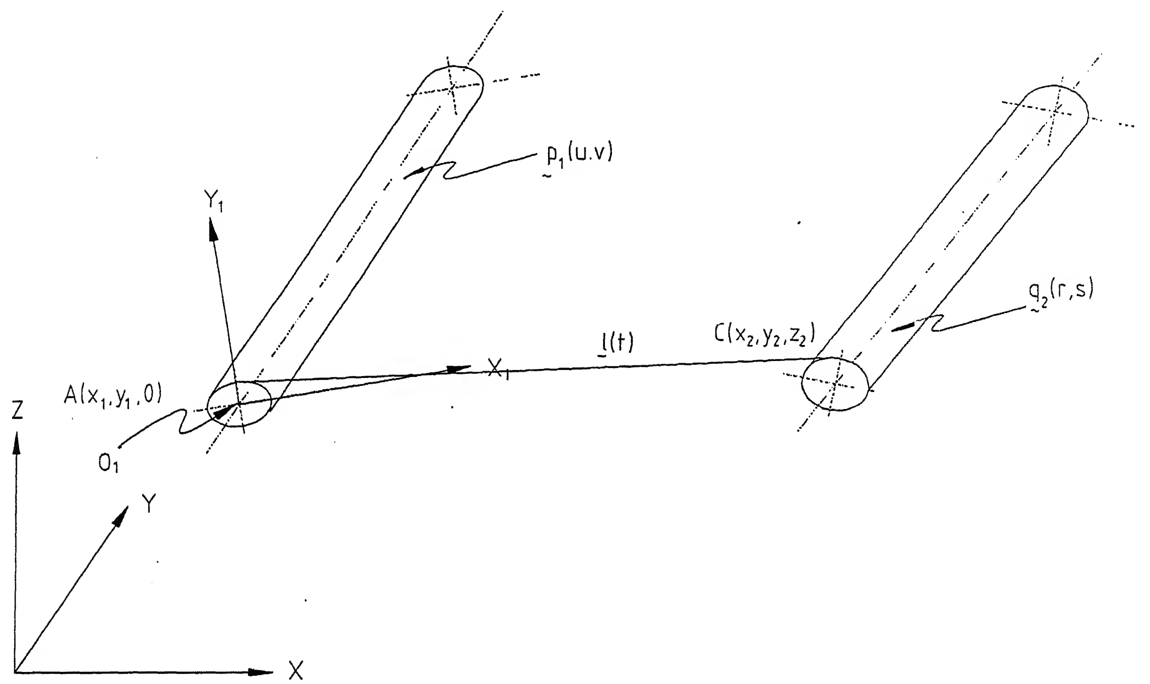

Figure 3.7: Tangent Points A and C in the frame $X_1Y_1Z_1$

The parametric representation of the line AC in the frame $X_1Y_1Z_1$ is given by [38, pp. 55-56]

$$\mathbf{l}(t) = \begin{bmatrix} x_1 & y_1 & 0 & 1 \end{bmatrix} + t \begin{bmatrix} x_2 - x_1 & y_2 - y_1 & z_2 & 0 \end{bmatrix} \qquad 0 \leq t \leq 1 \qquad (3.9)$$

The tangent to the line $\mathbf{l}(t)$ is obtained by differentiating Eq. (3.9) with respect to t:

$$\mathbf{l}^t(t) = \begin{bmatrix} x_2 - x_1 & y_2 - y_1 & z_2 & 0 \end{bmatrix} \qquad (3.10)$$

The surface $\mathbf{p}_1(u,v)$ in the frame $X_1Y_1Z_1$ is given by Eq. (3.1), i.e.,

$$\mathbf{p}_1(u,v) = \begin{bmatrix} r_1 \cos u & r_1 \sin u & -l_1 v & 1 \end{bmatrix}$$

The surface $\mathbf{q}_1(r,s)$ in the same frame $X_1Y_1Z_1$ is given by

$$\mathbf{q}_1(r,s) = \begin{bmatrix} r_2 \cos r & r_2 \sin r & -l_2 s & 1 \end{bmatrix} \begin{bmatrix} T_1^2 \end{bmatrix} \qquad (3.11)$$

There are four conditions (a), (b), (c) and (d) to find the tangent points A and C, as discussed below. The values of t on the line l(t) at the points A and C are 0 and 1 respectively. The values of v and s at the points A and C, respectively, are both 0.

(a) The normal to $\mathbf{p}_1(u,v)$ is orthogonal to the line $\mathbf{l}(t)$ at A(t=0, v=0), i.e.,

$$(\mathbf{p}_1^u \times \mathbf{p}_1^v) \cdot \mathbf{l}^t\Big|_{t=0,\, v=0} = 0$$

where the parametric derivatives $\mathbf{p}_1^u$ and $\mathbf{p}_1^v$ are the tangent vectors to $\mathbf{p}_1(u,v)$ [38, 90]. This yields

$$(y_2 - y_1)\sin u + (x_2 - x_1)\cos u = 0 \tag{3.12}$$

(b) The normal to $\mathbf{q}_1(r,s)$ is orthogonal to the line $\mathbf{l}(t)$ at C(t=1, s=0), i.e.,

$$(\mathbf{q}_1^r \times \mathbf{q}_1^s) \cdot \mathbf{l}^t\Big|_{t=1,\, s=0} = 0$$

where the parametric derivatives $\mathbf{q}_1^r$ and $\mathbf{q}_1^s$ are the tangent vectors to $\mathbf{q}_1(r,s)$. This yields

$$\begin{vmatrix} -a_{11}\sin r + a_{21}\cos r & -a_{12}\sin r + a_{22}\cos r & -a_{13}\sin r + a_{23}\cos r \\ -a_{31}l_2 & -a_{32}l_2 & -a_{33}l_2 \\ x_2 - x_1 & y_2 - y_1 & z_2 \end{vmatrix} = 0 \tag{3.13}$$

where a_{ij} is the element in the i^{th} row and j^{th} column of the matrix $[T_1^2]$.

(c) The line $\mathbf{l}(t)$ touches $\mathbf{p}_1(u,v)$ at A(t=0, v=0), i.e.,

$$\mathbf{p}_1(u,0) - \mathbf{l}(0) = 0$$

This yields

$$x_1 = r_1\cos u \tag{3.14}$$

$$y_1 = r_1\sin u \tag{3.15}$$

(d) The line $\mathbf{l}(t)$ touches $\mathbf{q}_1(r,s)$ at C(t=1, s=0), i.e.,

$$\mathbf{q}_1(r,0) - \mathbf{l}(1) = 0$$

This yields

$$x_2 = r_2(a_{11}\cos r + a_{21}\sin r) + a_{41} \tag{3.16}$$

$$y_2 = r_2(a_{12}\cos r + a_{22}\sin r) + a_{42} \tag{3.17}$$

$$z_2 = r_2(a_{13}\cos r + a_{23}\sin r) + a_{43} \tag{3.18}$$

Substituting x_1, y_1, x_2, y_2 and z_2 from Eqs. (3.14), (3.15), (3.16), (3.17) and (3.18) respectively, into Eqs. (3.12) and (3.13) gives two transcendental equations in two unknowns u and r.

3.1.4 Solving for u and r by Newton-Raphson Method

The two equations, Eqs. (3.12) and (3.13) are to be solved for the two variables u and r. The two equations, being transcendental, have to be solved by an iterative technique. Newton-Raphson method [97] is adopted to solve the two equations as follows:

Let the left hand sides of Eqs. (3.12) and (3.13) be expressed as F_1 and F_2 respectively. Therefore, the two transcendental equations in two unknowns u and r are given by

$$F_1 = (y_2 - y_1)\sin u + (x_2 - x_1)\cos u = 0 \tag{3.19}$$

$$F_2 = \begin{vmatrix} f & g & h \\ p & q & r \\ u & v & w \end{vmatrix} = 0 \tag{3.20}$$

where Eq. (3.13) is written as

$$\begin{vmatrix} f & g & h \\ p & q & r \\ u & v & w \end{vmatrix} = 0$$

The terms x_1, y_1, x_2, y_2 and z_2 in the above are given by Eqs. (3.14) to (3.18).

The system of equations is given by $[F] = \begin{bmatrix} F_1 \\ F_2 \end{bmatrix} = \begin{bmatrix} 0 \\ 0 \end{bmatrix}$. The Jacobian of [F] is given by

$$[J] = \begin{bmatrix} \dfrac{\partial F_1}{\partial u} & \dfrac{\partial F_1}{\partial r} \\ \dfrac{\partial F_2}{\partial u} & \dfrac{\partial F_2}{\partial r} \end{bmatrix} \tag{3.21}$$

where

$$\frac{\partial F_1}{\partial u} = (y_2 - y_1)\cos u + \left(\frac{\partial y_2}{\partial u} - \frac{\partial y_1}{\partial u}\right)\sin u - (x_2 - x_1)\sin u + \left(\frac{\partial x_2}{\partial u} - \frac{\partial x_1}{\partial u}\right)\cos u \tag{3.22}$$

$$\frac{\partial F_1}{\partial r} = \left(\frac{\partial y_2}{\partial r} - \frac{\partial y_1}{\partial r}\right)\sin u + \left(\frac{\partial x_2}{\partial r} - \frac{\partial x_1}{\partial r}\right)\cos u \tag{3.23}$$

$$\frac{\partial F_2}{\partial u} = \frac{\partial}{\partial u}\begin{vmatrix} f & g & h \\ p & q & r \\ u & v & w \end{vmatrix}$$

The partial derivatives of the determinant F_2 can be expressed as the sum of the

three determinants [71, pp. 243] as follows

$$\frac{\partial F_2}{\partial u} = \begin{vmatrix} f' & g' & h' \\ p & q & r \\ u & v & w \end{vmatrix} + \begin{vmatrix} f & g & h \\ p' & q' & r' \\ u & v & w \end{vmatrix} + \begin{vmatrix} f & g & h \\ p & q & r \\ u' & v' & w' \end{vmatrix} \tag{3.24}$$

where prime denotes partial derivatives with respect to u. Since the first and second rows of F_2 do not depend upon u, therefore,

$$\frac{\partial F_2}{\partial u} = \begin{vmatrix} f & g & h \\ p & q & r \\ u' & v' & w' \end{vmatrix} \tag{3.25}$$

The second row of F_2 does not depend upon r too. Therefore,

$$\frac{\partial F_2}{\partial r} = \begin{vmatrix} f' & g' & h' \\ p & q & r \\ u & v & w \end{vmatrix} + \begin{vmatrix} f & g & h \\ p & q & r \\ u' & v' & w' \end{vmatrix} \tag{3.26}$$

where the prime denotes partial derivatives with respect to r.

So the Jacobian of [F] can be expressed analytically.

There are four tangents to the cylinders at the front end. If our initial guess for both u and r are close to $\pi/2$, then the desired result, i.e., the one for which both y_1 and y_2 are positive, is obtained (Fig. 3.7). Newton-Raphson method, on solving the two transcendental equations, gives the values of the parameters u and r for the tangent AC. Let these values of u and r at the points A and C, respectively, be given by

$$\begin{aligned} u &= u_A \\ r &= r_C \end{aligned} \tag{3.27}$$

3.1.5 The Four Corner Points of the Work Surface in the Base Frame XYZ

The four corner points of the work surface ABDC are described in Section 3.1.2. Once the tangent line AC is found, the corner points $\mathbf{p}(0,0)$, $\mathbf{p}(0,1)$, $\mathbf{p}(1,0)$ and $\mathbf{p}(1,1)$ correspond to $(u_A, v = 0)$, $(u_A, v = 1)$, $(r_C, s = 0)$ and $(r_C, s = 1)$ respectively. Hence the corner points $\mathbf{p}(0,0)$ and $\mathbf{p}(0,1)$ in the frame XYZ are given by

$$\begin{bmatrix} \mathbf{p}(0,0) \\ \mathbf{p}(0,1) \end{bmatrix} = \begin{bmatrix} r_1 \cos u_A & r_1 \sin u_A & 0 & 1 \\ r_1 \cos u_A & r_1 \sin u_A & -l_1 & 1 \end{bmatrix} [T_0^1] \tag{3.28}$$

The other two corner points $\mathbf{p}(1,0)$ and $\mathbf{p}(1,1)$ in the frame XYZ are given by

$$\begin{bmatrix} \mathbf{p}(1,0) \\ \mathbf{p}(1,1) \end{bmatrix} = \begin{bmatrix} r_2 \cos r_C & r_2 \sin r_C & 0 & 1 \\ r_2 \cos r_C & r_2 \sin r_C & -l_2 & 1 \end{bmatrix} [T_0^2] \tag{3.29}$$

And the bilinear surface is given by Eq. (3.8).

3.1.6 Parametric Representation of the Laser Beam

The optical attachment emits the laser beam to draw a contour on the work surface and cut the sheet. To find the intersection of the beam and the work surface, it is necessary to represent the incident beam mathematically.

Let **EF** be the incident laser beam emitted from the optical attachment at $E(a_3, b_3, c_3)$ and intersecting the XY plane at G as shown in Fig. 3.8.

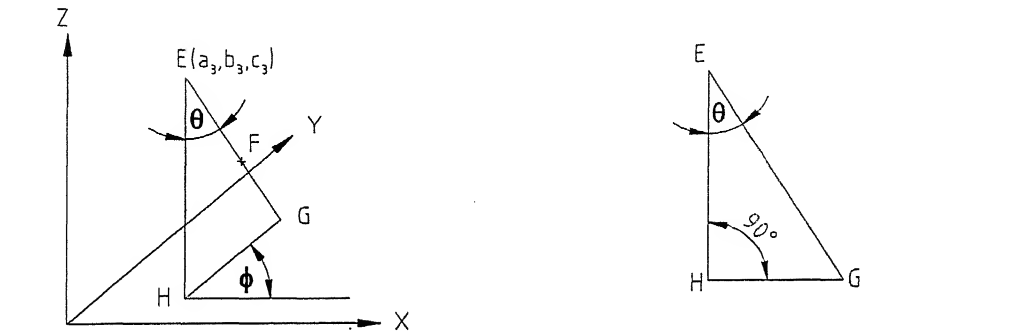

(a) The Incident Laser Beam **EG** (b) Rightangle Triangle EGH

Figure 3.8: The Incident Laser Beam

The parametric equation of the line EG is given by

$$\mathbf{Q}(t) = \left[\begin{array}{cccc} a_3 & b_3 & c_3 & 1 \end{array}\right] + t\left[\begin{array}{cccc} c_3 \tan\theta\cos\phi & c_3\tan\theta\sin\phi & -c_3 & 0 \end{array}\right] \tag{3.30}$$

The above equation holds for a vertical laser beam too, by substituting $\theta = 0^o$ and any value of ϕ, say $\phi = 0^o$.

3.1.7 Intersection of the Laser Beam and the Work Surface

The laser beam **EG** in the base frame XYZ is given by

$$\mathbf{Q}(t) = \left[\begin{array}{cccc} a_3 & b_3 & c_3 & 1 \end{array}\right] + t\left[\begin{array}{cccc} c_3 \tan\theta\cos\phi & c_3\tan\theta\sin\phi & -c_3 & 0 \end{array}\right]$$

The surface ABDC in the frame XYZ is given by

$$\mathbf{q}(u, w) = \left[\begin{array}{cc} 1-u & u \end{array}\right] \left[\begin{array}{cc} \mathbf{p}(0,0) & \mathbf{p}(0,1) \\ \mathbf{p}(1,0) & \mathbf{p}(1,1) \end{array}\right] \left[\begin{array}{c} 1-w \\ w \end{array}\right]$$

as in Eq. (3.8). The defining points **p**(0,0), **p**(0,1), **p**(1,0) and **p**(1,1) are given by Eqs. (3.28) and (3.29).

Hence the point of intersection of **Q**(t) and **q**(u,w) is given by [38, 90, 133]

$$\mathbf{q}(u, w) = \mathbf{Q}(t) \qquad 0 \leq t \leq \infty \tag{3.31}$$

A frame $X^{\star}Y^{\star}Z^{\star}$ is obtained by a transformation with respect to the frame XYZ such that the $Z^{\star}$-axis coincides with **GE**. See Fig. 3.9. The transformation of the base frame XYZ with respect to the $X^{\star}Y^{\star}Z^{\star}$ is given by

$$\left[T_{\star}^{base}\right] \equiv Rot(Y^{\star},\theta) \rightarrow Rot(Z_2,-\phi) \rightarrow Trans(-\mathbf{OG})$$

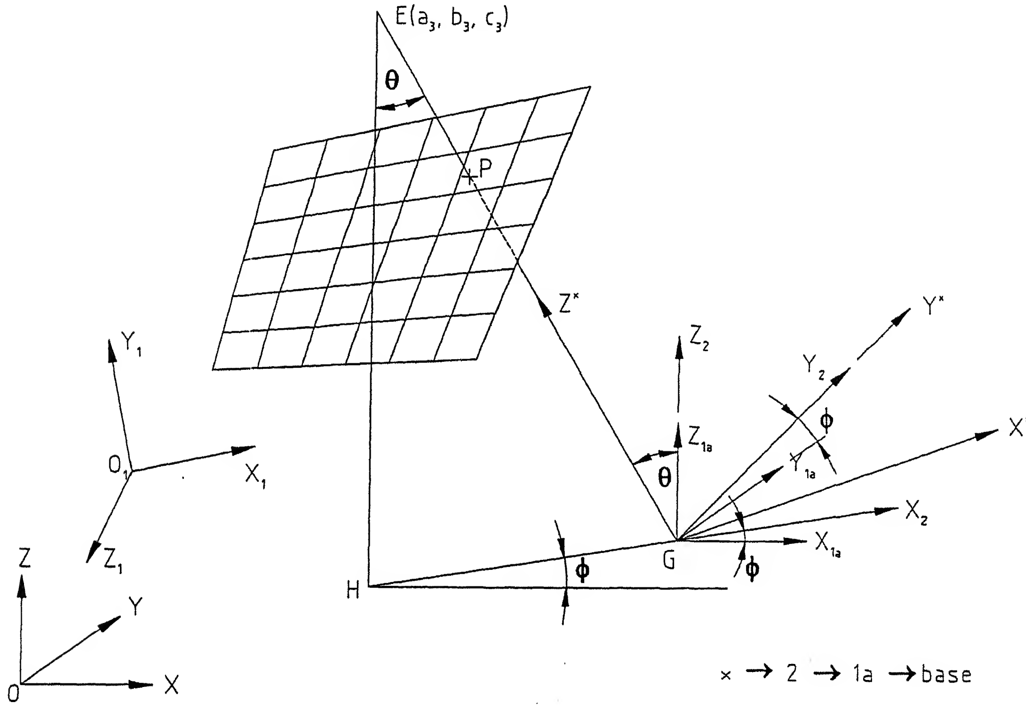

Figure 3.9: Intersection of the Laser Beam and the Work Surface

Let the above transformation matrix $[T_{\star}^{base}]$ be simply represented by [T],

$$[T] = \left[T_{\star}^{base}\right]$$

Hence

$$[T] = Trans(-\mathbf{OG})\; Rot(Z_2,-\phi)\; Rot(Y^{\star},\theta)$$

The translation **OG** is given by

$$\mathbf{OG} = \left[\begin{array}{cccc} a_3 + c_3\tan\theta\cos\phi & b_3 + c_3\tan\theta\sin\phi & 0 & 0 \end{array}\right]$$

Let

$$\mathbf{OG} = \left[\begin{array}{cccc} g_x & g_y & 0 & 0 \end{array}\right] \tag{3.32}$$

where

$$g_x = a_3 + c_3\tan\theta\cos\phi$$

and

$$g_y = b_3 + c_3\tan\theta\sin\phi$$

Therefore,

$$[T] = Trans(-g_x, -g_y, 0)\ Rot(Z_2, -\phi)\ Rot(Y^\star, \theta) \tag{3.33}$$

Or,

$$[T] = \left[\begin{array}{c|c|c|c} \cos\theta\cos\phi & -\sin\phi & -\sin\theta\cos\phi & 0 \\ \hline \cos\theta\sin\phi & \cos\phi & -\sin\theta\sin\phi & 0 \\ \hline \sin\theta & 0 & \cos\theta & 0 \\ \hline -\cos\theta(a_3\cos\phi + b_3\sin\phi & a_3\sin\phi - b_3\cos\phi & \sin\theta(a_3\cos\phi + b_3\sin\phi & 1 \\ +c_3\tan\theta) & & +c_3\tan\theta) & \end{array}\right] \tag{3.34}$$

The transformed surface is given by

$$\begin{aligned} \mathbf{q}^\star(u,w) &= \mathbf{q}(u,w)\,[T] \\ &= \begin{bmatrix} x & y & z & 1 \end{bmatrix} [T] \end{aligned}$$

Let

$$\mathbf{q}^\star(u,w) = \begin{bmatrix} x^\star(u,w) & y^\star(u,w) & z^\star(u,w) & 1 \end{bmatrix} \tag{3.35}$$

where

$$\begin{bmatrix} x^\star(u,w) & y^\star(u,w) & z^\star(u,w) & 1 \end{bmatrix} = \begin{bmatrix} x(u,w) & y(u,w) & z(u,w) & 1 \end{bmatrix} [T] \tag{3.36}$$

and

$$\begin{bmatrix} x(u,w) & y(u,w) & z(u,w) & 1 \end{bmatrix} = \begin{bmatrix} 1-u & u \end{bmatrix} \begin{bmatrix} \mathbf{p}(0,0) & \mathbf{p}(0,1) \\ \mathbf{p}(1,0) & \mathbf{p}(1,1) \end{bmatrix} \begin{bmatrix} 1-w \\ w \end{bmatrix} \tag{3.37}$$

The transformed line is given by

$$\mathbf{Q}^\star(t) = \mathbf{Q}(t)\,[T]$$

The line EG is coincident with the $Z^\star$-axis. Hence the x and y coordinates of the line EG in the frame $X^\star Y^\star Z^\star$ are both zeroes. Therefore, $\mathbf{Q}^\star(t)$ is given by

$$\mathbf{Q}^\star(t) = \begin{bmatrix} 0 & 0 & z(t)|_{Q^\star} & 1 \end{bmatrix} \tag{3.38}$$

Equating right hand sides of Eqs. (3.35) and (3.38) gives the point of intersection as

$$\begin{aligned} x^\star(u,w) &= 0 & (3.39) \\ y^\star(u,w) &= 0 & (3.40) \end{aligned}$$

The defining points $\mathbf{p}$(0,0), $\mathbf{p}$(0,1), $\mathbf{p}$(1,0) and $\mathbf{p}$(1,1), and the transformation matrix [T] do not depend upon the parameters u and w. It can be seen that the

expressions for $x^\star$ and $y^\star$ are non-linear in u and w. Eqs. (3.42) and (3.43) can be solved for u and w by Newton-Raphson method, an iterative technique [97].

For the intersection

$$F_1 = x^\star(u,w) = 0 \tag{3.41}$$

$$F_2 = y^\star(u,w) = 0 \tag{3.42}$$

The Jacobian [J] of $[F] = \begin{bmatrix} F_1 \\ F_2 \end{bmatrix}$ is given by

$$[J] = \begin{bmatrix} \dfrac{\partial F_1}{\partial u} & \dfrac{\partial F_1}{\partial w} \\ \dfrac{\partial F_2}{\partial u} & \dfrac{\partial F_2}{\partial w} \end{bmatrix} \tag{3.43}$$

The Jacobian [J] can be expressed analytically as the expressions for F_1 and F_2 involve only multiplication terms of u and w. Since the elements of [T] do not depend upon u and w, therefore, the partial derivatives of F_1 and F_2 with respect to u are given by

$$\begin{aligned} \begin{bmatrix} \dfrac{\partial F_1}{\partial u} & \dfrac{\partial F_2}{\partial u} & \dfrac{\partial z^\star}{\partial u} & 0 \end{bmatrix} &= \frac{\partial}{\partial u}\begin{bmatrix} x^\star & y^\star & z^\star & 1 \end{bmatrix} \\ &= \frac{\partial}{\partial u}\begin{bmatrix} x & y & z & 1 \end{bmatrix}[T] \\ &= \begin{bmatrix} -1 & 1 \end{bmatrix}\begin{bmatrix} \mathbf{p}(0,0) & \mathbf{p}(0,1) \\ \mathbf{p}(1,0) & \mathbf{p}(1,1) \end{bmatrix}\begin{bmatrix} 1-w \\ w \end{bmatrix}[T] \end{aligned} \tag{3.44}$$

and the partial derivatives of F_1 and F_2 with respect to w are given by

$$\begin{aligned} \begin{bmatrix} \dfrac{\partial F_1}{\partial w} & \dfrac{\partial F_2}{\partial w} & \dfrac{\partial z^\star}{\partial w} & 0 \end{bmatrix} &= \frac{\partial}{\partial w}\begin{bmatrix} x^\star & y^\star & z^\star & 1 \end{bmatrix} \\ &= \frac{\partial}{\partial w}\begin{bmatrix} x & y & z & 1 \end{bmatrix}[T] \\ &= \begin{bmatrix} 1-u & u \end{bmatrix}\begin{bmatrix} \mathbf{p}(0,0) & \mathbf{p}(0,1) \\ \mathbf{p}(1,0) & \mathbf{p}(1,1) \end{bmatrix}\begin{bmatrix} -1 \\ 1 \end{bmatrix}[T] \end{aligned} \tag{3.45}$$

Hence the elements of Jacobian [J] are given by Eqs. (3.44) and (3.45). Solving Eqs. (3.41) and (3.42) by Newton-Raphson method gives u and w. Substituting u and w in Eq. (3.37) gives x, y and z. Hence the point of intersection P is given by

$$\mathbf{q} = \begin{bmatrix} x & y & z & 1 \end{bmatrix}$$

where **q** is the position vector of a point on the contour of a slice cut by the laser beam.

3.2 Stochastic Error Analysis of the LOM Process

Chapter 2 discusses stochastic modeling of an RP process. Following the approach given there, the stochastic error analysis of the LOM process can be carried out as follows.

The dimensions in error in the LOM process are shown in Fig. 3.10. The dimensions in error are the coordinates a_1, b_1, c_1, a_2, b_2, c_2, a_3, b_3 and c_3; the angles α_1, β_1, α_2, β_2, θ and ϕ; and the link lengths r_1, l_1, r_2 and l_2. The error in a_1 is $\triangle a_1$, the error in b_1 is $\triangle b_1$, and so on. There are 19 dimensions in error. Let V_i, i=1 to 19, be the random variables involved in the process. Using the approach given in Chapter 2, the random variables involved in the LOM process are as follows:

$$
\begin{array}{llll}
V_1 = a_1 + \epsilon_1, & V_2 = b_1 + \epsilon_2, & V_3 = c_1 + \epsilon_3, & V_4 = \alpha_1 + \epsilon_4, \\
V_5 = \beta_1 + \epsilon_5, & V_6 = r_1(1 + \epsilon_6), & V_7 = l_1(1 + \epsilon_7), & \\
V_8 = a_2 + \epsilon_8, & V_9 = b_2 + \epsilon_9, & V_{10} = c_2 + \epsilon_{10}, & V_{11} = \alpha_2 + \epsilon_{11}, \\
V_{12} = \beta_2 + \epsilon_{12}, & V_{13} = r_2(1 + \epsilon_{13}), & V_{14} = l_2(1 + \epsilon_{14}), & \\
V_{15} = a_3 + \epsilon_{15}, & V_{16} = b_3 + \epsilon_{16}, & V_{17} = c_3 + \epsilon_{17}, & V_{18} = \theta + \epsilon_{18}, \\
V_{19} = \phi + \epsilon_{19}, & & &
\end{array}
\tag{3.46}
$$

where ϵ_1, ϵ_2, ϵ_3, ϵ_8, ϵ_9, ϵ_{10}, ϵ_{15}, ϵ_{16} and ϵ_{17} are absolute tolerances in meters(m) on coordinates; ϵ_4, ϵ_5, ϵ_{11}, ϵ_{12}, ϵ_{18} and ϵ_{19} are absolute tolerances in radians on angles; and ϵ_6, ϵ_7, ϵ_{13} and ϵ_{14} are tolerances per unit nominal lengths on r_1, l_1, r_2 and l_2 respectively. The random variables V_i are independent of each other.

The mean values of the random variables m$[V_i]$, i=1 to 19, are a_1, b_1, c_1, α_1, β_1, r_1, l_1, a_2, b_2, c_2, α_2, β_2, r_2, l_2, a_3, b_3, c_3, θ and ϕ respectively.

The variances D$[V_i]$ are given as follows:

$$
\begin{aligned}
D[V_i] &= \left(\frac{\epsilon_i}{3}\right)^2 \quad \text{i} = 1 \text{ to } 5,\ 8 \text{ to } 12,\ 15 \text{ to } 19 \\
D[V_6] &= \left(\frac{\epsilon_6 r_1}{3}\right)^2 \\
D[V_7] &= \left(\frac{\epsilon_7 l_1}{3}\right)^2 \\
D[V_{13}] &= \left(\frac{\epsilon_{13} r_2}{3}\right)^2 \\
D[V_{14}] &= \left(\frac{\epsilon_{14} l_2}{3}\right)^2
\end{aligned}
\tag{3.47}
$$

The coordinates of a point on the work surface traced by the laser beam are given by

$$
\begin{aligned}
x &= x\left(V_1, V_2, \ldots, V_{19}\right) \\
y &= y\left(V_1, V_2, \ldots, V_{19}\right) \\
z &= z\left(V_1, V_2, \ldots, V_{19}\right)
\end{aligned}
\tag{3.48}
$$

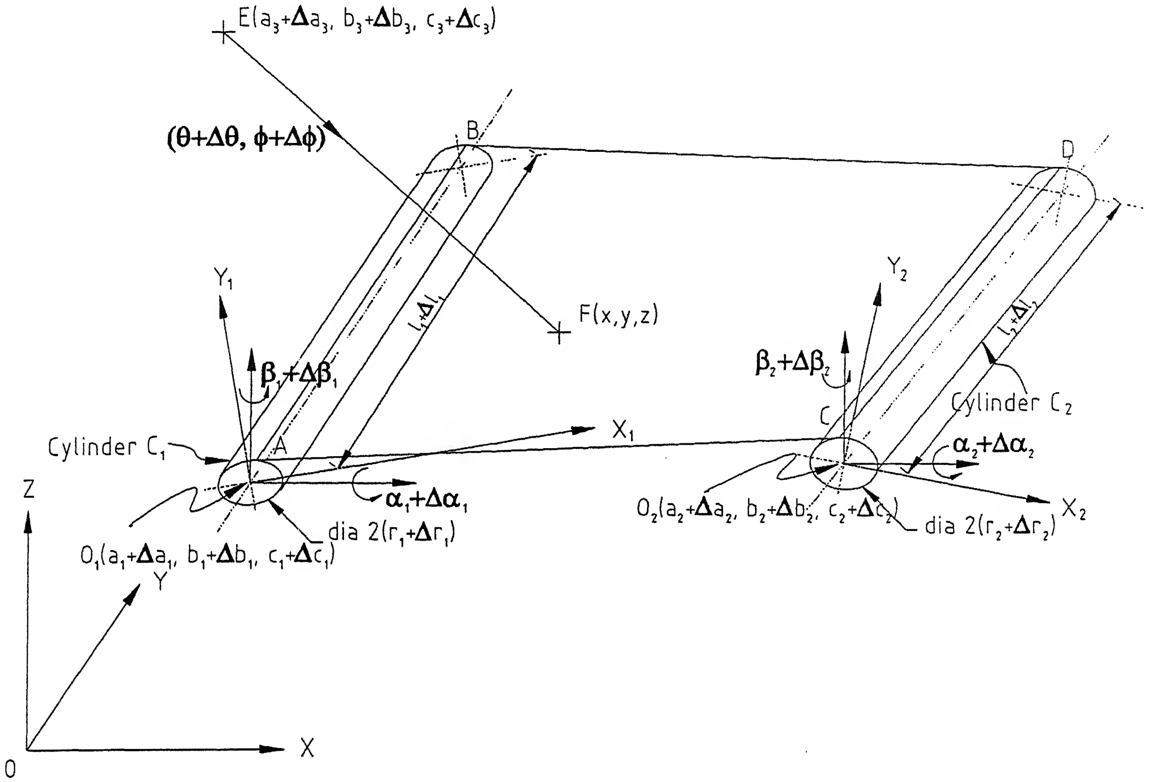

Figure 3.10: Geometric Model of the LOM Process Showing Errors in Dimensions

The means and the variances of the dependent variables x, y and z are given as follows:

$$\begin{aligned}
m[x] &= x\,(m\,[V_i]\,,\quad \mathrm{i} = 1,2,\ldots,19) \\
m[y] &= y\,(m\,[V_i]\,,\quad \mathrm{i} = 1,2,\ldots,19) \\
m[z] &= z\,(m\,[V_i]\,,\quad \mathrm{i} = 1,2,\ldots,19) \\
D[x] &= \sum_{i=1}^{19} \left(\frac{\partial x}{\partial V_i}\right)_m^2 D[V_i] \\
D[y] &= \sum_{i=1}^{19} \left(\frac{\partial y}{\partial V_i}\right)_m^2 D[V_i] \\
D[z] &= \sum_{i=1}^{19} \left(\frac{\partial z}{\partial V_i}\right)_m^2 D[V_i]
\end{aligned} \tag{3.49}$$

The partial derivatives are evaluated at the mean values of the variables V_i as denoted by the subscript m. The mean values m[V_i] of the variables V_i are as given earlier in this subsection. The necessary expressions for the influence coefficients $\left(\frac{\partial x}{\partial V_i}\right)^2$, $\left(\frac{\partial y}{\partial V_i}\right)^2$ and $\left(\frac{\partial z}{\partial V_i}\right)^2$ can be derived as in the following.

The coordinates of a point on the work surface is given by Eq. (3.8):

$$\mathbf{q}(u,w) = \begin{bmatrix} x & y & z & 1 \end{bmatrix} = \begin{bmatrix} 1-u & u \end{bmatrix} \begin{bmatrix} \mathbf{p}(0,0) & \mathbf{p}(0,1) \\ \mathbf{p}(1,0) & \mathbf{p}(1,1) \end{bmatrix} \begin{bmatrix} 1-w \\ w \end{bmatrix}$$

Therefore,

$$
\begin{aligned}
x &= q[1] = p_{11}(1-u)(1-w) + p_{21}(1-u)w + p_{31}u(1-w) + p_{41}uw && (3.50)\\
y &= q[2] = p_{12}(1-u)(1-w) + p_{22}(1-u)w + p_{32}u(1-w) + p_{42}uw && (3.51)\\
z &= q[3] = p_{13}(1-u)(1-w) + p_{23}(1-u)w + p_{33}u(1-w) + p_{43}uw && (3.52)
\end{aligned}
$$

where p_{ij} is given by

$$
[p] = \begin{bmatrix} p_{11} & p_{12} & p_{13} & 1 \\ p_{21} & p_{22} & p_{23} & 1 \\ p_{31} & p_{32} & p_{33} & 1 \\ p_{41} & p_{42} & p_{43} & 1 \end{bmatrix} = \begin{bmatrix} \mathbf{p}(0,0) \\ \mathbf{p}(0,1) \\ \mathbf{p}(1,0) \\ \mathbf{p}(1,1) \end{bmatrix} = \begin{bmatrix} \begin{bmatrix} r_1\cos u & r_1\sin u & 0 & 1 \\ r_1\cos u & r_1\sin u & -l_1 & 1 \end{bmatrix} [T_0^1] \\ \begin{bmatrix} r_2\cos r & r_2\sin r & 0 & 1 \\ r_2\cos r & r_2\sin r & -l_2 & 1 \end{bmatrix} [T_0^2] \end{bmatrix} \tag{3.53}
$$

The expressions for $\mathbf{p}(0,0)$, $\mathbf{p}(0,1)$, $\mathbf{p}(1,0)$ and $\mathbf{p}(1,1)$ in the above equation are given in Eqs. (3.28) and (3.29). The coordinates p_{ij} in the above equation are with respect to the base frame XYZ. Therefore, the points on the surface $\mathbf{q}$ are also given with respect to the frame XYZ.

Equations (3.5) and (3.6) give

$$
\begin{aligned}
\left[T_0^1\right] &= T_0^1\left(a_1, b_1, c_1, \alpha_1, \beta_1\right) && (3.54)\\
\left[T_0^2\right] &= T_0^2\left(a_2, b_2, c_2, \alpha_2, \beta_2\right) && (3.55)
\end{aligned}
$$

Therefore,

$$
\begin{aligned}
p_{1i} \text{ and } p_{2i} &\rightarrow \text{fn}(a_1, b_1, c_1, \alpha_1, \beta_1, r_1, l_1, u) \quad \text{i} = 1 \text{ to } 4 && (3.56)\\
p_{3i} \text{ and } p_{4i} &\rightarrow \text{fn}(a_2, b_2, c_2, \alpha_2, \beta_2, r_2, l_2, r) \quad \text{i} = 1 \text{ to } 4 && (3.57)
\end{aligned}
$$

The parameters u and r in the expressions for p_{ij} are the solution of Eqs. (3.12) and (3.13). Rewriting Eqs. (3.12) and (3.13)

$$
(y_2 - y_1)\sin u + (x_2 - x_1)\cos u = 0
$$

$$
\begin{vmatrix} -a_{11}\sin r + a_{21}\cos r & -a_{12}\sin r + a_{22}\cos r & -a_{13}\sin r + a_{23}\cos r \\ -a_{31}l_2 & -a_{32}l_2 & -a_{33}l_2 \\ x_2 - x_1 & y_2 - y_1 & z_2 \end{vmatrix} = 0
$$

where

$$
\begin{aligned}
x_1 &= r_1\cos u\\
y_1 &= r_1\sin u\\
x_2 &= r_2(a_{11}\cos r + a_{21}\sin r) + a_{41}\\
y_2 &= r_2(a_{12}\cos r + a_{22}\sin r) + a_{42}\\
z_2 &= r_2(a_{13}\cos r + a_{23}\sin r) + a_{43}
\end{aligned}
$$

Therefore,

$$x = q[1] = p_{11}(1-u)(1-w) + p_{21}(1-u)w + p_{31}u(1-w) + p_{41}uw \quad (3.50)$$

$$y = q[2] = p_{12}(1-u)(1-w) + p_{22}(1-u)w + p_{32}u(1-w) + p_{42}uw \quad (3.51)$$

$$z = q[3] = p_{13}(1-u)(1-w) + p_{23}(1-u)w + p_{33}u(1-w) + p_{43}uw \quad (3.52)$$

where p_{ij} is given by

$$[p] = \begin{bmatrix} p_{11} & p_{12} & p_{13} & 1 \\ p_{21} & p_{22} & p_{23} & 1 \\ p_{31} & p_{32} & p_{33} & 1 \\ p_{41} & p_{42} & p_{43} & 1 \end{bmatrix} = \begin{bmatrix} \mathbf{p}(0,0) \\ \mathbf{p}(0,1) \\ \mathbf{p}(1,0) \\ \mathbf{p}(1,1) \end{bmatrix} = \begin{bmatrix} \begin{bmatrix} r_1\cos u & r_1\sin u & 0 & 1 \\ r_1\cos u & r_1\sin u & -l_1 & 1 \end{bmatrix} [T_0^1] \\ \begin{bmatrix} r_2\cos r & r_2\sin r & 0 & 1 \\ r_2\cos r & r_2\sin r & -l_2 & 1 \end{bmatrix} [T_0^2] \end{bmatrix} \quad (3.53)$$

The expressions for $\mathbf{p}(0,0)$, $\mathbf{p}(0,1)$, $\mathbf{p}(1,0)$ and $\mathbf{p}(1,1)$ in the above equation are given in Eqs. (3.28) and (3.29). The coordinates p_{ij} in the above equation are with respect to the base frame XYZ. Therefore, the points on the surface $\mathbf{q}$ are also given with respect to the frame XYZ.

Equations (3.5) and (3.6) give

$$[T_0^1] = T_0^1(a_1, b_1, c_1, \alpha_1, \beta_1) \quad (3.54)$$

$$[T_0^2] = T_0^2(a_2, b_2, c_2, \alpha_2, \beta_2) \quad (3.55)$$

Therefore,

$$p_{1i} \text{ and } p_{2i} \rightarrow \text{fn}(a_1, b_1, c_1, \alpha_1, \beta_1, r_1, l_1, u) \quad i = 1 \text{ to } 4 \quad (3.56)$$

$$p_{3i} \text{ and } p_{4i} \rightarrow \text{fn}(a_2, b_2, c_2, \alpha_2, \beta_2, r_2, l_2, r) \quad i = 1 \text{ to } 4 \quad (3.57)$$

The parameters u and r in the expressions for p_{ij} are the solution of Eqs. (3.12) and (3.13). Rewriting Eqs. (3.12) and (3.13)

$$(y_2 - y_1)\sin u + (x_2 - x_1)\cos u = 0$$

$$\begin{vmatrix} -a_{11}\sin r + a_{21}\cos r & -a_{12}\sin r + a_{22}\cos r & -a_{13}\sin r + a_{23}\cos r \\ -a_{31}l_2 & -a_{32}l_2 & -a_{33}l_2 \\ x_2 - x_1 & y_2 - y_1 & z_2 \end{vmatrix} = 0$$

where

$$x_1 = r_1\cos u$$

$$y_1 = r_1\sin u$$

$$x_2 = r_2(a_{11}\cos r + a_{21}\sin r) + a_{41}$$

$$y_2 = r_2(a_{12}\cos r + a_{22}\sin r) + a_{42}$$

$$z_2 = r_2(a_{13}\cos r + a_{23}\sin r) + a_{43}$$

In the above expressions (x_1, y_1) and (x_2, y_2, z_2) are coordinates with respect to the frame $X_1Y_1Z_1$.

Let Eq. (3.13) be represented by

$$\begin{vmatrix} f_{11} & f_{12} & f_{13} \\ f_{21} & f_{22} & f_{23} \\ f_{31} & f_{32} & f_{33} \end{vmatrix} = 0 \tag{3.58}$$

Differentiating Eqs. (3.12) and (3.58) with respect to the random variables V_i gives

$$\frac{\partial (y_2 - y_1)}{\partial Vi} \sin u + (y_2 - y_1) \cos u \frac{\partial u}{\partial Vi} + \frac{\partial (x_2 - x_1)}{\partial Vi} \cos u - (x_2 - x_1) \sin u \frac{\partial u}{\partial Vi} = 0 \tag{3.59}$$

$$\begin{vmatrix} f'_{11} & f'_{12} & f'_{13} \\ f_{21} & f_{22} & f_{23} \\ f_{31} & f_{32} & f_{33} \end{vmatrix} + \begin{vmatrix} f_{11} & f_{12} & f_{13} \\ f'_{21} & f'_{22} & f'_{23} \\ f_{31} & f_{32} & f_{33} \end{vmatrix} + \begin{vmatrix} f_{11} & f_{12} & f_{13} \\ f_{21} & f_{22} & f_{23} \\ f'_{31} & f'_{32} & f'_{33} \end{vmatrix} = 0 \tag{3.60}$$

where prime denotes derivative with respect to V_i

Equations (3.59) and (3.60) involve derivatives of the elements of the matrix $[T_1^2]$, given by Eq. (3.7). Let $[T_1^2]$ in Eq. (3.7) be represented by

$$[T_1^2] = \begin{bmatrix} a_{11} & a_{12} & a_{13} & 0 \\ a_{21} & a_{22} & a_{23} & 0 \\ a_{31} & a_{32} & a_{33} & 0 \\ a_{41} & a_{42} & a_{43} & 1 \end{bmatrix} \tag{3.61}$$

Equation (3.7) gives $[T_1^2]$ in terms of the mean values of the variables V_i. In terms of the variables V_i, a_{ij} is given by

$$a_{ij} = a_{ij}(V_1, V_2, \ldots, V_5, V_8, V_9, \ldots, V_{12}) \tag{3.62}$$

In addition to $V_1, V_2, \ldots, V_5$ and $V_8, V_9, \ldots, V_{12}$ the coordinates of x_1, y_1, x_2, y_2 and z_2 are functions of $V_6 = r_1$ and $V_{13} = r_2$ (and, of course, u and r). Hence Eqs. (3.12) and (3.13) which are two equations in two variables u and r, involve V_1 to V_{13} except V_7, i.e.,

$$u = u(V_1, V_2, \ldots, V_6, V_8, V_9, \ldots, V_{13}) \tag{3.63}$$

$$r = r(V_1, V_2, \ldots, V_6, V_8, V_9, \ldots, V_{13}) \tag{3.64}$$

Also

$$x_1, y_1, x_2, y_2, z_2 \rightarrow \text{fn}(V_1, V_2, \ldots, V_6, V_8, V_9, \ldots, V_{13}) \tag{3.65}$$

Partial derivatives of the elements of $[T_1^2]$ and x_1, y_1, x_2, y_2 and z_2 with respect to the variables V_i are derived in the following subsections. These derivatives are needed in solving Eqs. (3.59) and (3.60) for $\frac{\partial u}{\partial V_i}$ and $\frac{\partial r}{\partial V_i}$ for all V_i's. The derivatives $\frac{\partial u}{\partial V_i}$ and $\frac{\partial r}{\partial V_i}$ are needed for the influence coefficients $\frac{\partial x}{\partial V_i}$, $\frac{\partial y}{\partial V_i}$ and $\frac{\partial z}{\partial V_i}$.

3.2.1 Partial Derivatives of the Elements of $[T_1^2]$

Equation (3.7) gives $[T_1^2]$ in terms of the mean values of the random variables. The elements a_{ij} of $[T_1^2]$ are given by Eq. (3.61). The expressions for each a_{ij} is written comparing Eqs. (3.7) and (3.61). The partial derivatives of a_{ij} is derived at the mean values of random variables in the following.

$$a_{11} = \cos(V_5 - V_{12})$$

Hence,

$$\begin{aligned}
\left.\frac{\partial a_{11}}{\partial V_5}\right|_m &= -\sin(\beta_1 - \beta_2) \\
\left.\frac{\partial a_{11}}{\partial V_{12}}\right|_m &= \sin(\beta_1 - \beta_2) \\
\left.\frac{\partial a_{11}}{\partial V_i}\right|_m &= 0 \qquad \text{i} = 1 \text{ to } 4,\ 6 \text{ to } 11,\ 13 \text{ to } 19
\end{aligned} \tag{3.66}$$

$$a_{12} = \sin V_4 \sin(V_5 - V_{12})$$

Hence,

$$\begin{aligned}
\left.\frac{\partial a_{12}}{\partial V_4}\right|_m &= \cos\alpha_1 \sin(\beta_1 - \beta_2) \\
\left.\frac{\partial a_{12}}{\partial V_5}\right|_m &= \sin\alpha_1 \cos(\beta_1 - \beta_2) \\
\left.\frac{\partial a_{12}}{\partial V_{12}}\right|_m &= -\sin\alpha_1 \cos(\beta_1 - \beta_2) \\
\left.\frac{\partial a_{12}}{\partial V_i}\right|_m &= 0 \qquad \text{i} = 1 \text{ to } 3,\ 6 \text{ to } 11,\ 13 \text{ to } 19
\end{aligned} \tag{3.67}$$

$$a_{13} = \cos V_4 \sin(V_5 - V_{12})$$

Hence,

$$\begin{aligned}
\left.\frac{\partial a_{13}}{\partial V_4}\right|_m &= -\sin\alpha_1 \sin(\beta_1 - \beta_2) \\
\left.\frac{\partial a_{13}}{\partial V_5}\right|_m &= \cos\alpha_1 \cos(\beta_1 - \beta_2) \\
\left.\frac{\partial a_{13}}{\partial V_{12}}\right|_m &= -\cos\alpha_1 \cos(\beta_1 - \beta_2) \\
\left.\frac{\partial a_{13}}{\partial V_i}\right|_m &= 0 \qquad \text{i} = 1 \text{ to } 3,\ 6 \text{ to } 11,\ 13 \text{ to } 19
\end{aligned} \tag{3.68}$$

$$a_{21} = \sin V_{11} \sin(V_{12} - V_5)$$

Hence,

$$\begin{aligned}
\left.\frac{\partial a_{21}}{\partial V_5}\right|_m &= -\sin\alpha_2 \cos(\beta_2 - \beta_1) \\
\left.\frac{\partial a_{21}}{\partial V_{11}}\right|_m &= \cos\alpha_2 \sin(\beta_2 - \beta_1) \\
\left.\frac{\partial a_{21}}{\partial V_{12}}\right|_m &= \sin\alpha_2 \cos(\beta_2 - \beta_1) \\
\left.\frac{\partial a_{21}}{\partial V_i}\right|_m &= 0 \qquad \text{i = 1 to 4, 6 to 10, 13 to 19}
\end{aligned} \tag{3.69}$$

$$a_{22} = \sin V_4 \sin V_{12} \cos(V_5 - V_{12}) + \cos V_4 \cos V_{11}$$

Hence,

$$\begin{aligned}
\left.\frac{\partial a_{22}}{\partial V_4}\right|_m &= \cos\alpha_1 \sin\alpha_2 \cos(\beta_1 - \beta_2) - \sin\alpha_1 \cos\alpha_2 \\
\left.\frac{\partial a_{22}}{\partial V_5}\right|_m &= -\sin\alpha_1 \sin\alpha_2 \sin(\beta_1 - \beta_2) \\
\left.\frac{\partial a_{22}}{\partial V_{11}}\right|_m &= \sin\alpha_1 \cos\alpha_2 \cos(\beta_1 - \beta_2) - \cos\alpha_1 \sin\alpha_2 \\
\left.\frac{\partial a_{22}}{\partial V_{12}}\right|_m &= \sin\alpha_1 \sin\alpha_2 \sin(\beta_1 - \beta_2) \\
\left.\frac{\partial a_{22}}{\partial V_i}\right|_m &= 0 \qquad \text{i = 1 to 3, 6 to 10, 13 to 19}
\end{aligned} \tag{3.70}$$

$$a_{23} = \sin V_{11} \cos V_4 \cos(V_5 - V_{12}) - \sin V_4 \cos V_{11}$$

Hence,

$$\begin{aligned}
\left.\frac{\partial a_{23}}{\partial V_4}\right|_m &= -\sin\alpha_1 \sin\alpha_2 \cos(\beta_1 - \beta_2) - \cos\alpha_1 \cos\alpha_2 \\
\left.\frac{\partial a_{23}}{\partial V_5}\right|_m &= -\cos\alpha_1 \sin\alpha_2 \sin(\beta_1 - \beta_2) \\
\left.\frac{\partial a_{23}}{\partial V_{11}}\right|_m &= \cos\alpha_1 \cos\alpha_2 \cos(\beta_1 - \beta_2) + \sin\alpha_1 \sin\alpha_2 \\
\left.\frac{\partial a_{23}}{\partial V_{12}}\right|_m &= \cos\alpha_1 \sin\alpha_2 \sin(\beta_1 - \beta_2) \\
\left.\frac{\partial a_{23}}{\partial V_i}\right|_m &= 0 \qquad \text{i = 1 to 3, 6 to 10, 13, to 19}
\end{aligned} \tag{3.71}$$

$$a_{31} = \cos V_{11} \sin(V_{12} - V_5)$$

Hence,

$$\begin{aligned}
\left.\frac{\partial a_{31}}{\partial V_5}\right|_m &= -\cos\alpha_2 \cos(\beta_2 - \beta_1) \\
\left.\frac{\partial a_{31}}{\partial V_{11}}\right|_m &= -\sin\alpha_2 \sin(\beta_2 - \beta_1) \\
\left.\frac{\partial a_{31}}{\partial V_{12}}\right|_m &= \cos\alpha_2 \cos(\beta_2 - \beta_1) \\
\left.\frac{\partial a_{31}}{\partial V_i}\right|_m &= 0 \qquad \mathrm{i} = 1 \text{ to } 4,\ 6 \text{ to } 10,\ 13 \text{ to } 19
\end{aligned} \tag{3.72}$$

$$a_{32} = \sin V_4 \cos V_{11} \cos(V_5 - V_{12}) - \cos V_4 \cos V_{11}$$

Hence,

$$\begin{aligned}
\left.\frac{\partial a_{32}}{\partial V_4}\right|_m &= \cos\alpha_1 \cos\alpha_2 \cos(\beta_1 - \beta_2) + \sin\alpha_1 \sin\alpha_2 \\
\left.\frac{\partial a_{32}}{\partial V_5}\right|_m &= -\sin\alpha_1 \cos\alpha_2 \sin(\beta_1 - \beta_2) \\
\left.\frac{\partial a_{32}}{\partial V_{11}}\right|_m &= -\sin\alpha_1 \sin\alpha_2 \cos(\beta_1 - \beta_2) - \cos\alpha_1 \cos\alpha_2 \\
\left.\frac{\partial a_{32}}{\partial V_{12}}\right|_m &= \sin\alpha_1 \cos\alpha_2 \sin(\beta_1 - \beta_2) \\
\left.\frac{\partial a_{32}}{\partial V_i}\right|_m &= 0 \qquad \mathrm{i} = 1 \text{ to } 3,\ 6 \text{ to } 10,\ 13 \text{ to } 19
\end{aligned} \tag{3.73}$$

$$a_{33} = \cos V_4 \cos V_{11} \cos(V_5 - V_{12}) + \sin V_4 \sin V_{11}$$

Hence,

$$\begin{aligned}
\left.\frac{\partial a_{33}}{\partial V_4}\right|_m &= -\sin\alpha_1 \cos\alpha_2 \cos(\beta_1 - \beta_2) + \cos\alpha_1 \sin\alpha_2 \\
\left.\frac{\partial a_{33}}{\partial V_5}\right|_m &= -\cos\alpha_1 \cos\alpha_2 \sin(\beta_1 - \beta_2) \\
\left.\frac{\partial a_{33}}{\partial V_{11}}\right|_m &= -\cos\alpha_1 \sin\alpha_2 \cos(\beta_1 - \beta_2) + \sin\alpha_1 \cos\alpha_2 \\
\left.\frac{\partial a_{33}}{\partial V_{12}}\right|_m &= \cos\alpha_1 \cos\alpha_2 \sin(\beta_1 - \beta_2) \\
\left.\frac{\partial a_{33}}{\partial V_i}\right|_m &= 0 \qquad \mathrm{i} = 1 \text{ to } 3,\ 6 \text{ to } 10,\ 13 \text{ to } 19
\end{aligned} \tag{3.74}$$

$$a_{41} = (V_8 - V_1)\cos V_5 + (V_9 - V_2)\sin V_5$$

Hence,

$$\begin{aligned}
\left.\frac{\partial a_{41}}{\partial V_1}\right|_m &= -\cos\beta_1 \\
\left.\frac{\partial a_{41}}{\partial V_2}\right|_m &= -\sin\beta_1 \\
\left.\frac{\partial a_{41}}{\partial V_5}\right|_m &= -(a_2 - a_1)\sin\beta_1 + (b_2 - b_1)\cos\beta_1 \\
\left.\frac{\partial a_{41}}{\partial V_8}\right|_m &= \cos\beta_1 \\
\left.\frac{\partial a_{41}}{\partial V_9}\right|_m &= \sin\beta_1 \\
\left.\frac{\partial a_{41}}{\partial V_i}\right|_m &= 0 \qquad \text{i} = 3,\ 4,\ 6,\ 7,\ 10 \text{ to } 19
\end{aligned} \tag{3.75}$$

$$a_{42} = (V_8 - V_1)\sin V_4 \sin V_5 - (V_9 - V_2)\sin V_4 \cos V_5 + (V_{10} - V_3)\cos V_4$$

Hence,

$$\begin{aligned}
\left.\frac{\partial a_{42}}{\partial V_1}\right|_m &= -\sin\alpha_1 \sin\beta_1 \\
\left.\frac{\partial a_{42}}{\partial V_2}\right|_m &= \sin\alpha_1 \cos\beta_1 \\
\left.\frac{\partial a_{42}}{\partial V_3}\right|_m &= -\cos\alpha_1 \\
\left.\frac{\partial a_{42}}{\partial V_4}\right|_m &= (a_2 - a_1)\cos\alpha_1 \sin\beta_1 - (b_2 - b_1)\cos\alpha_1 \cos\beta_1 - (c_2 - c_1)\sin\alpha_1 \\
\left.\frac{\partial a_{42}}{\partial V_5}\right|_m &= (a_2 - a_1)\sin\alpha_1 \cos\beta_1 + (b_2 - b_1)\sin\alpha_1 \sin\beta_1 \\
\left.\frac{\partial a_{42}}{\partial V_8}\right|_m &= \sin\alpha_1 \sin\beta_1 \\
\left.\frac{\partial a_{42}}{\partial V_9}\right|_m &= -\sin\alpha_1 \cos\beta_1 \\
\left.\frac{\partial a_{42}}{\partial V_{10}}\right|_m &= \cos\alpha_1 \\
\left.\frac{\partial a_{42}}{\partial V_i}\right|_m &= 0 \qquad \text{i} = 6,\ 7,\ 11 \text{ to } 19
\end{aligned} \tag{3.76}$$

$$a_{43} = (V_8 - V_1)\cos V_4 \sin V_5 - (V_9 - V_2)\cos V_4 \cos V_5 - (V_{10} - V_3)\sin V_4$$

Hence,

$$
\begin{aligned}
\left.\frac{\partial a_{43}}{\partial V_1}\right|_m &= -\cos\alpha_1 \sin\beta_1 \\
\left.\frac{\partial a_{43}}{\partial V_2}\right|_m &= \cos\alpha_1 \cos\beta_1 \\
\left.\frac{\partial a_{43}}{\partial V_3}\right|_m &= \sin\alpha_1 \\
\left.\frac{\partial a_{43}}{\partial V_4}\right|_m &= -(a_2 - a_1)\sin\alpha_1 \sin\beta_1 + (b_2 - b_1)\sin\alpha_1 \cos\beta_1 - (c_2 - c_1)\cos\alpha_1 \\
\left.\frac{\partial a_{43}}{\partial V_5}\right|_m &= (a_2 - a_1)\cos\alpha_1 \cos\beta_1 + (b_2 - b_1)\cos\alpha_1 \sin\beta_1 \\
\left.\frac{\partial a_{43}}{\partial V_8}\right|_m &= \cos\alpha_1 \sin\beta_1 \\
\left.\frac{\partial a_{43}}{\partial V_9}\right|_m &= -\cos\alpha_1 \cos\beta_1 \\
\left.\frac{\partial a_{43}}{\partial V_{10}}\right|_m &= -\sin\alpha_1 \\
\left.\frac{\partial a_{43}}{\partial V_i}\right|_m &= 0 \qquad \text{i} = 6,\ 7,\ 11 \text{ to } 19
\end{aligned}
\tag{3.77}
$$

$$a_{j4} = \text{constant} \qquad \text{j} = 1 \text{ to } 4$$

Hence,

$$\left.\frac{\partial a_{j4}}{\partial V_i}\right|_m = 0 \qquad \text{j} = 1 \text{ to } 4, \quad \text{i} = 1 \text{ to } 19. \tag{3.78}$$

This completes the derivation of partial derivatives of the elements of matrix $[T_1^2]$ needed for solving Eqs. (3.59) and (3.60). The partial derivatives of x_1, y_1, x_2, y_2 and z_2, which are also needed to solve the two equations, are derived in the following subsection.

3.2.2 Partial Derivatives of x_1, y_1, x_2, y_2 and z_2

The coordinates x_1, y_1, x_2, y_2 and z_2 are given by Eqs. (3.14), (3.15), (3.16), (3.17) and (3.18) in terms of the mean values of the random variables V_i. These coordinates involve the parameters u and r. From Eqs. (3.63) and (3.64),

$$
\begin{aligned}
u &= u\,(V_1, V_2, \ldots, V_6, V_8, V_9, \ldots, V_{13}) \\
r &= r\,(V_1, V_2, \ldots, V_6, V_8, V_9, \ldots, V_{13})
\end{aligned}
$$

Also

$$a_{ij} = a_{ij}\left(V_1, V_2, \ldots, V_5, V_8, V_9, \ldots, V_{12}\right)$$

Keeping these in mind the partial derivatives of the coordinates at the mean values of the random variables are derived in the following:

(i)

$$x_1 = V_6 \cos u$$

Hence,

$$\begin{aligned}
\left.\frac{\partial x_1}{\partial V_6}\right|_m &= \cos u - r_1 \sin u \left.\frac{\partial u}{\partial V_6}\right|_m \\
\left.\frac{\partial x_1}{\partial V_i}\right|_m &= -r_1 \sin u \left.\frac{\partial u}{\partial V_i}\right|_m \qquad \text{i} = 1 \text{ to } 5,\ 8 \text{ to } 13 \\
\left.\frac{\partial x_1}{\partial V_i}\right|_m &= 0 \qquad \text{i} = 7,\ 14 \text{ to } 19
\end{aligned} \tag{3.79}$$

(ii)

$$y_1 = V_6 \sin u$$

Hence,

$$\begin{aligned}
\left.\frac{\partial y_1}{\partial V_6}\right|_m &= \sin u + r_1 \cos u \left.\frac{\partial u}{\partial V_6}\right|_m \\
\left.\frac{\partial y_1}{\partial V_i}\right|_m &= r_1 \cos u \left.\frac{\partial u}{\partial v_i}\right|_m \qquad \text{i} = 1 \text{ to } 5,\ 8 \text{ to } 13 \\
\left.\frac{\partial y_1}{\partial V_i}\right|_m &= 0 \qquad \text{i} = 7,\ 14 \text{ to } 19
\end{aligned} \tag{3.80}$$

(iii)

$$x_2 = V_{13}(a_{11} \cos r + a_{21} \sin r) + a_{41}$$

Since a_{ij} is not a function of $V_{13} = r_2$, but r is a function of $V_{13} = r_2$, therefore, it follows that

$$\begin{aligned}
\left.\frac{\partial x_2}{\partial V_6}\right|_m &= r_2(-a_{11} \sin r + a_{21} \cos r) \left.\frac{\partial r}{\partial V_6}\right|_m \\
\left.\frac{\partial x_2}{\partial V_i}\right|_m &= r_2(-a_{11} \sin r + a_{21} \cos r) \left.\frac{\partial r}{\partial V_i}\right|_m + r_2(\left.\frac{\partial a_{11}}{\partial V_i}\right|_m \cos r + \left.\frac{\partial a_{21}}{\partial V_i}\right|_m \sin r) \\
&\quad + \left.\frac{\partial a_{41}}{\partial V_i}\right|_m \qquad \text{i} = 1 \text{ to } 5,\ 8 \text{ to } 12 \\
\left.\frac{\partial x_2}{\partial V_{13}}\right|_m &= a_{11} \cos r + a_{21} \sin r + r_2(-a_{11} \sin r + a_{21} \cos r) \left.\frac{\partial r}{\partial V_{13}}\right|_m \\
\left.\frac{\partial x_2}{\partial V_i}\right|_m &= 0 \qquad \text{i} = 7,\ 14 \text{ to } 19
\end{aligned} \tag{3.81}$$

(iv)

$$y_2 = V_{13}(a_{12}\cos r + a_{22}\sin r) + a_{42}$$

Hence,

$$\begin{aligned}
\left.\frac{\partial y_2}{\partial V_6}\right|_m &= r_2(-a_{12}\sin r + a_{22}\cos r)\left.\frac{\partial r}{\partial V_6}\right|_m \\
\left.\frac{\partial y_2}{\partial V_i}\right|_m &= r_2(-a_{12}\sin r + a_{22}\cos r)\left.\frac{\partial r}{\partial V_i}\right|_m + r_2(\left.\frac{\partial a_{12}}{\partial V_i}\right|_m \cos r + \left.\frac{\partial a_{22}}{\partial V_i}\right|_m \sin r) \\
&\quad + \left.\frac{\partial a_{42}}{\partial V_i}\right|_m \qquad \text{i} = 1 \text{ to } 5,\ 8 \text{ to } 12 \\
\left.\frac{\partial y_2}{\partial V_{13}}\right|_m &= a_{12}\cos r + a_{22}\sin r + r_2(-a_{12}\sin r + a_{22}\cos r)\left.\frac{\partial r}{\partial V_{13}}\right|_m \\
\left.\frac{\partial y_2}{\partial V_i}\right|_m &= 0 \qquad \text{i} = 7,\ 14 \text{ to } 19
\end{aligned} \tag{3.82}$$

(v)

$$z_2 = V_{13}(a_{13}\cos r + a_{23}\sin r) + a_{43}$$

Hence,

$$\begin{aligned}
\left.\frac{\partial z_2}{\partial V_6}\right|_m &= r_2(-a_{13}\sin r + a_{23}\cos r)\left.\frac{\partial r}{\partial V_6}\right|_m \\
\left.\frac{\partial z_2}{\partial V_i}\right|_m &= r_2(-a_{13}\sin r + a_{23}\cos r)\left.\frac{\partial r}{\partial V_i}\right|_m + r_2(\left.\frac{\partial a_{13}}{\partial V_i}\right|_m \cos r + \left.\frac{\partial a_{23}}{\partial V_i}\right|_m \sin r) \\
&\quad + \left.\frac{\partial a_{43}}{\partial V_i}\right|_m \qquad \text{i} = 1 \text{ to } 5,\ 8 \text{ to } 12 \\
\left.\frac{\partial z_2}{\partial V_{13}}\right|_m &= a_{13}\cos r + a_{23}\sin r + r_2(-a_{13}\sin r + a_{23}\cos r)\left.\frac{\partial r}{\partial V_{13}}\right|_m \\
\left.\frac{\partial z_2}{\partial V_i}\right|_m &= 0 \qquad \text{i} = 7,\ 14 \text{ to } 19
\end{aligned} \tag{3.83}$$

3.2.3 Partial Derivatives of the Elements f_{ij}

Consider Eq. (3.58) which is a representation of Eq. (3.13). The derivatives of the elements f_{ij} in Eq. (3.58) are needed in solving Eqs. (3.59) and (3.60). Expressions for f_{ij} are written and differentiated in the following:

(i) The elements f_{1j} for j=1,2,3 are given by

$$f_{1j} = -a_{1j}\sin r + a_{2j}\cos r \qquad \text{j} = 1,2,3$$

Hence,

$$\begin{aligned}
\frac{\partial f_{1j}}{\partial V_i} &= (-a_{1j}\cos r - a_{2j}\sin r)\frac{\partial r}{\partial V_i} + (-\frac{\partial a_{1j}}{\partial V_i}\sin r + \frac{\partial a_{2j}}{\partial V_i}\cos r) \\
& \qquad \mathrm{j} = 1,2,3. \quad \mathrm{i} = 1 \text{ to } 5,\ 8 \text{ to } 12 \\
\frac{\partial f_{1j}}{\partial V_i} &= (-a_{1j}\cos r - a_{2j}\sin r)\frac{\partial r}{\partial V_i} \qquad \mathrm{j} = 1,2,3. \quad \mathrm{i} = 6,13 \\
\frac{\partial f_{1j}}{\partial V_i} &= 0 \qquad \mathrm{j} = 1,2,3. \quad \mathrm{i} = 7,\ 14 \text{ to } 19
\end{aligned} \tag{3.84}$$

(ii) The elements f_{2j} for j=1,2,3 are given by

$$f_{2j} = a_{3j} \qquad \mathrm{j} = 1,2,3$$

Hence,

$$\frac{\partial f_{2j}}{\partial V_i} = \frac{\partial a_{3j}}{\partial V_i} \qquad \mathrm{j} = 1,2,3. \quad \mathrm{i} = 1 \text{ to } 19 \tag{3.85}$$

(iii)

$$f_{31} = x_2 - x_1$$

Hence,

$$\frac{\partial f_{31}}{\partial V_i} = \frac{\partial x_2}{\partial V_i} - \frac{\partial x_1}{\partial V_i} \qquad \mathrm{i} = 1 \text{ to } 19 \tag{3.86}$$

where $\frac{\partial x_1}{\partial V_i}$ and $\frac{\partial x_2}{\partial V_i}$ are given by Eqs. (3.79) and (3.81) respectively.

(iv)

$$f_{32} = y_2 - y_1$$

Hence,

$$\frac{\partial f_{32}}{\partial V_i} = \frac{\partial y_2}{\partial V_i} - \frac{\partial y_1}{\partial V_i} \qquad \mathrm{i} = 1 \text{ to } 19 \tag{3.87}$$

where $\frac{\partial y_1}{\partial V_i}$ and $\frac{\partial y_2}{\partial V_i}$ are given by Eqs. (3.80) and (3.82) respectively.

(v) Finally,

$$f_{33} = z_2$$

Hence,

$$\frac{\partial f_{33}}{\partial V_i} = \frac{\partial z_2}{\partial V_i} \qquad \mathrm{i} = 1 \text{ to } 19 \tag{3.88}$$

where $\frac{\partial z_2}{\partial V_i}$ is given by Eqs. (3.83).

3.2.4 Partial Derivatives of the Parameters u and r

The partial derivatives of the parameters u and r with respect to a variable V_i are the solution of Eqs. (3.59) and (3.60). The two equations are to be solved one by one for each variable V_i to obtain $\frac{\partial u}{\partial V_i}$ and $\frac{\partial r}{\partial V_i}$, i=1 to 19. Rewriting the equations gives

$$\frac{\partial\left(y_2-y_1\right)}{\partial V_i}\sin u+\left(y_2-y_1\right)\cos u\frac{\partial u}{\partial V_i}+\frac{\partial\left(x_2-x_1\right)}{\partial V_i}\cos u$$
$$-\left(x_2-x_1\right)\sin u\frac{\partial u}{\partial Vi} = 0 \qquad i=1\text{ to }19$$

$$\begin{vmatrix} f'_{11} & f'_{12} & f'_{13} \\ f_{21} & f_{22} & f_{23} \\ f_{31} & f_{32} & f_{33} \end{vmatrix} + \begin{vmatrix} f_{11} & f_{12} & f_{13} \\ f'_{21} & f'_{22} & f'_{23} \\ f_{31} & f_{32} & f_{33} \end{vmatrix} + \begin{vmatrix} f_{11} & f_{12} & f_{13} \\ f_{21} & f_{22} & f_{23} \\ f'_{31} & f'_{32} & f'_{33} \end{vmatrix} = 0$$

where prime denotes derivative with respect to V_i, i=1 to 19.

The terms in the above two equations contain the partial derivatives $\frac{\partial u}{\partial V_i}$ and $\frac{\partial r}{\partial V_i}$. There is no multiplication of these two derivatives. Hence, the above two equations have linear terms of $\frac{\partial u}{\partial V_i}$ and $\frac{\partial r}{\partial V_i}$ for a particular V_i. The two equations are not linear in u and r because the trigonometric functions of u and r are also present in the equations. But the two equations are solved for particular values of the parameters u and r. The parameters u and r in these equations correspond to the tangent line AC, as shown in Fig. (3.5). Their values are given by $u = u_A$ and $r = r_C$. Therefore, the two equations are linear in $\frac{\partial u}{\partial V_i}$ and $\frac{\partial r}{\partial V_i}$ for a particular V_i.

Even though Eqs. (3.59) and (3.60) are linear in $\frac{\partial u}{\partial V_i}$ and $\frac{\partial r}{\partial V_i}$, it is a tedious process to express them explicitly in terms of these partial derivatives. This is because the derivatives of coordinates x_1, y_1, x_2, y_2 and z_2 involve $\frac{\partial u}{\partial V_i}$ and $\frac{\partial r}{\partial V_i}$, there are third order determinants involved, and moreover the process has to be repeated for the 19 variables as the derivatives of the coordinates x_1, y_1, etc, are different for these variables. Therefore, an iterative technique is needed to solve the two equations. The two equations are solved by Newton-Raphson method [97]. Since it is difficult to compute the Jacobian matrix [J] analytically, the Jacobian is found numerically by the finite difference method.

Solving the two equations by Newton-Raphson method give $\frac{\partial u}{\partial V_i}$ and $\frac{\partial r}{\partial V_i}$ at $u = u_A$ and $r = r_C$. The two equations are solved one by one for each random variable V_i.

3.2.5 Partial Derivatives of the Elements of $[T_0^1]$

The dependent variables x, y and z are given by Eqs. (3.50), (3.51) and (3.52), and involve the elements p_{ij}. The matrix [p] having elements p_{ij} is given by Eq. (3.53). Rewriting it gives

$$[p] = \begin{bmatrix} \begin{bmatrix} r_1 \cos u & r_1 \sin u & 0 & 1 \\ r_1 \cos u & r_1 \sin u & -l_1 & 1 \end{bmatrix} [T_0^1] \\ \begin{bmatrix} r_2 \cos r & r_2 \sin r & 0 & 1 \\ r_2 \cos r & r_2 \sin r & -l_2 & 1 \end{bmatrix} [T_0^2] \end{bmatrix}$$

The derivatives of p_{ij} need the derivatives of matrices $[T_0^1]$ and $[T_0^2]$. The derivatives of the elements of $[T_0^1]$, $[T_0^2]$ and [p] are found in the present and following subsections.

The matrix $[T_0^1]$, in terms of the mean values of the random variables, is given by Eq. (3.5). Writing $[T_0^1]$ in terms of the variables V_i yields

$$\left[T_0^1\right] = \begin{bmatrix} \cos V_5 & \sin V_5 & 0 & 0 \\ \sin V_4 \sin V_5 & -\sin V_4 \cos V_5 & \cos V_4 & 0 \\ \cos V_4 \sin V_5 & -\cos V_4 \cos V_5 & -\sin V_4 & 0 \\ V_1 & V_2 & V_3 & 1 \end{bmatrix} \tag{3.89}$$

It follows that

$$\left[T_0^1\right] = T_0^1 \left(V_1, V_2, \ldots, V_5\right) \tag{3.90}$$

Differentiating $[T_0^1]$ with respect to the variables V_i yields

$$
\begin{aligned}
\left.\frac{\partial\,[T_0^1]}{\partial V_1}\right|_m &= \begin{bmatrix} 0 & 0 & 0 & 0 \\ 0 & 0 & 0 & 0 \\ 0 & 0 & 0 & 0 \\ 1 & 0 & 0 & 0 \end{bmatrix} \\
\left.\frac{\partial\,[T_0^1]}{\partial V_2}\right|_m &= \begin{bmatrix} 0 & 0 & 0 & 0 \\ 0 & 0 & 0 & 0 \\ 0 & 0 & 0 & 0 \\ 0 & 1 & 0 & 0 \end{bmatrix} \\
\left.\frac{\partial\,[T_0^1]}{\partial V_3}\right|_m &= \begin{bmatrix} 0 & 0 & 0 & 0 \\ 0 & 0 & 0 & 0 \\ 0 & 0 & 0 & 0 \\ 0 & 0 & 1 & 0 \end{bmatrix} \\
\left.\frac{\partial\,[T_0^1]}{\partial V_4}\right|_m &= \begin{bmatrix} 0 & 0 & 0 & 0 \\ \cos\alpha_1 \sin\beta_1 & -\cos\alpha_1\cos\beta_1 & -\sin\alpha_1 & 0 \\ -\sin\alpha_1\sin\beta_1 & \sin\alpha_1\cos\beta_1 & -\cos\alpha_1 & 0 \\ 0 & 0 & 0 & 0 \end{bmatrix} \\
\left.\frac{\partial\,[T_0^1]}{\partial V_5}\right|_m &= \begin{bmatrix} -\sin\beta_1 & \cos\beta_1 & 0 & 0 \\ \sin\alpha_1\cos\beta_1 & \sin\alpha_1\sin\beta_1 & 0 & 0 \\ \cos\alpha_1\cos\beta_1 & \cos\alpha_1\sin\beta_1 & 0 & 0 \\ 0 & 0 & 0 & 0 \end{bmatrix} \\
\left.\frac{\partial\,[T_0^1]}{\partial V_i}\right|_m &= 0 \qquad \text{i} = 6 \text{ to } 19
\end{aligned}
\tag{3.91}
$$

3.2.6 Partial Derivatives of the Elements of $[T_0^2]$

The matrix $[T_0^2]$ in terms of the mean values of the random variables, is given by Eq. (3.6). Writing $[T_0^2]$ in terms of the variables V_i yields

$$[T_0^2] = \begin{bmatrix} \cos V_{12} & \sin V_{12} & 0 & 0 \\ \sin V_{11}\sin V_{12} & -\sin V_{11}\cos V_{12} & \cos V_{11} & 0 \\ \cos V_{11}\sin V_{12} & -\cos V_{11}\cos V_{12} & -\sin V_{11} & 0 \\ V_8 & V_9 & V_{10} & 1 \end{bmatrix} \tag{3.92}$$

It follows that

$$[T_0^2] = T_0^2\,(V_8, V_9, \ldots, V_{12}) \tag{3.93}$$

Differentiating $[T_0^2]$ with respect to the variables V_i yields

$$\begin{aligned}
\left.\frac{\partial\,[T_0^2]}{\partial V_8}\right|_m &= \begin{bmatrix} 0&0&0&0\\0&0&0&0\\0&0&0&0\\1&0&0&0 \end{bmatrix} \\
\left.\frac{\partial\,[T_0^2]}{\partial V_9}\right|_m &= \begin{bmatrix} 0&0&0&0\\0&0&0&0\\0&0&0&0\\0&1&0&0 \end{bmatrix} \\
\left.\frac{\partial\,[T_0^2]}{\partial V_{10}}\right|_m &= \begin{bmatrix} 0&0&0&0\\0&0&0&0\\0&0&0&0\\0&0&1&0 \end{bmatrix} \\
\left.\frac{\partial\,[T_0^2]}{\partial V_{11}}\right|_m &= \begin{bmatrix} 0 & 0 & 0 & 0 \\ \cos\alpha_2\sin\beta_2 & -\cos\alpha_2\cos\beta_2 & -\sin\alpha_2 & 0 \\ -\sin\alpha_2\sin\beta_2 & \sin\alpha_2\cos\beta_2 & -\cos\alpha_2 & 0 \\ 0 & 0 & 0 & 0 \end{bmatrix} \\
\left.\frac{\partial\,[T_0^2]}{\partial V_{12}}\right|_m &= \begin{bmatrix} -\sin\beta_2 & \cos\beta_2 & 0 & 0 \\ \sin\alpha_2\cos\beta_2 & \sin\alpha_2\sin\beta_2 & 0 & 0 \\ \cos\alpha_2\cos\beta_2 & \cos\alpha_2\sin\beta_2 & 0 & 0 \\ 0 & 0 & 0 & 0 \end{bmatrix} \\
\left.\frac{\partial\,[T_0^2]}{\partial V_i}\right|_m &= 0 \qquad \text{i} = 1 \text{ to } 7,\ 13 \text{ to } 19
\end{aligned} \tag{3.94}$$

3.2.7 Partial Derivatives of the Elements of [p]

The matrix [p] in terms of the mean values of the random variables is given by Eq. (3.53). Differentiating it with respect to the variables V_i yields,

$$\frac{\partial[p]}{\partial V_i} = \frac{\partial}{\partial V_i}\left[\begin{array}{c} \begin{bmatrix} V_6\cos u & V_6\sin u & 0 & 1 \\ V_6\cos u & V_6\sin u & -V_7 & 1 \end{bmatrix}[T_0^1] \\ \begin{bmatrix} V_{13}\cos r & V_{13}\sin r & 0 & 1 \\ V_{13}\cos r & V_{13}\sin r & -V_{14} & 1 \end{bmatrix}[T_0^2] \end{array}\right]$$

where as mentioned earlier,

$$\begin{aligned} u &= u\,(V_1, V_2, \ldots, V_6, V_8, V_9, \ldots, V_{13}) \\ r &= r\,(V_1, V_2, \ldots, V_6, V_8, V_9, \ldots, V_{13}) \\ \left[T_0^1\right] &= T_0^1\,(V_1, V_2, \ldots, V_5) \\ \left[T_0^2\right] &= T_0^2\,(V_8, V_9, \ldots, V_{12}) \end{aligned}$$

Keeping these in mind, it follows that

$$\left.\frac{\partial[p]}{\partial V_i}\right|_m = \left[\begin{array}{c} \begin{bmatrix} -r_1\sin u\dfrac{\partial u}{\partial V_i}+ & r_1\cos u\dfrac{\partial u}{\partial V_i} & 0 & 0 \\ -r_1\sin u\dfrac{\partial u}{\partial V_i}+ & r_1\cos u\dfrac{\partial u}{\partial V_i} & 0 & 0 \end{bmatrix}[T_0^1] \\ \begin{bmatrix} -r_2\sin r\dfrac{\partial r}{\partial V_i} & r_2\cos r\dfrac{\partial r}{\partial V_i} & 0 & 0 \\ -r_2\sin r\dfrac{\partial r}{\partial V_i} & r_2\cos r\dfrac{\partial r}{\partial V_i} & 0 & 0 \end{bmatrix}[T_0^2] \end{array}\right] + \left[\begin{array}{c} \begin{bmatrix} r_1\cos u & r_1\sin u & 0 & 1 \\ r_1\cos u & r_1\sin u & -l_1 & 1 \end{bmatrix}\left.\dfrac{\partial[T_0^1]}{\partial V_i}\right|_m \\ \begin{bmatrix} 0 & 0 & 0 & 0 \\ 0 & 0 & 0 & 0 \end{bmatrix} \end{array}\right] \quad \text{i} = 1 \text{ to } 5$$

$$\left.\frac{\partial[p]}{\partial V_6}\right|_m = \left[\begin{array}{c} \begin{bmatrix} -r_1\sin u\dfrac{\partial u}{\partial V_6}+\cos u & r_1\cos u\dfrac{\partial u}{\partial V_6}+\sin u & 0 & 0 \\ -r_1\sin u\dfrac{\partial u}{\partial V_6}+\cos u & r_1\cos u\dfrac{\partial u}{\partial V_6}+\sin u & 0 & 0 \end{bmatrix}[T_0^1] \\ \begin{bmatrix} -r_2\sin r\dfrac{\partial r}{\partial V_6} & r_2\cos r\dfrac{\partial r}{\partial V_6} & 0 & 0 \\ -r_2\sin r\dfrac{\partial r}{\partial V_6} & r_2\cos r\dfrac{\partial r}{\partial V_6} & 0 & 0 \end{bmatrix}[T_0^2] \end{array}\right]$$

$$\left.\frac{\partial[p]}{\partial V_7}\right|_m = \begin{bmatrix} 0 & 0 & 0 & 0 \\ -\cos\alpha_1\sin\beta_1 & \cos\alpha_1\cos\beta_1 & \sin\alpha_1 & 0 \\ 0 & 0 & 0 & 0 \\ 0 & 0 & 0 & 0 \end{bmatrix} \tag{3.95}$$

$$\left.\frac{\partial[p]}{\partial V_i}\right|_m = \begin{bmatrix} \begin{bmatrix} -r_1 \sin u \frac{\partial u}{\partial V_i} & r_1 \cos u \frac{\partial u}{\partial V_i} & 0 & 0 \\ -r_1 \sin u \frac{\partial u}{\partial V_i} & r_1 \cos u \frac{\partial u}{\partial V_i} & 0 & 0 \end{bmatrix} [T_0^1] \\ \begin{bmatrix} -r_2 \sin r \frac{\partial r}{\partial V_i} & r_2 \cos r \frac{\partial r}{\partial V_i} & 0 & 0 \\ -r_2 \sin r \frac{\partial r}{\partial V_i} & r_2 \cos r \frac{\partial r}{\partial V_i} & 0 & 0 \end{bmatrix} [T_0^2] \end{bmatrix} + \begin{bmatrix} \begin{bmatrix} 0 & 0 & 0 & 0 \\ 0 & 0 & 0 & 0 \end{bmatrix} \\ \begin{bmatrix} r_2 \cos r & r_2 \sin r & 0 & 1 \\ r_2 \cos r & r_2 \sin r & -l_2 & 1 \end{bmatrix} \left.\frac{\partial [T_0^2]}{\partial V_i}\right|_m \end{bmatrix} \qquad \mathrm{i} = 8 \text{ to } 12$$

$$\left.\frac{\partial[p]}{\partial V_{13}}\right|_m = \begin{bmatrix} \begin{bmatrix} -r_1 \sin u \frac{\partial u}{\partial V_{13}} & r_1 \cos u \frac{\partial u}{\partial V_{13}} & 0 & 0 \\ -r_1 \sin u \frac{\partial u}{\partial V_{13}} & r_1 \cos u \frac{\partial u}{\partial V_{13}} & 0 & 0 \end{bmatrix} [T_0^1] \\ \begin{bmatrix} -r_2 \sin r \frac{\partial r}{\partial V_{13}} + \cos r & r_2 \cos r \frac{\partial r}{\partial V_{13}} + \sin r & 0 & 0 \\ -r_2 \sin r \frac{\partial r}{\partial V_{13}} + \cos r & r_2 \cos r \frac{\partial r}{\partial V_{13}} + \sin r & 0 & 0 \end{bmatrix} [T_0^2] \end{bmatrix}$$

$$\left.\frac{\partial[p]}{\partial V_{14}}\right|_m = \begin{bmatrix} 0 & 0 & 0 & 0 \\ 0 & 0 & 0 & 0 \\ 0 & 0 & 0 & 0 \\ -\cos\alpha_2 \sin\beta_2 & \cos\alpha_2 \cos\beta_2 & \sin\alpha_2 & 0 \end{bmatrix}$$

$$\left.\frac{\partial[p]}{\partial V_i}\right|_m = 0 \qquad \mathrm{i} = 15 \text{ to } 19 \tag{3.96}$$

Hence,

$$[p] = p(V_1, V_2, \ldots, V_{14}) \tag{3.97}$$

The partial derivatives of the elements of [p] have been derived as in Eqs. (3.95) and (3.96) above.

3.2.8 Partial Derivatives of u and w

The parameters u and w on the surface **q**(u,w) are given by Eq. (3.39) and (3.40):

$$\begin{aligned} x^\star(u,w) &= 0 \\ y^\star(u,w) &= 0 \end{aligned}$$

where, from Eqs. (3.36) and (3.37)

$$\begin{aligned}\begin{bmatrix} x^\star(u,w) & y^\star(u,w) & z^\star(u,w) & 1 \end{bmatrix} &= \begin{bmatrix} x(u,w) & y(u,w) & z(u,w) & 1 \end{bmatrix}[T] \\ &= \begin{bmatrix} 1-u & u \end{bmatrix}\begin{bmatrix} \mathbf{p}(0,0) & \mathbf{p}(0,1) \\ \mathbf{p}(1,0) & \mathbf{p}(1,1) \end{bmatrix}\begin{bmatrix} 1-w \\ w \end{bmatrix}[T]\end{aligned} \tag{3.98}$$

Hence u and w are given by

$$\begin{bmatrix} 1-u & u \end{bmatrix}\begin{bmatrix} \mathbf{p}(0,0) & \mathbf{p}(0,1) \\ \mathbf{p}(1,0) & \mathbf{p}(1,1) \end{bmatrix}\begin{bmatrix} 1-w \\ w \end{bmatrix}[T] = \begin{bmatrix} 0 & 0 & z^\star(u,w) & 1 \end{bmatrix} \tag{3.99}$$

From Eq. (3.97), $[p] = p\,(V_1, V_2, \ldots, V_{14})$. Equation (3.34) gives [T] in terms of the mean values of variables V_i.

$$[T] = T\,(a_3, b_3, c_3, \theta, \phi)$$

[T], in terms of the variables V_i, is given by

$$[T] = T\,(V_{15}, V_{16} \ldots, V_{19}) \tag{3.100}$$

Hence, from Eq. (3.99) it follows that

$$u = u(V_1, V_2, \ldots, V_{19}) \tag{3.101}$$

$$w = w(V_1, V_2, \ldots, V_{19}) \tag{3.102}$$

where u and w are parameters of the surface $\mathbf{q}$(u,w).

Differentiating Eqs. (3.39) and (3.40) yields

$$\frac{\partial x^\star}{\partial V_i} = 0 \tag{3.103}$$

$$\frac{\partial y^\star}{\partial V_i} = 0 \tag{3.104}$$

where, using Eq. (3.100),

$$\begin{aligned}\begin{bmatrix} \frac{\partial x^\star}{\partial V_i} & \frac{\partial y^\star}{\partial V_i} & \frac{\partial z^\star}{\partial V_i} & 0 \end{bmatrix} &= \begin{bmatrix} \frac{\partial x}{\partial V_i} & \frac{\partial y}{\partial V_i} & \frac{\partial z}{\partial V_i} & 0 \end{bmatrix}[T] \qquad \text{i} = 1 \text{ to } 14 \\ \begin{bmatrix} \frac{\partial x^\star}{\partial V_i} & \frac{\partial y^\star}{\partial V_i} & \frac{\partial z^\star}{\partial V_i} & 0 \end{bmatrix} &= \begin{bmatrix} \frac{\partial x}{\partial V_i} & \frac{\partial y}{\partial V_i} & \frac{\partial z}{\partial V_i} & 0 \end{bmatrix}[T] \\ &\quad +[\, x \;\; y \;\; z \;\; 1 \,]\frac{\partial [T]}{\partial V_i} \qquad \text{i} = 15 \text{ to } 19\end{aligned} \tag{3.105}$$

Partial derivatives of the dependent variables x, y, and z, and those of the elements of [T] are derived in the next two subsections. For each V_i, i=1 to 19, Eqs. (3.103) and (3.104) are solved for $\frac{\partial u}{\partial V_i}$ and $\frac{\partial w}{\partial V_i}$. This gives $\frac{\partial u}{\partial V_i}$ and $\frac{\partial w}{\partial V_i}$ for all i, i=1 to 19.

Although Eqs. (3.103) and (3.104) are linear in $\frac{\partial u}{\partial V_i}$ and $\frac{\partial w}{\partial V_i}$ it is quite cumbersome to solve them by collecting the coefficients of $\frac{\partial u}{\partial V_i}$ and $\frac{\partial w}{\partial V_i}$. So an iterative technique is adopted. They are solved by Newton-Raphson method with the Jacobian computed numerically [97].

3.2.9 Partial Derivatives of the Elements of [T]

The transformation matrix [T] in terms of the mean values of the random variables is given by Eq. (3.34). Writing [T] in terms of the variables V_i yields

$$[T] = \begin{bmatrix} \cos V_{18}\cos V_{19} & -\sin V_{19} & -\sin V_{18}\cos V_{19} & 0 \\ \cos V_{18}\sin V_{19} & \cos V_{19} & -\sin V_{18}\sin V_{19} & 0 \\ \sin V_{18} & 0 & \cos V_{18} & 0 \\ \begin{array}{r} -\cos V_{18}(V_{15}\cos V_{19}+V_{16}\sin V_{19} \\ +V_{17}\tan V_{18}) \end{array} & V_{15}\sin V_{19}-V_{16}\cos V_{19} & \begin{array}{r} \sin V_{18}(V_{15}\cos V_{19}+V_{16}\sin V_{19} \\ +V_{17}\tan V_{18}) \end{array} & 1 \end{bmatrix} \tag{3.106}$$

Therefore, as in Eq. (3.100)

$$[T] = T\,(V_{15}, V_{16}, \ldots, V_{19})$$

Hence,

$$\begin{aligned}
\left.\frac{\partial [T]}{\partial V_i}\right|_m &= 0 \qquad\qquad \mathrm{i} = 1 \text{ to } 14 \\
\left.\frac{\partial [T]}{\partial V_{15}}\right|_m &= \begin{bmatrix} 0 & 0 & 0 & 0 \\ 0 & 0 & 0 & 0 \\ 0 & 0 & 0 & 0 \\ -\cos\theta\cos\phi & \sin\phi & \sin\theta\cos\phi & 0 \end{bmatrix} \\
\left.\frac{\partial [T]}{\partial V_{16}}\right|_m &= \begin{bmatrix} 0 & 0 & 0 & 0 \\ 0 & 0 & 0 & 0 \\ 0 & 0 & 0 & 0 \\ -\cos\theta\sin\phi & -\cos\phi & \sin\theta\sin\phi & 0 \end{bmatrix} \\
\left.\frac{\partial [T]}{\partial V_{17}}\right|_m &= \begin{bmatrix} 0 & 0 & 0 & 0 \\ 0 & 0 & 0 & 0 \\ 0 & 0 & 0 & 0 \\ -\sin\theta & 0 & \sin\theta\tan\theta & 0 \end{bmatrix} \\
\left.\frac{\partial [T]}{\partial V_{18}}\right|_m &= \begin{bmatrix} -\sin\theta\cos\phi & 0 & -\cos\theta\cos\phi & 0 \\ -\sin\theta\sin\phi & 0 & -\cos\theta\sin\phi & 0 \\ \cos\theta & 0 & -\sin\theta & 0 \\ \begin{array}{r} \sin\theta(a_3\cos\phi+b_3\sin\phi) \\ -c_3\cos\theta \end{array} & 0 & \begin{array}{r} \cos\theta(a_3\cos\phi+b_3\sin\phi) \\ c_3\sin\theta(1+\sec^2\theta) \end{array} & 0 \end{bmatrix} \\
\left.\frac{\partial [T]}{\partial V_{19}}\right|_m &= \begin{bmatrix} -\cos\theta\sin\phi & -\cos\phi & \sin\theta\sin\phi & 0 \\ \cos\theta\cos\phi & -\sin\phi & -\sin\theta\cos\phi & 0 \\ 0 & 0 & 0 & 0 \\ \begin{array}{r} -\cos\theta(-a_3\sin\phi \\ +b_3\cos\phi) \end{array} & a_3\cos\phi+b_3\sin\phi & \begin{array}{r} \sin\theta(-a_3\sin\phi \\ +b_3\cos\phi) \end{array} & 0 \end{bmatrix}
\end{aligned} \tag{3.107}$$

3.2.10 The Influence Coefficients $\left(\frac{\partial x}{\partial V_i}\right)^2$, $\left(\frac{\partial y}{\partial V_i}\right)^2$ and $\left(\frac{\partial z}{\partial V_i}\right)^2$

The dependent variables $[\ x \quad y \quad z \quad 1\ ] = [q]$ are given by Eqs. (3.50), (3.51) and (3.52). It follows that

$$q[j] = p_{1j}(1-u)(1-w) + p_{2j}(1-u)w + p_{3j}u(1-w) + p_{4j}uw \qquad j = 1,2,3 \tag{3.108}$$

where, as has been mentioned earlier

$$p_{ij} = p_{ij}(V_1 \text{ to} V_{14})$$

$$\begin{aligned} u &= u(V_1, V_2, \ldots, V_{19}) \\ w &= w(V_1, V_2, \ldots, V_{19}) \end{aligned}$$

Hence, differentiating q[j] in Eq. (3.108) with respect to V_i gives

$$\begin{aligned} \frac{\partial q[j]}{\partial V_i} &= \frac{\partial p_{ij}}{\partial V_i}(1-u)(1-w) + \frac{\partial p_{2j}}{\partial V_i}(1-u)w + \frac{\partial p_{3j}}{\partial V_i}u(1-w) + \frac{\partial p_{4j}}{\partial V_i}uw \\ &\quad + \left[-p_{1j}(1-w) - p_{2j}w + p_{3j}(1-w) + p_{4j}w\right]\frac{\partial u}{\partial V_i} \\ &\quad + \left[-p_{1j}(1-u) + p_{2j}(1-u) - p_{3j}u + p_{4j}u\right]\frac{\partial w}{\partial V_i} \qquad i = 1 \text{ to } 14 \\ \frac{\partial q[j]}{\partial V_i} &= \left[-p_{1j}(1-w) - p_{2j}w + p_{3j}(1-w) + p_{4j}w\right]\frac{\partial u}{\partial V_i} \\ &\quad + \left[-p_{1j}(1-u) + p_{2j}(1-u) - p_{3j}u + p_{4j}u\right]\frac{\partial w}{\partial V_i} \qquad i = 15 \text{ to } 19 \end{aligned} \tag{3.109}$$

where $\frac{\partial p_{kj}}{\partial V_i}$, $\frac{\partial u}{\partial V_i}$ and $\frac{\partial w}{\partial V_i}$, i=1 to 19, have been derived earlier. Substituting, we get the partial derivatives $\frac{\partial x}{\partial V_i}$, $\frac{\partial y}{\partial V_i}$ and $\frac{\partial z}{\partial V_i}$, i=1 to 19, from Eqs. (3.109) above. The influence coefficients $\left(\frac{\partial x}{\partial V_i}\right)^2$, $\left(\frac{\partial y}{\partial V_i}\right)^2$ and $\left(\frac{\partial z}{\partial V_i}\right)^2$, i=1 to 19, are then obtained by squaring these partial derivatives.

3.3 Numerical Results

Numerical results are obtained with the following input values (See Fig. 3.1):

$$\begin{array}{llllllll} a_1 = & 0.1 \text{ m} & b_1 = & 0.1 \text{ m} & c_1 = & 0.1 \text{ m} & \alpha_1 = & 0.5° \\ & & \beta_1 = & 1.0° & r_1 = & 0.03 \text{ m} & l_1 = & 0.50 \text{ m} \\ a_2 = & 1.04 \text{ m} & b_2 = & 0.1 \text{ m} & c_2 = & 0.1 \text{ m} & \alpha_2 = & -1.0° \\ & & \beta_2 = & -0.5° & r_2 = & 0.03 \text{ m} & l_2 = & 0.05 \text{ m} \\ c_3 = & 0.6 \text{ m} & \theta = & 0.0° & \phi = & 0.0° & & \end{array}$$

Absolute tolerances on x-coordinates: $\epsilon_1 = \epsilon_8 = \epsilon_{15} = 0.0001$ m

Absolute tolerances on y-coordinates: $\epsilon_2 = \epsilon_9 = \epsilon_{16} = 0.0001$ m
Absolute tolerances on z-coordinates: $\epsilon_3 = \epsilon_{10} = \epsilon_{17} = 0.0001$ m
Absolute tolerances on angles: $\epsilon_4 = \epsilon_5 = \epsilon_{11} = \epsilon_{12} = \epsilon_{18} = \epsilon_{19} = 0.008°$
Tolerance per unit nominal length on radii and lengths of the two rollers:
$\epsilon_7 = \epsilon_8 = \epsilon_{13} = \epsilon_{14} = 0.005$ m/m

The nominal values of the angles θ and ϕ are both zero, so that the laser beam is vertical. The standard deviation σ of error at a point on the work surface is given by [110]

$$\begin{aligned} \sigma &= \sqrt{\mathrm{D[x]} + \mathrm{D[y]} + \mathrm{D[z]}} \\ &= \sqrt{\mathrm{DSUM}}, \qquad \text{say.} \end{aligned}$$

where

$$\mathrm{DSUM} = \mathrm{D[x]} + \mathrm{D[y]} + \mathrm{D[z]}$$

Hence,

$$\mathrm{DSUM} = \sigma^2$$

i.e., DSUM is the square of the standard deviation of error at a point.

The variances D[x], D[y] and D[z] are obtained at several points on **q**(u,w), the bilinear surface ABDC. These points are obtained by varying the parameters u and w in the ranges, $0 \le u \le 1.0$ and $0 \le w \le 1.0$ with increments of 0.1. Table 3.1 tabulates the variances D[x], D[y] and D[z], and their sum DSUM for these values of u and w.

From the table it is observed that the variances D[x], D[y] and D[z] are of the same order. The variance D[z] varies significantly over the work surface compared to D[x] and D[y]. The variance D[y] doesn't vary over the work surface. The influence coefficient $\left(\frac{\partial y}{\partial V_{16}}\right)_m = 1.0$ throughout the work surface as can be easily seen; and $\left(\frac{\partial y}{\partial V_i}\right)_m$, for other i's, are negligible compared to it. Hence, the variance D[y] is equal to the variance ρ_{16} throughout the work surface and, therefore, it doesn't vary.

The variance D[x] varies slightly over the work surface. The influence coefficient $\left(\frac{\partial x}{\partial V_{15}}\right)_m = 1.0$ on the work surface, as can be easily seen. Here V_{15} is the x-coordinate of the source of the laser beam. For m[V_{18}] = 0° and m[V_{19}] = 0°, increasing V_{18} increases the x-coordinate, whereas increasing V_{19} doesn't change the coordinates of a point. That is why $\left(\frac{\partial x}{\partial V_{18}}\right)_m$ is significantly large but $\left(\frac{\partial x}{\partial V_{19}}\right)_m$, $\left(\frac{\partial y}{\partial V_{19}}\right)_m$ and $\left(\frac{\partial z}{\partial V_{19}}\right)_m$ are negligibly small. The influence coefficients $\left(\frac{\partial x}{\partial V_{18}}\right)_m$ varies slightly over the work surface causing small variation of the variance D[x] over it. Table 3.2 lists the influence coefficients at (u=1.0, w=1.0) for the input values mentioned above.

From the error analysis above, the maximum value of the sum of variances DSUM is found at (u=1.0, w=1.0).

Variances and Their Sum					
q_x m	q_y m	D[x] $10^{-9}m^2$	D[y] $10^{-9}m^2$	D[z] $10^{-9}m^2$	DSUM $10^{-9}m^2$
0.00	0.00	1.5896	1.1111	2.50028	5.2010
0.00	0.10	1.5887	1.1111	2.50050	5.2003
0.00	0.20	1.5878	1.1111	2.50074	5.1997
0.00	0.30	1.5870	1.1111	2.50098	5.1991
0.00	0.40	1.5861	1.1111	2.50124	5.1984
0.00	0.50	1.5852	1.1111	2.50150	5.1978
0.00	0.60	1.5843	1.1111	2.50178	5.1972
0.00	0.70	1.5834	1.1111	2.50206	5.1966
0.00	0.80	1.5825	1.1111	2.50235	5.1960
0.00	0.90	1.5817	1.1111	2.50265	5.1954
0.00	1.00	1.5808	1.1111	2.50296	5.1949
0.10	0.00	1.5896	1.1111	2.05010	4.7508
0.10	0.10	1.5890	1.1111	2.05036	4.7505
0.10	0.20	1.5884	1.1111	2.05078	4.7503
0.10	0.30	1.5878	1.1111	2.05136	4.7502
0.10	0.40	1.5871	1.1111	2.05210	4.7503
0.10	0.50	1.5865	1.1111	2.05300	4.7506
0.10	0.60	1.5859	1.1111	2.05405	4.7511
0.10	0.70	1.5853	1.1111	2.05526	4.7517
0.10	0.80	1.5847	1.1111	2.05663	4.7524
0.10	0.90	1.5840	1.1111	2.05815	4.7533
0.10	1.00	1.5834	1.1111	2.05981	4.7543
0.20	0.00	1.5896	1.1111	1.69996	4.4007
0.20	0.10	1.5893	1.1111	1.70034	4.4007
0.20	0.20	1.5889	1.1111	1.70121	4.4012
0.20	0.30	1.5886	1.1111	1.70257	4.4022
0.20	0.40	1.5882	1.1111	1.70441	4.4037
0.20	0.50	1.5878	1.1111	1.70674	4.4057
0.20	0.60	1.5875	1.1111	1.70954	4.4081
0.20	0.70	1.5871	1.1111	1.71281	4.4111
0.20	0.80	1.5868	1.1111	1.71655	4.4144
0.20	0.90	1.5864	1.1111	1.72075	4.4183
0.20	1.00	1.5861	1.1111	1.72541	4.4226
0.30	0.00	1.5896	1.1111	1.44986	4.1506
0.30	0.10	1.5895	1.1111	1.45037	4.1510
0.30	0.20	1.5894	1.1111	1.45172	4.1523
0.30	0.30	1.5894	1.1111	1.45391	4.1544
0.30	0.40	1.5893	1.1111	1.45692	4.1573
0.30	0.50	1.5892	1.1111	1.46076	4.1610
0.30	0.60	1.5891	1.1111	1.46540	4.1656
0.30	0.70	1.5890	1.1111	1.47086	4.1710
0.30	0.80	1.5889	1.1111	1.47711	4.1771
0.30	0.90	1.5888	1.1111	1.48416	4.1841
0.30	1.00	1.5887	1.1111	1.49199	4.1918
0.40	0.00	1.5896	1.1111	1.29982	4.0005
0.40	0.10	1.5898	1.1111	1.30041	4.0013
0.40	0.20	1.5900	1.1111	1.30210	4.0032
0.40	0.30	1.5902	1.1111	1.30488	4.0061
0.40	0.40	1.5903	1.1111	1.30873	4.0102
0.40	0.50	1.5905	1.1111	1.31366	4.0153
0.40	0.60	1.5907	1.1111	1.31964	4.0214
0.40	0.70	1.5909	1.1111	1.32668	4.0287
0.40	0.80	1.5910	1.1111	1.33475	4.0369
0.40	0.90	1.5912	1.1111	1.34386	4.0462
0.40	1.00	1.5914	1.1111	1.35400	4.0565
0.50	0.00	1.5896	1.1111	1.24983	3.9506
0.50	0.10	1.5901	1.1111	1.25043	3.9516
0.50	0.20	1.5905	1.1111	1.25221	3.9538
0.50	0.30	1.5910	1.1111	1.25518	3.9572
0.50	0.40	1.5914	1.1111	1.25931	3.9618

Variances and Their Sum					
q_x m	q_y m	D[x] $10^{-9}m^2$	D[y] $10^{-9}m^2$	D[z] $10^{-9}m^2$	DSUM $10^{-9}m^2$
0.50	0.50	1.5918	1.1111	1.26460	3.9676
0.50	0.60	1.5923	1.1111	1.27104	3.9744
0.50	0.70	1.5927	1.1111	1.27862	3.9825
0.50	0.80	1.5932	1.1111	1.28733	3.9916
0.50	0.90	1.5936	1.1111	1.29716	4.0019
0.50	1.00	1.5941	1.1111	1.30811	4.0133
0.60	0.00	1.5896	1.1111	1.29991	4.0007
0.60	0.10	1.5903	1.1111	1.30042	4.0019
0.60	0.20	1.5910	1.1111	1.30202	4.0042
0.60	0.30	1.5918	1.1111	1.30471	4.0076
0.60	0.40	1.5925	1.1111	1.30848	4.0121
0.60	0.50	1.5932	1.1111	1.31332	4.0176
0.60	0.60	1.5939	1.1111	1.31921	4.0242
0.60	0.80	1.5953	1.1111	1.33415	4.0406
0.60	0.90	1.5960	1.1111	1.34317	4.0503
0.60	1.00	1.5968	1.1111	1.35322	4.0611
0.70	0.00	1.5896	1.1111	1.45008	4.1508
0.70	0.10	1.5906	1.1111	1.45041	4.1521
0.70	0.20	1.5916	1.1111	1.45159	4.1543
0.70	0.30	1.5926	1.1111	1.45360	4.1573
0.70	0.40	1.5935	1.1111	1.45643	4.1611
0.70	0.50	1.5945	1.1111	1.46009	4.1657
0.70	0.60	1.5955	1.1111	1.46456	4.1712
0.70	0.70	1.5965	1.1111	1.46984	4.1774
0.70	0.80	1.5975	1.1111	1.47592	4.1845
0.70	0.90	1.5985	1.1111	1.48279	4.1924
0.70	1.00	1.5994	1.1111	1.49045	4.2010
0.80	0.00	1.5896	1.1111	1.70032	4.4011
0.80	0.10	1.5909	1.1111	1.70044	4.4024
0.80	0.20	1.5921	1.1111	1.70104	4.4043
0.80	0.30	1.5934	1.1111	1.70214	4.4066
0.80	0.40	1.5946	1.1111	1.70372	4.4094
0.80	0.50	1.5959	1.1111	1.70578	4.4128
0.80	0.60	1.5971	1.1111	1.70831	4.4165
0.80	0.70	1.5984	1.1111	1.71132	4.4208
0.80	0.80	1.5996	1.1111	1.71480	4.4255
0.80	0.90	1.6009	1.1111	1.71875	4.4307
0.80	1.00	1.6021	1.1111	1.72315	4.4364
0.90	0.00	1.5896	1.1111	2.05066	4.7514
0.90	0.10	1.5911	1.1111	2.05056	4.7528
0.90	0.20	1.5927	1.1111	2.05063	4.7544
0.90	0.30	1.5942	1.1111	2.05086	4.7561
0.90	0.40	1.5957	1.1111	2.05125	4.7580
0.90	0.50	1.5972	1.1111	2.05179	4.7601
0.90	0.60	1.5987	1.1111	2.05250	4.7623
0.90	0.70	1.6003	1.1111	2.05336	4.7647
0.90	0.80	1.6018	1.1111	2.05438	4.7673
0.90	0.90	1.6033	1.1111	2.05555	4.7700
0.90	1.00	1.6048	1.1111	2.05687	4.7728
1.00	0.00	1.5896	1.1111	2.50110	5.2018
1.00	0.10	1.5914	1.1111	2.50088	5.2034
1.00	0.20	1.5932	1.1111	2.50067	5.2050
1.00	0.30	1.5950	1.1111	2.50048	5.2066
1.00	0.40	1.5968	1.1111	2.50029	5.2082
1.00	0.50	1.5986	1.1111	2.50012	5.2098
1.00	0.60	1.6003	1.1111	2.49995	5.2114
1.00	0.70	1.6021	1.1111	2.49980	5.2131
1.00	0.80	1.6039	1.1111	2.49966	5.2147
1.00	0.90	1.6058	1.1111	2.49953	5.2164
1.00	1.00	1.6076	1.1111	2.49941	5.2181

Table 3.1: Variances and Their Sum at Several Points in uw Parametric Space on the Bilinear Surface ABDC in LOM

The Influence Coefficients			
i	$\left(\frac{\partial x}{\partial V_i}\right)_m$	$\left(\frac{\partial y}{\partial V_i}\right)_m$	$\left(\frac{\partial z}{\partial V_i}\right)_m$
1	−7.553e−14	1.981e−13	−4.784e−09
2	4.797e−13	1.982e−13	7.651e−06
3	−7.335e−14	−3.546e−13	4.383e−04
4	−7.548e−14	1.982e−13	−3.443e−07
5	−7.548e−14	1.982e−13	−4.869e−11
6	−7.327e−14	−3.546e−13	4.382e−04
7	−7.546e−14	1.982e−13	−2.400e−15
8	−6.110e−12	−2.942e−13	1.372e−02
9	−7.553e−14	1.981e−13	−7.651e−06
10	−7.769e−14	1.964e−13	−4.383e−04
11	4.797e−13	−3.570e−13	3.940e−06
12	−7.552e−14	1.982e−13	7.192e−06
13	−8.315e−14	−3.811e−13	9.997e−01
14	−3.896e−13	3.760e−12	−1.490e−09
15	1.000e+00	1.369e−13	−1.372e−02
16	2.392e−13	1.000e−00	−1.734e−02
17	−7.546e−14	1.982e−13	−2.400e−15
18	4.787e−01	1.689e−13	−6.570e−03
19	−7.546e−14	1.982e−13	−2.400e−15

Table 3.2: The Influence Coefficients at (u = 1.0, w = 1.0) in *uw* Parametric Space on the Bilinear Surface ABDC in LOM

The three-sigma bands of error in tracing several lines on the bilinear surface q(u,w) is obtained. The three-sigma band is the band of 3σ and -3σ values of error at a point. Figure 3.11 shows the three-sigma band for a horizontal line in *uw* parametric space from (.1, .1) to (.9, .1). Figure 3.12 shows the three-sigma band for a vertical line from (.9, .1) to (.9, .9). Figure 3.13 shows the three-sigma band for an inclined line from (.1, .1) to (.9,.9). The three-sigma bands for the horizontal and inclined lines decreases and then increases. The three-sigma band for the vertical line is almost constant. This is because the sum of variances DSUM doesn't vary much in the vertical direction in *uw* parametric space as can be seen from Table 3.1. From Table 3.1 and the three-sigma band it is seen that the overall error doesn't vary much over the work surface and it is immaterial where on the work surface, the contour is drawn.

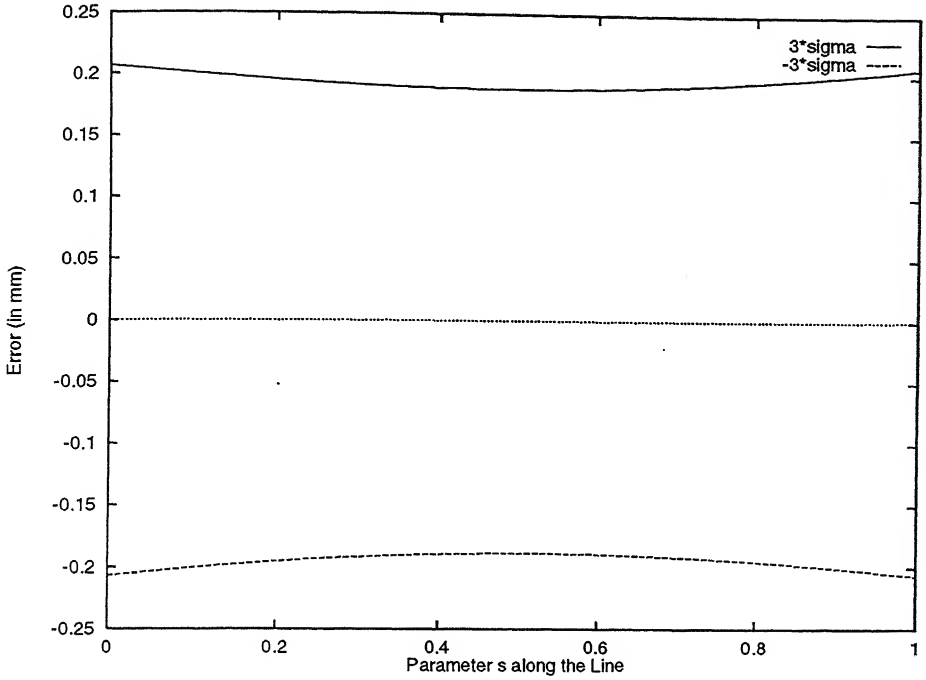

Figure 3.11: The 3σ band for a Horizontal Line in uw Parametric Space from (.1,.1) to (.9,.1)

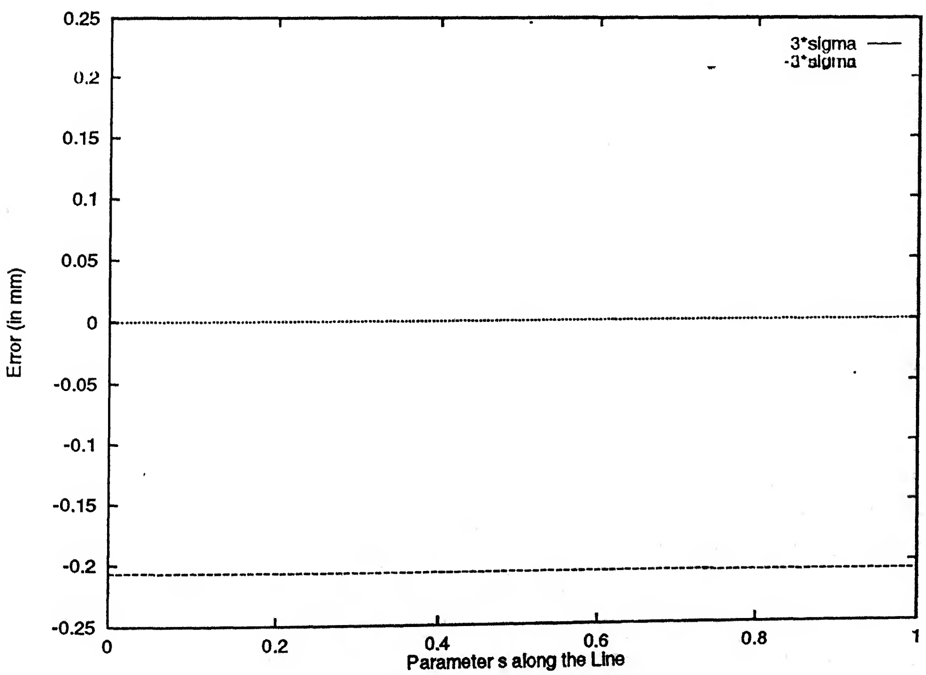

Figure 3.12: The 3σ band for a Vertical Line in uw Parametric Space from (.9,.1) to (.9,.9)

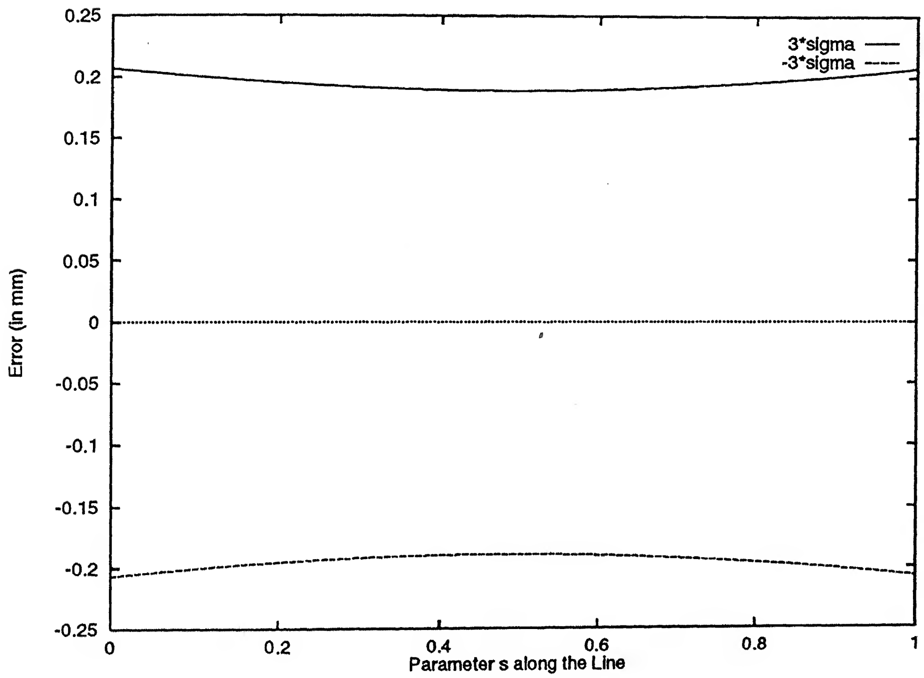

Figure 3.13: The 3σ band for an Inclined Line in uw Parametric Space from (.1,.1) to (.9,.9)

Chapter 4

ANALYSIS OF MECHANICAL ERROR IN FDM

4.1 Geometric Modeling for Description of the FDM Process

The Fused Deposition Modeling (FDM) process comprises of an extruder head moving in the horizontal plane (Fig. 1.3). The extruder head slides along a link in X direction. Figure 4.1 shows the motion of extruder head on the head rails. This link itself slides along another link in Y direction. When the part is built progressively, the Z-stage platen moves downwards. The tip of the extruder head deposits material on the Z-stage platen. It draws the contour of a slice, and fills the contour with roads [63, 95, 13, 45]. The FDM process has been discussed in detail in Section 1.1.2.2.

The geometric model of the FDM process is as follows. There is a kinematic chain consisting of links and other members causing the movement of the extruder head in FDM (Fig. 4.2). The extruder head slides on member 3. The sub-assembly consisting of member 3 and the extruder head slides on link 1. The members $\overline{DE}$ and $\overline{EG}$ constitute a rigid link. The members $\overline{DE}$ and $\overline{EG}$ are called the sliding member 2 and member 3 respectively. The sliding member 2 is taken to be parallel to Z_0 direction. There is a sliding pair between link 1 and the sliding member 2. It is called pair 12.

The present model is being done for a particular layer of the part being built. Consider the Z-stage platen for that layer. A base frame $X_0Y_0Z_0$ is attached at the front end of the Z-stage platen such that the surface of the foam foundation is the X_0Y_0-plane (Fig. 4.2). The frame $X_0Y_0Z_0$ is fixed in space, it does not move with the

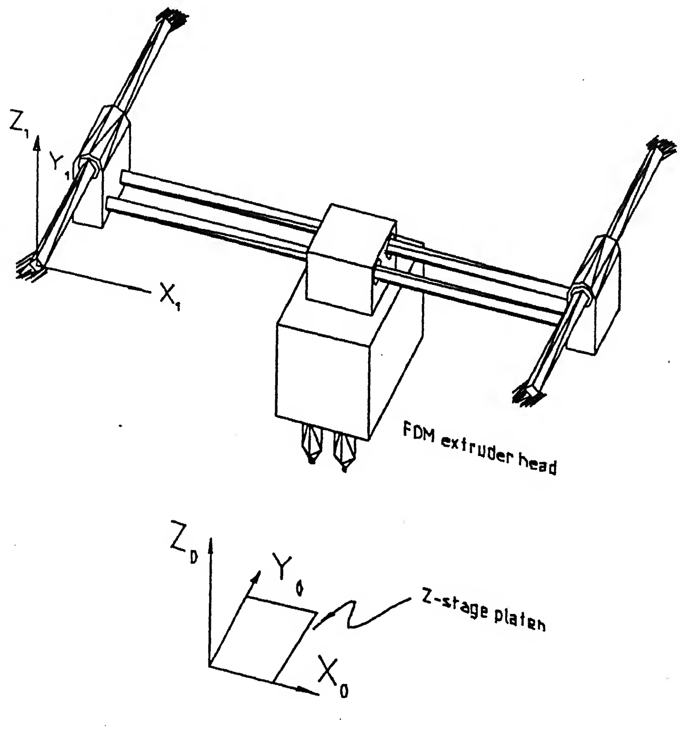

Figure 4.1: Motion of Extruder Head in FDM

platen.

Ideally, link 1 and Y_0 direction should be parallel, and member 3 and X_0 direction should be parallel. However, due to mechanical errors the members 1 and 3 are oblique in space. A frame $X_1Y_1Z_1$ is attached at the front end A of link 1 such that Y_1 axis is along link 1(Fig. 4.2). The frame $X_1Y_1Z_1$ is obtained by a rotation α_1 about X_0-axis, a rotation β_1 about Y_0-axis and a translation (a_1, b_1, c_1) in $X_0Y_0Z_0$ successively.

Another frame $X_2Y_2Z_2$ is attached at the left end E of member 3 such that the X_2-axis is along member 3 (Fig. 4.2). The frame $X_2Y_2Z_2$ is obtained from $X_1Y_1Z_1$ as follows. The frame $X_2Y_2Z_2$ is obtained by a translation **AD** along link 1, a translation **DE** along link 2, a rotation α_2 about a direction parallel to X_1-axis and passing through E and rotation β_2 about a direction parallel to Y_1-axis and passing through E successively.

The extruder head is modeled by two members 4 and 5 such that they are parallel to Y_2 and Z_2 directions respectively. As shown in Fig. 4.2, the line segments $\overline{HI}$ and $\overline{IQ}$ are members 4 and 5 respectively. The nozzle tip is at the point Q. The members 4 and 5 are rigidly connected to each other and, therefore, make a single link. The extruder head being a rigid body can always be modeled by two such members parallel to Y_2 and Z_2 directions. There is a sliding pair between link 3 and member 4. This

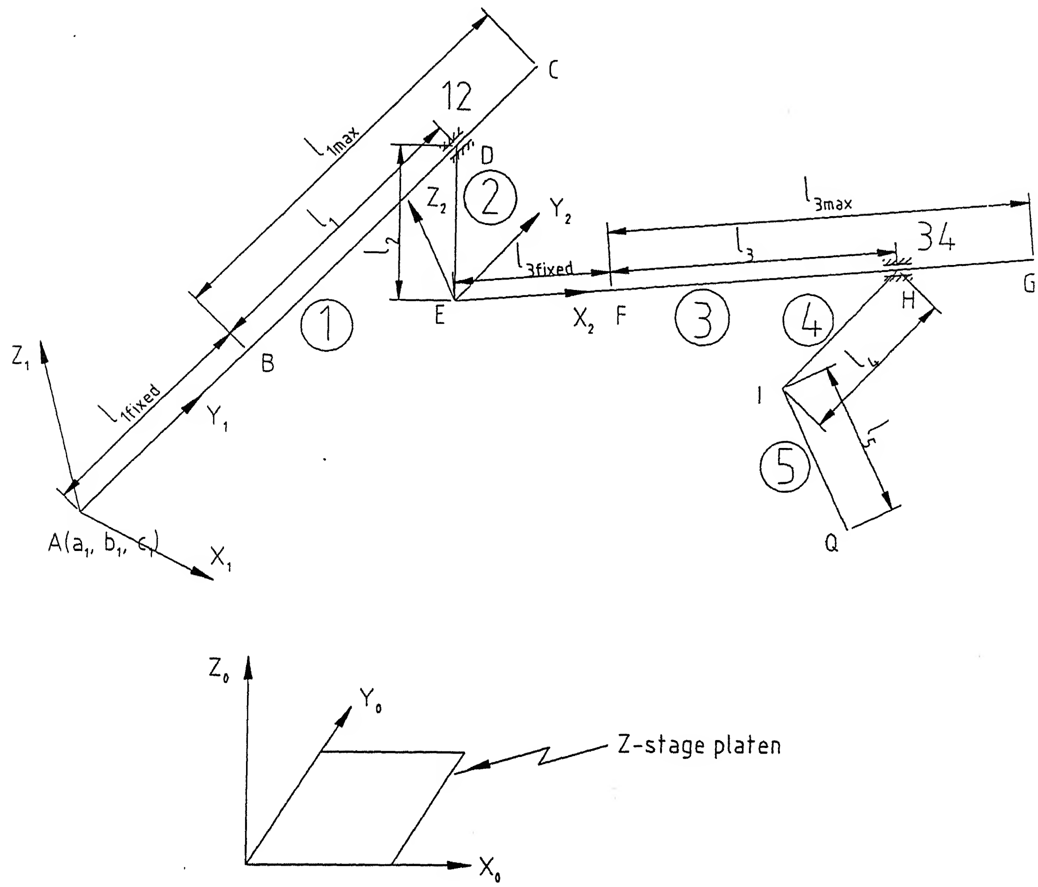

Figure 4.2: Geometric Model of the FDM Process

pair is called pair 34.

The kinematic chain is an open link mechanism. The left and right head-rails are fixed links and, therefore only the head-rail on the left is considered. The nominal lengths of various links and members are as follows. The sliding member 2 is constrained to move between two points B and C on link 1 such that the lengths of $\overline{AB}$ and $\overline{BC}$ are l_{1fixed} and l_{1max} respectively. At any position D of the sliding member 2 the lengths of link 1 is $l_{1fixed} + l_1$

The nominal length of the sliding member 2 is l_2. The sliding member 4 is constrained to move between two points F and G on member 3 such that the lengths of $\overline{EF}$ and $\overline{FG}$ are l_{3fixed} and l_{3max} respectively. At any position H of the sliding member 2 the length of member 3 is $l_{3fixed} + l_3$. The nominal length of members 4 and 5 are l_4 and l_5 respectively. The dimensions are taken in S.I. units, i.e., the lengths in meters and the angles in radians.

4.2 Stochastic Model of the FDM Process

Chapter 2 discusses stochastic modeling of the RP process. Following that approach, the stochastic modeling of FDM is done as follows. The sliding members 2 and 4 are driven by belt and pulley drive mechanism. There is an error in positioning 2 and 4 by the corresponding drive mechanism. Let ϵ_1 be the absolute error, in meters, in positioning the sliding member 2 along link 1 by the drive mechanism. Let ϵ_2, ϵ_4 and ϵ_5 be the tolerances per unit nominal length in m/m on members 2, 4, 5 respectively. Let ϵ_3 be the absolute error, in meters, in positioning the sliding member 4 along member 3 by the drive mechanism. The actual lengths R_i of links are given by

$$R_1 = l_{1fixed} + l_1 + \epsilon_1 \tag{4.1}$$
$$R_2 = l_2(1+\epsilon_2) \tag{4.2}$$
$$R_3 = l_{3fixed} + l_3 + \epsilon_3 \tag{4.3}$$
$$R_4 = l_4(1+\epsilon_4) \tag{4.4}$$
$$R_5 = l_5(1+\epsilon_5) \tag{4.5}$$

where R_i are now random variables.

The effective clearance error ϵ along a link axis in a spatial revolute joint is given by Eq. (2.8). It is as follows.

$$\epsilon = \frac{r\cos\alpha}{\cos\gamma}$$

where r and α are parameters, random in nature as illustrated in Fig. 2.5. γ is the angle made by the link with a plane perpendicular to the socket axis.

Although the pairs 12 and 34 are sliding pairs, they comprise of the cylindrical elements socket and pin. Therefore the clearance in them is given by Eq. (2.8), as above.

Let ϵ_6 be the effective clearance error in pair 12 along member 3, i.e., along X_2 direction (Fig. 4.3). Therefore,

$$\epsilon_6 = \frac{r_b\cos\alpha_b}{\cos\gamma_b} \tag{4.6}$$

where r_b and α_b are the parameters for ϵ_6. They are random in nature with their ranges given by $0 \le r_b \le c_{12}$ and $0 \le \alpha_b \le 2\pi$; where c_{12} is the radial clearance in pair 12. It is assumed that the radial clearances in both the left and right head-rails are equal, and they are c_{12}. γ_b is the angle made by member 3 with a plane perpendicular to link 1.

Let ϵ_7 be the effective clearance error in pair 12 along the sliding member 2, i.e., along Z_0 direction (Fig. 4.3). Therefore,

$$\epsilon_7 = \frac{r_a\cos\alpha_a}{\cos\gamma_a} \tag{4.7}$$

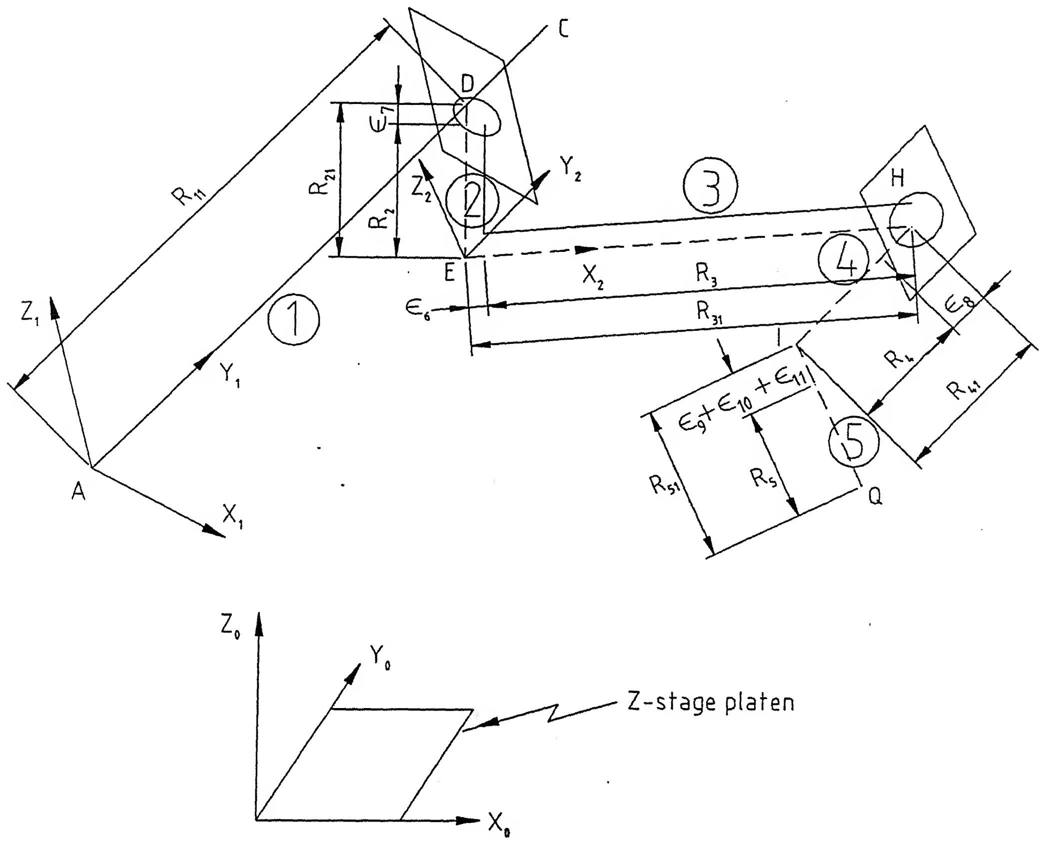

Figure 4.3: Equivalent Kinematic Chain

where r_a and α_a are the parameters for ϵ_7. They are random in nature with their ranges given by $0 \leq r_a \leq c_{12}$ and $0 \leq \alpha_a \leq 2\pi$. γ_a is the angle made by the sliding member 2 with a plane perpendicular to link 1.

Let ϵ_8 be the effective clearance error in pair 34 along the sliding member 4 which lies along Y_2 direction (Fig. 4.3). Therefore,

$$\epsilon_8 = \frac{r_c \cos \alpha_c}{\cos \gamma_c}$$

where r_c and α_c are the parameters for ϵ_8. They are random in nature with their ranges given by $0 \leq r_c \leq c_{34}$ and $0 \leq \alpha_c \leq 2\pi$; where c_{34} is the radial clearance in pair 34. γ_c is the angle made by the sliding member 4 with a plane perpendicular to member 3. Since the sliding member 4, being parallel to Y_2-axis, lies in a plane perpendicular to member 3, therefore,

$$\gamma_c = 0^o$$

Hence,

$$\epsilon_8 = r_c \cos \alpha_c \tag{4.8}$$

direction (Fig. 4.3). Therefore,

$$\epsilon_9 = \frac{r_d \cos \alpha_d}{\cos \gamma_d}$$

where r_d and α_d are the parameters for ϵ_9. They are random in nature with their ranges given by $0 \leq r_d \leq c_{34}$ and $0 \leq \alpha_d \leq 2\pi$. γ_d is the angle made by member 5 with a plane perpendicular to member 3. Since member 5, being parallel to Z_2-axis, lies in a plane perpendicular to member 3, therefore,

$$\gamma_d = 0^o$$

Hence,

$$\epsilon_9 = r_d \cos \alpha_d \tag{4.9}$$

The effective clearance errors ϵ_i, i= 6 to 9, are random variables.

The extruder head is fixed by screws to the slider which slides on member 3. This head attachment causes an error in Z_2 direction. Let ϵ_{10} be the absolute error, in meters, in Z_2 direction at the head attachment. This modifies the length of member 5.

The nozzle tip is screwed to the extruder head. This nozzle tip attachment too causes an error in Z_2 direction. Let ϵ_{11} be the absolute error, in meters, in Z_2 direction at the nozzle tip attachment. The error ϵ_{11} too modifies the length of member 5. The errors ϵ_{10} and ϵ_{11} are also random variables.

Let ϵ_{12}, ϵ_{13}, ϵ_{14} and ϵ_{15} be the absolute tolerances, in radians, on angles α_1, β_1, α_2 and β_2 respectively. The actual angle is then given by the sum of the nominal angle and its corresponding tolerance. The actual angles are now random variables.

So, in all, there are fifteen random variables involved in the present model. If these are denoted by V_1, V_2, ..., V_{15} then

$$\begin{aligned}
V_i &= R_i & \text{i} = 1 \text{ to } 5 \\
V_i &= \epsilon_i & \text{i} = 6 \text{ to } 11 \\
V_{12} &= \alpha_1 + \epsilon_{12} \\
V_{13} &= \beta_1 + \epsilon_{13} \\
V_{14} &= \alpha_2 + \epsilon_{14} \\
V_{15} &= \beta_2 + \epsilon_{15}
\end{aligned} \tag{4.10}$$

These random variables are independent of each other.

The equivalent lengths of the members in terms of the random variables are given as follows:

$$\begin{aligned}
R_{11} &= R_1 &&= V_1 \\
R_{21} &= R_2 + \epsilon_7 &&= V_2 + V_7 \\
R_{31} &= R_3 + \epsilon_6 &&= V_3 + V_6 \\
R_{41} &= R_4 + \epsilon_8 &&= V_4 + V_8 \\
R_{51} &= R_5 + \epsilon_9 + \epsilon_{10} + \epsilon_{11} &&= V_5 + V_9 + V_{10} + V_{11}
\end{aligned} \tag{4.11}$$

where R_{i1} is the equivalent length of the i^{th} member. The kinematic chain with equivalent lengths of members is shown in Fig. 4.3. The above is a good approximation for R_{21} and R_{31}. When members 1, 2 and 3 are perpendicular to each other, as in the ideal case, then the expressions for R_{21} and R_{31} holds exactly.

When the first layer of the part is being built, the nozzle tip is buried .01 in into the foam foundation on the Z-stage platen. The foam foundation deforms as the first few layers are made, and the layer comes out as traced by the nozzle tip. So the error in the Z-stage platen does not give rise to any error in the part.

4.2.1 Mean Values of the Random Variables

From Section 2.2.1, the mean values of actual member lengths are given by

$$\begin{aligned} m[V_1] &= l_{1fixed} + l_1 \\ m[V_2] &= l_2 \\ m[V_3] &= l_{3fixed} + l_3 \\ m[V_4] &= l_4 \\ m[V_5] &= l_5 \end{aligned}$$

Section 2.2.2, which discusses effective clearance error in a spatial revolute joint, yields

$$m[V_i] = 0 \qquad \text{i} = 6,7,8,9$$

ϵ_{10} and ϵ_{11} are absolute error on member lengths. They are normally distributed with zero nominal value. Hence

$$m[V_i] = 0 \qquad \text{i} = 10,11$$

Section 2.2.4 yields

$$\begin{aligned} m[V_{12}] &= \alpha_1 \\ m[V_{13}] &= \beta_1 \\ m[V_{14}] &= \alpha_2 \\ m[V_{15}] &= \beta_2 \end{aligned}$$

4.2.2 Variances of the Random Variables

Variances ρ_i of the random variables V_i are discussed below. Let ϵ_i be the tolerance per unit nominal length of a link. From Section 2.2.1, the variance of the actual length of a link is given by

$$\rho_i = (\epsilon_i l_i / 3)^2$$

where l_i is the nominal length of the link.

Therefore, if ϵ_i is the absolute tolerance on the nominal length of a link then the variance is given by

$$\rho_i = (\epsilon_i/3)^2 \tag{4.12}$$

Hence for the random variables in the present model, it follows that

$$\rho_i = (\epsilon_i/3)^2 \qquad \text{i} = 1,3,10,11$$

$$\rho_i = (\epsilon_i l_i/3)^2 \qquad \text{i} = 2,4,5$$

Section 2.2.2 yields

$$\begin{aligned}
\rho_6 &= \frac{c_{12}^2}{4\cos\gamma_a} \\
\rho_7 &= \frac{c_{12}^2}{4\cos\gamma_b} \\
\rho_8 &= \frac{c_{34}^2}{4} \\
\rho_9 &= \frac{c_{34}^2}{4}
\end{aligned}$$

From Section 2.2.4,

$$\rho_i = (\epsilon_i/3)^2 \qquad \text{i} = 12,\ 13,\ 14,\ 15$$

The angles γ_a and γ_b, which appear in the expressions for ρ_6 and ρ_7, respectively, are derived in the following subsections.

4.2.3 The Angle γ_a

γ_a is the angle made by the sliding member 2 with a plane perpendicular to link 1. A frame $X_5Y_5Z_5$ parallel to $X_1Y_1Z_1$ is attached at D as shown in Fig. 4.4.

So γ_a is the angle made by link 2, i.e., the line segment $\overline{DE}$ with the X_5Z_5-plane. Figure 4.5 shows a frame XYZ with O as its origin. A line **OP** from a point P(x,y,z) makes an angle γ with the XZ-plane. The angle γ is given by

$$\gamma = \tan^{-1}\frac{|y|}{\sqrt{z^2+x^2}} \tag{4.13}$$

Using this, the angle γ_a can be derived as follows. The point E in $X_2Y_2Z_2$ frame, being its origin, is given by

$$[e_2] = \begin{bmatrix} 0 & 0 & 0 & 1 \end{bmatrix}$$

Therefore, the point E in $X_5Y_5Z_5$ frame is given by

$$[e_5] = \begin{bmatrix} 0 & 0 & 0 & 1 \end{bmatrix}\begin{bmatrix} T_5^2 \end{bmatrix}$$

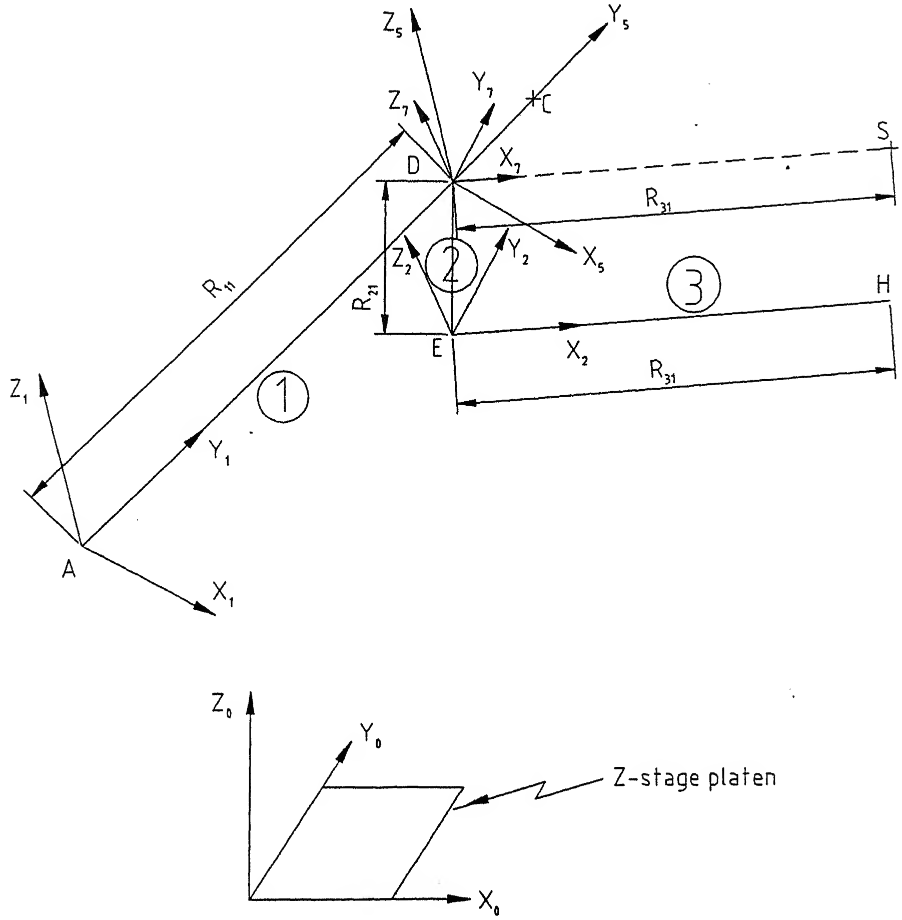

Figure 4.4: The Angles γ_a and γ_b

The transformation $[T_5^2]$ involves a translation R_{21} along Z_0 direction. So the transformation $[T_0^5]$ of frame $X_5Y_5Z_5$ with respect to $X_0Y_0Z_0$ is found and using it the transformation $[T_5^2]$ is derived. The transformation $[T_0^2]$ is given by

$$\left[T_0^2\right] \equiv \left[T_0^5\right] \rightarrow \left[T_5^2\right]$$

Or,

$$\left[T_0^2\right] = \left[T_5^2\right]\left[T_0^5\right]$$

Hence,

$$\left[T_5^2\right] = \left[T_0^2\right]\left[T_0^5\right]^{-1} \tag{4.14}$$

The transformation $[T_0^2]$ and $[T_0^5]$ are derived in the following subsections. They are evaluated at the nominal values of link lengths and angles for calculating $[e_5]$. Both $[T_0^2]$ and $[T_0^5]$ involve R_1, the actual length of link 1. The mean value of R_1 is $l_{1fixed} + l_1$. However, the angle γ_a does not depend upon the length of link 1 and it can be taken to be any arbitrary positive value. So the mean value of R_1 is taken to

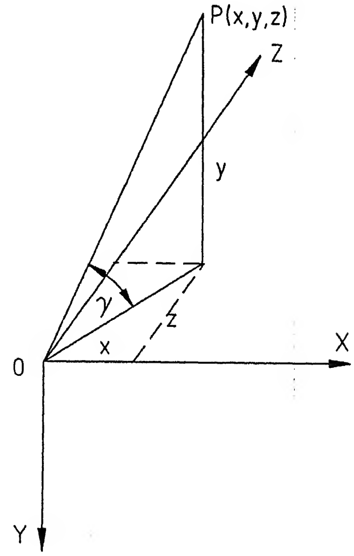

Figure 4.5: Angle γ Made by a line OP With the XZ-plane

be l_{1fixed}, i.e., l_1 is taken to be zero. Hence $[e_5]$ is given by

$$[e_5] = \begin{bmatrix} 0 & 0 & 0 & 1 \end{bmatrix} \left[T_5^2\right]_{m,\ l_1=0} \tag{4.15}$$

where $[T_5^2]$ is evaluated at $l_1 = 0$. The subscript m signifies that $[T_5^2]$ is being evaluated at the mean values of link lengths and angles.

Hence, from Eq. (4.13), the angle γ_a is given by

$$\gamma_a = \tan^{-1}\frac{|e_{5y}|}{\sqrt{e_{5z}^2 + e_{5x}^2}} \tag{4.16}$$

where e_{5x}, e_{5y} and e_{5z} are the x, y and z coordinates of $[e_5]$ respectively.

4.2.4 The Angle γ_b

γ_b is the angle made by member 3 with a plane perpendicular to link 1. A line **DS** is drawn parallel to member 3 and passing through D as shown in Fig. 4.4. So γ_b is the angle made by **DS** with the X_5Z_5-plane.

A frame $X_7Y_7Z_7$ parallel to $X_2Y_2Z_2$ is attached at point D. The angle γ_b does not depend upon the length of member 3 and it can be taken any arbitrary positive value. So the mean value of R_3 is taken to be l_{3fixed}, i.e., l_3 is taken to be zero. Hence the point S in $X_7Y_7Z_7$ frame is given by

$$[s_7] = \begin{bmatrix} l_{3fixed} & 0 & 0 & 1 \end{bmatrix} \tag{4.17}$$

The point S in $X_5Y_5Z_5$ frame is given by

$$[s_5] = [s_7]\left[T_5^7\right]$$

where

$$\left[T_5^7\right] \equiv \text{Rot}(X_5, \alpha_2) \rightarrow \text{Rot}(Y_5, \beta_2)$$

Or,

$$\begin{aligned}[T_5^7] &= \text{Rot}(X_5, \alpha_2)\ \text{Rot}(Y_5, \beta_2) \\ &= \begin{bmatrix} \cos\beta_2 & 0 & -\sin\beta_2 & 0 \\ \sin\alpha_2 \sin\beta_2 & \cos\alpha_2 & \sin\alpha_2 \cos\beta_2 & 0 \\ \cos\alpha_2 \sin\beta_2 & -\sin\alpha_2 & \cos\alpha_2 \cos\beta_2 & 0 \\ 0 & 0 & 0 & 1 \end{bmatrix}\end{aligned} \tag{4.18}$$

The transformation $[T_5^7]$ is evaluated at the mean values of angles α_2 and β_2. Hence

$$[s_5] = \left[\ l_{3fixed}\ \ 0\ \ 0\ \ 1\ \right] \left[T_5^7\right]_m \tag{4.19}$$

where m signifies that $[T_5^7]$ is being evaluated at the mean values of angles α_2 and β_2. The angle γ_b is then given by

$$\gamma_b = \tan^{-1} \frac{|s_{5y}|}{\sqrt{s_{5z}^2 + s_{5x}^2}} \tag{4.20}$$

where s_{5x}, s_{5y} and s_{5z} are the x, y and z coordinates of $[s_5]$ respectively.

4.3 The Transformation Matrix $[T_0^1]$

The frame $X_1Y_1Z_1$ is obtained by a rotation α_1 about X_0 axis, a rotation β_1 about Y_0 axis and a translation (a_1, b_1, c_1) with respect to the base frame $X_0Y_0Z_0$ (Fig. 4.6).

The transformation $[T_0^1]$ is then given by [103]

$$\left[T_0^1\right] \equiv \text{Rot}(X_0, \alpha_1) \rightarrow \text{Rot}(Y_0, \beta_1) \rightarrow \text{Trans}(Base, a_1, b_1, c_1)$$

Or,

$$\left[T_0^1\right] = \text{Rot}(X_0, \alpha_1)\text{Rot}(Y_0, \beta_1)\text{Trans}(Base, a_1, b_1, c_1)$$

Hence

$$\left[T_0^1\right] = \begin{bmatrix} \cos\beta_1 & 0 & -\sin\beta_1 & 0 \\ \sin\alpha_1 \sin\beta_1 & \cos\alpha_1 & \sin\alpha_1 \cos\beta_1 & 0 \\ \cos\alpha_1 \sin\beta_1 & -\sin\alpha_1 & \cos\alpha_1 \cos\beta_1 & 0 \\ a_1 & b_1 & c_1 & 1 \end{bmatrix} \tag{4.21}$$

4.4 The Transformation Matrix $[T_0^2]$

The frame $X_5Y_5Z_5$ in Fig. 4.4 have axes parallel to those of $X_1Y_1Z_1$. Another frame $X_6Y_6Z_6$ is drawn parallel to $X_5Y_5Z_5$ with origin at E as shown in Fig. 4.7.

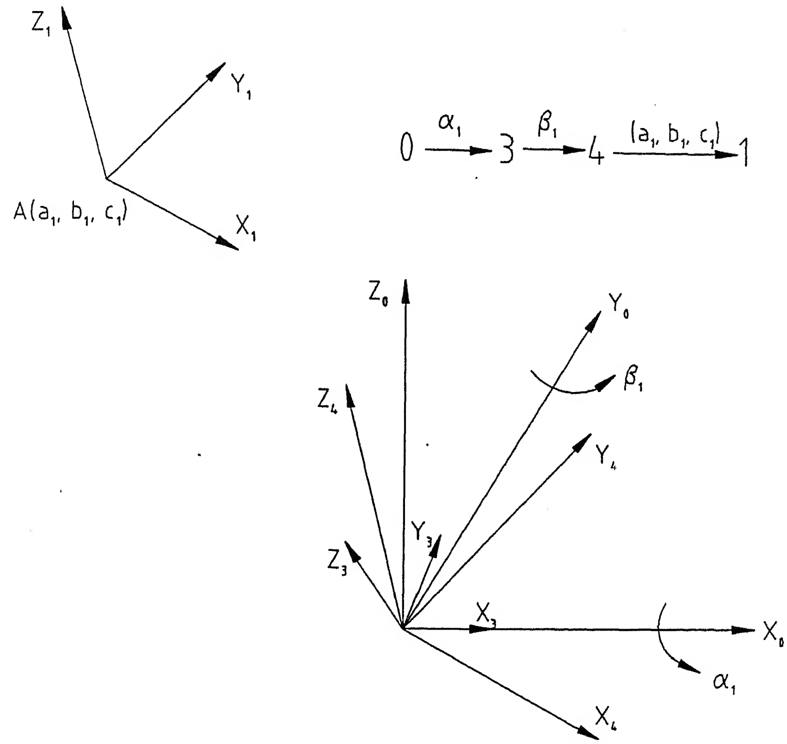

Figure 4.6: The Transformation $[T_0^1]$

The frame $X_5Y_5Z_5$ with respect to the base frame $X_0Y_0Z_0$ is given by

$$\left[T_0^5\right] \equiv \left[T_0^1\right] \rightarrow \text{Trans}(Y_1, R_{11})$$

Or,

$$\left[T_0^5\right] = \text{Trans}(Y_1, R_{11}) \left[T_0^1\right] \tag{4.22}$$

The frame $X_6Y_6Z_6$ with respect to the base frame $X_0Y_0Z_0$ is given by

$$\left[T_0^6\right] \equiv \left[T_0^5\right] \rightarrow \text{Trans}(Base, 0, 0, -R_{21})$$

Or,

$$\left[T_0^6\right] = \left[T_0^5\right] \text{Trans}(Base, 0, 0, -R_{21})$$

Substituting $[T_0^5]$ from Eq. (4.22) in the above equation yields

$$\left[T_0^6\right] = \text{Trans}(Y_1, R_{11}) \left[T_0^1\right] \text{Trans}(Base, 0, 0, -R_{21}) \tag{4.23}$$

The frame $X_2Y_2Z_2$ is obtained by two successive rotations α_2 and β_2 about X_6 and Y_6 axes respectively. Hence the frame $X_2Y_2Z_2$ with respect to $X_6Y_6Z_6$ is given by

$$\left[T_6^2\right] \equiv \text{Rot}(X_6, \alpha_2) \rightarrow \text{Rot}(Y_6, \beta_2)$$

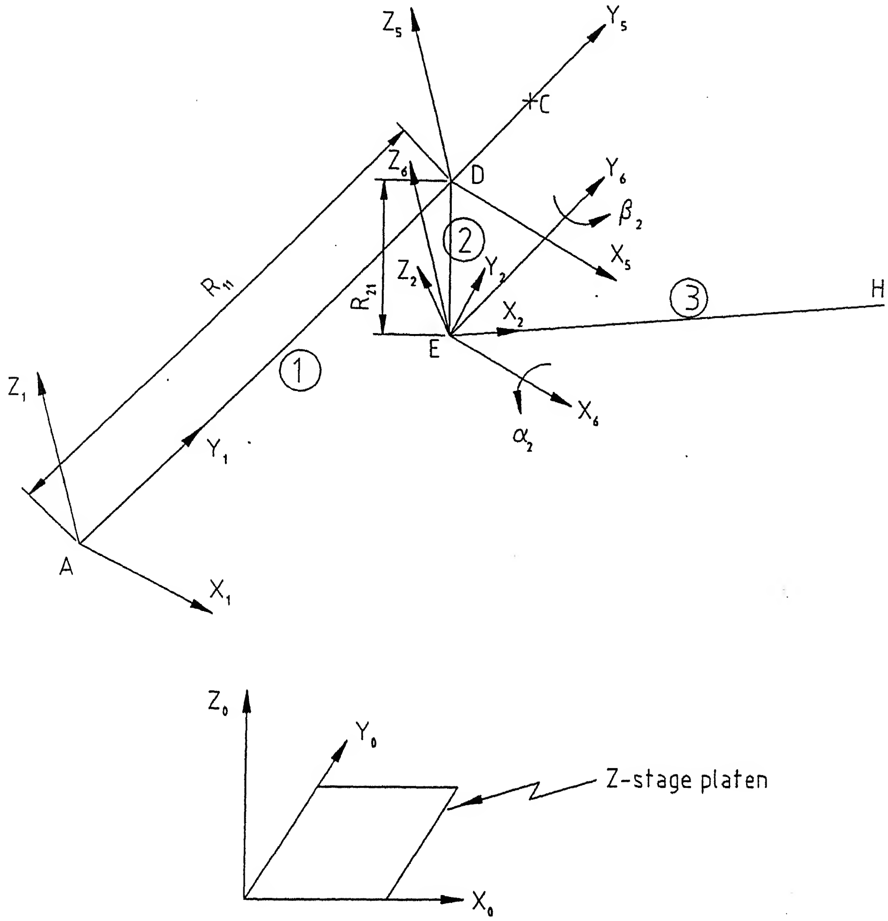

Figure 4.7: The Transformation $[T_0^2]$

Or,

$$[T_6^2] = \text{Rot}(X_6, \alpha_2)\ \text{Rot}(Y_6, \beta_2)$$

$$= \begin{bmatrix} \cos\beta_2 & 0 & -\sin\beta_2 & 0 \\ \sin\alpha_2 \sin\beta_2 & \cos\alpha_2 & \sin\alpha_2\cos\beta_2 & 0 \\ \cos\alpha_2\sin\beta_2 & -\sin\alpha_2 & \cos\alpha_2\cos\beta_2 & 0 \\ 0 & 0 & 0 & 1 \end{bmatrix} \quad (4.24)$$

Now the frame $X_2Y_2Z_2$ with respect to the base frame $X_0Y_0Z_0$ is given by

$$\left[T_0^2\right] = \left[T_0^6\right] \rightarrow \left[T_6^2\right]$$

Or,

$$\left[T_0^2\right] = \left[T_6^2\right]\left[T_0^6\right]$$

Substituting $[T_0^6]$ from Eq. (4.23) into $[T_0^2]$ above yields

$$\left[T_0^2\right] = \left[T_6^2\right]\ \text{Trans}(Y_1, R_{11})\left[T_0^1\right]\ \text{Trans}(Base, 0, 0, -R_{21})$$

Let $[T_A]$ and $[T_B]$ be the two transformation matrices such that

$$[T_A] = \left[T_6^2\right]\ \text{Trans}(Y_1, R_{11})$$

and

$$[T_B] = \left[T_0^1\right] \text{ Trans}(Base, 0, 0, -R_{21})$$

Therefore,

$$[T_A] = \begin{bmatrix} \cos\beta_2 & 0 & -\sin\beta_2 & 0 \\ \sin\alpha_2\sin\beta_2 & \cos\alpha_2 & \sin\alpha_2\cos\beta_2 & 0 \\ \cos\alpha_2\sin\beta_2 & -\sin\alpha_2 & \cos\alpha_2\cos\beta_2 & 0 \\ 0 & R_{11} & 0 & 1 \end{bmatrix} \tag{4.25}$$

and

$$[T_B] = \begin{bmatrix} \cos\beta_1 & 0 & -\sin\beta_1 & 0 \\ \sin\alpha_1\sin\beta_1 & \cos\alpha_1 & \sin\alpha_1\cos\beta_1 & 0 \\ \cos\alpha_1\sin\beta_1 & -\sin\alpha_1 & \cos\alpha_1\cos\beta_1 & 0 \\ a_1 & b_1 & c_1 - R_{21} & 1 \end{bmatrix} \tag{4.26}$$

The transformation $[T_0^2]$ is now given by

$$\left[T_0^2\right] = [T_A][T_B] \tag{4.27}$$

where $[T_A]$ and $[T_B]$ are given by Eqs. (4.25) and (4.26) respectively.

4.5 The Point Q on the Contour of a Slice Traced by the Nozzle Tip

The nozzle tip traces the contour of a slice. It deposits the material over the previous layer of a part as the part is progressively built. When the first layer is being built the nozzle tip is buried .01 inch into the foam foundation [113]. So the nozzle tip is always in touch with either a previously built layer or the foam foundation. Therefore the coordinates of the nozzle tip are the coordinates of a point on the part being built.

The coordinates of the nozzle tip Q in the frame $X_2Y_2Z_2$ is given by

$$[q_2] = \begin{bmatrix} R_{31} & -R_{41} & -R_{51} & 1 \end{bmatrix} \tag{4.28}$$

Therefore, the coordinates of the nozzle tip Q in $X_0Y_0Z_0$ frame is given by

$$[q] = [q_2]\left[T_0^2\right] \tag{4.29}$$

Substituting $[T_0^2]$ from Eq. (4.27) yields

$$[q] = [q_2]\,[T_A]\,[T_B] \tag{4.30}$$

The above equation gives the coordinates of a point on the contour of a slice traced by the nozzle tip. Let

$$[q] = \begin{bmatrix} x & y & z & 1 \end{bmatrix} \tag{4.31}$$

4.6 The Means and the Variances of the Dependent Variables x, y and z

From Eqs. (4.30) and (4.31) the coordinates of a point on the contour of a slice traced by the nozzle tip are given by

$$\begin{aligned} x &= x(V_1, V_2, \ldots, V_{15}) \\ y &= y(V_1, V_2, \ldots, V_{15}) \\ z &= z(V_1, V_2, \ldots, V_{15}) \end{aligned} \tag{4.32}$$

Using the approach given in Chapter 2, the means and the variances of the dependent variables x, y and z are as follows:

$$\begin{aligned} m[x] &= x(m[V_i], \quad i = 1,2, \ldots, 15) \\ m[y] &= y(m[V_i], \quad i = 1,2, \ldots, 15) \\ m[z] &= z(m[V_i], \quad i = 1,2, \ldots, 15) \\ D[x] &= \sum_{i=1}^{15} \left(\frac{\partial x}{\partial V_i}\right)_m^2 D[V_i] \\ D[y] &= \sum_{i=1}^{15} \left(\frac{\partial y}{\partial V_i}\right)_m^2 D[V_i] \\ D[z] &= \sum_{i=1}^{15} \left(\frac{\partial z}{\partial V_i}\right)_m^2 D[V_i] \end{aligned} \tag{4.33}$$

The partial derivatives are evaluated at the mean values of the variables V_i as denoted by the subscript m. The mean values m$[V_i]$ of the variables V_i are as given in Section 4.2.1. The influence coefficients $\left(\frac{\partial x}{\partial V_i}\right)^2$, $\left(\frac{\partial y}{\partial V_i}\right)^2$ and $\left(\frac{\partial z}{\partial V_i}\right)^2$ need the partial derivatives of matrices $[T_A]$ and $[T_B]$ and are derived in the following subsections.

4.7 Partial Derivatives of the Elements of $[T_A]$

The transformation matrix $[T_A]$ is given by Eq. (4.25). Expressing it in terms of the random variables V_i, it follows that

$$[T_A] = \begin{bmatrix} \cos V_{15} & 0 & -\sin V_{15} & 0 \\ \sin V_{14} \sin V_{15} & \cos V_{14} & \sin V_{14} \cos V_{15} & 0 \\ \cos V_{14} \sin V_{15} & -\sin V_{14} & \cos V_{14} \cos V_{15} & 0 \\ 0 & V_1 & 0 & 1 \end{bmatrix} \tag{4.34}$$

Hence the elements of $[T_A]$ are functions of V_1, V_{14} and V_{15} only, i.e.,

$$[T_A] = T_A(V_1, V_{14}, V_{15}) \tag{4.35}$$

Therefore, the partial derivatives of the elements of $[T_A]$ with respect to the variables V_i are given by

$$
\begin{aligned}
\frac{\partial[T_A]}{\partial V_1} &= \begin{bmatrix} 0 & 0 & 0 & 0 \\ 0 & 0 & 0 & 0 \\ 0 & 0 & 0 & 0 \\ 0 & 1 & 0 & 0 \end{bmatrix} \\
\frac{\partial[T_A]}{\partial V_{14}} &= \begin{bmatrix} 0 & 0 & 0 & 0 \\ \cos V_{14}\sin V_{15} & -\sin V_{14} & \cos V_{14}\cos V_{15} & 0 \\ -\sin V_{14}\sin V_{15} & -\cos V_{14} & -\sin V_{14}\cos V_{15} & 0 \\ 0 & 0 & 0 & 0 \end{bmatrix} \\
\frac{\partial[T_A]}{\partial V_{15}} &= \begin{bmatrix} -\sin V_{15} & 0 & -\cos V_{15} & 0 \\ \sin V_{14}\cos V_{15} & 0 & -\sin V_{14}\sin V_{15} & 0 \\ \cos V_{14}\cos V_{15} & 0 & -\cos V_{14}\sin V_{15} & 0 \\ 0 & 0 & 0 & 0 \end{bmatrix} \\
\frac{\partial[T_A]}{\partial V_i} &= 0 \qquad \text{i} = 2 \text{ to } 13
\end{aligned}
\tag{4.36}
$$

4.8 Partial Derivatives of the Elements of $[T_B]$

The transformation matrix $[T_B]$ is given by Eq. (4.26). Expressing it in terms of the random variables V_i, it follows that

$$
[T_B] = \begin{bmatrix} \cos V_{13} & 0 & -\sin V_{13} & 0 \\ \sin V_{12}\sin V_{13} & \cos V_{12} & \sin V_{12}\cos V_{13} & 0 \\ \cos V_{12}\sin V_{13} & -\sin V_{12} & \cos V_{12}\cos V_{13} & 0 \\ a_1 & b_1 & c_1 - V_2 - V_7 & 1 \end{bmatrix} \tag{4.37}
$$

Hence the elements of $[T_B]$ are functions of V_2, V_7, V_{12} and V_{13} only, i.e.,

$$
[T_B] = T_B(V_2, V_7, V_{12}, V_{13}) \tag{4.38}
$$

Therefore, the partial derivatives of the elements of $[T_B]$ with respect to the vari-

ables V_i are given by

$$\begin{aligned}
\frac{\partial[T_B]}{\partial V_2} &= \frac{\partial[T_B]}{\partial V_7} \\
&= \begin{bmatrix} 0 & 0 & 0 & 0 \\ 0 & 0 & 0 & 0 \\ 0 & 0 & 0 & 0 \\ 0 & 0 & -1 & 0 \end{bmatrix} \\
\frac{\partial[T_B]}{\partial V_{12}} &= \begin{bmatrix} 0 & 0 & 0 & 0 \\ \cos V_{12}\sin V_{13} & -\sin V_{12} & \cos V_{12}\cos V_{13} & 0 \\ -\sin V_{12}\sin V_{13} & -\cos V_{12} & -\sin V_{12}\cos V_{13} & 0 \\ 0 & 0 & 0 & 0 \end{bmatrix} \\
\frac{\partial[T_B]}{\partial V_{13}} &= \begin{bmatrix} -\sin V_{13} & 0 & -\cos V_{13} & 0 \\ \sin V_{12}\cos V_{13} & 0 & -\sin V_{12}\sin V_{13} & 0 \\ \cos V_{12}\cos V_{13} & 0 & -\cos V_{12}\sin V_{13} & 0 \\ 0 & 0 & 0 & 0 \end{bmatrix} \\
\frac{\partial[T_B]}{\partial V_i} &= 0 \qquad \text{i} = 1, 3 \text{ to } 6, 8 \text{ to } 11, 14 \text{ to } 15
\end{aligned} \tag{4.39}$$

4.9 The Influence Coefficients $\left(\frac{\partial x}{\partial V_i}\right)^2$, $\left(\frac{\partial y}{\partial V_i}\right)^2$ and $\left(\frac{\partial z}{\partial V_i}\right)^2$

The point Q on the contour of a slice is given by Eq. (4.30),

$$[q] = [q_2]\,[T_A]\,[T_B]$$

where $[q_2]$ is given by Eq. (4.28), that is

$$[q_2] = \begin{bmatrix} R_{31} & -R_{41} & -R_{51} & 1 \end{bmatrix}$$

Taking partial derivatives of [q] with respect to a variable V_i yields

$$\frac{\partial[q]}{\partial V_i} = \frac{\partial[q_2]}{\partial V_i}[T_A][T_B] + [q_2]\left[\frac{\partial[T_A]}{\partial V_i}[T_B] + [T_A]\frac{\partial[T_B]}{\partial V_i}\right] \qquad \text{i} = 1 \text{ to } 19 \tag{4.40}$$

The derivatives of the elements of the matrices $[T_A]$ and $[T_B]$ with respect to the variables V_i have been found in the previous subsections. The position vector $[q_2]$ can be expressed in terms of the variables V_i as follows:

$$[q_2] = \begin{bmatrix} V_3 + V_6 & -V_4 - V_8 & -V_5 - V_9 - V_{10} - V_{11} & 1 \end{bmatrix}$$

Hence

$$[q_2] = q_2(V_3, V_4, \ldots, V_6, V_8, V_9, \ldots, V_{11})$$

Taking partial derivatives of $[q_2]$ with respect to the variables V_i yields

$$
\begin{aligned}
\frac{\partial[q_2]}{\partial V_3} &= [\,1 \;\; 0 \;\; 0 \;\; 0\,] \\
\frac{\partial[q_2]}{\partial V_4} &= [\,0 \;\; -1 \;\; 0 \;\; 0\,] \\
\frac{\partial[q_2]}{\partial V_5} &= [\,0 \;\; 0 \;\; -1 \;\; 0\,] \\
\frac{\partial[q_2]}{\partial V_6} &= [\,1 \;\; 0 \;\; 0 \;\; 0\,] \\
\frac{\partial[q_2]}{\partial V_8} &= [\,0 \;\; -1 \;\; 0 \;\; 0\,] \\
\frac{\partial[q_2]}{\partial V_9} &= [\,0 \;\; 0 \;\; -1 \;\; 0\,] \\
\frac{\partial[q_2]}{\partial V_{10}} &= [\,0 \;\; 0 \;\; -1 \;\; 0\,] \\
\frac{\partial[q_2]}{\partial V_{11}} &= [\,0 \;\; 0 \;\; -1 \;\; 0\,] \\
\frac{\partial[q_2]}{\partial V_i} &= [\,0 \;\; 0 \;\; 0 \;\; 0\,] \qquad \text{i =1, 2, 7, 12 to 15}
\end{aligned}
\tag{4.41}
$$

The x, y and z coordinates of Eq. (4.40) gives $\frac{\partial x}{\partial V_i}$, $\frac{\partial y}{\partial V_i}$ and $\frac{\partial z}{\partial V_i}$ respectively. Squaring them gives the influence coefficients $\left(\frac{\partial x}{\partial V_i}\right)^2$, $\left(\frac{\partial y}{\partial V_i}\right)^2$ and $\left(\frac{\partial z}{\partial V_i}\right)^2$. The influence coefficients are obtained by substituting $[q_2]$, $[T_A]$, $[T_B]$ and their partial derivatives into Eq. (4.40).

4.10 Numerical Results

Numerical results are obtained with the following input values (See Figs. 4.2 and 4.3):

$$
\begin{array}{llllllllllll}
a_1 & = & -0.15\text{ m} & b_1 & = & -0.10\text{ m} & c_1 & = & 0.22\text{ m} & & & \\
l_{1fixed} & = & 0.09\text{ m} & l_{1max} & = & 0.25\text{ m} & l_2 & = & 0.07\text{ m} & & & \\
l_{3fixed} & = & 0.12\text{ m} & l_{3max} & = & 0.25\text{ m} & l_4 & = & 0.01\text{ m} & l_5 & = & 0.15\text{ m} \\
\alpha_1 & = & 1.0^\circ & \beta_1 & = & 0.0^\circ & \alpha_2 & = & 0.0^\circ & \beta_2 & = & -1.0^\circ
\end{array}
$$

Absolute Error in positioning member 2 along link 1: $\epsilon_1 = 0.0001$ m

Tolerance per unit length on links 2, 4 and 5: $\epsilon_2 = \epsilon_4 = \epsilon_5 = 0.001$ m/m

Absolute error in positioning member 4 along member 3: $\epsilon_3 = 0.0001$ m

Radial clearance in pair 12: $c_{12} = 0.0001$ m

Radial clearance in pair 34: $c_{34} = 0.0001$ m

Absolute tolerance in Z_2 direction at the head attachment: $\epsilon_{10} = 0.0002$ m

Absolute tolerance in Z_2 direction at the nozzle tip attachment: $\epsilon_{11} = 0.0002$ m

Absolute tolerances on angles: $\epsilon_{12} = \epsilon_{13} = \epsilon_{14} = \epsilon_{15} = 0.03°$

The standard deviation σ of error at a point on the work surface is given by [110]

$$\begin{aligned} \sigma &= \sqrt{\mathrm{D[x]} + \mathrm{D[y]} + \mathrm{D[z]}} \\ &= \sqrt{\mathrm{DSUM}}, \qquad \text{say.} \end{aligned}$$

where

$$\mathrm{DSUM} = \mathrm{D[x]} + \mathrm{D[y]} + \mathrm{D[z]}$$

Hence,

$$\mathrm{DSUM} = \sigma^2$$

i.e., DSUM is the square of the standard deviation of error at a point.

The variance D[x], D[y] and D[z] are obtained at the nozzle tip Q by varying the link lengths l_1 and l_3 in the ranges $0 \leq l_1 \leq .25$ and $0 \leq l_3 \leq .25$ with increments of .025 each. Table 4.1 lists the variances D[x], D[y] and D[z], and their sum DSUM for these values of l_1 and l_3.

From the table it is seen that the variances D[x] and D[y] are of the same order and they vary slightly over the work surface. The variance D[z] is an order higher. This is because the influence coefficients $\left(\frac{\partial z}{\partial V_i}\right)_m$ have larger magnitudes compared to $\left(\frac{\partial x}{\partial V_i}\right)_m$ and $\left(\frac{\partial y}{\partial V_i}\right)_m$. Table 4.2 lists the influence coefficients for $l_1 = .25$ m and $l_3 = .25$ m for the input values mentioned above. The variance D[z] varies significantly over the work surface causing DSUM to vary over it. The maximum value of DSUM is found at $l_1 = .25$ m and $l_3 = .25$ m.

The three-sigma bands of error in tracing several curves by the nozzle tip is obtained. The three-sigma band is the band of 3σ and -3σ values of error at a point. Figure 4.8 shows the three-sigma band for tracing a curve by the nozzle tip whose projection on the X_0Y_0-plane is a line from (.05, .05) to (.20, .20). The three-sigma band increases with parameter s along the line. Figure 4.9 shows the three-sigma band for tracing a curve whose projection on the X_0Y_0-plane is a circle with center at (.15, .1) and radius .05 m. The three-sigma band decreases with angle psi along the circle and then increases. From Table 4.1 it is observed that the overall error varies appreciably over the work surface.

Variances and Their Sum						Variances and Their Sum					
l_1	l_3	D[x]	D[y]	D[z]	DSUM	l_1	l_3	D[x]	D[y]	D[z]	DSUM
m	m	$10^{-9}m^2$	$10^{-9}m^2$	$10^{-8}m^2$	$10^{-8}m^2$	m	m	$10^{-9}m^2$	$10^{-9}m^2$	$10^{-8}m^2$	$10^{-8}m^2$
0.000	0.000	4.9343	4.9657	1.8052	2.7952	0.125	0.125	4.8764	4.9278	2.1974	3.1778
0.000	0.025	4.9264	4.9619	1.8463	2.8352	0.125	0.150	4.8688	4.9242	2.2766	3.2559
0.000	0.050	4.9187	4.9581	1.8951	2.8828	0.125	0.175	4.8611	4.9205	2.3634	3.3416
0.000	0.075	4.9109	4.9543	1.9514	2.9380	0.125	0.200	4.8536	4.9169	2.4578	3.4349
0.000	0.100	4.9032	4.9506	2.0154	3.0008	0.125	0.225	4.8460	4.9133	2.5599	3.5358
0.000	0.125	4.8954	4.9468	2.0870	3.0712	0.125	0.250	4.8384	4.9098	2.6695	3.6443
0.000	0.150	4.8877	4.9431	2.1662	3.1493	0.150	0.000	4.9111	4.9426	1.9492	2.9345
0.000	0.175	4.8801	4.9394	2.2530	3.2350	0.150	0.025	4.9034	4.9388	1.9903	2.9745
0.000	0.200	4.8724	4.9358	2.3474	3.3282	0.150	0.050	4.8956	4.9351	2.0390	3.0221
0.000	0.225	4.8648	4.9321	2.4495	3.4292	0.150	0.100	4.8803	4.9277	2.1594	3.1401
0.000	0.250	4.8572	4.9285	2.5591	3.5377	0.150	0.125	4.8726	4.9240	2.2309	3.2106
0.025	0.000	4.9304	4.9618	1.8197	2.8089	0.150	0.150	4.8650	4.9204	2.3101	3.2887
0.025	0.025	4.9226	4.9580	1.8608	2.8489	0.150	0.175	4.8574	4.9168	2.3969	3.3743
0.025	0.050	4.9148	4.9542	1.9096	2.8965	0.150	0.200	4.8498	4.9132	2.4913	3.4676
0.025	0.075	4.9070	4.9505	1.9659	2.9517	0.150	0.225	4.8423	4.9096	2.5934	3.5685
0.025	0.100	4.8993	4.9467	2.0299	3.0145	0.150	0.250	4.8347	4.9061	2.7030	3.6771
0.025	0.125	4.8916	4.9430	2.1015	3.0849	0.175	0.000	4.9073	4.9388	1.9865	2.9711
0.025	0.150	4.8839	4.9393	2.1807	3.1630	0.175	0.025	4.8996	4.9350	2.0276	3.0111
0.025	0.175	4.8763	4.9356	2.2675	3.2487	0.175	0.050	4.8919	4.9313	2.0763	3.0587
0.025	0.200	4.8686	4.9320	2.3619	3.3420	0.175	0.075	4.8842	4.9276	2.1327	3.1139
0.025	0.225	4.8610	4.9284	2.4639	3.4429	0.175	0.100	4.8765	4.9239	2.1967	3.1767
0.025	0.250	4.8534	4.9248	2.5736	3.5514	0.175	0.125	4.8689	4.9203	2.2682	3.2472
0.050	0.000	4.9265	4.9580	1.8380	2.8264	0.175	0.150	4.8613	4.9166	2.3474	3.3252
0.050	0.025	4.9187	4.9542	1.8791	2.8664	0.175	0.175	4.8537	4.9130	2.4342	3.4109
0.050	0.050	4.9109	4.9504	1.9278	2.9140	0.175	0.200	4.8461	4.9095	2.5286	3.5042
0.050	0.075	4.9032	4.9466	1.9842	2.9692	0.175	0.225	4.8385	4.9059	2.6307	3.6051
0.050	0.100	4.8955	4.9429	2.0482	3.0320	0.175	0.250	4.8310	4.9024	2.7403	3.7136
0.050	0.125	4.8878	4.9392	2.1198	3.1024	0.200	0.000	4.9035	4.9349	2.0276	3.0114
0.050	0.150	4.8801	4.9355	2.1989	3.1805	0.200	0.025	4.8958	4.9312	2.0687	3.0514
0.050	0.175	4.8725	4.9318	2.2858	3.2662	0.200	0.050	4.8881	4.9275	2.1175	3.0990
0.050	0.200	4.8648	4.9282	2.3802	3.3595	0.200	0.075	4.8804	4.9238	2.1738	3.1542
0.050	0.225	4.8572	4.9246	2.4822	3.4604	0.200	0.100	4.8727	4.9202	2.2378	3.2171
0.050	0.250	4.8497	4.9210	2.5918	3.5689	0.200	0.125	4.8651	4.9165	2.3094	3.2875
0.075	0.000	4.9226	4.9541	1.8601	2.8477	0.200	0.150	4.8575	4.9129	2.3885	3.3656
0.075	0.025	4.9149	4.9503	1.9012	2.8877	0.200	0.175	4.8499	4.9093	2.4753	3.4513
0.075	0.050	4.9071	4.9465	1.9499	2.9353	0.200	0.200	4.8424	4.9057	2.5698	3.5446
0.075	0.075	4.8994	4.9428	2.0063	2.9905	0.200	0.225	4.8348	4.9022	2.6718	3.6455
0.075	0.100	4.8917	4.9391	2.0703	3.0533	0.200	0.250	4.8273	4.8987	2.7814	3.7540
0.075	0.125	4.8840	4.9354	2.1418	3.1238	0.225	0.000	4.8997	4.9312	2.0725	3.0556
0.075	0.150	4.8763	4.9317	2.2210	3.2018	0.225	0.025	4.8920	4.9274	2.1137	3.0956
0.075	0.175	4.8687	4.9281	2.3078	3.2875	0.225	0.050	4.8843	4.9237	2.1624	3.1432
0.075	0.200	4.8611	4.9244	2.4023	3.3808	0.225	0.075	4.8766	4.9201	2.2187	3.1984
0.075	0.225	4.8535	4.9208	2.5043	3.4817	0.225	0.100	4.8690	4.9164	2.2827	3.2612
0.075	0.250	4.8459	4.9172	2.6139	3.5902	0.225	0.125	4.8614	4.9128	2.3543	3.3317
0.100	0.000	4.9188	4.9502	1.8859	2.8728	0.225	0.150	4.8538	4.9092	2.4335	3.4098
0.100	0.025	4.9110	4.9465	1.9271	2.9128	0.225	0.175	4.8462	4.9056	2.5203	3.4954
0.100	0.050	4.9033	4.9427	1.9758	2.9604	0.225	0.200	4.8387	4.9020	2.6147	3.5887
0.100	0.075	4.8956	4.9390	2.0322	3.0156	0.225	0.225	4.8312	4.8985	2.7167	3.6897
0.100	0.100	4.8879	4.9353	2.0961	3.0785	0.225	0.250	4.8237	4.8950	2.8263	3.7982
0.100	0.125	4.8802	4.9316	2.1677	3.1489	0.250	0.000	4.8959	4.9274	2.1213	3.1036
0.100	0.150	4.8725	4.9279	2.2469	3.2270	0.250	0.025	4.8882	4.9237	2.1624	3.1436
0.100	0.175	4.8649	4.9243	2.3337	3.3126	0.250	0.050	4.8805	4.9200	2.2111	3.1912
0.100	0.200	4.8573	4.9207	2.4281	3.4059	0.250	0.075	4.8729	4.9163	2.2675	3.2464
0.100	0.225	4.8497	4.9171	2.5302	3.5068	0.250	0.100	4.8653	4.9127	2.3314	3.3092
0.100	0.250	4.8422	4.9135	2.6398	3.6154	0.250	0.125	4.8577	4.9091	2.4030	3.3797
0.125	0.000	4.9149	4.9464	1.9157	2.9018	0.250	0.150	4.8501	4.9055	2.4822	3.4578
0.125	0.025	4.9072	4.9426	1.9568	2.9418	0.250	0.175	4.8425	4.9019	2.5690	3.5434
0.125	0.050	4.8995	4.9389	2.0055	2.9894	0.250	0.200	4.8350	4.8984	2.6634	3.6367
0.125	0.075	4.8917	4.9352	2.0619	3.0446	0.250	0.225	4.8275	4.8948	2.7654	3.7377
0.125	0.100	4.8841	4.9315	2.1258	3.1074	0.250	0.250	4.8200	4.8913	2.8751	3.8462

Table 4.1: Variances and Their Sum at the Nozzle Tip Q in FDM Obtained by Varying l_1 and l_3

The Influence Coefficients			
i	$\left(\frac{\partial x}{\partial V_i}\right)_m$	$\left(\frac{\partial y}{\partial V_i}\right)_m$	$\left(\frac{\partial z}{\partial V_i}\right)_m$
1	0.000e+00	9.998e−01	1.745e−02
2	0.000e+00	0.000e+00	−1.000e+00
3	9.998e−01	−3.046e−04	1.745e−02
4	0.000e+00	−9.998e−01	−1.745e−02
5	1.745e−02	1.745e−02	−9.997e−01
6	9.998e−01	−3.046e−04	1.745e−02
7	0.000e+00	0.000e+00	−1.000e+00
8	0.000e+00	−9.998e−01	−1.745e−02
9	1.745e−02	1.745e−02	−9.997e−01
10	1.745e−02	1.745e−02	−9.997e−01
11	1.745e−02	1.745e−02	−9.997e−01
12	0.000e+00	1.377e−01	3.325e−01
13	−1.377e−01	0.000e+00	−3.726e−01
14	1.745e−04	1.502e−01	−7.379e−03
15	−1.435e−01	6.502e−03	−3.725e−01

Table 4.2: The Influence Coefficients for $l_1 = .25$ and $l_3 = .25$ in FDM

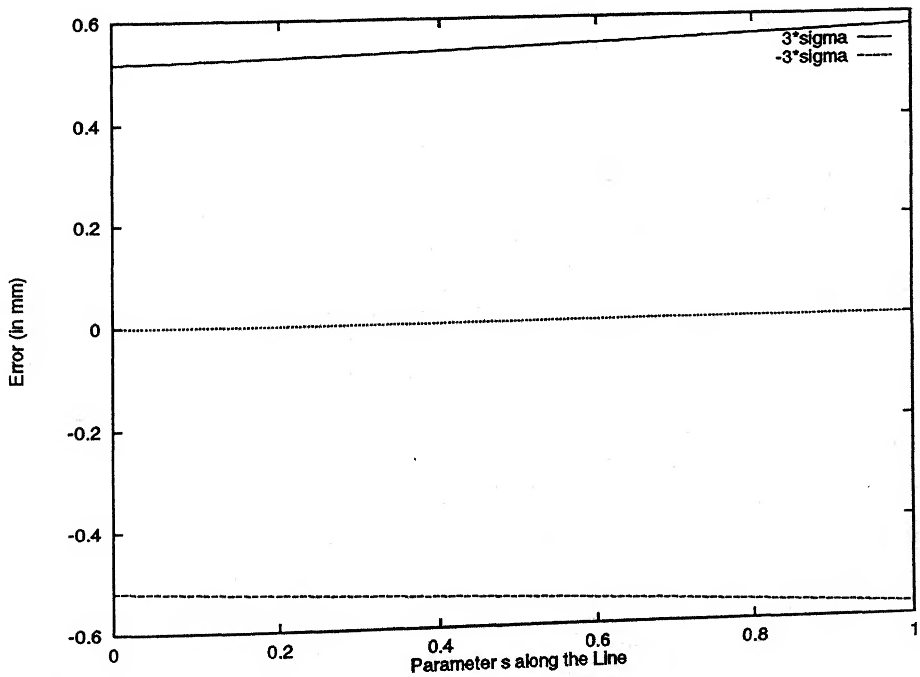

Figure 4.8: The 3σ band for Tracing a Curve by the Nozzle Tip whose Projection in X_0Y_0-Plane is an Inclined Line from (.05, .05) to (.20, .20)

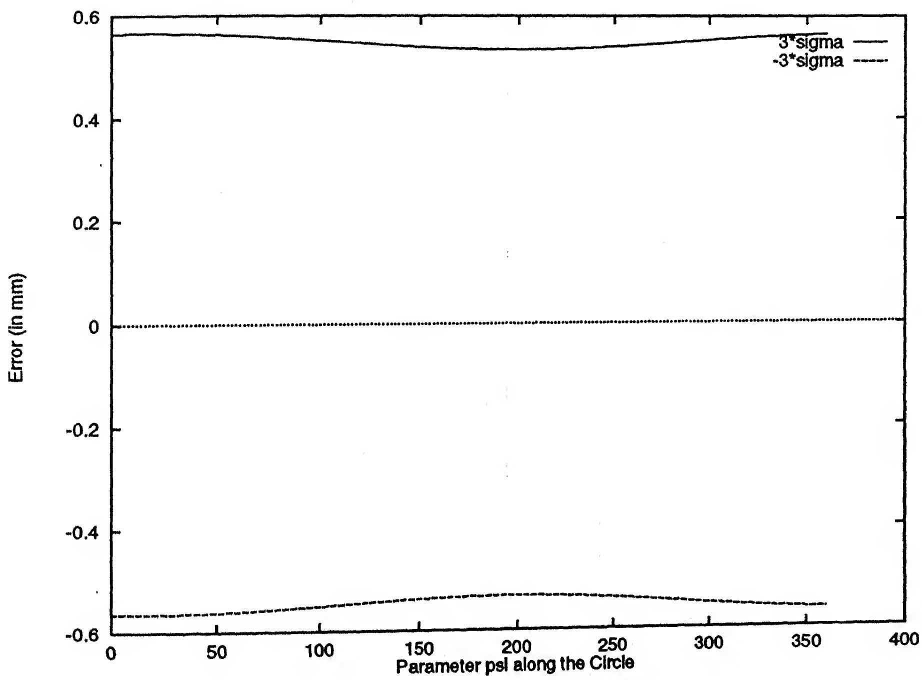

Figure 4.9: The 3σ Band for Tracing a Curve by the Nozzle Tip whose Projection in X_0Y_0-Plane is a Circle With Center at (.15, .10) and Radius .05 m

Chapter 5

ANALYSIS OF MECHANICAL ERROR IN SL

5.1 Geometric Modeling for Description of the SL Process

The StereoLithography (SL) process comprises of a laser which emits a laser beam (Fig. 1.4). An elevator platform rests below the surface of a photocurable liquid acrylate resin in a vat. Initially, the elevator platform is located at a distance from the surface equal to the thickness of the first bottom-most layer of the part to be built. The laser beam, deflected by the galvanometer-driven mirrors, scribes the contour of the slice of a part. It then hatches the interior of the contour. The liquid when exposed to the beam solidifies. The elevator platform is then lowered by a distance equal to the thickness of the next slice. The subsequent layers are produced similarly [31, 60, 63, 45]. The SL process is discussed in detail in Section 1.1.2.3.

The geometric model of the SL process is as follows. The laser beam emitted by the laser strikes the mirror GHIJ and gets deflected towards the resin surface (Fig. 5.1). It is assumed that there is a reflection from a single mirror. The ray **EF** is the centerline of the beam incident on the mirror. The ray **FQ** is the centerline of the beam reflected from the mirror (Fig. 5.1). A frame $X_0Y_0Z_0$ with X_0Y_0-plane being horizontal is chosen as the base frame.

The elevator platform moves vertically up and down. Therefore the bottom of the current layer being built is horizontal as is the liquid surface. Let a_3 and b_3 be the x and y coordinates of the front left end of the elevator platform. Let the surface of the liquid is given by $Z_0 = c_3$. A coordinate frame $X_1Y_1Z_1$ is attached at $O_1(a_3, b_3, c_3)$

with X_1Y_1-plane horizontal. Hence the X_1Y_1-plane is the free surface of the liquid. The corresponding axes of $X_0Y_0Z_0$ and $X_1Y_1Z_1$ are parallel.

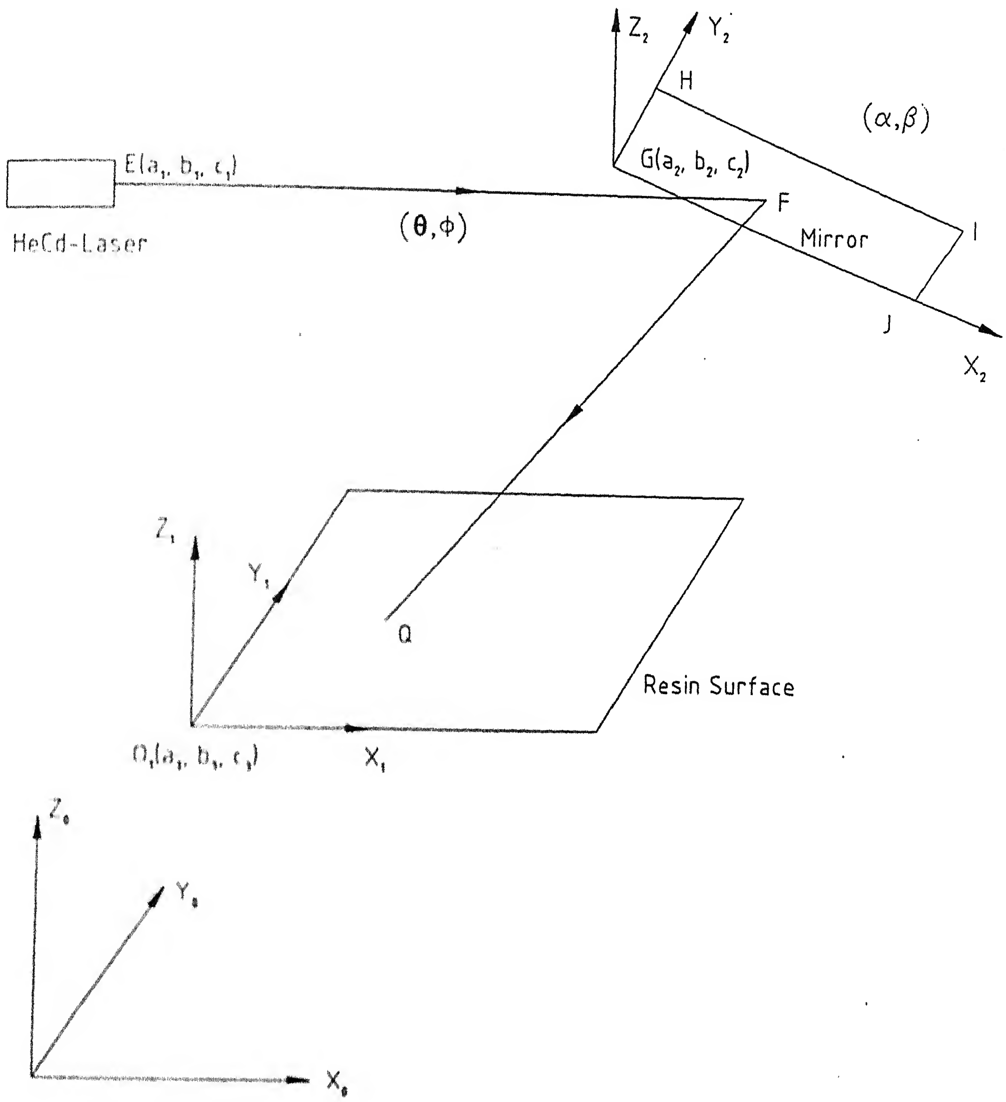

Figure 5.1: Geometric Model of the SL Process

The ray **EF** emanating from E(a_1, b_1, c_1) strikes the mirror at F and is reflected towards the point Q on the X_1Y_1-plane. Ideally the ray **EF** is along X_1 direction. However, due to mechanical errors it is oblique in space and its direction is given by two angles θ and ϕ as shown in Figs. 5.1 and 5.3. Nominal values of θ and ϕ are taken such that the ray **EF** is along X_0 direction.

The corner point G(a_2, b_2, c_2) of the mirror is taken to be fixed in space. The mirror rotates in space such that the point G is fixed. A frame $X_2Y_2Z_2$ is chosen with origin at G and the X_2Y_2-plane being the mirror plane. The frame $X_2Y_2Z_2$ is obtained from the frame $X_0Y_0Z_0$ by a rotation α about X_0-axis, a rotation β about Y_0-axis and a translation (a_2, b_2, c_2) in the base frame $X_0Y_0Z_0$. The angles α and β

are obtained such that the ray **EF** is reflected towards the desired point Q on the work surface X_1Y_1.

5.2 Stochastic Model of the SL Process

Chapter 2 discusses stochastic modeling of an RP process. Following the approach given there, the stochastic modeling of the SL process is done in the following.

Due to mechanical errors, the locations of the source E(a_1, b_1, c_1) and the corner point G(a_2, b_2, c_2) are in error (Fig. 5.2). The ray **EF** is not along X_0 direction due to mechanical errors and there are tolerances on the angles θ and ϕ. When oriented to achieve the desired reflection, the mirror is not exactly rotated by the angles α and β but the angles α and β are achieved with some tolerances.

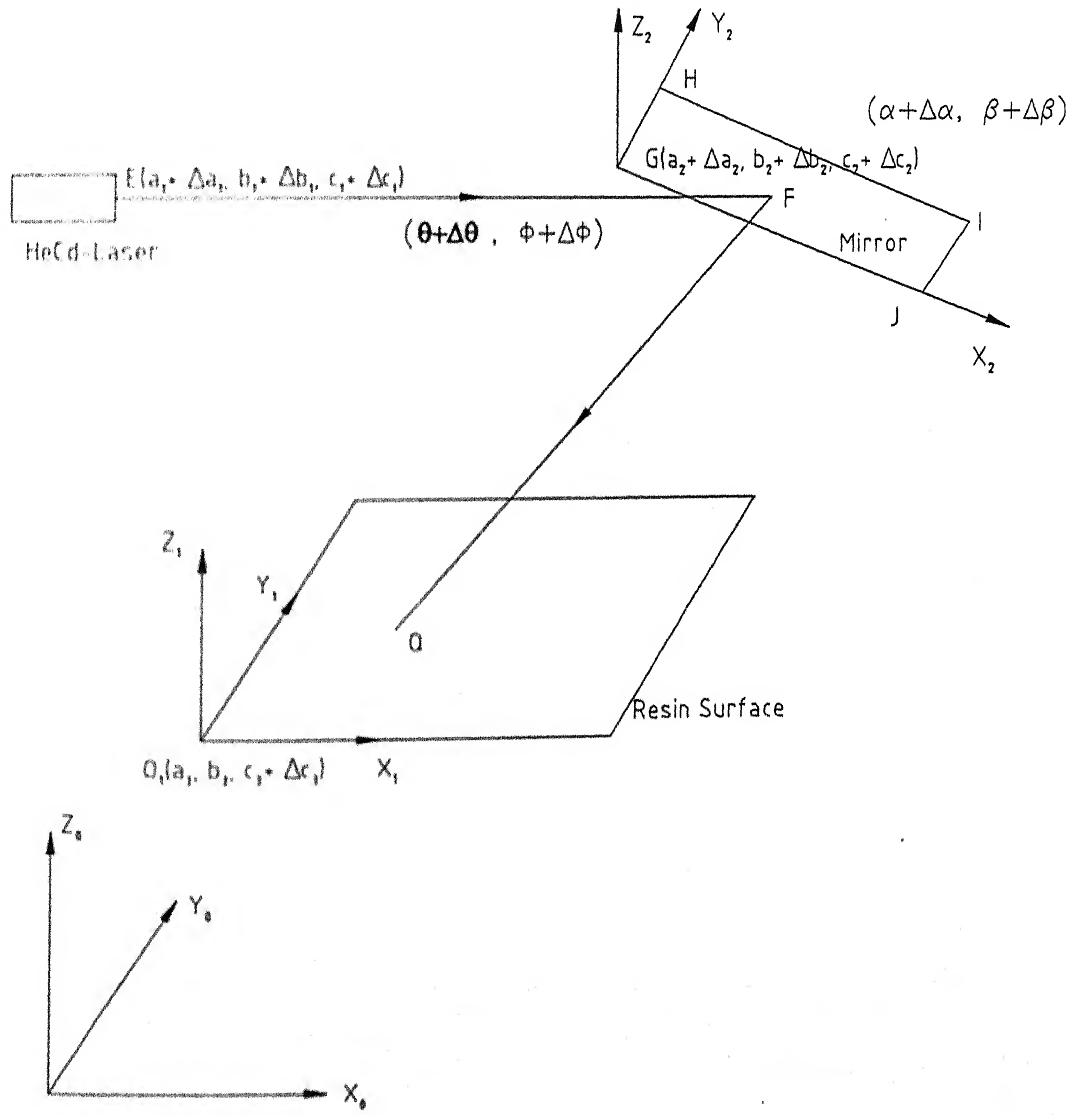

Figure 5.2: Geometric Model of the SL Process Showing Error in Dimensions

The X_1Y_1-plane is the resin level and is given by $Z_0 = c_3$ in the base frame. The liquid resin shrinks upon polymerization. Therefore the resin level decreases after laser drawing of each layer. A sensors checks the resin level upon completion of laser drawing of each layer. In the event that the sensor detects a resin level that is not within the tolerance limits, resin is displaced in the vat using a plunger. When the resin level lies within the tolerance limits, the levelling operation is completed [60, pp. 13]. Hence c_3, the Z_0-coordinate of the point G, is in error and there is a tolerance in it. The tolerance in c_3 takes into account the error in positioning the platform in Z_0direction and the error in the thickness of the current layer swept by the recoater blade also.

So, in all, there are eleven dimensions in error. Therefore there are eleven random variables V_i, i = 1 to 11, involved in the process corresponding to these eleven dimensions. These random variables are independent of each other. The random variables are given as follows:

$$\begin{array}{lllll} V_1 = a_1 + \epsilon_1, & V_2 = b_1 + \epsilon_2, & V_3 = c_1 + \epsilon_3, & V_4 = \theta + \epsilon_4, & V_5 = \phi + \epsilon_5, \\ V_6 = a_2 + \epsilon_6, & V_7 = b_2 + \epsilon_7, & V_8 = c_2 + \epsilon_8, & V_9 = \alpha + \epsilon_9, & V_{10} = \beta + \epsilon_{10}, \\ V_{11} = c_3 + \epsilon_{11}, & & & & \end{array} \tag{5.1}$$

where ϵ_i, i = 1,2,3,6,7,8 and 11 are absolute tolerances in meters on respective coordinates. ϵ_i, i = 4,5,9 and 10, are absolute tolerances in radians on angles θ, ϕ, α and β respectively.

The mean values of the variables V_i, i = 1 to 11, are given by

$$\begin{array}{lllll} m[V_1] = a_1, & m[V_2] = b_1, & m[V_3] = c_1, & m[V_4] = \theta, & m[V_5] = \phi, \\ m[V_6] = a_2, & m[V_7] = b_2, & m[V_8] = c_2, & m[V_9] = \alpha, & m[V_{10}] = \beta, \\ m[V_{11}] = c_3, & & & & \end{array} \tag{5.2}$$

The variance $D[V_i]$ of the variable V_i is given by

$$D[V_i] = \left(\frac{\epsilon_i}{3}\right)^2 \qquad i = 1 \text{ to } 11 \tag{5.3}$$

5.3 The Incident Ray EF

Consider the ray **EF** in Fig. 5.1 which emanates from the source E and strikes the mirror GHIJ at F. Let $[ef]$ be a unit vector along **EF** in the base frame. The orientation of **EF** is given by two angles θ and ϕ as shown in Fig. 5.3. Due to mechanical errors the ray **EF** is oblique in space and it intersects the X_0Y_0-plane at say, K. Therefore the unit vector $[ef]$ is given by

$$[ef] = \begin{bmatrix} \sin\theta\cos\phi & \sin\theta\sin\phi & -\cos\theta & 0 \end{bmatrix} \tag{5.4}$$

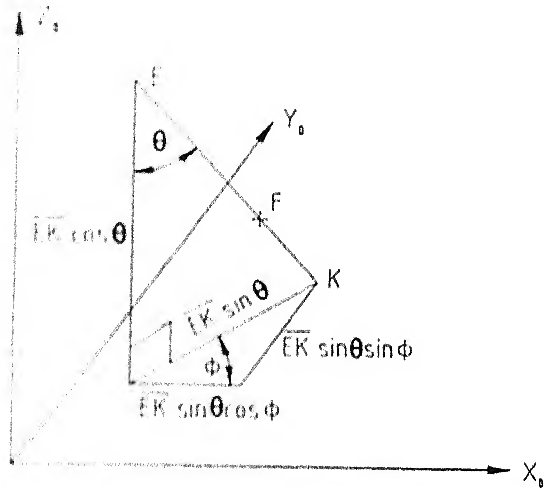

Figure 5.3: The vector **EF**

The ray **EF** is then given by [38]

$$[r(t)] = [e] + t[ef] \qquad 0 \le t \le \infty \tag{5.5}$$

where

$$[e] = \begin{bmatrix} a_1 & b_1 & c_1 & 1 \end{bmatrix} \tag{5.6}$$

5.4 The Transformation Matrices $[T_0^2]$ and $[T_2^0]$

The frame $X_2Y_2Z_2$ is obtained by a rotation α about X_0 axis, a rotation β about Y_0 axis and a translation (a_2, b_2, c_2) in the base frame $X_0Y_0Z_0$ (Fig. 5.4). The transformation $[T_0^2]$ is given by [103]

$$\left[T_0^2\right] \equiv \mathrm{Rot}(X_0, \alpha) \to \mathrm{Rot}(Y_0, \beta) \to \mathrm{Trans}(Base, a_2, b_2, c_2)$$

Or,

$$\left[T_0^2\right] = \mathrm{Rot}(X_0, \alpha)\mathrm{Rot}(Y_0, \beta)\mathrm{Trans}(Base, a_2, b_2, c_2)$$

This yields

$$\left[T_0^2\right] = \begin{bmatrix} \cos\beta & 0 & -\sin\beta & 0 \\ \sin\alpha\sin\beta & \cos\alpha & \sin\alpha\cos\beta & 0 \\ \cos\alpha\sin\beta & -\sin\alpha & \cos\alpha\cos\beta & 0 \\ a_2 & b_2 & c_2 & 1 \end{bmatrix} \tag{5.7}$$

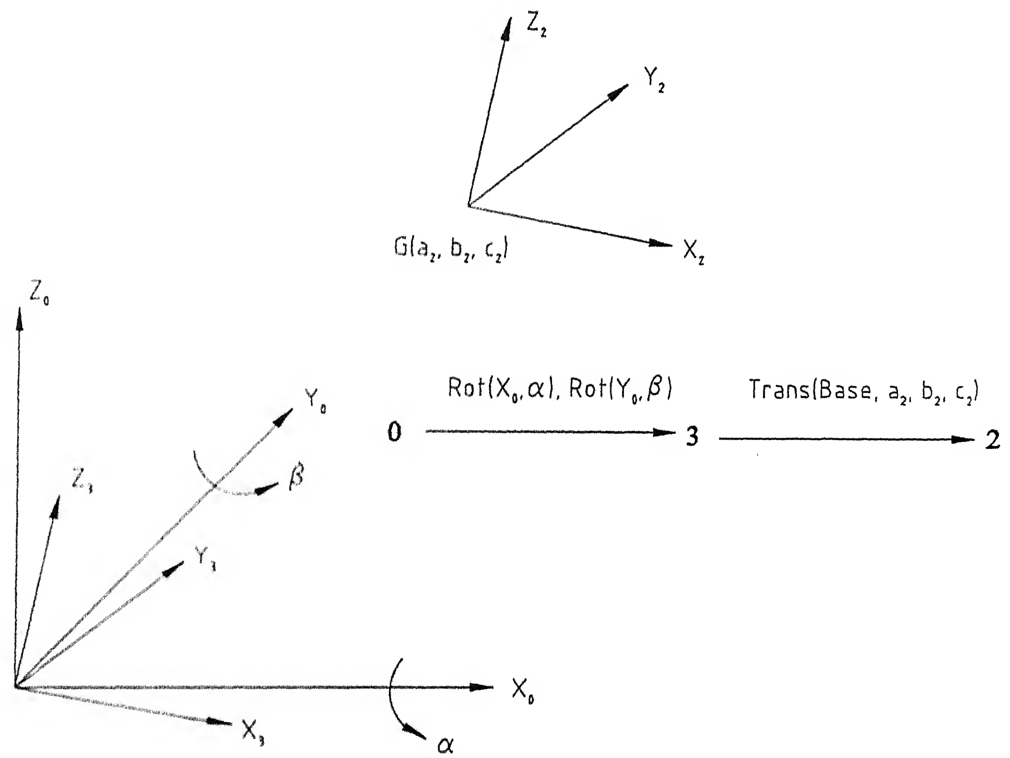

Figure 5.4: The Transformations $[T_0^2]$ and $[T_2^0]$

The transformation $[T_2^0]$, the inverse of $[T_0^2]$ is given by

$$[T_2^0] = \begin{bmatrix} \cos\beta & \sin\alpha\sin\beta & \cos\alpha\sin\beta & 0 \\ 0 & \cos\alpha & -\sin\alpha & 0 \\ -\sin\beta & \sin\alpha\cos\beta & \cos\alpha\cos\beta & 0 \\ -a_2\cos\beta & -a_2\sin\alpha\sin\beta - b_2\cos\alpha & -a_2\cos\alpha\sin\beta + b_2\sin\alpha & 1 \\ +c_2\sin\beta & -c_2\sin\alpha\cos\beta & -c_2\cos\alpha\cos\beta & \end{bmatrix} \quad (5.8)$$

5.5 Solving for the Mirror Plane and the Intersection Point F

This section finds the normal to the mirror plane such that the ray **EF** from the given source E is reflected towards the point Q on the resin surface. The mirror plane passes through the fixed point G. The normal gives the orientation of the plane of mirror in space. This section also finds the point of intersection F of the incident ray and the mirror plane.

The point E as in Eq. (5.6) is given by

$$[e] = \begin{bmatrix} a_1 & b_1 & c_1 & 1 \end{bmatrix}$$

All the position vectors including [e] above and other derivations in this section

are in the base frame $X_0Y_0Z_0$. The fixed point G on the mirror plane is given by

$$[g] = \begin{bmatrix} a_2 & b_2 & c_2 & 1 \end{bmatrix} \tag{5.9}$$

Let the point Q on the resin surface is given by

$$[q] = \begin{bmatrix} q_x & q_y & q_z & 1 \end{bmatrix} \tag{5.10}$$

The nominal values of θ and ϕ are as follows:

$$\theta = \pi/2.0, \quad \phi = 0.0 \tag{5.11}$$

At these nominal values the plane of reflection EFQ, as shown in Fig. 5.5, has a normal vector with zero X_0-coordinate. That is, the plane of reflection is normal to the Y_0Z_0-plane. This is a degenerate case and should be taken care of separately, rather than solving for the mirror plane with arbitrary values, θ and ϕ. This facilitates obtaining the solution. Let f_x be the X_0-coordinate of point F. Since ray **EF** is along X_0 direction, therefore, the point F is given by

$$[f] = \begin{bmatrix} f_x & b_1 & c_1 & 1 \end{bmatrix} \tag{5.12}$$

Let the unit vector $\mathbf{FN_1}$, normal to the mirror plane GHIJ at F, is given by

$$[fn1] = \begin{bmatrix} A & B & C & 0 \end{bmatrix} \tag{5.13}$$

The mirror plane passes through $G(a_2, b_2, c_2)$ and $\mathbf{FN_1}$ is a unit normal vector to it. A point P(x,y,z) lies on the mirror plane GHIJ if and only if **GP** is perpendicular to $\mathbf{FN_1}$; that is, if and only if

$$\mathbf{FN_1.GP} = 0 \tag{5.14}$$

This gives the mirror plane as

$$A(x - a_2) + B(y - b_2) + C(z - c_2) = 0 \tag{5.15}$$

Since the point F lies on the mirror plane given by Eq. (5.15), therefore,

$$A(f_x - a_2) + B(b_1 - b_2) + C(c_1 - c_2) = 0 \tag{5.16}$$

Moreover, $[fn_1]$ is a unit normal vector. Therefore,

$$A^2 + B^2 + C^2 = 1 \tag{5.17}$$

Let the plane of reflection, which passes through E, F and Q, is given by

$$Lx + My + Nz = 1 \tag{5.18}$$

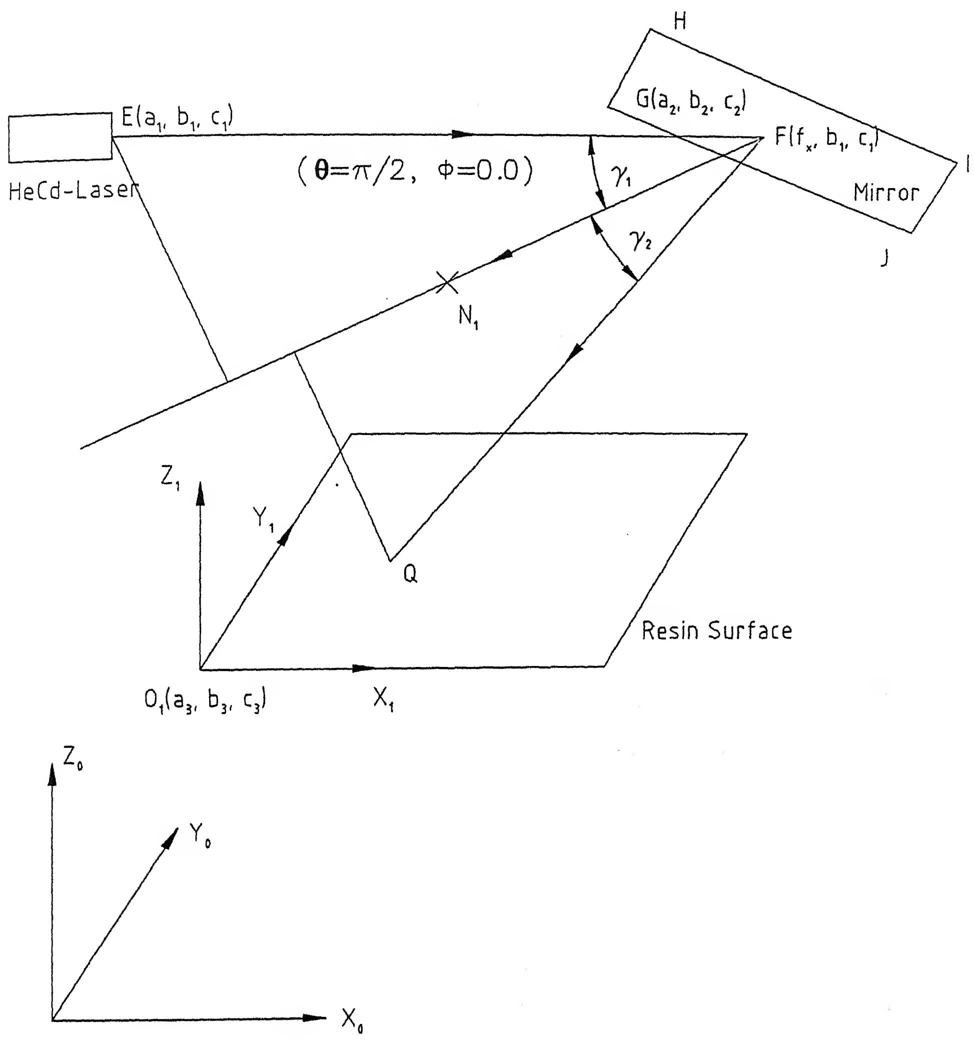

Figure 5.5: The Mirror Plane and the Plane of Reflection

Since the points E, Q and F lie on the plane given by Eq. (5.18), therefore, it follows that

$$La_1 + Mb_1 + Nc_1 = 1 \tag{5.19}$$

$$Lq_x + Mq_y + Nq_z = 1 \tag{5.20}$$

and

$$Lf_x + Mb_1 + Nc_1 = 1 \tag{5.21}$$

Equations (5.19), (5.20), (5.21) constitute a set of three equations in four unknowns L, M, N and f_x. Subtracting Eq. (5.21) from Eq. (5.19) yields

$$L = 0 \tag{5.22}$$

So the above set reduces to the following two equations in two unknowns M and N:

$$Mb_1 + Nc_1 \quad = \quad 1 \tag{5.23}$$

$$Mq_y + Nq_z = 1 \tag{5.24}$$

Solving Eqs. (5.23) and (5.24) yields

$$M = \frac{q_z - c_1}{b_1 q_z - c_1 q_y} \tag{5.25}$$

and

$$N = \frac{b_1 - q_y}{b_1 q_z - c_1 q_y} \tag{5.26}$$

The plane of reflection EFQ is now given by

$$My + Nz = 1 \tag{5.27}$$

The coefficients A, B and C of the mirror plane and the coordinate f_x of the point F are found in the following.

First Law of Reflection:

From the first law of reflection, the normal vector $\mathbf{FN_1}$ to the mirror plane, and hence the point N_1, lies on the plane of reflection EFQ given by Eq. (5.27). The point N_1 is given by

$$[n] = \left[\begin{array}{cccc} f_x{+}A & b_1{+}B & c_1{+}C & 1 \end{array}\right] \tag{5.28}$$

Since N_1 lies on the plane (5.27), therefore

$$M(b_1 + B) + N(c_1 + C) = 1 \tag{5.29}$$

Subtracting Eq. (5.19) from Eq. (5.29) and substituting $L = 0$ yields

$$MB + NC = 0$$

Or,

$$B = kC \tag{5.30}$$

where

$$k = \frac{q_y - b_1}{q_z - c_1} \tag{5.31}$$

Substituting Eq. (5.30) into Eq. (5.17) yields

$$A^2 = 1 - (1 + k^2)C^2 \tag{5.32}$$

Or,

$$A = \pm\sqrt{1 - (1 + k^2)C^2} \tag{5.33}$$

Second Law of Reflection:

From the second law of reflection, the angle of incidence γ_1 is equal to the angle of reflection γ_2 (Fig. 5.5). That is

$$\gamma_1 = \gamma_2$$

Hence,

$$\cos\gamma_1 = \cos\gamma_2$$

Or,

$$\frac{\mathbf{FE.FN_1}}{|\mathbf{FE}|\,|\mathbf{FN_1}|} = \frac{\mathbf{FN_1.FQ}}{|\mathbf{FN_1}|\,|\mathbf{FQ}|} \tag{5.34}$$

This yields

$$-A = \frac{A(q_x - f_x) + B(q_y - b_1) + C(q_z - c_1)}{\sqrt{(q_x - f_x)^2 + (q_y - b_1)^2 + (q_z - c_1)^2}} \tag{5.35}$$

Squaring both sides of the above equation gives

$$A^2 = \frac{\{A(q_x - f_x) + B(q_y - b_1) + C(q_z - c_1)\}^2}{(q_x - f_x)^2 + (q_y - b_1)^2 + (q_z - c_1)^2} \tag{5.36}$$

Consider the following equation,

$$A = \frac{A(q_x - f_x) + B(q_y - b_1) + C(q_z - c_1)}{\sqrt{(q_x - f_x)^2 + (q_y - b_1)^2 + (q_z - c_1)^2}} \tag{5.37}$$

The solutions (A_1, B_1, C_1) and (A_2, B_2, C_2) satisfying Eqs. (5.35) and (5.37), respectively, satisfy Eq. (5.36) also. Moreover, if (A_1, B_1, C_1) and (A_2, B_2, C_2) satisfy Eqs. (5.35) and (5.37), respectively, then $(-A_1, -B_1, -C_1)$ and $(-A_2, -B_2, -C_2)$ also satisfy Eqs. (5.35) and (5.37) respectively. Equation (5.35) as well as Eq. (5.16) are homogeneous in A, B and C. It follows that there are four values of the unit normal vector $[fn_1] = [\ A \quad B \quad C \quad 0\ ]$ possible on solving Eqs. (5.16), (5.30), (5.32) and (5.36).

Squaring Eq. (5.35) to obtain Eq. (5.36) is equivalent to finding the unit normal vector $\mathbf{FN_1}$ such that

$$\left[\frac{(\pm\mathbf{FE}).\mathbf{FN_1}}{|\mathbf{FE}|\,|\mathbf{FN_1}|}\right]^2 = \left[\frac{\mathbf{FN_1}.(\pm\mathbf{FQ})}{|\mathbf{FN_1}|\,|\mathbf{FQ}|}\right]^2$$

For the given points F, E and Q there are four combinations possible: (**FE**, **FQ**), (**FE**, -**FQ**), (-**FE**, **FQ**) and (-**FE**, -**FQ**). So there are four solutions to unit normal vector $\mathbf{FN_1}$ possible. Let the vectors $\mathbf{FE_1}$ and $\mathbf{FQ_1}$ be in the direction opposite to **FE** and **FQ** respectively. Then the four solutions to unit normal vector are $\mathbf{FN_{1a}}$, $\mathbf{FN_{1b}}$, $\mathbf{FN_{1c}}$ and $\mathbf{FN_{1d}}$ as shown in Fig. 5.6. $\mathbf{FN_{1a}}$ and $\mathbf{FN_{1c}}$ are bisectors of angles QFE and EFQ_1 respectively. Therefore $\mathbf{FN_{1a}}$ and $\mathbf{FN_{1c}}$ are perpendicular to each

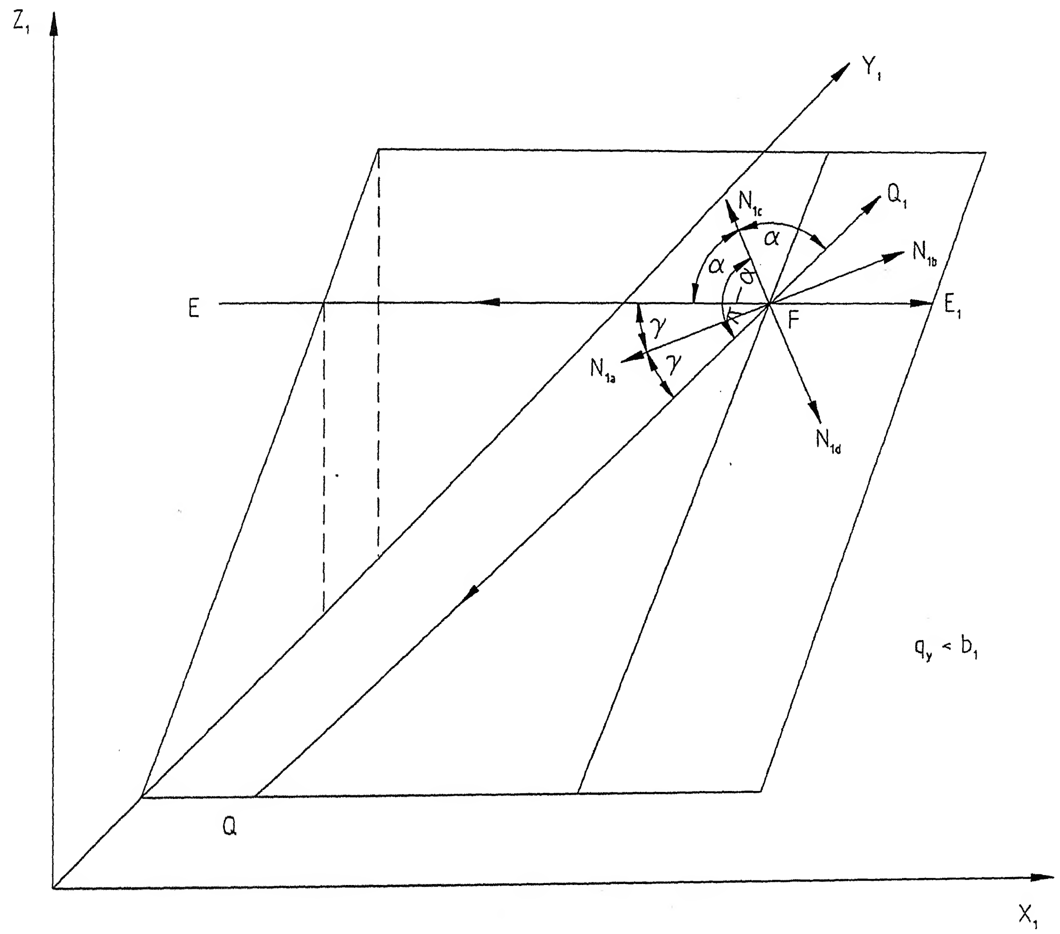

Figure 5.6: Four Possible Solutions to Unit Normal Vector on the Plane of Reflection

other. Similarly $\mathbf{FN_{1b}}$ and $\mathbf{FN_{1d}}$ are perpendicular to each other. Also the vectors $\mathbf{FN_{1a}}$ and $\mathbf{FN_{1c}}$ are collinear with vectors $\mathbf{FN_{1b}}$ and $\mathbf{FN_{1d}}$ respectively.

The vector $\mathbf{FN_{1a}}$ is the desired solution. This is because the incident ray is to be reflected downwards, towards the resin surface which is on the X_1Y_1-plane. For such a reflection, the unit normal to the mirror plane is given by

$$[fn1] = [fn1a] = [\ A \quad B \quad C \quad 0\ ]$$

where

$$\begin{aligned} C &< 0 \\ A &< 0 \end{aligned} \tag{5.38}$$

As mentioned earlier, all the derivations and position vectors are in the base frame $X_0Y_0Z_0$. The coordinate B is given by Eq. (5.30). It follows that

$$\begin{aligned} B &\geq 0 \qquad \text{for } q_y \geq b_1 \\ &< 0 \qquad \text{for } q_y < b_1 \end{aligned} \tag{5.39}$$

So there are two equations, Eqs. (5.16) and (5.36) in two unknowns C and f_x as follows:

$$\begin{aligned} A(f_x - a_2) + B(b_1 - b_2) + C(c_1 - c_2) &= 0 \\ A^2\{(q_x - f_x)^2 + (q_y - b_1)^2 + (q_z - c_1)^2\} - \{A(q_x - f_x) & \\ + B(q_y - b_1) + C(q_z - c_1)\}^2 &= 0 \end{aligned} \tag{5.40}$$

where B is given by Eq. (5.30), i.e.,

$$B = kC$$

Since $A < 0$, therefore, from Eq. (5.32) it follows that

$$A = -\sqrt{1 - (1 + k^2)C^2} \tag{5.41}$$

Since A is a real number, therefore, Eq. (5.41) gives the upper limit of $|C|$. Moreover, using Eq. (5.38) it follows that

$$-\frac{1}{\sqrt{1 + k^2}} \leq C < 0 \tag{5.42}$$

The set of equations, Eq. (5.40) above are non-linear in C and f_x. Newton-Raphson method, an iterative technique, is used to solve them [97]. Let F_1 and F_2 represent the left hand sides of Eqs. (5.16) and (5.36) above, i.e.,

$$F_1 = A(f_x - a_2) + B(b_1 - b_2) + C(c_1 - c_2) \tag{5.43}$$

$$\begin{aligned} F_2 = {} & A^2\left\{(q_x - f_x)^2 + (q_y - b_1)^2 + (q_z - c_1)^2\right\} \\ & - \{A(q_x - f_x) + B(q_y - b_1) + C(q_z - c_1)\}^2 \end{aligned} \tag{5.44}$$

Taking partial derivative of B in Eq. (5.30) with respect to C gives

$$\frac{\partial B}{\partial C} = k \tag{5.45}$$

Taking partial derivative of A in Eq. (5.32) with respect to C gives

$$\frac{\partial A}{\partial C} = -(1 + k^2)C/A \tag{5.46}$$

The Jacobian matrix [J] of the set of equation $[F] = \begin{bmatrix} F_1 \\ F_2 \end{bmatrix}$ is given by

$$[J] = \begin{bmatrix} \dfrac{\partial F_1}{\partial C} & \dfrac{\partial F_1}{\partial f_x} \\ \dfrac{\partial F_2}{\partial C} & \dfrac{\partial F_2}{\partial f_x} \end{bmatrix} \tag{5.47}$$

The partial derivatives of F_1 and F_2 are as follows:

$$\frac{\partial F_1}{\partial C} = (f_x - a_2)\frac{\partial A}{\partial C} + k(b_1 - b_2) + (c_1 - c_2) \tag{5.48}$$

$$\frac{\partial F_1}{\partial f_x} = A \tag{5.49}$$

$$\begin{aligned}\frac{\partial F_2}{\partial C} = & -2(1+k^2)C\left\{(q_x - f_x)^2 + (q_y - b_1)^2 + (q_z - c_1)^2\right\} \\ & -2\left\{A(q_x - f_x) + B(q_y - b_1) + C(q_z - c_1)\right\} \\ & \left\{(q_x - f_x)\frac{\partial A}{\partial C} + k(q_y - b_1) + (q_z - c_1)\right\}\end{aligned} \tag{5.50}$$

$$\frac{\partial F_2}{\partial f_x} = -2A^2(q_x - f_x) + 2A\left\{A(q_x - f_x) + B(q_y - b_1) + C(q_z - c_1)\right\} \tag{5.51}$$

The initial value of C for Newton-Raphson iteration is taken such that it lies in the range given by Eq. (5.42).

5.6 Orientation of the Frame $X_2Y_2Z_2$ Using Direction Cosines of X_2 and Z_2 axes

The frame $X_2Y_2Z_2$ is obtained by a rotation α about X_0-axis, a rotation β about Y_0-axis and a translation (a_2, b_2, c_2) in the base frame $X_0Y_0Z_0$ successively. For these two successive rotations, the X_2-axis lies on a plane parallel to X_0Z_0-plane for any values of α and β. So once the mirror plane is obtained, the X_2-axis is parallel to the line of intersection of the mirror plane and the X_0Z_0-plane. In Fig. 5.7, RST is the mirror plane and the line RS is the line of intersection.

The point F lies on the X_2Y_2-plane. Let the point F in the frame $X_2Y_2Z_2$ be given by

$$[f_2] = \begin{bmatrix} f_{2x} & f_{2y} & 0 & 1 \end{bmatrix} \tag{5.52}$$

The position vector $[f_2]$ can be obtained from [f] as follows:

$$[f_2] = [f]\left[T_2^0\right] \tag{5.53}$$

where $[T_2^0]$ is as given in Eq. (5.9).

The directions of X_2, Y_2 and Z_2 axes are chosen such that both f_{2x} and f_{2y} are positive. This ensures that the ray physically falls on the mirror (Fig. 5.8). The angles α and β for these X_2, Y_2 and Z_2 axes are obtained.

The mirror plane given by Eq. (5.15) can be rewritten as

$$Ax + By + Cz = D \tag{5.54}$$

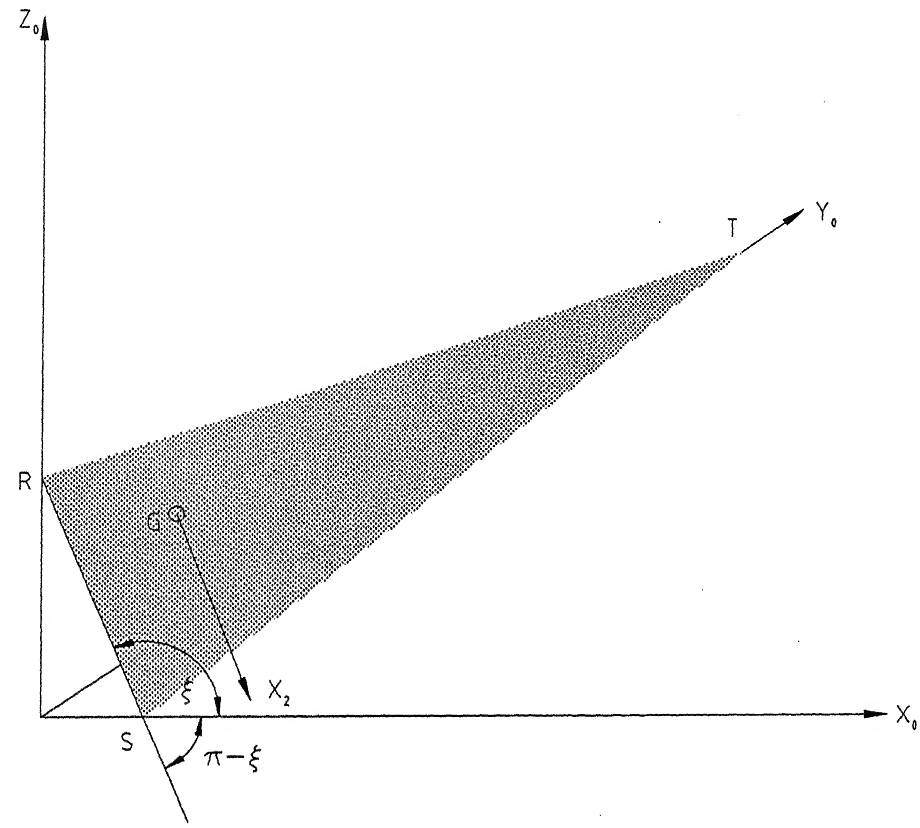

Figure 5.7: Direction of X_2 Axis

where D is a constant given by

$$D = Aa_2 + Bb_2 + Cc_2 \tag{5.55}$$

The coefficients A, B and C have already been obtained in the previous sections.

Let the line of intersection RS makes an angle ξ from X_0-axis as shown in Fig. 5.7. For the plane given by Eq. (5.54), the angle ξ is given by

$$\tan\xi = \frac{\partial z}{\partial x}$$

Or,

$$\tan\xi = -\frac{A}{C} \tag{5.56}$$

Since the coefficients A and C are negative for any point on the resin surface, therefore, the slope of line RS

$$\tan\xi < 0 \tag{5.57}$$

The choice of X_2 and Y_2 axes depends upon the coordinates of the points E and G. The points E and G are chosen such that $e_y = f_y > g_y$ and $e_z = f_z < g_z$. Then for F to lie in the first quadrant of X_2Y_2 plane, X_2-axis should be directed downwards and Y_2-axis should lie away from the line RS, as shown in Fig. 5.8. The directions of X_2 and Y_2 are chosen in this manner.

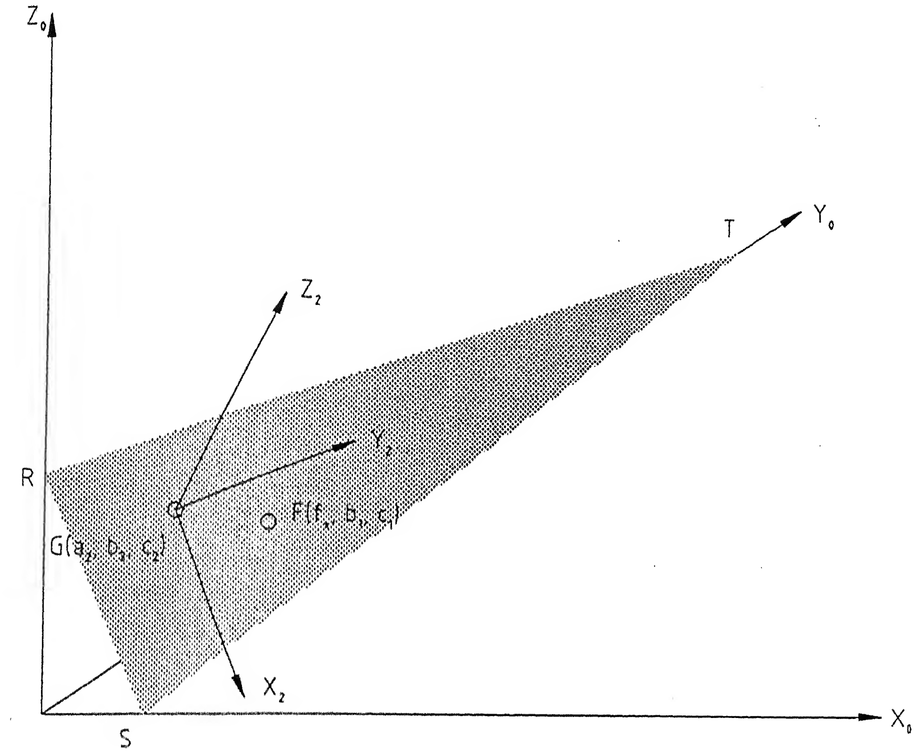

Figure 5.8: Directions of X_2 and Y_2 Axes

Since reflection is taking place in the first octant of the frame $X_0Y_0Z_0$, therefore there are points on the miror lying in the first octant. Moreover, since both the coefficients A and C are negative, therefore, the mirror plane has positive X_0 and Z_0 intercepts as shown in Fig. 5.8. Therefore from Eq. (5.57) it follows that

$$90^o < \xi < 180^o \tag{5.58}$$

Therefore,

$$\cos\xi = \frac{C}{\sqrt{A^2 + C^2}} \tag{5.59}$$

and

$$\sin\xi = -\frac{A}{\sqrt{A^2 + C^2}} \tag{5.60}$$

Hence the direction cosines of X_2-axis are given by

$$[x_2] = \left[-\frac{C}{\sqrt{A^2 + C^2}} \quad 0 \quad \frac{A}{\sqrt{A^2 + C^2}} \quad 0 \right] \tag{5.61}$$

For the chosen X_2 and Y_2 axes, the Z_2-axis is opposite to $[fn1]$. Hence the direction cosines of Z_2-axis are given by

$$[z_2] = \left[-A \quad -B \quad -C \quad 0 \right] \tag{5.62}$$

Consider the transformation $[T_0^2]$ given in Eq. (5.7). The first, second and third rows of $[T_0^2]$ give direction cosines of X_2, Y_2 and Z_2 axes in the base frame $X_0Y_0Z_0$. The fourth row of $[T_0^2]$ gives the coordinates of origin G of $X_2Y_2Z_2$ frame.

Comparing Eq. (5.61) and the first row of $[T_0^2]$ gives

$$\sin\beta = -\frac{A}{\sqrt{A^2+C^2}}$$

and

$$\cos\beta = -\frac{C}{\sqrt{A^2+C^2}}$$

Since both A and C are negative, therefore, $\sin\beta$ and $\cos\beta$ both are positive. Hence β lies in the first quadrant and is given by

$$\beta = \sin^{-1}\left[-\frac{A}{\sqrt{A^2+C^2}}\right] \tag{5.63}$$

Comparing Eqs. (5.62) and the third row of $[T_0^2]$ gives

$$\sin\alpha = B$$

and

$$\cos\alpha\sin\beta = -A$$

Substituting $\sin\beta$ in the above gives

$$\cos\alpha = \sqrt{(A^2+C^2)}$$

Therefore $\cos\alpha$ is always positive. And using Eq. (5.39) it follows that $\sin\alpha$ is positive for $q_y \geq b_1$ and negative for $q_y < b_1$. Hence the angle α is given by

$$\alpha = \sin^{-1} B \tag{5.64}$$

From Eq. (5.53) the coordinates f_{2x} and f_{2y} are given by

$$f_{2x} = (f_x - a_2)\cos\beta + (c_2 - c_1)\sin\beta \tag{5.65}$$

$$f_{2y} = (b_1 - b_2)\sec\alpha \tag{5.66}$$

With both A and C negative the mirror plane is oriented such that $f_x > a_2$. Therefore from Eq. (5.65) it follows that f_{2x} is positive. From Eq. (5.66) it follows that f_{2y} is positive. So f_{2x} and f_{2y} are always positive as desired.

5.7 Expression for *tf*, the Value of the Parameter t at the Point F

The ray **EF** in the frame $X_2Y_2Z_2$ is given by

$$[r_2(t)] = [r(t)]\left[T_2^0\right] \tag{5.67}$$

where [r(t)] is given by Eq. (5.5). Let the coordinates of $[r_2(t)]$ be given by

$$[r_2(t)] = \left[\begin{array}{cccc} r_{2x}(t) & r_{2y}(t) & r_{2z}(t) & 1 \end{array}\right]$$

The ray **EF** intersects the plane of mirror GHIJ in the X_2Y_2-plane. Therefore the point of intersection is given by

$$r_{2z}(t) = 0 \tag{5.68}$$

Let [t02_3] be the third column of $[T_2^0]$. That is

$$[t02\_3] = \left[\begin{array}{l} \cos\alpha\sin\beta \\ -\sin\alpha \\ \cos\alpha\cos\beta \\ -a_2\cos\alpha\sin\beta + b_2\sin\alpha - c_2\cos\alpha\cos\beta \end{array}\right] \tag{5.69}$$

Therefore Eq. (5.68) yields

$$\Big[[e] + tf\ [ef]\Big]\ [t02\_3] = 0 \tag{5.70}$$

where tf is the value of the parameter t at the point F. On solving it follows that

$$tf = -\frac{[e][t02\_3]}{[ef][t02\_3]} \tag{5.71}$$

Let the position vectors $[r_2(t)]$ and [r(t)] at $t = tf$ be given by $[r2\_tf]$ and $[r\_tf]$ respectively. Therefore, from Eq. (5.5),

$$[r\_tf] = [e] + tf\ [ef] \tag{5.72}$$

and from Eq. (5.67),

$$[r2\_tf] = [r\_tf]\left[T_2^0\right] \tag{5.73}$$

The point F in the frame $X_2Y_2Z_2$ is given by

$$[f_2] = [r2\_tf] \tag{5.74}$$

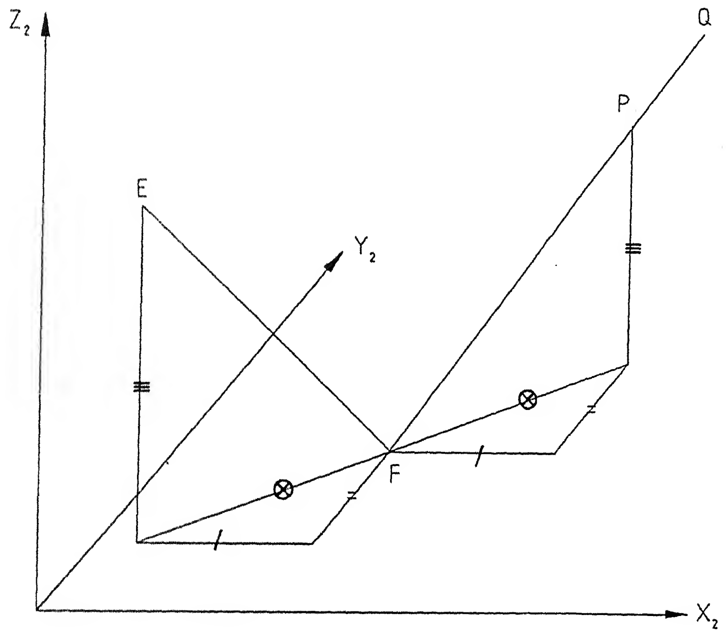

Figure 5.9: The Reflected Ray **FQ**

5.8 The Reflected Ray FQ

The ray **EF** is reflected from the mirror as the ray **FQ** (Fig. 5.9). Let P be a point on the ray **FQ** such that $|\mathbf{EF}| = |\mathbf{FP}|$.

The point E in the frame $X_2Y_2Z_2$ is given by

$$[e_2] = [e]\left[T_2^0\right] \tag{5.75}$$

Let the coordinates of $[e_2]$ be given by

$$[e_2] = \left[\begin{array}{cccc} e_{2x} & e_{2y} & e_{2z} & 1 \end{array}\right] \tag{5.76}$$

The point F in the frame $X_2Y_2Z_2$, $[f_2]$ is given by Eq. (5.52). Hence the vector **FP** in the frame $X_2Y_2Z_2$ is given by

$$[fp2] = \left[\begin{array}{cccc} f_{2x}-e_{2x} & f_{2y}-e_{2y} & +e_{2z} & 0 \end{array}\right] \tag{5.77}$$

The reflected ray **FQ** is, therefore, given by

$$[w_2] = [f_2] + s[fp2] \qquad 0 \leq s \leq sq \tag{5.78}$$

where sq is the value of the parameter s at the point Q. The ray **FQ** in the frame $X_1Y_1Z_1$ is given by

$$[w_1] = [w_2]\left[T_1^2\right] \tag{5.79}$$

where

$$[T_1^2] = [T_0^2]\left[T_1^0\right] \tag{5.80}$$

The transformation $[T_0^2]$ is given by Eq. (5.7). $[T_0^1]$ is given by

$$[T_0^1] = \begin{bmatrix} 1 & 0 & 0 & 0 \\ 0 & 1 & 0 & 0 \\ 0 & 0 & 1 & 0 \\ a_3 & b_3 & c_3 & 1 \end{bmatrix} \tag{5.81}$$

Therefore $[T_1^0]$, the inverse of $[T_0^1]$, is given by

$$[T_1^0] = \begin{bmatrix} 1 & 0 & 0 & 0 \\ 0 & 1 & 0 & 0 \\ 0 & 0 & 1 & 0 \\ -a_3 & -b_3 & -c_3 & 1 \end{bmatrix} \tag{5.82}$$

Substituting Eqs. (5.7) and (5.82) into Eq. (5.80), it follows that

$$\left[T_1^2\right] = \begin{bmatrix} \cos\beta & 0 & -\sin\beta & 0 \\ \sin\alpha\sin\beta & \cos\alpha & \sin\alpha\cos\beta & 0 \\ \cos\alpha\sin\beta & -\sin\alpha & \cos\alpha\cos\beta & 0 \\ a_2 - a_3 & b_2 - b_3 & c_2 - c_3 & 1 \end{bmatrix} \tag{5.83}$$

Let the coordinates of $[w_1]$ in Eq. (5.79) be given by

$$[w_1] = \begin{bmatrix} w_{1x} & w_{1y} & w_{1z} & 1 \end{bmatrix} \tag{5.84}$$

5.9 The Point Q on the Contour of a slice Drawn by the Laser on the Resin Surface

The point Q drawn by the laser on the resin surface is the intersection of the reflected ray **FQ** with the resin surface, i.e., the X_1Y_1-plane. From Eqs. (5.79) and (5.83), the point Q in the frame $X_1Y_1Z_1$ is given by

$$w_{1z} = 0 \tag{5.85}$$

Let [t21_3] be the third column of $[T_1^2]$. That is

$$[t21\_3] = \begin{bmatrix} -\sin\beta \\ \sin\alpha\cos\beta \\ \cos\alpha\cos\beta \\ c_2 - c_3 \end{bmatrix} \tag{5.86}$$

Therefore Eq. (5.85) yields

$$\Big[[f_2] + sq\,[fp2]\Big]\,[t21\_3] = 0 \tag{5.87}$$

where sq is the value of the parameter at the point Q. It follows that

$$sq = -\frac{[f_2][t21\_3]}{[fp2][t21\_3]} \tag{5.88}$$

Substituting the value of sq in Eq. (5.79) gives $[w_1]$ at sq. Let $[w_1]$ at sq be given by $[w1\_sq]$. Let $w1x\_sq$ and $w1y\_sq$ be the x and y coordinates of $[w1\_sq]$. Therefore,

$$[w1\_sq] = \left[\begin{array}{cccc} w1x\_sq & w1y\_sq & 0 & 1 \end{array} \right] \tag{5.89}$$

Let the coordinates of the point Q in the frame $X_1Y_1Z_1$ be given by

$$[q_1] = \left[\begin{array}{cccc} q_{1x} & q_{1y} & q_{1z} & 1 \end{array} \right] \tag{5.90}$$

Therefore,

$$\begin{aligned} q_{1x} &= w1x\_sq \\ q_{1y} &= w1y\_sq \\ q_{1z} &= 0 \end{aligned} \tag{5.91}$$

The point Q in the frame $X_0Y_0Z_0$ is given by

$$[q] = [q_1]\left[T_0^1\right] \tag{5.92}$$

This yields

$$[q] = \left[\begin{array}{cccc} w1x\_sq + a_3 & w1y\_sq + b_3 & c_3 & 1 \end{array} \right] \tag{5.93}$$

Let the coordinates of point [q] be given by

$$[q] = \left[\begin{array}{cccc} x & y & z & 1 \end{array} \right] \tag{5.94}$$

5.10 The Means and the Variances of the Dependent Variables x, y and z

From Eqs. (5.93) and (5.94) the coordinates of a point on the contour of a slice drawn by the laser beam are given by

$$\begin{aligned} x &= x\left(V_1, V_2, \ldots, V_{11}\right) \\ y &= y\left(V_1, V_2, \ldots, V_{11}\right) \\ z &= z\left(V_1, V_2, \ldots, V_{11}\right) \end{aligned} \tag{5.95}$$

Using the approach given in Chapter 2, the means and the variances of the dependent variables x, y and z are as follows:

$$
\begin{aligned}
m[x] &= x\,(m\,[V_i]\,, \quad \mathrm{i} = 1,2, \ldots, 11) \\
m[y] &= y\,(m\,[V_i]\,, \quad \mathrm{i} = 1,2, \ldots, 11) \\
m[z] &= z\,(m\,[V_i]\,, \quad \mathrm{i} = 1,2, \ldots, 11) \\
D[x] &= \sum_{i=1}^{11} \left(\frac{\partial x}{\partial V_i}\right)_m^2 D[V_i] \\
D[y] &= \sum_{i=1}^{11} \left(\frac{\partial y}{\partial V_i}\right)_m^2 D[V_i] \\
D[z] &= \sum_{i=1}^{11} \left(\frac{\partial z}{\partial V_i}\right)_m^2 D[V_i]
\end{aligned}
\tag{5.96}
$$

The partial derivatives are evaluated at the mean values of the variables V_i as denoted by the subscript m. The mean values $m[V_i]$ of the variables V_i are as given in Section 5.2. The necessary expressions for the influence coefficients $\left(\frac{\partial x}{\partial V_i}\right)^2$, $\left(\frac{\partial y}{\partial V_i}\right)^2$ and $\left(\frac{\partial z}{\partial V_i}\right)^2$ can be derived as in the following sections.

5.11 The influence coefficients $\left(\frac{\partial x}{\partial V_i}\right)^2$, $\left(\frac{\partial y}{\partial V_i}\right)^2$ and $\left(\frac{\partial z}{\partial V_i}\right)^2$

The point Q on the contour of a slice drawn on the resin surface is given by Eq. (5.93). It gives [q] in the base frame $X_0Y_0Z_0$ in terms of the nominal values of the variables. Writing [q] in terms of the variables V_i yields

$$
[q] = \begin{bmatrix} w1x\_sq{+}a_3 & w1y\_sq{+}b_3 & V_{11} & 1 \end{bmatrix} \tag{5.97}
$$

Therefore the partial derivatives of [q] with respect to the variables V_i are given by

$$
\begin{aligned}
\frac{\partial}{\partial V_i}[q] &= \begin{bmatrix} \frac{\partial w1x\_sq}{\partial V_i} & \frac{\partial w1y\_sq}{\partial V_i} & 0 & 0 \end{bmatrix} \qquad \mathrm{i} = 1 \text{ to } 10 \\
\frac{\partial}{\partial V_{11}}[q] &= \begin{bmatrix} \frac{\partial w1x\_sq}{\partial V_{11}} & \frac{\partial w1y\_sq}{\partial V_{11}} & 1 & 0 \end{bmatrix}
\end{aligned}
\tag{5.98}
$$

5.11.1 Partial Derivatives of [w1_sq]

The position vector $[w_1]$ at sq on the resin surface is given by Eq. (5.89). Therefore,

$$
\frac{\partial}{\partial V_i}[w1\_sq] = \begin{bmatrix} \frac{\partial w1x\_sq}{\partial V_i} & \frac{\partial w1y\_sq}{\partial V_i} & 0 & 0 \end{bmatrix}
$$

Taking partial derivative of Eq. (5.79) gives

$$
\begin{aligned}
\frac{\partial}{\partial V_i}[w1\_sq] &= \left[\frac{\partial [f_2]}{\partial V_i} + \frac{\partial sq}{\partial V_i}[fp2] + sq\,\frac{\partial [fp2]}{\partial V_i}\right][T_1^2] \\
&+ \Big[[f_2] + sq\,[fp2]\Big]\frac{\partial}{\partial V_i}[T_1^2] \qquad \mathrm{i} = 1 \text{ to } 11
\end{aligned}
\tag{5.99}
$$

5.11.2 Partial Derivatives of sq

The value of the parameter s at the point Q, sq is given by Eq. (5.87). It can be rewritten as

$$sq\ [fp2]\ \ [t21\_3] = -[f_2]\ \ [t21\_3]$$

Therefore the partial derivative of sq with respect to the variables V_i are given by

$$\frac{\partial sq}{\partial V_i} = -\frac{1}{[fp2][t21\_3]}\left[\frac{\partial[f_2]}{\partial V_i}[t21\_3] + [f_2]\frac{\partial[t21\_3]}{\partial V_i} + sq\ \frac{\partial[fp2]}{\partial V_i}[t21\_3] + sq\ [fp2]\frac{\partial[t21\_3]}{\partial V_i}\right] \qquad \mathrm{i} = 1 \text{ to } 11 \tag{5.100}$$

5.11.3 Partial Derivatives of $[fp2]$, $[f_2]$, $[r2\_tf]$, $[r\_tf]$ and tf

The vector $[fp2]$ given by Eq. (5.77) has its partial derivatives as follows:

$$\frac{\partial}{\partial V_i}[fp2] = \left[\begin{array}{cccc} \frac{\partial f_{2x}}{\partial V_i} - \frac{\partial e_{2x}}{\partial V_i} & \frac{\partial f_{2y}}{\partial V_i} - \frac{\partial e_{2y}}{\partial V_i} & \frac{\partial e_{2z}}{\partial V_i} & 0 \end{array}\right] \qquad \mathrm{i} = 1 \text{ to } 11 \tag{5.101}$$

Taking partial derivatives of Eqs. (5.74), (5.73)(5.72) and (5.70) it follows that

$$\frac{\partial}{\partial V_i}[f_2] = \left[\begin{array}{cccc} \frac{\partial f_{2x}}{\partial V_i} & \frac{\partial f_{2y}}{\partial V_i} & 0 & 0 \end{array}\right] = \frac{\partial}{\partial V_i}[r2\_tf] \qquad \mathrm{i} = 1 \text{ to } 11 \tag{5.102}$$

$$\frac{\partial}{\partial V_i}[r2\_tf] = \frac{\partial[r\_tf]}{\partial V_i}[T_2^0] + [r\_tf]\frac{\partial[T_2^0]}{\partial V_i} \qquad \mathrm{i} = 1 \text{ to } 11 \tag{5.103}$$

$$\frac{\partial}{\partial V_i}[r\_tf] = \frac{\partial[e]}{\partial V_i} + \frac{\partial tf}{\partial V_i}[ef] + tf\ \frac{\partial[ef]}{\partial V_i} \qquad \mathrm{i} = 1 \text{ to } 11 \tag{5.104}$$

$$\frac{\partial tf}{\partial V_i} = -\frac{1}{[ef][t02\_3]}\left[\frac{\partial[e]}{\partial V_i}[t02\_3] + [e]\frac{\partial[t02\_3]}{\partial V_i} + tf\ \frac{\partial[ef]}{\partial V_i}[t02\_3] + tf\ [ef]\frac{\partial[t02\_3]}{\partial V_i}\right] \qquad \mathrm{i} = 1 \text{ to } 11 \tag{5.105}$$

5.11.4 Partial Derivatives of $[ef]$, $[e_2]$ and $[e]$

Equation (5.4) gives $[ef]$ in terms of the nominal values of the variables. Writing $[ef]$ in terms of the variables V_i yields

$$[ef] = \left[\begin{array}{cccc} \sin V_4 \cos V_5 & \sin V_4 \sin V_5 & -\cos V_4 & 0 \end{array}\right] \tag{5.106}$$

Therefore the partial derivatives of $[ef]$ with respect to the variables V_i are given

by

$$\begin{aligned}
\frac{\partial}{\partial V_4}[ef] &= \begin{bmatrix} \cos V_4 \cos V_5 & \cos V_4 \sin V_5 & \sin V_4 & 0 \end{bmatrix} \\
\frac{\partial}{\partial V_5}[ef] &= \begin{bmatrix} -\sin V_4 \sin V_5 & \sin V_4 \cos V_5 & 0 & 0 \end{bmatrix} \\
\frac{\partial}{\partial V_i}[ef] &= \begin{bmatrix} 0 & 0 & 0 & 0 \end{bmatrix} \qquad \text{i} = 1 \text{ to } 3,\ 6 \text{ to } 11
\end{aligned} \tag{5.107}$$

Taking the partial derivative of Eq. (5.75) with respect to the variables V_i gives

$$\frac{\partial}{\partial V_i}[e_2] = \frac{\partial [e]}{\partial V_i}[T_2^0] + [e]\frac{\partial [T_2^0]}{\partial V_i} \qquad \text{i} = 1 \text{ to } 11 \tag{5.108}$$

Equation (5.6) gives the point [e] in terms of the nominal values of the variables. Writing [e] in terms of the variables V_i yields

$$[e] = \begin{bmatrix} V_1 & V_2 & V_3 & 1 \end{bmatrix} \tag{5.109}$$

Therefore the partial derivatives of [e] with respect to the variables V_i are given by

$$\begin{aligned}
\frac{\partial}{\partial V_1}[e] &= \begin{bmatrix} 1 & 0 & 0 & 0 \end{bmatrix} \\
\frac{\partial}{\partial V_2}[e] &= \begin{bmatrix} 0 & 1 & 0 & 0 \end{bmatrix} \\
\frac{\partial}{\partial V_3}[e] &= \begin{bmatrix} 0 & 0 & 1 & 0 \end{bmatrix} \\
\frac{\partial}{\partial V_i}[e] &= \begin{bmatrix} 0 & 0 & 0 & 0 \end{bmatrix} \qquad \text{i} = 4 \text{ to } 11
\end{aligned} \tag{5.110}$$

5.11.5 Partial Derivatives of the Elements of $[T_1^2]$ and $[t21\_3]$

Equation (5.83) gives the transformation $[T_1^2]$ in terms of the nominal values of the variables. Writing $[T_1^2]$ in terms of the variables V_i yields

$$[T_1^2] = \begin{bmatrix} \cos V_{10} & 0 & -\sin V_{10} & 0 \\ \sin V_9 \sin V_{10} & \cos V_9 & \sin V_9 \cos V_{10} & 0 \\ \cos V_9 \sin V_{10} & -\sin V_9 & \cos V_9 \cos V_{10} & 0 \\ V_6 - a_3 & V_7 - b_3 & V_8 - V_{11} & 1 \end{bmatrix} \tag{5.111}$$

Therefore the partial derivatives of $[T_1^2]$ with respect to the variables V_i are given

by

$$
\begin{aligned}
\frac{\partial}{\partial V_i}[T_1^2] &= 0 \qquad\qquad \text{i} = 1 \text{ to } 5 \\
\frac{\partial}{\partial V_6}[T_1^2] &= \begin{bmatrix} 0 & 0 & 0 & 0 \\ 0 & 0 & 0 & 0 \\ 0 & 0 & 0 & 0 \\ 1 & 0 & 0 & 0 \end{bmatrix} \\
\frac{\partial}{\partial V_7}[T_1^2] &= \begin{bmatrix} 0 & 0 & 0 & 0 \\ 0 & 0 & 0 & 0 \\ 0 & 0 & 0 & 0 \\ 0 & 1 & 0 & 0 \end{bmatrix} \\
\frac{\partial}{\partial V_8}[T_1^2] &= \begin{bmatrix} 0 & 0 & 0 & 0 \\ 0 & 0 & 0 & 0 \\ 0 & 0 & 0 & 0 \\ 0 & 0 & 1 & 0 \end{bmatrix} \\
\frac{\partial}{\partial V_9}[T_1^2] &= \begin{bmatrix} 0 & 0 & 0 & 0 \\ \cos V_9 \sin V_{10} & -\sin V_9 & \cos V_9 \cos V_{10} & 0 \\ -\sin V_9 \sin V_{10} & -\cos V_9 & -\sin V_9 \cos V_{10} & 0 \\ 0 & 0 & 0 & 0 \end{bmatrix} \\
\frac{\partial}{\partial V_{10}}[T_1^2] &= \begin{bmatrix} -\sin V_{10} & 0 & -\cos V_{10} & 0 \\ \sin V_9 \cos V_{10} & 0 & -\sin V_9 \sin V_{10} & 0 \\ \cos V_9 \cos V_{10} & 0 & -\cos V_9 \sin V_{10} & 0 \\ 0 & 0 & 0 & 0 \end{bmatrix} \\
\frac{\partial}{\partial V_{11}}[T_1^2] &= \begin{bmatrix} 0 & 0 & 0 & 0 \\ 0 & 0 & 0 & 0 \\ 0 & 0 & 0 & 0 \\ 0 & 0 & -1 & 0 \end{bmatrix}
\end{aligned} \qquad (5.112)
$$

The partial derivative of $[t21\_3]$ with respect to a variable V_i is the third column of the partial derivative of $[T_1^2]$ with respect to that variable V_i, i.e.,

$$
\frac{\partial}{\partial V_i}[t21\_3] = \text{third column of } \frac{\partial}{\partial V_i}[T_1^2] \qquad \text{i} = 1 \text{ to } 11 \qquad (5.113)
$$

5.11.6 Partial Derivatives of the Elements of $[T_2^0]$ and $[t02\_3]$

Equation (5.8) gives the transformation $[T_2^0]$ in terms of the nominal values of the variables. The transformation $[T_2^0]$ in terms of the variables V_i is given by

$$[T_2^0] = \begin{bmatrix} \cos V_{10} & \sin V_9 \sin V_{10} & \cos V_9 \sin V_{10} & 0 \\ 0 & \cos V_9 & -\sin V_9 & 0 \\ -\sin V_{10} & \sin V_9 \cos V_{10} & \cos V_9 \cos V_{10} & 0 \\ \begin{array}{r} -V_6 \cos V_{10} \\ +V_8 \sin V_{10} \end{array} & \begin{array}{r} -V_6 \sin V_9 \sin V_{10} - V_7 \cos V_9 \\ -V_8 \sin V_9 \cos V_{10} \end{array} & \begin{array}{r} -V_6 \cos V_9 \sin V_{10} + V_7 \sin V_9 \\ -V_8 \cos V_9 \cos V_{10} \end{array} & 1 \end{bmatrix} \tag{5.114}$$

Therefore the partial derivatives of the elements of $[T_2^0]$ with respect to the variables V_i is given by

$$\begin{aligned}
\frac{\partial}{\partial V_i}[T_2^0] &= 0 \qquad \mathrm{i} = 1 \text{ to } 5,\ 11 \\
\frac{\partial}{\partial V_6}[T_2^0] &= \begin{bmatrix} 0 & 0 & 0 & 0 \\ 0 & 0 & 0 & 0 \\ 0 & 0 & 0 & 0 \\ -\cos V_{10} & -\sin V_9 \sin V_{10} & -\cos V_9 \sin V_{10} & 0 \end{bmatrix} \\
\frac{\partial}{\partial V_7}[T_2^0] &= \begin{bmatrix} 0 & 0 & 0 & 0 \\ 0 & 0 & 0 & 0 \\ 0 & 0 & 0 & 0 \\ 0 & -\cos V_9 & \sin V_9 & 0 \end{bmatrix} \\
\frac{\partial}{\partial V_8}[T_2^0] &= \begin{bmatrix} 0 & 0 & 0 & 0 \\ 0 & 0 & 0 & 0 \\ 0 & 0 & 0 & 0 \\ \sin V_{10} & -\sin V_9 \cos V_{10} & -\cos V_9 \cos V_{10} & 0 \end{bmatrix} \\
\frac{\partial}{\partial V_9}[T_2^0] &= \begin{bmatrix} 0 & \cos V_9 \sin V_{10} & -\sin V_9 \sin V_{10} & 0 \\ 0 & -\sin V_9 & -\cos V_9 & 0 \\ 0 & \cos V_9 \cos V_{10} & -\sin V_9 \cos V_{10} & 0 \\ 0 & \begin{array}{r} -V_6 \cos V_9 \sin V_{10} + V_7 \sin V_9 \\ -V_8 \cos V_9 \cos V_{10} \end{array} & \begin{array}{r} V_6 \sin V_9 \sin V_{10} + V_7 \cos V_9 \\ +V_8 \sin V_9 \cos V_{10} \end{array} & 0 \end{bmatrix} \\
\frac{\partial}{\partial V_{10}}[T_2^0] &= \begin{bmatrix} -\sin V_{10} & \sin V_9 \cos V_{10} & \cos V_9 \cos V_{10} & 0 \\ 0 & 0 & 0 & 0 \\ -\cos V_{10} & -\sin V_9 \sin V_{10} & -\cos V_9 \sin V_{10} & 0 \\ \begin{array}{r} V_6 \sin V_{10} \\ +V_8 \cos V_{10} \end{array} & \begin{array}{r} -V_6 \sin V_9 \cos V_{10} \\ +V_8 \sin V_9 \sin V_{10} \end{array} & \begin{array}{r} -V_6 \cos V_9 \cos V_{10} \\ +V_8 \cos V_9 \sin V_{10} \end{array} & 0 \end{bmatrix}
\end{aligned} \tag{5.115}$$

The partial derivative of $[t02\_3]$ with respect to a variable V_i is the third column

of the partial derivatives of the elements of $[T_2^0]$ with respect to that variable V_i, i.e.,

$$\frac{\partial}{\partial V_i}[t02\_3] = \text{ third column of } \frac{\partial}{\partial V_i}[T_2^0] \qquad i = 1 \text{ to } 11 \tag{5.116}$$

5.12 Numerical Results

Numerical results are obtained with the following input values (see Figs. 5.1 and 5.2):

$$\begin{array}{lllll} a_1 = 0.0\text{ m} & b_1 = 0.15\text{ m} & c_1 = 1.0\text{ m} & \theta = 90.0^\circ & \phi = 0.0^\circ \\ a_2 = 0.25\text{ m} & b_2 = 0.05\text{ m} & c_2 = 1.02\text{ m} & & \\ a_3 = 0.0\text{ m} & b_3 = 0.0\text{ m} & c_3 = 0.5\text{ m} & & \end{array}$$

Length of the platform: 0.30 m

Width of the platform: 0.30 m

Absolute tolerances on x-coordinates: $\epsilon_1 = \epsilon_6 = 0.0001$ m

Absolute tolerances on y-coordinates: $\epsilon_2 = \epsilon_7 = 0.0009$ m

Absolute tolerances on z-coordinates: $\epsilon_3 = \epsilon_8 = \epsilon_{11} = 0.0008$ m

Absolute tolerances on angles: $\epsilon_4 = \epsilon_5 = \epsilon_9 = \epsilon_{10} = 0.03^\circ$

As mentioned in Section 5.6, the coordinates b_2 and c_2 are chosen such that $b_2 < b_1$ and $c_2 > c_1$.

For the laser beam to be horizontal and along X_1 direction, the angles θ and ϕ are taken to be 90° and 0° respectively. For these values of θ and ϕ, the plane of reflection EFQ is normal to the Y_0Z_0-plane as discussed in Section 5.5. This is a degenerate case and should be taken care of separately. The mirror plane is obtained for these nominal values and they cannot be varied in the present formulation.

The standard deviation σ of error at a point on the work surface is given by [110]

$$\begin{aligned} \sigma &= \sqrt{\mathrm{D[x] + D[y] + D[z]}} \\ &= \sqrt{\mathrm{DSUM}}, \qquad \text{say.} \end{aligned}$$

where

$$\mathrm{DSUM = D[x] + D[y] + D[z]}$$

Hence,

$$\mathrm{DSUM} = \sigma^2$$

i.e., DSUM is the square of the standard deviation of error at a point.

The variance D[x], D[y] and D[z] are obtained at several points Q on the resin surface, i.e., the X_1Y_1-plane. The x and y coordinates of Q, which lie in the range $0 \le q_x \le .30$ and $0 \le q_y \le .30$, are incremented by .03 each. Table 5.1 lists the variances D[x], D[y] and D[z], and their sum DSUM for these values of q_x and q_y.

Variances and Their Sum					
q_x	q_y	D[x]	D[y]	D[z]	DSUM
m	m	$10^{-7}m^2$	$10^{-7}m^2$	$10^{-7}m^2$	$10^{-7}m^2$
0.00	0.00	2.1056	1.5646	0.71111	4.3814
0.00	0.03	2.1071	1.4983	0.71111	4.3165
0.00	0.06	2.1131	1.4480	0.71111	4.2723
0.00	0.09	2.1238	1.4137	0.71111	4.2486
0.00	0.12	2.1392	1.3951	0.71111	4.2454
0.00	0.15	2.1592	1.3925	0.71111	4.2627
0.00	0.18	2.1837	1.4057	0.71111	4.3005
0.00	0.21	2.2127	1.4349	0.71111	4.3587
0.00	0.24	2.2460	1.4804	0.71111	4.4375
0.00	0.27	2.2834	1.5424	0.71111	4.5369
0.00	0.30	2.3249	1.6212	0.71111	4.6572
0.03	0.00	1.9988	1.5354	0.71111	4.2452
0.03	0.03	1.9980	1.4699	0.71111	4.1790
0.03	0.06	2.0019	1.4203	0.71111	4.1333
0.03	0.09	2.0104	1.3864	0.71111	4.1079
0.03	0.12	2.0236	1.3681	0.71111	4.1029
0.03	0.15	2.0415	1.3655	0.71111	4.1181
0.03	0.18	2.0640	1.3785	0.71111	4.1536
0.03	0.21	2.0909	1.4074	0.71111	4.2094
0.03	0.24	2.1223	1.4523	0.71111	4.2856
0.03	0.27	2.1578	1.5134	0.71111	4.3823
0.03	0.30	2.1973	1.5912	0.71111	4.4996
0.06	0.00	1.9170	1.5087	0.71111	4.1368
0.06	0.03	1.9138	1.4441	0.71111	4.0690
0.06	0.06	1.9152	1.3951	0.71111	4.0214
0.06	0.09	1.9213	1.3616	0.71111	3.9940
0.06	0.12	1.9322	1.3436	0.71111	3.9869
0.06	0.15	1.9478	1.3410	0.71111	3.9999
0.06	0.18	1.9680	1.3539	0.71111	4.0330
0.06	0.21	1.9929	1.3823	0.71111	4.0863
0.06	0.24	2.0221	1.4267	0.71111	4.1599
0.06	0.27	2.0556	1.4871	0.71111	4.2537
0.06	0.30	2.0931	1.5639	0.71111	4.3680
0.09	0.00	1.8600	1.4848	0.71111	4.0559
0.09	0.03	1.8540	1.4209	0.71111	3.9860
0.09	0.06	1.8527	1.3724	0.71111	3.9363
0.09	0.09	1.8562	1.3393	0.71111	3.9066
0.09	0.12	1.8645	1.3215	0.71111	3.8971
0.09	0.15	1.8776	1.3189	0.71111	3.9076
0.09	0.18	1.8954	1.3316	0.71111	3.9381
0.09	0.21	1.9180	1.3597	0.71111	3.9888
0.09	0.24	1.9450	1.4035	0.71111	4.0596
0.09	0.27	1.9763	1.4632	0.71111	4.1506
0.09	0.30	2.0117	1.5391	0.71111	4.2619
0.12	0.00	1.8278	1.4634	0.71111	4.0023
0.12	0.03	1.8188	1.4001	0.71111	3.9300
0.12	0.06	1.8145	1.3522	0.71111	3.8778
0.12	0.09	1.8150	1.3194	0.71111	3.8455
0.12	0.12	1.8204	1.3017	0.71111	3.8332
0.12	0.15	1.8307	1.2991	0.71111	3.8409
0.12	0.18	1.8459	1.3117	0.71111	3.8687
0.12	0.21	1.8659	1.3395	0.71111	3.9165
0.12	0.24	1.8905	1.3828	0.71111	3.9844
0.12	0.27	1.9195	1.4418	0.71111	4.0724
0.12	0.30	1.9527	1.5168	0.71111	4.1806
0.15	0.00	1.8206	1.4445	0.71111	3.9762
0.15	0.03	1.8082	1.3818	0.71111	3.9011
0.15	0.06	1.8005	1.3343	0.71111	3.8459
0.15	0.09	1.7977	1.3018	0.71111	3.8106
0.15	0.12	1.7998	1.2843	0.71111	3.7952
0.15	0.15	1.8071	1.2817	0.71111	3.7999
0.15	0.18	1.8194	1.2940	0.71111	3.8245
0.15	0.21	1.8366	1.3215	0.71111	3.8692
0.15	0.24	1.8585	1.3643	0.71111	3.9340
0.15	0.27	1.8850	1.4227	0.71111	4.0188
0.15	0.30	1.9158	1.4970	0.71111	4.1239
0.18	0.00	1.8387	1.4280	0.71111	3.9778
0.18	0.03	1.8225	1.3658	0.71111	3.8995
0.18	0.06	1.8110	1.3187	0.71111	3.8408
0.18	0.09	1.8045	1.2865	0.71111	3.8021
0.18	0.15	1.8068	1.2664	0.71111	3.7843
0.18	0.18	1.8158	1.2786	0.71111	3.8055
0.18	0.21	1.8299	1.3058	0.71111	3.8468
0.18	0.24	1.8489	1.3481	0.71111	3.9082
0.18	0.27	1.8726	1.4059	0.71111	3.9897
0.18	0.30	1.9008	1.4795	0.71111	4.0914
0.21	0.00	1.8827	1.4138	0.71111	4.0076
0.21	0.03	1.8623	1.3521	0.71111	3.9255
0.21	0.06	1.8466	1.3053	0.71111	3.8630
0.21	0.09	1.8358	1.2732	0.71111	3.8202
0.21	0.12	1.8303	1.2559	0.71111	3.7973
0.21	0.15	1.8302	1.2532	0.71111	3.7945
0.21	0.18	1.8355	1.2653	0.71111	3.8119
0.21	0.21	1.8461	1.2922	0.71111	3.8494
0.21	0.24	1.8618	1.3341	0.71111	3.9070
0.21	0.27	1.8824	1.3914	0.71111	3.9849
0.21	0.30	1.9077	1.4643	0.71111	4.0831
0.24	0.00	1.9533	1.4018	0.71111	4.0662
0.24	0.03	1.9282	1.3405	0.71111	3.9797
0.24	0.06	1.9077	1.2940	0.71111	3.9127
0.24	0.09	1.8922	1.2621	0.71111	3.8654
0.24	0.12	1.8821	1.2448	0.71111	3.8381
0.24	0.15	1.8776	1.2421	0.71111	3.8308
0.24	0.18	1.8787	1.2540	0.71111	3.8438
0.24	0.21	1.8853	1.2806	0.71111	3.8770
0.24	0.24	1.8973	1.3222	0.71111	3.9306
0.24	0.27	1.9145	1.3789	0.71111	4.0046
0.24	0.30	1.9366	1.4512	0.71111	4.0989
0.27	0.00	2.0512	1.3920	0.71111	4.1542
0.27	0.03	2.0209	1.3310	0.71111	4.0629
0.27	0.06	1.9951	1.2847	0.71111	3.9908
0.27	0.09	1.9743	1.2529	0.71111	3.9384
0.27	0.12	1.9590	1.2357	0.71111	3.9058
0.27	0.15	1.9495	1.2329	0.71111	3.8935
0.27	0.18	1.9458	1.2447	0.71111	3.9016
0.27	0.21	1.9480	1.2710	0.71111	3.9301
0.27	0.24	1.9558	1.3123	0.71111	3.9792
0.27	0.27	1.9691	1.3685	0.71111	4.0488
0.27	0.30	1.9876	1.4402	0.71111	4.1389
0.30	0.00	2.1775	1.3841	0.71111	4.2727
0.30	0.03	2.1413	1.3234	0.71111	4.1758
0.30	0.06	2.1096	1.2773	0.71111	4.0980
0.30	0.09	2.0829	1.2457	0.71111	4.0397
0.30	0.12	2.0618	1.2284	0.71111	4.0013
0.30	0.15	2.0466	1.2256	0.71111	3.9833
0.30	0.18	2.0376	1.2372	0.71111	3.9859
0.30	0.21	2.0347	1.2633	0.71111	4.0091
0.30	0.24	2.0378	1.3042	0.71111	4.0531
0.30	0.27	2.0467	1.3601	0.71111	4.1179
0.30	0.30	2.0610	1.4313	0.71111	4.2034

Table 5.1: Variances and Their Sum at Several Points on the Resin Surface obtained by varying q_x and q_y

From the table it is observed that the variances D[x], D[y] and D[z] are of the same order. The variance D[z] doesn't vary over the resin surface. This is because the influence coefficient $\left(\frac{\partial z}{\partial V_i}\right)_m$ is non-zero for i=11 only, and $\left(\frac{\partial z}{\partial V_i}\right)_m$ is constant over the resin surface. This can be verified from Eq. (5.93). Table 5.2 lists the influence coefficients at $(q_x = 0.0, q_y = 0.30)$. The variances D[x] and D[y] vary over the resin surface causing DSUM to vary over it. The maximum value of the sum of variances DSUM occurs at $(q_x = 0.0, q_y = 0.30)$.

The Influence Coefficients			
i	$\left(\frac{\partial x}{\partial V_i}\right)_m$	$\left(\frac{\partial y}{\partial V_i}\right)_m$	$\left(\frac{\partial z}{\partial V_i}\right)_m$
1	1.687e−09	−4.470e−10	3.338e−16
2	1.723e−01	1.000e+00	6.085e−17
3	−1.132e+00	3.000e−01	−1.876e−16
4	−9.852e−01	2.611e−01	−1.036e−16
5	1.500e−01	8.705e−01	2.936e−18
6	1.000e−00	4.470e−10	1.094e−16
7	−1.723e−01	−7.703e−11	−4.865e−17
8	5.744e−01	2.568e−10	0.000e+00
9	2.947e−01	1.026e+00	4.163e−17
10	−1.362e+00	2.611e−01	5.551e−17
11	5.574e−01	−3.000e−01	1.000e+00

Table 5.2: The Influence Coefficients at $q_x = 0.0$ m and $q_y = 0.3$ m in SL

The three-sigma bands of error in tracing several curves on the resin surface is obtained. The three-sigma band is the band of 3σ and -3σ values of error at a point. Figure 5.10 shows the three-sigma band for an inclined line from (.01, .28) to (.28, .1) in the X_1Y_1-plane. The three-sigma band decreases and then increases with the parameter s along the line. Figure 5.11 shows the three-sigma band for an ellipse with center at (.15, .15), semimajor axis .14 and semiminor axis .10 in the X_1Y_1-plane. The inclination angle of ellipse from X_1 direction is 0°. The three-sigma band varies slightly with the parameter psi along the ellipse. From Table 5.1 it is observed that the three-sigma band varies appreciably over the resin surface for this set of input values.

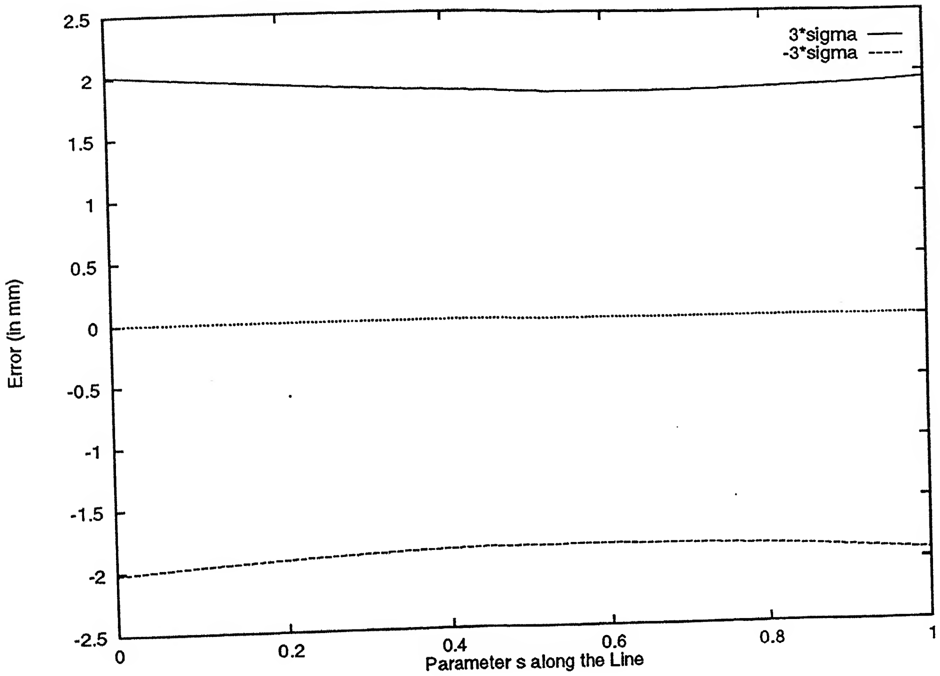

Figure 5.10: The 3σ band for an Inclined Line in Object Space from (.01, .28) to (.28, .01)

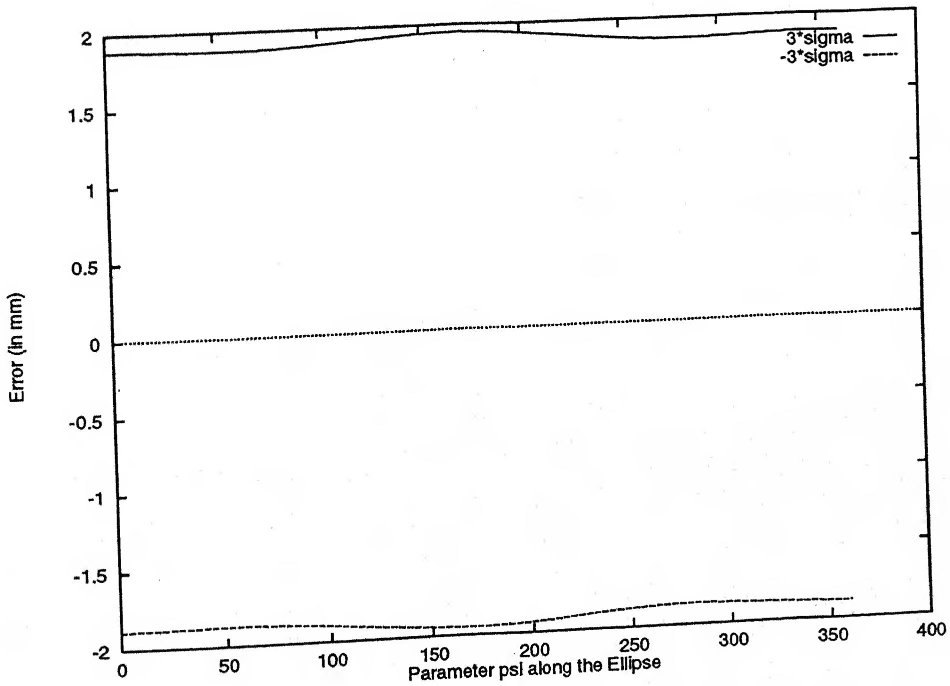

Figure 5.11: The 3σ Band for an Ellipse With Center at $X_1Y_1 = (.15, .15)$, Semimajor Axis = .14, Semiminor Axis = .10 and Inclination Angle = $0°$

Chapter 6

OPTIMAL ALLOCATION OF TOLERANCES AND CLEARANCES

The stochastic model of an RP process is discussed in Section 2.2.5. The coordinates of a point on the work surface traced by the laser beam or the tip of the extruder head is expressed as a function of random variables involved in the process. If there are n random variables $V_1, V_2, \ldots, V_n$ involved in the process then the coordinates of the point are given by $x(V_1, V_2, \ldots, V_n)$, $y(V_1, V_2, \ldots, V_n)$ and $z(V_1, V_2, \ldots, V_n)$. The section gives the methodology to associate any given range of a dependent variable x, y or z with its corresponding probability. For normally distributed random variables, the dependent variable may as well be taken as normal for more than five random variables. For a given probability, the range of a dependent variable is evaluated from the variance of the dependent variable. Equations (2.22) and (2.24) give expressions for the variances of the dependent variables x, y and z in terms of the influence coefficients $\left(\frac{\partial x}{\partial V_i}\right)^2$, $\left(\frac{\partial y}{\partial V_i}\right)^2$ and $\left(\frac{\partial z}{\partial V_i}\right)^2$.

Chapters 3, 4 and 5 derive expressions for the influence coefficients in the Laminated Object Manufacturing (LOM), the Fused Deposition Modeling (FDM) and the Stereolithography (SL) process. The variances D[x], D[y] and D[z] are tabulated at the mean values of the random variables at several points on the work surface. The three-sigma bands of mechanical error in tracing several curves on the work surface for given tolerances and clearances are plotted. This forms the analysis part of the problem. The synthesis part is the inverse of the above problem. In synthesis, the designer has to decide about the levels of tolerances on V_i's for certain allowable tolerance limits on x, y and z. One very obvious solution is to keep very strict tolerances

on V_i's so that the output errors on x, y and z will be less than the specified limits. However, such a solution is impractical since it is very expensive to manufacture any component or assembly with allowances close to zero. As a matter of fact, it is desirable to give as much of tolerance as possible to keep the manufacturing costs low.

Consider an RP process with n random variables V_i involved in its stochastic model. The random variables V_i have variances D[V_i]. The problem of optimal allocation of tolerances and clearances can be stated as follows:

$$\text{minimize} \quad C = \sum_{i=1}^{n} \frac{1}{\rho_i} \tag{6.1}$$

where

$$\rho_i = D[V_i]$$

subject to

$$\sum_{i=1}^{n} a_i \rho_i = D[x] \tag{6.2}$$

$$\sum_{i=1}^{n} b_i \rho_i = D[y] \tag{6.3}$$

$$\sum_{i=1}^{n} c_i \rho_i = D[z] \tag{6.4}$$

where

$$a_i = \left(\frac{\partial x}{\partial V_i}\right)_m^2, \quad b_i = \left(\frac{\partial y}{\partial V_i}\right)_m^2 \quad \text{and} \quad c_i = \left(\frac{\partial z}{\partial V_i}\right)_m^2$$

The minimization problem is stated at that point P(x,y,z) on the work surface where the errors in x, y and z have been observed to be critical while conducting the error analysis. In other words, some study in analyzing mechanical errors should be made prior to undertaking the synthesis. On the basis of this study values of variances D[x], D[y] and D[z] should be specified at a particular point P(x,y,z) on the work surface. Moreover, in the statement of the problem above, it has been assumed that the production cost C is inversely proportional to the variances D[V_i].

6.1 Optimization Using Lagrange Multiplier Technique

The coefficients $\left(\frac{\partial x}{\partial V_i}\right)_m^2$ in the above minimization problem are evaluated at the mean value of V_i. The expressions for the mean values of the random variables m[V_i] discussed earlier do not depend upon ϵ_i or c_{ij} and hence on ρ_i. So ρ_i and a_i are

independent. Hence the constraints are linear functions of design variables for the optimization of ρ_i's. We can take derivatives easily. So the optimization problem is solved using Lagrange multiplier technique.

Using Lagrange multiplier technique, the modified cost function can be written as

$$\begin{aligned} M &= C + \lambda_1 \left\{ \sum_{i=1}^{n} a_i \rho_i - D[x] \right\} \\ &\quad + \lambda_2 \left\{ \sum_{i=1}^{n} b_i \rho_i - D[y] \right\} \\ &\quad + \lambda_3 \left\{ \sum_{i=1}^{n} c_i \rho_i - D[z] \right\} \end{aligned} \tag{6.5}$$

where

$$C = \sum_{i=1}^{n} \frac{1}{\rho_i}$$

and λ_1, λ_2 and λ_3 are Lagrange multipliers [100, 101].

The optimality conditions for minimum M are

$$\begin{aligned} \frac{\partial M}{\partial \rho_i} &= 0 \qquad\qquad i = 1,2,\ldots,n \\ \frac{\partial M}{\partial \lambda_1} &= \frac{\partial M}{\partial \lambda_2} = \frac{\partial M}{\partial \lambda_3} = 0 \end{aligned}$$

Applying the optimality conditions to the above problem gives

$$\begin{aligned} \frac{1}{\rho_i^2} &= \lambda_1 a_i + \lambda_2 b_i + \lambda_3 c_i \\ & \qquad\qquad i = 1,2,\ldots,n \\ \sum_{i=1}^{n} a_i \rho_i - D[x] &= 0 \\ \sum_{i=1}^{n} b_i \rho_i - D[y] &= 0 \\ \sum_{i=1}^{n} c_i \rho_i - D[z] &= 0 \end{aligned} \tag{6.6}$$

Let

$$\begin{aligned} \sigma_1 &= \frac{\lambda_2}{\lambda_1}, & \sigma_2 &= \frac{\lambda_3}{\lambda_1}, \\ K_1 &= \frac{D[x]}{D[y]}, \quad \text{and} & K_2 &= \frac{D[x]}{D[z]} \end{aligned}$$

then σ_1 and σ_2 can be obtained by solving the following two equations:

$$f(\sigma_1, \sigma_2) = K_1$$

and

$$g(\sigma_1, \sigma_2) = K_2$$

where

$$f(\sigma_1, \sigma_2) = \frac{\sum_i a_i \rho_i}{\sum_i b_i \rho_i} = \frac{\sum_i \frac{a_i}{\sqrt{\lambda_1 a_i + \lambda_2 b_i + \lambda_3 c_i}}}{\sum_i \frac{b_i}{\sqrt{\lambda_1 a_i + \lambda_2 b_i + \lambda_3 c_i}}}$$

Or,

$$f(\sigma_1, \sigma_2) = \frac{\sum_i \sqrt{\frac{a_i^2}{a_i + \sigma_1 b_i + \sigma_2 c_i}}}{\sum_i \sqrt{\frac{b_i^2}{a_i + \sigma_1 b_i + \sigma_2 c_i}}} \tag{6.7}$$

Similarly

$$g(\sigma_1, \sigma_2) = \frac{\sum_i \sqrt{\frac{a_i^2}{a_i + \sigma_1 b_i + \sigma_2 c_i}}}{\sum_i \sqrt{\frac{c_i^2}{a_i + \sigma_1 b_i + \sigma_2 c_i}}} \tag{6.8}$$

For σ_1 and σ_2 to be real, it is necessary that

$$a_i + \sigma_1 b_i + \sigma_2 c_i > 0, \qquad \text{i = 1,2,...,n} \tag{6.9}$$

The region given by the expression (6.9) is plotted in Fig. 6.1 for $a_i < 0$ and $a_j > 0$. Feasible region of σ_1 and σ_2 is where the expression (6.9) is satisfied for all i.

The feasible region is bounded by two convex hulls (Fig. 6.2). One convex hull is formed by the straight lines $a_i + \sigma_1 b_i + \sigma_2 c_i = 0$, for those i for which $a_i > 0$. The other convex hull is formed by $a_i < 0$.

The function $f(\sigma_1, \sigma_2)$ and $g(\sigma_1, \sigma_2)$ can be plotted in the feasible region of (σ_1, σ_2). This will give allowable range of K_1 and K_2. Then for given values of K_1 and K_2 in the allowable range, σ_1 and σ_2 can be found by solving Eqs. (6.7) and (6.8).

There is a feasible region of σ_1 and σ_2. Therefore arbitrary choice of K_1 and K_2 is not allowed. A real solution of (λ_1, λ_2, λ_3) cannot be obtained for K_1 and K_2 chosen in the infeasible region. But if a real solution is obtained then the expression (6.9) is verified. The solution satisfies the first of equations (6.6). This gives

$$a_i + \sigma_1 b_i + \sigma_2 c_i = \frac{1}{\lambda_1 \rho_i^2}, \qquad \text{i = 1,2,...,n} \tag{6.10}$$

So the expression (6.9) is verified if λ_1 obtained in the solution is positive. This verification avoids plotting $f(\sigma_1, \sigma_2)$ and $g(\sigma_1, \sigma_2)$ to find the allowable range of K_1 and K_2.

The first of equations (6.6) can be rewritten as

$$\rho_i = \frac{1}{\sqrt{\lambda_1 a_i + \lambda_2 b_i + \lambda_3 c_i}} \qquad \text{i = 1,2,...,n} \tag{6.11}$$

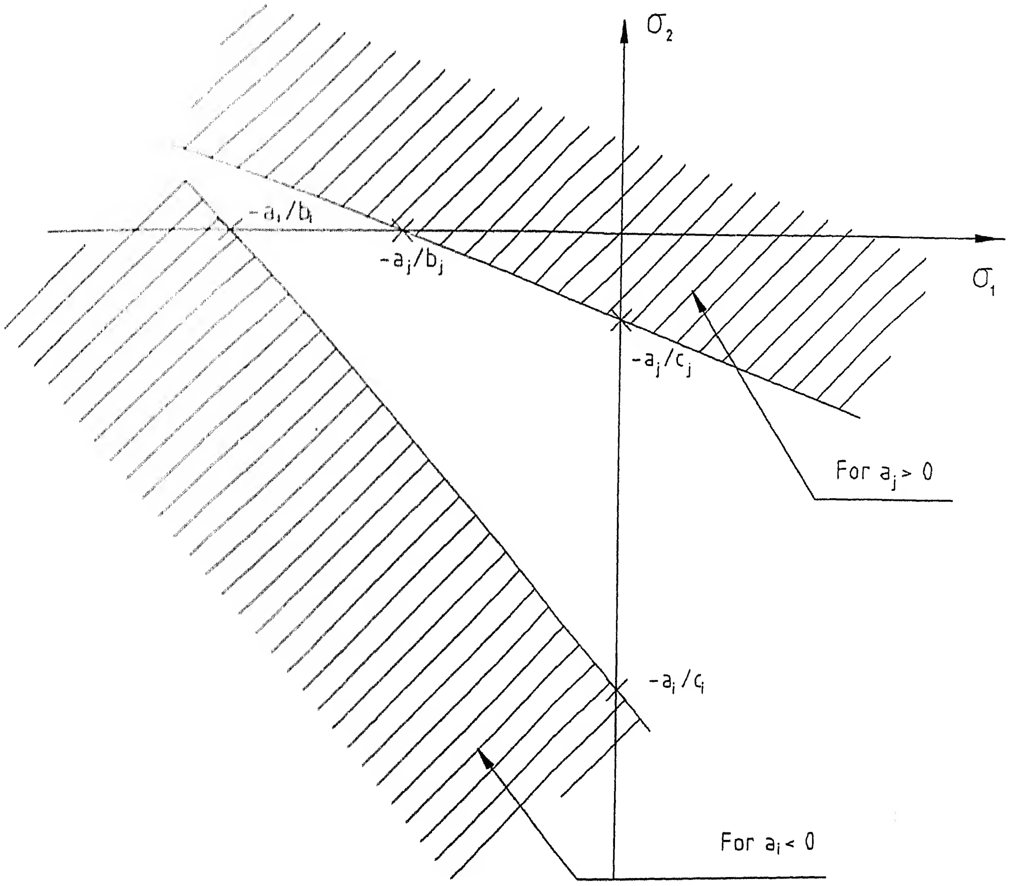

Figure 6.1: The region $a_i + \sigma_1 b_i + \sigma_2 c_i > 0$

Substituting the above expression for ρ_i in the last three equations of (6.6) gives three non-linear equations in three unknowns λ_1, λ_2 and λ_3 as follows:

$$\begin{aligned} h_1(\lambda_1, \lambda_2, \lambda_3) &= \sum_{i=1}^{n} a_i(\lambda_1 a_i + \lambda_2 b_i + \lambda_3 c_i)^{-1/2} - D[x] &= 0 \\ h_2(\lambda_1, \lambda_2, \lambda_3) &= \sum_{i=1}^{n} b_i(\lambda_1 a_i + \lambda_2 b_i + \lambda_3 c_i)^{-1/2} - D[y] &= 0 \\ h_3(\lambda_1, \lambda_2, \lambda_3) &= \sum_{i=1}^{n} c_i(\lambda_1 a_i + \lambda_2 b_i + \lambda_3 c_i)^{-1/2} - D[z] &= 0 \end{aligned} \tag{6.12}$$

The above set of non-linear equations can be solved by Newton-Raphson method. The elements of the Jacobian [J] can be derived as follows:

$$\begin{aligned} \frac{\partial h_1}{\partial \lambda_1} &= \sum_{i=1}^{n} a_i(-\frac{a_i}{2})(\lambda_1 a_i + \lambda_2 b_i + \lambda_3 c_i)^{-3/2} \\ \frac{\partial h_1}{\partial \lambda_2} &= \sum_{i=1}^{n} a_i(-\frac{b_i}{2})(\lambda_1 a_i + \lambda_2 b_i + \lambda_3 c_i)^{-3/2} \\ \frac{\partial h_1}{\partial \lambda_3} &= \sum_{i=1}^{n} a_i(-\frac{c_i}{2})(\lambda_1 a_i + \lambda_2 bi + \lambda_3 c_i)^{-3/2} \end{aligned}$$

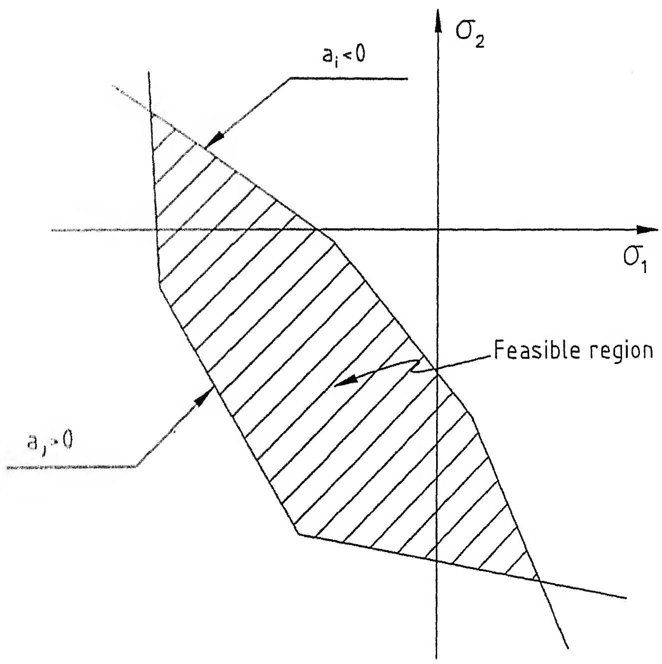

Figure 6.2: Feasible Region of σ_1 and σ_2

Similarly the expressions for $\frac{\partial h_2}{\partial \lambda_i}$, i = 1,2,3 and $\frac{\partial h_3}{\partial \lambda_i}$, i = 1,2,3 can be obtained. Then the Jacobian [J] can be written as follows:

$$[J] = \sum_{i=1}^{n} (-\frac{1}{2})(\lambda_1 a_i + \lambda_2 b_i + \lambda_3 c_i)^{-3/2} \begin{bmatrix} a_i^2 & a_i b_i & a_i c_i \\ b_i a_i & b_i^2 & b_i c_i \\ c_i a_i & c_i b_i & c_i^2 \end{bmatrix} \tag{6.13}$$

So analytical expression for Jacobian [J] is available and it is not needed to find the numerical derivatives of h_i, i = 1,2,3. On solving Eq. (6.12) by Newton-Raphson method the values of λ_1, λ_2 and λ_3 can be obtained. Then ρ_i's can be obtained from expression (6.11).

6.2 Optimization Using Genetic Algorithms

Genetic algorithms (GAs) are computerized search and optimization algorithms based on the mechanics of natural genetics and natural selection. GAs mimic the survival-of-the-fittest principle of nature to make a search process [25]. The variables in GA are coded in some string structures. Mostly binary coded strings are used. The length of the string is usually determined according to the desired solution accuracy.

In general, a fitness function $\mathcal{F}(x)$ is first derived from the objective function and used in successive genetic operation. For maximization problem, the fitness function can be considered to be the same as the objective function or $\mathcal{F}(x) = f(x)$. For

minimization problem the following function is often used.

$$\mathcal{F}(x) = \frac{1}{1+f(x)}$$

The fitness function value of a string is known as the string's fitness.

The operation of GAs begins with a population of random strings representing design or decision variables. Thereafter, each string is evaluated to find the fitness value. The population is then operated by three main operators — reproduction, crossover and mutation — to create a new population of points. The new population is further tested for termination. If the termination criterion is not met, the population is iteratively operated by the above three operators and evaluated. This procedure is continued until the termination criterion is met. One cycle of these operations and the subsequent evaluation procedure is known as a generation in GA's terminology.

As GAs use a coding of variables, they work with a discrete search space. Even though the underlying objective function is a continuous function, GAs convert the search space into a discrete set of points. GAs have also been developed to work directly with continuous variables (instead of discrete variables). In those GAs binary strings are not used. Instead, the variables are directly used. These are called real-coded GAs [25, 26].

A code developed by Deb et al [26] for real-coded GA is used in the present work.

6.3 Optimum Tolerances in LOM

Chapter 3 finds the position vector $\mathbf{q}(u,w) = [\ x \quad y \quad z \quad 1\ ]$ of a point on the contour of a slice traced by the laser beam in LOM. There are nineteen random variables involved in the stochastic model of the LOM process. The influence coefficients a_i, b_i and c_i and the partial derivatives required for them are derived in Section 3.2, pp. 50-66. The variance of the dependent variables x, y and z and their sum at several points on the work surface is tabulated in Table 3.1, Section 3.3. Sections 3.3 also gives the plots of three-sigma bands of error in tracing several lines on the bilinear surface $\mathbf{q}$(u,w). From the error analysis it is found that the maximum value of the sum of variances DSUM occurs at (u=1.0, w=1.0).

Numerical results for the optimal allocation of tolerances are obtained with the mean values of variables and other input values mentioned in Section 3.3. Optimal allocation is based on the point where DSUM is maximum, that is, at (u=1.0, w=1.0) in uw parametric space on the bilinear surface ABDC. Assuming D[x] = 1.6076 x $10^{-17}m^2$, D[y] = 1.1111 x $10^{-17}m^2$ and D[z] = 2.4994 x $10^{-17}m^2$, the optimal values of tolerances obtained are listed in Table 6.1. The optimal allocation is done using

Lagrange multiplier techniques. Since a real solution for the Lagrange multipliers $(\lambda_1, \lambda_2, \lambda_3)$ is obtained with positive λ_1, therefore, the ratio of variances, K_1 and K_2 are in the allowable range and the solution for $(\lambda_1, \lambda_2, \lambda_3)$ exists. The solution obtained for the Lagrange multipliers are as follows:

$$\lambda_1 = 8.4607 \times 10^{17} \quad \lambda_2 = 8.0997 \times 10^{17} \quad \lambda_3 = 1.6493 \times 10^{17}$$

Optimal Allocation of Tolerances			
		Tolerance	Units
Absolute tolerance on coordinate a_1	ϵ_1	$= 2.152e-04$	m
Absolute tolerance on coordinate b_1	ϵ_2	$= 5.382e-06$	m
Absolute tolerance on coordinate c_1	ϵ_3	$= 7.111e-07$	m
Absolute tolerance on angle α_1	ϵ_4	$= 2.537e-05$	rad
Absolute tolerance on angle β_1	ϵ_5	$= 2.133e-03$	rad
Tolerance per unit length on radius r_1	ϵ_6	$= 2.370e-05$	m/m
Tolerance per unit length on length l_1	ϵ_7	$= 4.337e-02$	m/m
Absolute tolerance on coordinate a_2	ϵ_8	$= 1.271e-07$	m
Absolute tolerance on coordinate b_2	ϵ_9	$= 5.382e-06$	m
Absolute tolerance on coordinate c_2	ϵ_{10}	$= 7.111e-07$	m
Absolute tolerance on angle α_2	ϵ_{11}	$= 7.500e-06$	rad
Absolute tolerance on angle β_2	ϵ_{12}	$= 5.551e-06$	rad
Tolerance per unit length on radius r_2	ϵ_{13}	$= 4.963e-07$	m/m
Tolerance per unit length on length l_2	ϵ_{14}	$= 7.712e-04$	m/m
Absolute tolerance on coordinate a_3	ϵ_{15}	$= 9.892e-09$	m
Absolute tolerance on coordinate b_3	ϵ_{16}	$= 1.000e-08$	m
Absolute tolerance on coordinate c_3	ϵ_{17}	$= 2.168e-02$	m
Absolute tolerance on angle θ	ϵ_{18}	$= 1.430e-08$	rad
Absolute tolerance on angle ϕ	ϵ_{19}	$= 2.168e-02$	rad

Table 6.1: Optimal Allocation of Tolerances in LOM

From Table 6.1 it is observed that much stricter tolerances are allocated on the variables V_{15}, V_{16} and V_{18} compared to other variables. This is because the corresponding influence coefficients are much larger. Stricter tolerances are also allocated on the variables V_3, V_8, V_{10} and V_{13}, whereas large tolerances are demanded on the variables V_7, V_{17} and V_{19}. Therefore, the error is most sensitive to V_{15}, V_{16} and V_{18}, and least sensitive to V_7, V_{17} and V_{19}.

6.4 Optimum Tolerances and Clearances in FDM

Chapter 4 finds the coordinates of a point on the contour of a slice traced by the nozzle tip Q. There are fifteen random variables V_1, V_2, ..., V_{15} involved in the stochastic model of the FDM process. The expressions for the influence coefficients a_i, b_i and c_i and the partial derivatives needed for them are given in Sections 4.7, 4.8 and 4.9, (pp. 86-88). The variances of the dependent variable x, y and z and their sum at several points on the work surface is tabulated in Table 4.1, Section 4.10. Section 4.10 also gives the plots of three-sigma bands of error in tracing several curves by the nozzle tip. From the error analysis it is found that the maximum value of the sum of variances DSUM occurs at $l_1 = 0.25$ m and $l_3 = 0.25$ m.

The optimal allocation of tolerances and clearances is done at the mean values of variables and other input values mentioned in Section 4.10. Optimal allocation is based on the location of nozzle tip where DSUM is maximum, that is, at $l_1 = 0.25$m and $l_3 = 0.25$ m. Assuming D[x] = 6.5 x $10^{-8}m^2$, D[y] = 3.0 x $10^{-7}m^2$ and D[z] = 19.5 x $10^{-8}m^2$, the optimal values of variances of variables V_i are obtained using Lagrange multiplier technique. Since a real solution for the Lagrange multipliers $(\lambda_1, \lambda_2, \lambda_3)$ is obtained with positive λ_1, therefore, the ratio of variances, K_1 and K_2 are in the allowable range and the solution for $(\lambda_1, \lambda_2, \lambda_3)$ exists. The solution obtained for the Lagrange multipliers are as follows:

$$\lambda_1 = 1.0396 \times 10^{15} \quad \lambda_2 = 1.2301 \times 10^{18} \quad \lambda_3 = 9.6734 \times 10^{14}$$

The optimal values of variances ρ_i of variables V_i obtained from Lagrange multiplier technique are listed in Table 6.2. The derivatives $\frac{\partial[q_2]}{\partial V_i}$, $\frac{\partial[T_A]}{\partial V_i}$ and $\frac{\partial[T_B]}{\partial V_i}$, and hence $\frac{\partial[q]}{\partial V_i}$ are identical for (i = 2,7). They are also identical for the indices i in each of the sets (i = 3,6), (i = 4,8) and (i = 5,9,10,11). Therefore, from Eq. (6.6) the optimum variances ρ_i are identical for the indices i in each of these sets as obtained by Lagrange multiplier technique in Table 6.2.

The optimum values of variances are also obtained using real coded genetic algorithm optimization method. The input values taken for GA runs are as follows:

Population size:	150
Number of variables:	15
Bounds on variables:	rigid
Crossover probability:	0.90
Mutation probability:	0.05
Random seed number:	0.15

Optimization is done by varying number of generation and number of runs. The optimum values of variances ρ_i on variables V_i, obtained for 600 generations and

single run, are listed in Table 6.2 alongwith those obtained from Lagrange multiplier technique.

Optimum Variances from Lagrange		Optimum Variances from Real GA	
i	Variance ρ_i	i	Variance ρ_i
1	9.018e−10	1	8.533e−10
2	3.215e−08	2	2.953e−08
3	3.101e−08	3	3.078e−08
4	9.018e−10	4	7.374e−10
5	2.730e−08	5	2.873e−08
6	3.101e−08	6	3.123e−08
7	3.215e−08	7	2.912e−08
8	9.018e−10	8	7.405e−10
9	2.730e−08	9	2.920e−08
10	2.730e−08	10	2.809e−08
11	2.730e−08	11	2.799e−08
12	6.531e−09	12	1.445e−08
13	8.058e−08	13	7.328e−08
14	6.005e−09	14	1.545e−08
15	6.940e−08	15	7.611e−08

Table 6.2: Optimum Values of Variances ρ_i in FDM from Lagrange Multiplier Technique and from Real Coded GA.

The optimum values obtained by real GA compare quite closely with those obtained by Lagrange method. The optimum values of ρ_{12} and ρ_{14} obtained by real GA differ from those obtained by Lagrange method. This needs to be investigated further. It has been observed that when the optimum values differ by several orders, then some of the optimum variances obtained by GA differ from those obtained by Lagrange method.

The tolerances and clearances are computed from the optimal values of variances ρ_i of variables V_i obtained from Lagrange method. Both ρ_6 and ρ_7 give the clearance c_{12} in pair 12. The smaller of the two values is chosen for the clearance c_{12} because narrower clearance will ensure that the variances on the dependent variables doesn't exceed the specified limit. Similarly smaller of the two values of clearances obtained from the variances ρ_8 and ρ_9 is chosen for the clearances c_{34} on pair 34. The optimal values of tolerances and clearances are listed in Table 6.3.

Converting the tolerance coefficients into absolute tolerances on the respective links and comparing the tolerances on links we find that stricter tolerances are de-

Optimal Allocation of Tolerances			
		Tolerance	Units
Absolute tolerance in positioning member 2 along link 1	ϵ_1	= 9.009e−05	m
Tolerance per unit length on link 2	ϵ_2	= 7.685e−03	m/m
Absolute tolerance in positioning member 4 along link 3	ϵ_3	= 5.283e−04	m
Tolerance per unit length on link 4	ϵ_4	= 9.009e−03	m/m
Tolerance per unit length on link 5	ϵ_5	= 3.305e−03	m/m
Radial Clearance in pair 12	c_{12}	= 3.522e−04	m
Radial Clearance in pair 34	c_{34}	= 6.006e−05	m
Absolute tolerance in Z_2 direction at the head attachment	ϵ_{10}	= 4.957e−04	m
Absolute tolerance in Z_2 direction at the nozzle tip attachment	ϵ_{11}	= 4.957e−04	m
Absolute tolerance on angle α_1	ϵ_{12}	= 2.424e−04	rad
Absolute tolerance on angle β_1	ϵ_{13}	= 8.516e−04	rad
Absolute tolerance on angle α_2	ϵ_{14}	= 2.325e−04	rad
Absolute tolerance on angle β_2	ϵ_{15}	= 7.903e−04	rad

Table 6.3: Optimal Allocation of Tolerances in FDM

manded on links 1 and 4. It may be noted that these two links are the only links in Y_0-direction. Stricter clearance is demanded in pair 34. Among angles, stricter tolerances are demanded on angles α_1 and α_2, i.e., the angles about X_0-direction. Therefore, the error is most sensitive to V_1, V_4, V_8, V_9, V_{12} and V_{14}.

6.5 Optimum Tolerances in SL

Chapter 5 finds the position vector $\mathbf{q}(u,w) = [\ x \quad y \quad z \quad 1\ ]$ of the point Q on the contour of a slice in SL. The laser beam in SL draws the contour on the resin surface. There are eleven random variables V_1, V_2, ..., V_{11} involved in the stochastic model of the process. The expressions for the influence coefficients a_i, b_i and c_i and the partial derivatives needed for them are given in Section 5.11, pp. 114-118. The variances of the dependent variable x, y and z and their sum is tabulated in Table 5.1, Section 5.12. Section 5.12 also gives the plots of three-sigma bands of error in tracing several curves on the resin surface. The maximum value of the sum of variances DSUM occurs at $(q_x = 0, q_y = .3)$.

The optimal allocation of tolerances is done at the mean values of variables and the other input values mentioned in Section 12. The optimal allocation is based on the point at which the sum of variances DSUM is maximum, that is, at $(q_x = 0, q_y = .3)$ on the resin surface. Assuming D[x] = 8.0 x $10^{-8}m^2$, D[y] = 12.0 x $10^{-8}m^2$ and D[z]

$= 5.0 \times 10^{-8} m^2$, the optimal values of variances of the variables V_i are obtained using Lagrange multiplier technique as discussed in Section 6.2. Since a real solution for the Lagrange multipliers $(\lambda_1, \lambda_2, \lambda_3)$ is obtained with positive λ_1, therefore, the ratio of variances, K_1 and K_2 are in the allowable range and the solution for λ_1, λ_2 and λ_3 exists. No real solution was found when $K_2 \simeq 5.0$. The solution obtained for the Lagrange multipliers are as follows:

$$\lambda_1 = 7.740 \times 10^{15} \quad \lambda_2 = 3.164 \times 10^{14} \quad \lambda_3 = -2.034 \times 10^{15}$$

The optimal values of variances ρ_i are listed in Table 6.4.

The optimum values of variances are also obtained using real coded genetic algorithm optimization method as discussed in Section 6.2. Since the error at the point Q doesn't depend upon the variable V_1, therefore, only the other ten variable are considered for optimization using GA. The influence coefficients with respect to variable V_1 are smaller by many orders compared to those for other variables. From Eq. (6.6) it can be seen that the terms corresponding to V_1 contribute negligibly to the constraints. The input values taken for GA runs are as follows:

Population size:	100
Number of variables:	10
Bounds on variables:	rigid
Crossover probability:	0.85
Mutation probability:	0.05
Random seed number:	0.51

Optimization is done by varying number of generation and number of runs. The optimum values of variances ρ_i on variables V_i, obtained for 600 generations and single run, are listed in Table 6.4 alongwith those obtained from Lagrange multiplier technique.

The optimum values of variances obtained by real GA compare very closely to those obtained by Lagrange multiplier technique. This confirms that the optimum values obtained are global optimum.

The tolerances on coordinates and angles, obtained from the optimal values of variances ρ_i, are listed in Table 6.5. The tolerance allocated on the variable V_1 is many orders higher compared to those on other variables. This only means that the error at the point Q doesn't depend upon the variable V_1. This can be easily seen that changing the x-coordinate of the laser beam doesn't affect the coordinates of the point Q. The absolute tolerance on other variables are of the same order for this set of input values. Among them, stricter tolerance are demanded on the z-coordinate of the source E and the x-coordinate of mirror. Stricter tolerance is demanded on the angle β. Therefore the error is most sensitive to V_3, V_6 and V_{10}.

Optimum Variances from Lagrange		Optimum Variances from Real GA	
i	Variance ρ_i	i	Variance ρ_i
1	6.730e+00		
2	4.279e-08	2	4.463e−08
3	1.003e-08	3	1.147e−08
4	1.152e-08	4	1.300e−08
5	4.915e-08	5	4.807e−08
6	1.137e-08	6	1.300e−08
7	6.596e-08	7	7.647e−08
8	1.979e-08	8	2.280e−08
9	3.153e-08	9	3.253e−08
10	8.341e-09	10	9.546e−09
11	5.000e-08	11	2.239e−08

Table 6.4: Optimum Values of Variances ρ_i in SL from Lagrange Multiplier Technique and from Real Coded GA.

Optimal Allocation of Tolerances			
		Tolerance	Units
Absolute tolerance on coordinate a_1	ϵ_1	$= 7.782e{+}00$	m
Absolute tolerance on coordinate b_1	ϵ_2	$= 6.205e{-}04$	m
Absolute tolerance on coordinate c_1	ϵ_3	$= 3.004e{-}04$	m
Absolute tolerance on angle α_1	ϵ_4	$= 3.220e{-}04$	rad
Absolute tolerance on angle β_1	ϵ_5	$= 6.651e{-}04$	rad
Absolute tolerance on coordinate a_2	ϵ_6	$= 3.198e{-}04$	m
Absolute tolerance on coordinate b_2	ϵ_7	$= 7.705e{-}04$	m
Absolute tolerance on coordinate c_2	ϵ_8	$= 4.220e{-}04$	m
Absolute tolerance on angle α_2	ϵ_9	$= 5.327e{-}04$	rad
Absolute tolerance on angle β_2	ϵ_{10}	$= 2.740e{-}04$	rad
Absolute tolerance on coordinate c_3	ϵ_{11}	$= 6.708e{-}04$	m

Table 6.5: Optimal Allocation of Tolerances in SL

The synthesis procedure in the present work enables the designer to allocate tolerances and clearances optimally. The synthesis procedure clearly shows that the allowances on different variables are different depending upon the influence of a particular variable.

Chapter 7

CONCLUSIONS

7.1 Conclusions

In the present work the mechanical error in rapid prototyping processes is studied using stochastic approach. Three RP processes, LOM, FDM and SL are considered. The coordinates of a point on the work surface traced by the laser beam or the tip of the extruder head is expressed as a function of random variables involved in the process. The methodology to associate any given range of a dependent variable x, y or z with its corresponding probability is given. The variances of the dependent variables x, y and z are expressed in terms of the influence coefficients $\left(\frac{\partial x}{\partial V_i}\right)^2$, $\left(\frac{\partial y}{\partial V_i}\right)^2$ and $\left(\frac{\partial z}{\partial V_i}\right)^2$.

In LOM, the variances D[x], D[y] and D[z] are of the same order. The variance D[z] varies significantly over the work surface compared to D[x] and D[y]. The variance D[y] does not vary over the work surface and is equal to the variance of the random variable V_{16}. The variances and their sum are listed in a table to show their variation across the work surface. The three-sigma bands of error in tracing few lines on the work surface is plotted. From the list of variances and the three-sigma bands it is observed that the overall error does not vary much over the work surface and a contour can be drawn anywhere on the work surface without much difference in accuracy. The error analysis in LOM is done when the laser beam traces the contour of a slice on the sheet held between idle rollers.

The variance D[x] and D[y] in FDM are of the same order. The variance D[z] is an order higher. This is because the influence coefficients $\left(\frac{\partial z}{\partial V_i}\right)^2$ have larger magnitudes compared to $\left(\frac{\partial x}{\partial V_i}\right)^2$ and $\left(\frac{\partial y}{\partial V_i}\right)^2$. The three-sigma bands in tracing few example curves by the nozzle tip is plotted. The variances and their sum are listed in a table to

show their variation across the work surface. The overall error is found to be varying appreciably across the work surface. The error is the least at the front-left end of the work surface and maximum at the rear-right end. The mechanical error in FDM was studied assuming that the material solidifies as it comes out of the nozzle tip.

The variances D[x], D[y] and D[z] in SL are of the same order. The variance D[z] does not vary over the work surface. The variances and their sum are listed in a table to show their variation across the work surface. The three-sigma bands of error in tracing a line and an ellipse on the resin surface is plotted.

A methodology for optimal allocation of tolerances and clearances is presented. Since the constraints are linear functions of design variables, therefore, the optimization is done using Lagrange multiplier technique. The optimal allocation is done at that point on the work surface where the sum of variances DSUM is found to be maximum while conducting error analysis. Optimization is also done using real coded Genetic Algorithm (real coded GA) for FDM and SL. The optimum values of variances for LOM differ from each other by several orders. The real GA code does not give good results for this case. Therefore, optimization in the case of LOM is not done using GA.

The synthesis procedure in the present work enables the designer to allocate tolerances and clearances optimally. The synthesis procedure clearly shows that the allowances on different variables are different depending upon the influence of that variable. In LOM, stricter tolerances are demanded in the x and y-coordinates of the source of the laser beam and the angle θ of the laser beam. In FDM, stricter tolerances are demanded on links 1 and 4, i.e., the links in Y_0-direction and on angles α_1 and α_2, i.e., the angles about X_0-direction. In SL, stricter tolerances are demanded on the z-coordinate of the source of the laser beam, the x-coordinate of the mirror and the angle of β of the mirror. It has been found that the error in SL is not sensitive to the location of the source of the laser beam along the direction of the laser beam.

7.2 Scope for Further Work

Geometric modeling of the LOM process can be improved by considering the mechanisms which cause the movement of the optics and the platform. The tolerances and clearances in these mechanisms can be considered in the error studies. The tolerances in the belt-driven mechanism for XY-positioning table can be considered.

There is a positive displacement belt drive for the motion of extruder head in FDM. The Z-stage platen moves on the power screws and there are two cylindrical rods for maintaining its alignment. The geometric model of FDM can be improved by considering these mechanisms. The manufacturing errors in them can be considered

in the error studies.

The geometric model of SL has considered the reflection through the mirror. It has considered the error in location and orientation of the mirror. In this way, it is an improvement over the geometric model of LOM. The geometric model can be further improved by considering the mechanisms which cause the movement of the optics and the elevator platform.

The study of mechanical error in FDM is carried out assuming the material solidifies as it comes out of the nozzle tip. The material flow characteristics and solidification properties can be considered in further work.

In the present work the mechanical error has been studied in drawing the slice of a part. The cumulative error in FDM, as the part is built progressively, depends upon the solidification and flow characteristics of modeling material and the error in the platform.

The cumulative error in LOM depends more on the error in the location and orientation of the platform and the heated roller. Geometric model is to be further refined taking them into consideration. The error at a particular layer is still stochastic as the thickness of the LOM sheet is sensed and the solid model is sliced on the fly.

The cumulative error in SL depends upon the error in positioning the platform and the error in sweeping by the recoater blade. Since the resin level is sensed after every layer, therefore, the error at any layer can be found out by stochastic approach. Further work is needed to find the cumulative error in RP processes as the part is built progressively.

In the present work synthesis has been carried out at a particular position on the work surface. The choice of the position is based on the trial analysis of the RP process. This approach seems to yield satisfactory results. However, a methodology can be developed for finding that critical point. For instance, the critical point can be chosen by repeating the synthesis procedure throughout the work surface. The critical point would be the point for which the maximum value of the sum of variances over the work surface is minimum. The optimal values of tolerances and clearances correspond to this point. The function $f(\sigma_1, \sigma_2)$ and $g(\sigma_1, \sigma_2)$ can be plotted in 3D in the feasible region of (σ_1, σ_2) to find the allowable range of K_1 and K_2 in Lagrange multiplier technique.

Optimization using real coded GA for the cases of FDM and SL gives optimal values comparable to those obtained by Lagrange multiplier technique. Results of real coded GA can be further refined. Optimization using real coded GA in the case of LOM needs to be further investigated. The optimum values of variances in LOM differ from each other by several orders. The code for real coded GA needs to be improved to take into account this case.

References

[1] 3D Systems Inc., 2000, Web Site, http://www.3dsystems.com/products/slaseries, October 2000.

[2] Ashley, Steven, 1991, "Rapid Prototyping Systems", Mechanical Engineering **113**, No. 4, pp. 34–43.

[3] Ashley, Steven, 1995, "Rapid Prototyping is Coming of Age", Mechanical Engineering **117**, No. 7, pp. 62–68.

[4] Austin, T.C., Denavit, J., and Hartenberg, R., S., 1965, "Analysis of Error in the Double Hooke Joint", ASME J. Engg. Ind. **87**, No. 2, pp. 251–257.

[5] Bakthavachalam, N., and Kimbrell, J. T., 1975, "Optimum Synthesis of Path-Generating Four-Bar Mechanisms", ASME J. Engg. Ind. **97**, No. 1, pp. 314–321.

[6] Balling, Richard J., Free, Joseph C., and Parkinson, Alan R., 1986, "Consideration of Worst-Case Manufacturing Tolerances in Design Optimization", ASME Journal of Mechanisms, Transmission and Automation in Design **108**, No. 4, pp. 438–441.

[7] Bandler, J. W., El-Kady, M. A., Kellermann, W., and Zuberek, W. M., 1984, "A Minimax Approach to the Best Mechanical Allignment Problem", ASME Journal of Mechanisms, Transmission and Automation in Design **106**, No. 1, pp. 31–40.

[8] Barker, C. R., and Bauman, J., 1987, "Characteristic Surfaces for Three-Position Motion Generation With Planar Four-Bar Mechanisms", ASME Journal of Mechanisms, Transmission and Automation in Design **109**, No. 2, pp. 183–188.

[9] Bartel, D. L., and Marks, R. W., 1974, "The Optimum Design of Mechanical Systems With Competing Design Objectives", ASME J. Engg. Ind. **96**, No. 1, pp. 171–178.

[10] Baumgarten, Josheph R., and van der Werff, K., 1985, "A Probabilistic Study Relating to Tolerancing and Path Generation Error", Mech. Mach. Theory **20**, No. 1, pp. 71–76.

[11] Beaman, J. J. Barlow, J. W., et al, 1997, Solid Freeform Fabrication: A New Direction in Manufacturing, Kluwer Academic Publishers. Boston, USA.

[12] Beightler, C. S., Lo, Ta-Chen, and Rylander, H. G., 1970, "Optimal Design by Geometric Programming", ASME J. Engg. Ind. **92**, No. 1, pp. 191–196.

[13] Bhatt, A. D., Agrawal, Sanat, and Dhande, S. G., 1997, "Rapid Prototyping and Tooling Technologies", National Seminar on Emerging Trends in Design Engineering, India, Vol. III, Section VI, pp. KN-118–136.

[14] Burns, Marshall, 1993, Automated Fabrication: Improving Productivity in Manufacturing, Ennex Corporation, Los Angels, USA.

[15] Chakraborty, J., 1975, "Synthesis of Mechanical Error in Linkages", Mech. Mach. Theory **10**, No. 2, pp. 155–165.

[16] Chatterjee, G. B., and Mallik, A. K., 1987, "Mechanical Error of a Four-Bar Linkage Coupler Curve", Mech. Mach. Theory **22**, No. 1, pp. 85–88.

[17] Chen, F. Y., and Chan, Ken-Lin, 1974, "Dimensional Synthesis of Mechanisms for Function Generation Using Marquardt's Compromise", ASME J. Engg. Ind. **96**, No. 1, pp. 131–137.

[18] Cheng, W., Fuh, ,J.Y.H., Nee, A.Y.C., Wong, Y.S., Loh, H.T. and Miyazawa, T., 1995, "Multi-objective Optimization of Part-Building Orientation in Stereo-lithography", Rapid Prototyping Journal **1**, No. 4, pp. 12–23.

[19] Childs, T. H. C., and Juster, N. P., 1994, "Linear and Geometric Accuracies from Layer Manufacturing", Annals of the CIRP **43**, No. 1, pp. 163–166.

[20] Chi-Yeh, Han, 1966, "A General Method for the Optimum Design of Mechanisms", J. Mechanisms**1**, No. 3–4, pp. 301–313.

[21] Choubey, M., and Rao, A. C., 1982, "Synthesizing Linkage with Minimal Structural and Mechanical Error Based upon Tolerance Allocation", Mech. Mach. Theory **17**, No. 2, pp. 91–97.

[22] Cleghorn, W. L., Fenton, R. G., and Fu, Jingfan 1993, "Optimum Tolerancing of Planar Mechanisms Based on Error Sensitivity Analysis", ASME J. Mech. Design **115**, No. 2, pp. 306–313.

[23] Coit, William G., and Riley, Donald R., 1981, "Sensitivity Analysis of Inverted Slider Crank Straight-Line Generator", Mech. Mach. Theory **16**, No. 4, pp. 303–310.

[24] Conley, J. G., and Marcus, H. L., 1997, "Rapid Prototyping and Solid Freeform Fabrication", ASME J. Manf. Sc. Engg. **119**, No. 4, pp. 811–816.

[25] Deb, Kalyanmoy, 1995, Optimization for Engineering Design, Prentice-Hall of India Private Limited, New Delhi.

[26] Deb, Kalyanmoy, and Agrawal, Ram Bhusan, 1995, "Simulated Binary Crossover for Continuous Search Space", Complex Systems **9**, pp. 115–148.

[27] Dhande, S. G., Bhadoria, B. S., and Chakraborty J., 1975, "A Unified Approach to the Analytical Design of Cam Mechanisms", ASME J. Engg. Ind. **97**, No. 1, pp. 327–333.

[28] Dhande, S. G., and Chakraborty, S. J., 1973, "Analysis and Synthesis of Mechanical Error in Linkages — A stochastic Approach", ASME J. Engg. Ind. **95**, No. 3, pp. 672–676.

[29] Dhande, S. G., and Chakraborty, J., 1975, "Mechanical Error Analysis of Cam-Follower Systems — A Stochastic Approach", Proceedings of the Fourth World Congress on Theory of Mechanisms and Machines, University of Newcastle upon Tyne, England, Vol. **4**, pp. 957–962.

[30] Dhande, S. G., and Chakraborty, J., 1978, "Mechanical Error Analysis of Spatial Linkages", ASME J. Mech. Design **100**, pp. 732–738.

[31] Dolenc, A., 1994, "An Overview of Rapid Prototyping Technology in Manufacturing", Otaniemi 1994/TKO-B116, ISBN 951-22-2123-3, Helsinki University of Technology, Finland.

[32] Dolenc, A., and Mäkelä, I., 1994, "Slicing Procedures for Layered Maufacturing Techniques", Computer-Aided Design **26**, No. 2, pp. 119–126.

[33] Dolenc, A., and Mäkelä, I., 1996, "Rapid Prototyping from a Computer Scientist's Point of View", Rapid Prototyping Journal **2**, No. 2, pp. 18–25.

[34] Dubowsky, S., Matuk, J., and Parreira, N. D., 1975, "A Parameter Identification Study of Kinematic Errors in Planar Mechanisms", ASME J. Engg. Ind. **97**, No. 2, pp. 635–642.

[35] Eason, E. D., and Fenton, R. G., 1974, "A Comparison of Numerical Optimization Methods for Engineering Design", ASME J. Engg. Ind. **96**, No. 1, pp. 196–200.

[36] Fadel, Georges M., and Kirschman, Chuck, 1996, "Accuracy Issues in CAD to RP Translations", Rapid Prototyping Journal **2**, No. 2, pp. 4–17.

[37] Faik, S., and Erdman, A. G., 1991, "Sensitivity Distribution in the Synthesis Solution Space of Four-Bar Linkages", ASME J. Mech. Design **113**, No. 1, pp. 3–9.

[38] Faux, I. D., and Pratt, M. J., 1979, Computational Geometry for Design and Manufacture, Ellis Horwood Limited, West Sussex, England.

[39] Fenton, R. G., Cleghorn, W. L., and Fu, Jing-Fan, 1989, "Allocation of Dimensional Tolerances for Multiple Loop Planar Mechanisms", ASME Journal of Mechanisms, Transmission and Automation in Design **111**, No. 4, pp. 465–470.

[40] Foley, J. D., van Dam, A., Feiner, S. K., and Hughes, J. F., 1996, Computer Graphics: Principles and Practice, Addison Wesley Publishing, Massachusets.

[41] Fox, R. L., and Gupta, K. C., 1973, "Optimization Technology as Applied to Mechanism Design", ASME J. Engg. Ind. **95**, No. 2, pp. 657–663.

[42] Garrett, R. E., and Hall, Jr, A. S., 1968, "Optimal Synthesis of Randomly Generated Linkages", ASME J. Engg. Ind. **68**, No. 3, pp. 475–480.

[43] Garrett, R. E., and Hall, Jr, A. S., 1969, "Effect of Tolerance and Clearance in Linkage Design", ASME J. Engg. Ind. **91**, No. 1, pp. 198–202.

[44] Ghosh, Amitabha, and Mallik, A. K., 1988, Theory of Mechanisms and Machines, Affiliated East West Press Private Limited, New Delhi, India.

[45] Ghosh, Amitabha, 1997, Rapid Prototyping: A Brief Introduction, Affiliated East West Press Private Limited, New Delhi, India.

[46] Graves, S. B., 1999, "A Total Cost Comparison of Alternating Tolerancing Formulae", ASME J. Manf. Sc. Engg. **121**, No. 4, pp. 720–726.

[47] Greenwood, W. H., and Chase, K. W., 1990, "Root Sum Squares Tolerance Analysis with Nonlinear Problems", ASME J. Engg. Ind. **112**, No. 4, pp. 382–384.

[48] Grigson, Angela, 1994, "Model Making", Mechanical Engineer **73**, No. 8, pp. 172–178.

[49] Gupta, V. K., and Radcliffe, Charles W., 1971, "Mobility Analysis of Plane and Spatial Mechanisms", ASME J. Engg. Ind. **93**, No. 1, pp. 125–130.

[50] Gupta, V. K., 1973, "Computer-Aided Synthesis of Mechanism Using Non-Linear Programming", ASME J. Engg. Ind. **95**, No. 1, pp. 339–344.

[51] Gupta, V. K., 1973, "Kinematic Analysis of Plane and Spatial Mechanisms", ASME J. Engg. Ind.. **95**, No. 2, pp. 481–486.

[52] Hall, Jr, A. S., 1961, "Coupler Curves", Kinematics and Linkage Design, Prentice-Hall, Inc. Englewood Cliffs, N. J., pp. 48–56.

[53] Hartenberg, R.S., and Denavit, J., 1964, Kinematic Synthesis of Linkages, McGraw-Hill, New York, pp. 316–319.

[54] Hati, S. K., and Rao, S. S., 1976, "Determination of Optimum Machining Conditions — Determinisitic and Probabilistic Approaches", ASME J. Engg. Ind. **98**, No. 1, pp. 354–359.

[55] Helisys Inc., 2000, Web Site, http://www.helisys.com/PAGE49.HTM, October 2000.

[56] Helstrom, Carl W., 1984, Probability and Stochastic Process for Engineers, Macmillan Publishing Company, New York.

[57] Hope, R. L., Jacobs, P. A., and Roth, R. N., 1997, "Rapid Prototyping With Sloping Surfaces", Rapid Prototyping Journal **3**, No. 1, pp. 12–19.

[58] Hope, R. L., Roth, R. N., and Jacobs, P. A., 1997, "Adaptive Slicing With Sloping Layer Surfaces", Rapid Prototyping Journal **3**, No. 3, pp. 89–98.

[59] Ippolito, R., Tuliano, L., and Gatto, A., 1995, "Benchmarking of Rapid Prototyping Techniques in Terms of Dimensional Accuracy and Surface Finish", Annals of the CIRP **44**, No. 1, pp. 157–160.

[60] Jacobs, Paul F., 1992, Rapid Prototyping and Manufacturing: Fundamentals of Stereolithography, SME, Dearborn, MI.

[61] Jamieson, Ron, and Hacker, Herbert, 1995, "Direct Slicing of CAD models for Rapid Prototyping", Rapid Prototyping Journal **1**, No. 2, pp. 4–12.

[62] Jurrens, Kevin K., 1993, "An Assessment of the State-of-the-Art in Rapid Prototyping Systems for Mechanical Parts", Final Report NISTIR 5335, U. S. Department of Commerce.

[63] Kai, Chua Chee, and Fai, Leong Kah, 1997, Rapid Prototyping: Principles & Applications in Manufacturing, John Wiley & Sons, N Y, USA.

[64] Kapur, J. N., 1988, Mathematical Modeling, Wiley Eastern Limited, New Delhi.

[65] Knappe, L. F., 1963, "Mechanism Tolerances", Machine Design **35**, pp. 155–157.

[66] Kochan, D., and Chua, C. K., 1995, "State-of-the-Art and Future Trends in Advanced Rapid Prototyping and Manufacturing", International Journal of Information Technology **1**, No. 2, pp. 173–184.

[67] Kochan, A., 1997, "RP Trends", Rapid Prototyping Journal **3**, No. 4, pp. 150–152.

[68] Kolhatkar, S. A., and Yajnik, K. S., 1970, "The Effects of Play in the Joints of a Function-Generating Mechanisms", J. Mechanisms **5**, No. 4, pp. 521–532.

[69] Koutsoyiannis, A., 1987, Theory of Econometrics, 2^{nd} ed., English Language Book Society/Macmillan, Hampshire, London.

[70] Kramer, S. N., and Sandor, G. N., 1975, "Selective Precision Synthesis — A General Method of Optimization for Planar Mechanisms", ASME J. Engg. Ind. **97**, No. 2, pp. 689–701.

[71] Kreyszig, Erwin, 1983, Advanced Engineering Mathematics, 3^{rd} ed., Wiley Eastern Limited, New Delhi, India.

[72] Kruth, J. P., 1991, "Material Incress Manufacturing by Rapid Prototyping Techniques", Annals of the CIRP **40**, No. 2, pp. 603–614.

[73] Kulkarni, Prashant, and Dutta, Debashish 1995, "An Accurate Slicing Procedure for Layered Manufacturing", Computer-Aided Design **28**, No. 9, pp. 683–697.

[74] Lacourse, Donald E., 1995, "Solid Modeling and Rapid Prototyping", Handbook of Solid Modeling, McGraw-Hill, New york, pp. 19.1–19.20.

[75] Lakshminarayana, K., and Narayanamurthi, R. G., 1971, "On the Analysis of Effect of Tolerances in Linkages", J. Mechanisms **6**, No. 1, pp. 59–67.

[76] Lee, T. W., and Freudenstein, F., 1976, "Heuristic Combinatorial Optimization in the Kinematic Design of Mechanisms Part1: Theory", ASME J. Engg. Ind. **98**, No. 4, pp. 1277–1280.

[77] Lee, T. W., and Freudenstein, F., 1976, "Heuristic Combinatorial Optimization in the Kinematic Design of Mechanisms Part2: Applications", ASME J. Engg. Ind. **98**, No. 4, pp. 1281–1284.

[78] Lee, W.-J., and Woo, T. C., 1989, "Optimum Selection of Descrete Tolerances", ASME Journal of Mechanisms, Transmission and Automation in Design **111**, No. 2, pp. 243–251.

[79] Lee, W.-J., and Woo, T. C., 1990, "Tolerances: Their Analysis and Synthesis", ASME J. Engg. Ind. **112**, No. 2, pp. 113–121.

[80] Lee, S. J., and Gilmore, B. J., 1991, "The Determination of the Probabilstic Properties of Velocities and Accelarations in Kinematic chains With Uncertainty", ASME J. Mech. Design **113**, No. 1, pp. 84–90.

[81] Lee, S. J., Gilmore, B. J., and Ogot, M. M., 1993, "Dimensional Tolerance Allocation of Stochastic Dynamic Mechanical Systems Through Performance and Sensitivity Analysis", ASME J. Mech. Design **115**, No. 3, pp. 392–402.

[82] Lee, S.-J.J., Sachs, E., and Cima, M., 1995, "Layer Position Accuracy in Powder-Based Rapid Prototyping", Rapid Prototyping Journal **1**, No. 4, pp. 24–37.

[83] Lin, Psang Dain, and Chen, Jen Fun, 1992, "Accuracy Analysis of Planar Linkages by the Matrix Method", Mech. Mach. Theory **27**, No. 5, pp. 507–516.

[84] Lynn-Charney, Charity, and Rosen, David W., 2000, "Usage of Accuracy Models in Stereolithography Process Planning", Rapid Prototyping Journal **6**, No. 2, pp. 77–86.

[85] Maddox, Roger, and Knesek, John, 1993, "A Glimpse at Rapid Prototyping Technologies", Aerospace America, June 1993, pp. 28–32.

[86] Mallik, Asok K., and Dhande, S. G., 1987, "Analysis and Synthesis of Path-Generating Linkages Using a Stochastic Approach", ASME J. Engg. Ind. **22**, No. 2, pp. 115–123.

[87] Mallik, Asok K., Ghosh, Amitabha, and Günter Dittrich, 1994, Kinematic Analysis and Synthesis of Mechanisms, CRC Press, Boca Raton (USA), pp. 308–314.

[88] Michael, W., and Siddal, J. N., 1981, "The Optimization Problem With Optimal Tolerance Assignment and Full Acceptance", ASME J. Mech. Design **103**, No. 4, pp. 842–848.

[89] Michael, W., and Siddal, J. N., 1982, "The Optimal Tolerance Assignment With Less Than Full Acceptance", ASME J. Mech. Design **104**, No. 4, pp. 855–60.

[90] Mortenson, M. E., 1985, Geometric Modeling, John Wiley & Sons, New York.

[91] Nechi, A. J., 1971, "A Relaxation and Gradient Combination Applied to the Computer Simulation of a Plane Four-Bar Chain", ASME J. Engg. Ind. **93**, No. 1, pp. 113–119.

[92] Nolle, H., and Hunt, K. H., 1971, "Optimum Synthesis of Planar Linkages to Generate Coupler Curves", J. Mechanisms **6**, pp. 267–287.

[93] Onuh, S. O., and Yusuf, Y. Y., 1999, "Rapid Prototyping Technology: Applications and Benefits for Rapid Product Development", J. Int. Manf. **10**, pp. 301–311.

[94] Ostwald, P. F., and Huang, J., 1977, "A Method for Optimal Tolerance Selection", ASME J. Engg. Ind. **99**, No. 3, pp. 558–565.

[95] Pham, D. T., and Gault, R. S., 1998, "A Comparison of Rapid Prototyping Technologies", Int. J. Mach. Tools Manf. **38**, pp. 1257–1287.

[96] Prasad, K. N., and Bagci, C., 1974, "Minimum Error Synthesis of Multiloop Plane Mechanisms for Rigid Body Guidance", ASME J. Engg. Ind. **96**, No. 1, pp. 107–116.

[97] Press, W. H., Teukolsky, S. A., Veterling, W. T., and Flannery, B. P., 1992, Numerical Recipes in C: The Art of Scientific Computing, Foundation Books, New Delhi.

[98] Rao, A. C., 1978, "Improved Method for the Design of Link Mechanisms", Indian Journal of Technlogy **16**, pp. 145–147.

[99] Rao, S. S., and Hati, S. K., 1979, "Game Theory Approach in Multicriteria Optimization of Function Generating Mechanisms", ASME J. Mech. Design **114**, No. 3, pp. 398–406.

[100] Rao, S. S., 1984, Optimization: Theory and Applications, Wiley Eastern Limited, New Delhi.

[101] Reklaitis, G.V., Ravindran, A., and Ragsdell, K. M., 1983, Engineering Opimization — Methods and Applications, Wiley, New York.

[102] Rhyu, Je Ha, and Kwak, Byung Man, 1988, "Optimal Stochastic Design of Four-Bar Mechanisms for Tolerance and Clearance", ASME Journal of Mechanisms, Transmission and Automation in Design **110**, No. 3, pp. 255–262.

[103] Rogers D. F., and Adams, J. A., 1990, Mathematical Elements for Computer Graphics, 2^{nd} ed., McGraw-Hill Publishing, New York.

[104] Root, R. R., and Ragsdell, K. M., 1976, "A Survey of Optimization Methods Applied to the Design of Mechanisms", ASME J. Engg. Ind. **98**, No. 3, pp. 1036–1041.

[105] Sabourin, Emmanuel, Houser, Scott A., and Bøhn, Jan Helge 1996, "Adaptive Slicing Using Stepwise Uniform Refinement", Rapid Prototyping Journal **2**, No. 4, pp. 20–26.

[106] Schade, G. R., 1981, "Probabilistic Models in Computer Automated Slider-Crank Function Generator Design", ASME J. Mech. Design **103**, No. 4, pp. 835–841.

[107] Sharfi, O. M. A., and Smith, M. R., 1983, "A Simple Method for the Allocation of Approximate Tolerance in Linkage Mechanisms", Mech. Mach. Theory **18**, No. 2, pp. 123–129.

[108] Shi, Z., 1997, "Synthesis of Mechanical Error in Spatial Linkages Based on Reliabilty Concept", Mech. Mach. Theory **32**, No. 2, pp. 255–259.

[109] Shigley, J. E., and Uicker, J. J., 1980, Theory of Machines and Mechanisms, McGraw-Hill Book Company, New York, pp. 342–344.

[110] Shigley, J. E., and Mitchell, L. D., 1983, Mechanical Engineering Design, McGraw-Hill, Singapore.

[111] Spotts, M. F., 1973, "Allocation of Tolerances to Minimize Cost of Assembly", ASME J. Engg. Ind. **95**, No. 3, pp. 762–764.

[112] Sprow, Eugene E., 1992, "Rapid Prototyping: Beyond the Wet Look", Mechanical Engineering, Nov. 1992, pp. 58–64.

[113] Stratasys Inc., 1998, FDM System Documentation, Stratasys Inc., 14950 Martin Drive, Eden Prairie, Minneapolis, 55344-2020, USA.

[114] Stratasys Inc., 2000, Web Site, http://www.stratasys.com/FDM2000.html, October 2000.

[115] Sukhija, R. P., and Rao, A. C., 1987, "Synthesis of Path-Generating Mechanisms and tolerance Allocation Using Information Theory", ASME Journal of Mechanisms, Transmission and Automation in Design **109**, No. 3, pp. 366–371.

[116] Sutherland, G., and Roth, B., 1973, "A Transmission Index for Spatial Mechanism", ASME J. Engg. Ind. **95**, No. 2, pp. 589–597.

[117] Sutherland, G. H., and Roth, B., 1975, "Mechanism Design: Accounting for Manufacturing Tolerances and Costs in Function Generating Problems", ASME J. Engg. Ind. **97**, No. 1, pp. 283–286.

[118] Tata, K., Fadel, G., Bagchi, A. and Aziz, N. 1998, "Efficient Slicing for Layered Manufacturing", Rapid Prototyping Journal **4**, No. 4, pp. 151–167.

[119] Ting, Kwun-Lon, and Long, Yufeng, 1996, "Performance Quality and Tolerance Sensitivity of Mechanisms", ASME J. Mech. Design **118**, No. 1, pp. 144–150.

[120] Ting, Kwun-Lon, Zhu, Jianmin, and Watkins, Derek, 2000, "The Effect of Joint Clearance on Position and Orientation Deviation of Linkages and Manipulators", Mech. Mach. Theory **35**, No. 3, pp. 391–401.

[121] Tuttle, S. B., 1960, "Error Analysis", Machine Design **32**, No. 12, pp. 153–158.

[122] Tyberg, Justin, and Bøhn, Jan Helge, 1998, "Local Adaptive Slicing", Rapid Prototyping Journal **4**, No. 3, pp. 118–127.

[123] Ventsel, E.S., 1964, Theory of Probability, Nauka, Moscow (In Russian).

[124] Wang, H. H. S., and Roth, B., 1989, "Positions Errors Due to Clearances in Journal Bearings", ASME Journal of Mechanisms, Transmission and Automation in Design **111**, No. 3, pp. 315–320.

[125] Weidermann, B., Dusel, K.-H., and Eschl, J., 1995, "Investigation into the Influence of Material and Process on Part Distortion", Rapid Prototyping Journal **1**, No. 3, pp. 17–22.

[126] Weiliang, Xu, and Qixian, Zhang, 1989, "Probablistic Analysis and Monte Carlo Simulatoin of the Kinematic Error in a Spatial Linkage", Mech. Mach. Theory **24**, No. 1, pp. 19–27.

[127] Wohlers, Terrey T., 1991, "Make Fiction Fact Fast", Mechanical Engineering , March 1991, pp. 44–49.

[128] Wu, S. M., and Dalal, J. G., 1971, "Stochastic Model for Machining Processes — Optimal Decision-Making and Control", ASME J. Engg. Ind. **93**, No. 2, pp. 593–602.

[129] Xu, F., Wong, Y. S., Loh, H. T., Fuh, J.Y.H., and Miyazawa, T., 1997, "Optimal Orientation With Variable Slicing in Stereolithography", Rapid Prototyping Journal **3**, No. 3, pp. 76–88.

[130] Xu, F., Loh, H. T., and Wong, Y. S., 1999, "Considerations and Selection of Optimal Orientation for different Rapid Prototyping Systems", Rapid Prototyping Journal **5**, No. 2, pp. 54–60.

[131] Young, J. S., Fox, S. R., and Anseth, K. S., 1999, "A Novel Device for Producing Three Dimensional Objects", ASME J. Manf. Sc. Engg. **121**, No. 3, pp. 474–477.

[132] Yufeng, Long, and Jiangqin, Lu, 1993, "On the Optimum Tolerances of Structural Parameters and Kinematic Parameters of Kinematic Parameters of Robot Manipulators", Mech. Mach. Theory **28**, No. 6, pp. 819–824.

[133] Zeid, Abrahim, 1991, CAD/CAM Theory and Practice, McGraw-Hill Publishing, New York.

[134] Zhu, Jianmin, and Ting, Kwun-Lon, 2000, "Uncertainty Analysis of Planar and Spatial Robots With Joint Clearances", Mech. Mach. Theory **35**, No. 9, pp. 1239–1256.